Faculdade de Engenharia da Universidade do Porto



Biomechanical analysis of low-cycle fatigue damage during the second stage of labor

Maria Castro Paupério Vila Pouca

Doctoral Program in Mechanical Engineering

Supervisor: Doctor Marco Paulo Lages Parente
Co-Supervisor: Doctor Renato Manuel Natal Jorge
Co-Supervisor: Doctor James Anthony Ashton-Miller

March 4, 2022

©Maria Vila Pouca, 2022

Biomechanical analysis of low-cycle fatigue damage during the second stage of labor

Maria Castro Paupério Vila Pouca

Doctoral Program in Mechanical Engineering

Approved by:

President: Doctor José Cesar de Sá

Referee: Doctor Gerhard Holzapfel

Referee: Doctor Nina Kimmich

Referee: Doctor Rita Rynkevic

Date: March 4, 2022

"Structural Engineering is the art of modelling materials we do not wholly understand, into shapes we cannot precisely analyse so as to withstand forces we cannot properly assess, in such a way that the public has no reason to suspect the extent of our ignorance."

Dr. A.R. Dykes

"There is nothing like looking if you want to find something."

J. R. R. Tolkien
In *The Hobbit,* 1937

Table of Contents

Acknowledgements xi

Resumo xiii

Abstract xv

List of Figures xvii

List of Tables xxiii

Acronyms and Symbols xxv

Introduction 1

Anatomy of the female pelvic floor – brief overview 1

Impact of vaginal delivery on the pelvic floor muscles 2

Biomechanics of the pelvic floor 6

Animal models and pelvic floor research 6

Mechanical testing and microscopic imaging in soft tissues and the pelvic floor 8

Constitutive modeling of soft tissues and the pelvic floor muscles 14

Material fatigue – brief description 21

Thesis outline and specific aims 23

Aim 1 – Material fatigue in the musculoskeletal system 23

Aim 2 – Material fatigue due to a difficult labor 23

Aim 3 – Experimental evidence of material fatigue in the levator ani 24

Aim 4 – Modeling low-cycle fatigue damage 24

Aim 5 – Modeling permanent deformation 24

References 25

Chapter 1 - Injuries in muscle-tendon-bone units 33

Abstract 36

1.1. Introduction 37

1.2. Methods 38

1.2.1. Search strategy 38

1.2.2. Data extraction 38

1.2.3. Quality assessment 39

1.2.4. Statistical analysis 40

1.3. Results 40

1.3.1. Search results 40

1.3.2. Laboratory studies employing mechanical failure tests 43

1.3.3. Observational studies 44
1.3.4. Injury site 45
1.3.5. Injury muscle/tendon groups 46
1.4. Discussion 52
1.5. Conclusion 56
References 57

Chapter 2 - Pelvic floor muscle injury during a difficult labor 65
Abstract 68
2.1. Introduction 69
2.2. What distinguishes muscle/ligament origins and insertions? 72
2.3. Characteristics of the origin of the pubovisceral muscle 74
2.4. Is there evidence of low-cycle fatigue damage occurring in soft tissues? 75
2.5. Can the origin of the pubovisceral muscle be susceptible to low-cycle fatigue damage in a difficult vaginal birth? 76
2.6. Conclusions 79
References 80

Chapter 3 - Investigating the birth-related caudal maternal pelvic floor muscle injury 83
Abstract 86
3.1. Introduction 87
3.2. Materials and methods 88
3.2.1. Animal model of the origin of the pubovisceral muscle 88
3.2.2. Specimens procurement and preparation 89
3.2.3. Experimental design and protocol 90
3.2.4. Digital image correlation 92
3.2.5. Permanent deformation 93
3.2.6. Microscopic damage assessment 93
3.2.7. Constitutive modeling and finite element simulation 94
3.3. Results 98
3.3.1. Ultimate tensile tests 99
3.3.2. Relaxation tests 99
3.3.3. Fatigue tests 99
3.3.4. Histologic assessment 99
3.3.5. Calibration of constitutive parameters 101
3.3.6. Numerical analysis and interpretation of the specimen behavior 105
3.4. Discussion 106
3.5. Conclusions 110
References 111

Chapter 4 - On the management of maternal pushing during the second stage of labor 115
Abstract 118
4.1. Introduction 119
4.2. Material and methods 122
4.2.1. Geometry model and Boundary Conditions 123
4.2.2. Material models 124
4.2.3. Maternal pushing 125

4.2.4. Biomechanical model evaluation 127
4.3. Results 128
4.4. Discussion 131
4.4.1. Principal findings 131
4.4.2. Results in the context of what is known 131
4.4.3. Clinical implications 133
4.4.4. Research implications 134
4.4.5. Strengths and limitations 134
4.4.6. Conclusions 136
References 137
Chapter 5 - Modeling permanent deformation during low-cycle fatigue 143
Abstract 146
5.1. Introduction 147
5.2. Material and methods 150
5.2.1. Kinematics 150
5.2.2. Constitutive and balance equations for hyperelastic materials 152
5.2.3. Evolution equations 154
5.2.4. Iterative scheme 156
5.3. Numerical examples 158
5.3.1. Convergence analysis 158
5.3.2. Tensile behavior of a dog bone-shaped sample 161
5.3.3. Behavior of rectangular specimen under biaxial stretch 163
5.3.4. Permanent deformation of the pelvic floor muscles after vaginal delivery 166
5.4. Discussion 170
5.5. Conclusions 171
References 172
Afterword 179
General discussion 179
Major findings 183
Final remarks and future work 183
Publications and presentations related with this study 185
Peer-reviewed publications 185
Oral communications 186
Appendix 187
A 189
B 191
C 203
D 205
E 221
F 226
G 228
References 234

Acknowledgements

First and foremost, I want to thank my advisors, Prof. Renato Natal and Prof. Marco Parente, for taking me in this journey, always believing in me and for the continuous support. I am also honored to work with Prof. James Ashton-Miller, who warmly welcomed me at the University of Michigan and taught me to be more confident, independent, and not to be afraid to try different methods, even if there is a chance of failure. For all the rides to the North Campus, the opportunity to participate in different meetings, for the support in the search of specimens and in those first difficult dissections, and for believing in me and pushing me forward. My appreciation extends to Kathy Ashton-Miller, whose genuine kindness was remarkable, for receiving me so well, always worried if I had a warm enough coat for Michigan winter. I also want to thank Dr. DeLancey for the helpful discussions and all the teaching moments during the hospital meetings and Dr. Ellen Arruda, for allowing me to use the laboratory equipment. I am also grateful to Andy Poli, for helping with the experimental design, teaching me how to use the tensile test and DIC equipment and for the good humored and friendly approach that always cheered me up, and to Carol Whitinger, who helped with the histology, training me to use the microtome and perform the specimens staining.

I gratefully acknowledge the support received from the Fulbright Scholarship for Research as well as Fundação para a Ciência e Tecnologia (FCT) under grant SFRH/BD/136213/2018.

I must thank my friends and colleagues at the Biomechanics Research Laboratory, INEGI and FEUP, for receiving me in their lab and for all the shared knowledge and support, particularly Luyun, Ali, Payam, Mariana, So Young, Dulce, Marco, Bruno and Madalena. To my closest friends in Ann Arbor, Andreia and Rita, who supported me during the difficult times, for all the nights out, the Portuguese dinners with the flaming chorizo, the rides to Kroger, my first American haunted house experience and much more. Thanks for all the shared laughs. A word of thanks to João and Francisca Soromenho, who organized Christmas dinner and the epic Game of Thrones viewing session and bingo, and to Nao, for the lovely talks at the end of the day and the Japanese-Portuguese dinner experiences.

Back home, to the friends from the running team, in particular Carla and Daniela, for always listening and supporting me, even when we were running. And to everyone from the artistic rollerskating team: a special word of thanks to Patrícia, whose joy is contagious, and to Filipe, my lifetime coach, thank you for teaching me to be determined and for making me more confident (or at least try…). To Xavier and Jaime, thank you for all the dinners and beer making days and Xavier, for listening and always be ready to help me whenever I needed to find a book, a paper or install new updated software. To Big Show, Mariana, Renata e Viktor, thank you for the

moments we shared. To my oldest and dearest friend, Maria João, a dedicated friend who is family, thank you for always being there.

A toda a minha família, obrigada por todo o apoio e carinho. Obrigada aos meus primos, por todas as gargalhadas partilhadas, momentos de descontração e diversão, aos meus tios pelo apoio incondicional. Às minhas sobrinhas por serem uma fonte de alegria. Um beijinho muito especial aos meus avós, cujo esforço e dedicação criou a família unida que temos, e sem dúvida, me ajudou a traçar este caminho: à minha avó, Margarida Paupério, obrigada por todos os almoços, incluindo os da 'tasquinha', pelas brincadeiras, lutas de água no quintal, pelas cartas quando estive fora e por todos os miminhos de avó; ao meu avô, José Paupério, obrigada por todas as histórias e canções, por todas as boleias para o treino, pelos jogos de bilhar, ping-pong, sueca e eleven, onde aprendemos desde cedo que é preciso dedicação e prática, para conseguirmos alcançar os nossos objetivos (e ganhar ao avô!); à minha avó, Lídia Vila Pouca, por me deixar ler banda desenhada a almoçar, por toda a dedicação, paciência, cuidados e brincadeiras com todos os netos.

Aos meus pais, por terem despoletado o meu gosto em Engenharia (apesar de eu ter escolhido a melhor vertente...), por todas as viagens que muito me fizeram crescer, por me terem sempre apoiado, acompanhado e acreditado em mim. Pelos sacrifícios, por vezes necessários para que não faltasse a um treino ou prova, e por estarem sempre nas bancadas, na patinagem e na vida. Mãe, obrigada por me mostrares que é preciso lutar pelos nossos objetivos, pela tua força e incrível multi-tasking, e por me ensinares que nunca é tarde para aprender. Pai, obrigada por toda a paciência, por todas as dúvidas esclarecidas durante o curso e pelas longas conversas de modelos de dano e deformação permanente, que tanto me ajudaram neste doutoramento.

Um obrigada gigante à melhor irmã do mundo, Catarina, por ser o meu exemplo. Por me mostrar que temos que agarrar as oportunidades, pela força e coragem que teve ao embarcar sozinha num doutoramento na Austrália e por ter terminado com louvor, passando ao próximo desafio. Mostrou-me que era possível e deu-me determinação. Obrigada pela nossas viagens, aventuras e cumplicidade, por me ensinares a tocar piano, a nadar e a fazer snorkeling. Por teres sido sempre paciente e presente, mesmo estando longe, por todas as proof-readings de trabalhos, ajuda nas candidaturas a bolsas e todas as dicas de formatação, que muito me ajudaram, incluindo agora no doutoramento. Obrigada por estares sempre presente.

As minhas últimas palavras vão para o João, que ao longo desta jornada se tornou meu marido, e a quem dedico esta tese. Obrigada por todo o apoio, pelas longas conversas de trabalho e brain-stormings, por me ajudares a desbloquear nas alturas mais complicadas e pelas várias proof-reading. Obrigada pelas longas viagens de autocarro de Cleveland para Ann Arbor, pelos croissants quando estava mais desanimada ao escrever a tese e por me fazeres rir constantemente com as tuas brincadeiras em casa. Muito obrigada por acreditares em mim e estares sempre ao meu lado.

Resumo

As lesões no pavimento pélvico são frequentes durante o parto vaginal, em particular na porção do músculo pubovisceral (PVM) pertencente ao *levator ani*. Para além das consequências imediatas associadas a uma qualquer lesão, as lesões no pavimento pélvico são um conhecido fator de risco para o desenvolvimento futuro de disfunções do pavimento pélvico. Estas disfunções, tal como a incontinência urinária, fecal e o prolapso dos órgãos pélvicos, têm um impacto significativo na qualidade de vida destas mulheres e as cirurgias de correção existentes ainda apresentam um elevado risco de recorrência e de complicações. Por este motivo, é essencial focarmo-nos na raiz do problema, aprofundar o nosso conhecimento relativamente ao porquê e como é que as lesões no pavimento pélvico ocorrem durante o parto vaginal para que se desenvolvam estratégias de prevenção e se reduzam as taxas deste tipo de lesões.

Nos últimos ~20 anos, as lesões no pavimento pélvico foram identificadas maioritariamente na origem do PVM, uma zona onde o músculo origina do osso e inclui a junção de três materiais distintos: músculo, colagénio e osso. No entanto, ainda não foi identificado em qual destes tecidos a lesão ocorre o que, consequentemente, faz com que o mecanismo de dano não seja verdadeiramente compreendido. Recentemente, a fadiga a baixos números de ciclos (~100) foi identificada como um possível mecanismo de dano na origem do ligamento cruzado anterior, na zona onde o ligamento conecta ao osso. Tendo em consideração que (1) durante o segundo estágio do parto, as contrações uterinas são complementadas com fortes esforços maternos e formam ciclos de carregamento repetitivos, com forças consideráveis, nos músculos do pavimento pélvico; e (2) a origem do PVM inclui duas junções de materiais distintos, que são zonas propensas a concentrações de tensões; esta tese explora a ideia de que a fadiga a baixos números de ciclos poderá causar a rápida acumulação e progressão de microdano durante o segundo estágio do parto, causando deformação permanente e até mesmo rutura do músculo.

Esta tese usa simultaneamente abordagens teóricas e experimentais para analisar a hipótese de fadiga de baixos ciclos no PVM e abordagens computacionais de modelação para investigar o impacto das atuais gestões do parto considerando a acumulação de microdano e deformação permanente. Em primeiro lugar, foi efetuada uma revisão sistemática para recolher evidências de lesões causadas por fadiga no sistema músculo-esquelético. De seguida, a hipótese foi avaliada de acordo com a informação encontrada e com o que é atualmente conhecido relativamente às

lesões no PVM, às suas especificidades anatómicas e às condições de carregamento. Estes estudos proporcionaram evidências indiretas que corroboraram a hipótese de fadiga a baixos números de ciclos como um potencial mecanismo de dano durante o parto vaginal. Assim, esta hipótese foi investigada mais a fundo através de ensaios experimentais, utilizando um protocolo de fadiga adequado e amostras da origem do PVM de um modelo animal. Deste estudo obteve-se curvas tensão-tempo onde é visível uma contínua relaxação das tensões, um sinal de acumulação de dano. Apesar de nenhuma amostra ter tido uma falha macroscópica, uma clara deformação permanente foi identificada em todas as amostras. A análise histológica permitiu a confirmação da acumulação de dano na microestrutura, com a visualização de fibras musculares tortuosas e rompimento individual de fibras musculares, numa zona perto da junção músculo-tendinosa. A partir destes resultados desenvolveu-se uma *framework* numérica à macro escala, incorporando ainda propriedades materiais fundamentais, como anisotropia e visco-hiperelasticidade. Um modelo de elementos finitos do segundo estágio do parto foi desenvolvido para testar diferentes gestões do parto, com o intuito de descobrir a melhor abordagem em termos de acumulação de dano nos tecidos musculares do pavimento pélvico. Os resultados mostraram que efetuar 3 esforços de 5 segundos por contração permitiram a menor acumulação de dano, sem prolongar o segundo estádio do parto. De forma a complementar a análise numérica, um estudo final foi efetuado para se incluir no modelo material, a deformação permanente associada à acumulação de dano na microestrutura. Este fenómeno pode impactar por si só o desenvolvimento de disfunções do pavimento pélvico, justificando a sua inclusão em modelos numéricos. O modelo material foi validado e testado através da realização de simulações numéricas com algum grau de complexidade, o que demonstrou a utilidade que poderá ter numa futura análise da gestão do parto, de forma a minimizar a deformação permanente.

Em síntese, esta tese apresenta uma nova hipótese relativamente ao mecanismo de dano do PVM durante o parto vaginal. Os resultados preliminares mostram o potencial deste mecanismo de dano e espera-se que despoletem a investigação complementar ainda necessária, para que se desenvolvam novas estratégias para a prevenção das lesões no PVM.

Abstract

Pelvic floor muscle injuries, particularly at the pubovisceral muscle (PVM) portion of the levator ani, are frequent during vaginal delivery. Besides the immediate consequences of the injury, they are also a known risk factor for the development of pelvic floor disorders later in life. These disorders, such as urinary and fecal incontinence and pelvic organ prolapse, have a significant impact in women's quality of life and the surgical repairs still present a high risk of reoccurrence and complications. So, it is essential to go to the root of the problem, improve our understanding regarding why and how pelvic muscle injuries occur during vaginal delivery and develop preventative measures to improve the injury rates.

In the past ~20 years, pelvic floor muscle injuries were reported to occur primarily at the origin of the PVM, a site where the muscle originates from the bone and includes the junction of three dissimilar materials: muscle, collagen tissue and bone. However, it is not yet known in which of these materials the injury occurs and consequently, the damage mechanism is not yet understood. Recently, low-cycle fatigue (~100 cycles) has been identified as a possible damage mechanism at the origin of the anterior cruciate ligament, at the location where the ligament connects to the bone. Since (1) during the second stage of labor strenuous maternal pushes are combined with the uterine contractions to form significant repetitive loading cycles on the pelvic floor muscles; and (2) the origin of the PVM includes two junctions of dissimilar materials, prone to stress concentration; this thesis explores the idea that low-cycle fatigue can cause microdamage to quickly accumulate and progress during the second stage of labor, causing permanent deformations or even a muscle tear.

This thesis uses both theoretical and experimental approaches to analyze the hypothesis of low-cycle fatigue damage in the PVM and modeling approaches to investigate the impact of the current managements of labor considering the microdamage accumulation and permanent deformation. First, a systematic review was performed to collect evidence of fatigue failure in the musculoskeletal system and then the hypothesis was evaluated in accordance with what was found and with what is currently known regarding the PVM injury, the loading conditions, and its anatomical features. These studies provided indirect evidence that corroborated the hypothesis of

low-cycle fatigue as a potential damage mechanism during vaginal delivery. This was further investigated by performing a low-cycle fatigue testing protocol on animal model specimens of the origin of the PVM. This study showed a continuous stress softening, which is an indication of damage accumulation. Despite the lack of macroscopic tears, all the specimens had visible permanent deformation. Histology confirmed these findings by showing microdamage in the form of tortuous muscle fibers and muscle fiber tears near the muscle-tendon junction. From these results, a numerical framework was developed at the macroscopic scale, incorporating also fundamental material properties, such as anisotropy and visco-hyperelasticity. A finite element model of the second stage of labor was developed to test different managements of labor, in search for the best approach in terms of maternal damage accumulation. It was found that performing 3 maternal pushes per contraction of 5 seconds each was the best approach, since it caused the less damage accumulation, and it did not prolong the second stage of labor. A final study was performed to complement the numerical framework to include the permanent deformation associated with the microdamage accumulation, since this permanent deformation can itself impact the development of pelvic floor disorders. The material model was validated and demonstrated against complex numerical simulations, which proved its usefulness to investigate the management of labor in terms of minimizing permanent deformation.

In summary, this thesis presented a novel hypothesis regarding the PVM damage mechanism during vaginal delivery and presented preliminary results that can trigger the additional research still needed to design new strategies for injury prevention.

List of Figures

Figure 1 - Schematic view from above of the levator ani muscles (pubovisceral, puborectal and iliococcygeus) and the coccygeus muscles. 1

Figure 2 - Schematic view from above of the type I (low-grade or minor) and type II (high grade or major) pubovisceral defect. Puborectal, iliococcygeus and the coccygeus muscles were removed for simplification. 5

Figure 3 - Schematic representation of the typical steps and timings in tissue processing and histological slide preparation. 13

Figure 4 - Schematic construction of a generic skeletal muscle, including its origin or insertion from bone. The muscle is composed of organized bundles muscle fibers involved by the endomysium. 15

Figure 5 - Schematic model of a viscoelastic material according to the Generalized Maxwell model. The total stress, **S**, decomposes according to (15) and (17). The spring in the first row represents the elastic stress, while each Maxwell element, characterized by a spring in series with a dashpot, represents the non-equilibrium stresses $\mathbf{Q}_\alpha$, $\alpha = 1, \dots, w$. The material parameters τ_α and β_α are the mechanical properties of the dashpots and the springs, respectively, and represent the relaxation times and free-energy parameters. 19

Figure 6 - Typical S-N curve of two materials with and without endurance limit and a common stress cycle used in fatigue testing. $\boldsymbol{\sigma}_a$: Cyclic stress amplitude. 22

Figure 7 - Strain control test and two possible stress responses, cycle-dependent hardening and softening. 22

Figure 1.1 - PRISMA flowchart detailing study identification and record screening process[98]. PRISMA, Preferred Reporting Items for Systematic Reviews and Meta-Analyses. 42

Figure 1.2 - Injury site distribution among the patient cohort (n = 3246). AV, tendon avulsion; M, muscle belly; MTJ, musculotendinous junction; T, tendon; TB, tendon-bone junction. 45

Figure 1.3 - Box-and-whisker plot (median, 25th percentile; range, 75th percentile) of patient age by injury site (n = 2,106). *P < .001. One-way analysis of variance. Dots appearing outside the whisker are outliers (observations numerically distant from the rest of data). AV, tendon avulsion; M, muscle belly; MTJ, musculotendinous junction; T, tendon; TB, tendon-bone junction. 45

Figure 1.4 - Distribution of proximal and distal locations within each muscle by injury site (n = 2,328). AV, tendon avulsion; MTJ, musculotendinous junction; T, tendon; TB, tendon-bone junction. 46

Figure 1.5 - Comparison of onset of injury category by injury sites (n = 1,772). AV, tendon avulsion; M, muscle belly; MTJ, musculotendinous junction; T, tendon; TB, tendon- bone junction. 47

Figure 1.6 - Injury distribution by muscle/tendon and injury site (n = 2,832) and mean ± SEM age by muscle/tendon (n = 2,106). Patient age was not reported for ADL, TMIN, and QF injuries. ACT, Achilles tendon; ADL, adductor longus; AV, tendon avulsion; BB, biceps brachii; BCH, brachialis; BF, biceps femoris; DLT, deltoid; ED, extensor digitorum; EDM, extensor digiti minimi; EHL, extensor hallucis longus; EIP, extensor indicis proprius; EPL, extensor pollicis longus; FPL, flexor pollicis longus; FPT, flexor profundus tendon; GMED, gluteus medius; GMIN, gluteus minimus; GRC, gracilis; GST, gastrocnemius; IAB, internal abdominal; IP, infraspinatus; LD, latissimus dorsi; M, muscle belly; MTJ, musculotendinous junction; PAT, patellar tendon; PB, peroneus brevis; PL, peroneus longus; PM, pectoralis major; POP, popliteus; QF, quadratus femoris; QT, quadriceps tendon; RF, rectus femoris; SC, subscapularis; SM, semimembranosus; SP, supraspinatus; ST, semitendinosus; T, tendon; TB, tendon-bone junction; TBL, tibialis posterior; TFL, tensor fasciae latae; TMIN, teres minor; TMJ, teres major; TR, triceps brachii; VI, vastus intermedius; VL, vastus lateralis; VM, vastus medialis..... 49

Figure 1.7 - Distribution of injuries by musculotendinous group and proximal and distal locations (n = 2,328). ACT, Achilles tendon; BB, biceps brachii; BCH, brachialis; BF, biceps femoris; DLT, deltoid; ED, extensor digitorum; EDM, extensor digiti minimi; EHL, extensor hallucis longus; EIP, extensor indicis proprius; EPL, extensor pollicis longus; FPL, flexor pollicis longus; FPT, flexor profundus tendon; GMED, gluteus medius; GMIN, gluteus minimus; GRC, gracilis; GST, gastrocnemius; IAB, internal abdominal; IP, infraspinatus; LD, latissimus dorsi; PAT, patellar tendon; PB, peroneus brevis; PM, pectoralis major; POP, popliteus; QF, quadratus femoris; QT, quadriceps tendon; RF, rectus femoris; SC, subscapularis; SM, semimembranosus; SP, supraspinatus; ST, semitendinosus; TBL, tibialis posterior; TFL, tensor fasciae latae; TMIN, teres minor; TMJ, teres major; TR, triceps brachii; VI, vastus intermedius; VM, vastus medialis. 50

Figure 1.8 - Comparison of onset of injury category (in percentages) by injured muscle/tendon (n = 1,415). ACT, Achilles tendon; BB, biceps brachii; BCH, brachialis; BF, biceps femoris; ED, extensor digitorum; EDM, extensor digiti minimi; EHL, extensor hallucis longus; EIP, extensor indicis proprius; EPL, extensor pollicis longus; FPL, flexor pollicis longus; FPT, flexor profundus tendon; GRC, gracilis; GST, gastrocnemius; IAB, internal abdominal; IP, infraspinatus; LD, latissimus dorsi; PAT, patellar tendon; PB, peroneus brevis; PL, peroneus longus; PM, pectoralis major; POP, popliteus; QF, quadratus femoris; QT, quadriceps tendon; RF, rectus femoris; SC, subscapularis; SM, semimembranosus; SP, supraspinatus; ST, semitendinosus; TBL, tibialis posterior; TFL, tensor fasciae latae; TMJ, teres major; TR, triceps brachii; VI, vastus intermedius; VL, vastus lateralis; VM, vastus medialis..... 51

Figure 2.1 - A left inferior view illustrating the pubovisceral muscle (PVM), which originates behind the pubic bone and forms the most distal portion of the levator ani muscle. It is particularly stretched late in the second stage of labor as the fetal head is driven by strong 2-3 maternal pushes, at three minutes intervals, through the birth canal to crown. EAS: External anal sphincter; ICM: iliococcygeal muscle; PRM: Puborectal muscle; ©DeLancey. 69

Figure 2.2 - Schematic illustration showing the relationship between material stress and strain as a tissue fails under an applied displacement (a) or applied load (b) load in a single loading cycle at each of three loading rates. The top row at left is the case when a linearly increasing displacement is applied to the material, at right (b) is the case when the same material is loaded instead by a linearly increasing tensile force. In the top row of (a) and (b) the three different curves in each plot are for a high strain rate (blue), a medium strain rate (pink) and a low strain rate (yellow). The lower panels for a) and b) show the corresponding

relationships between the tensile stress induced in the tissue and its strain. Note the effect of loading rate on the value of the tensile stress at failure (indicated by the arrow): the lower the rate of loading, the lower the stress, but the longer the length at which the material fails. 71

Figure 2.3 - Schematic representation of how low cycle fatigue can cause the failure of a soft tissue material subjected to cyclic sub-maximal stretch loading. (a) A cyclic linear increase and decrease in stretch is applied with the peak value less than the value that would cause failure in the first cycle. The lower figure shows the time course of the failure occurring at a lower stress than the peak stress induced by the first loading cycle, due to an accumulation of microdamage in the tissue. (b) A cyclic linear increase and decrease in tensile force is instead applied to the same material, with the peak force value being less than that required to cause failure in the first cycle. The lower panel shows the time course of the peak tensile strain induced by each loading cycle until failure occurs during the fifth loading cycle due to an accumulation of microdamage. Pushing during the second stage of labor loads the pelvic floor tissue most closely to the example shown at right in (b)..... 72

Figure 2.4 - Examples of medial, central and lateral region histology of the pubic origin of the PVM. Each row is from a different donor. Histological images showing the pubic origin of the levator ani from medial (column 1), central (column 2), and lateral (column 3) areas with the orientation picture below. All samples shown are stained in Masson's trichrome, and scale bars are 5mm for each row of images. Medial: The medial levator ani muscle fibers originate from multiple slips attaching in an enthesis to the pubis; oblique interface between the pubic bone (PB) and the levator ani muscle (LA) can also be observed. The thickness of the LA is greater than in other areas. N/A denotes missing data due to a technical issue during harvesting process. Central: The central portion originates from the PB in a single aponeurotic attachment, which is noticeably thinner than medial portion. The obturator internus muscle (OI) can be seen lateral to the LA. Lateral: The levator arch (LArch) appears as a dense blue connective tissue attaching to the PB and forming the lateral margin of the pubic origin of the LA. Note that relative preponderance of the three portions varies by individual. ©DeLancey 73

Figure 2.5 - Characteristic features of the origin of the right pubovisceral muscle (PVM). Medial and central portions attach to the pubic bone by an aponeurosis, while the lateral portion attaches to the levator arch (a.k.a arcus tendineus fascia pelvis). Laterally the structure is thin enough to visualize the forceps placed under it for demonstration purposes. ©DeLancey 74

Figure 3.1 - Superior view of the ovine pelvic floor. a) schematic representation showing the origin and insertion of the ishiococcygeous muscle, adapted from Basset. E.G[6]. b) posterolateral image showing the origin of the left ishiococcygeous muscle (pubic bone already trimmed at the proximal end) and the muscle fanning out and inserting onto to vaginal wall, anal canal, and coccygeal bone of tail. 89

Figure 3.2 - An anterolateral view of the ischiococcygeus muscle specimen after dissection: a) prior to preparation the medial surface of the (left) pubic bone can be seen at top with the bony origin (white collagenous tissue) of the muscle visible to the left of the small rectangular-shaped piece of clear skin tape (which itself lies over where the obturator foramen would normally be, the ischiococcygeus tendon with undisturbed margins, the MTJ and muscle proper below; b) after preparation consisting of adhering the ripstop nylon to both side of the muscle to within 15 mm of the MTJ. The jaws of the digital caliper serve as a 20 mm scale. 90

Figure 3.3 - Specimen inserted in the setup, hydrated with PBS, and ready for testing. 91

Figure 3.4 - Illustration showing how ischiococcygeal muscle specimens were divided (dashed lines with scissor logo) for histological evaluation: Tendon-Bone (TB) and Tendon-Muscle (TM) sections. Tendon-Bone samples were sliced with the microtome in the y-z

plane. Tendon-Muscle samples were divided in two, according to the figure, and one section was sliced in the y-x plane while the second was sliced in the y-z plane..... 93

Figure 3.5 - Finite Element model for the simulation of the experimental fatigue tests integrated in the micro-genetic algorithm for the calibration of the constitutive model parameters. The finite element model consists in a simplification of 1/8 of the averaged specimen. Representation of the boundary conditions and direction of the applied stretch. a) initial configuration b) deformed configuration at the peak displacement..... 97

Figure 3.6 - Force-displacement curves from the ultimate tensile tests (dashed lines). a) Averaged response: mean ± SD (standard deviation) (solid line). b) Averaged response of the relaxation tests: normalized engineering stress (current stress/peak stress) of all the experiments (dashed lines). Averaged response: mean ± SD (solid line). c-d) Averaged response of the fatigue tests c) engineering stress-grip to grip stretch d) engineering stress-time. 100

Figure 3.7 - Evolution of the engineering strain ε_{yy} distribution throughout the fatigue test in specimen 6R. 100

Figure 3.8 - Histological appearance of muscle-tendon sections with Masson's Trichrome stain. Comparison between untested controls (a-b) and fatigued specimens (c-h) (60 cycles between 60% and 45% of failure displacement). Fatigued specimens show kinked muscle fibers, individual fibers disruption and increase in interstitial spaces. a) Specimen 4L – control ($\sim 5-10$mm of MTJ, $\times 10$) b) Specimen 4L – control ($\sim 10-15$mm of MTJ, $\times 10$) c) Specimen 5R ($\sim 10-15$ mm of MTJ, $\times 10$) d) Specimen 10L ($\sim 10-15$mm of MTJ, $\times 10$) e) Specimen 10R ($\sim 10-15$mm of MTJ, $\times 10$). f) Specimen 5L (~10-15mm of MTJ, $\times 10$) g) Specimen 10L ($\sim 10-15$mm of MTJ, $\times 20$) h) Specimen 10L ($\sim 5-10$mm of MTJ, $\times 20$). 102

Figure 3.9 - Histological appearance of muscle-tendon sections at the MTJ with Masson's Trichrome stain. Collagen and muscle fibers with normal appearance in the MTJ and in the collagen fibers. a) Specimen 9L (×4). b) Specimen 10L (×20). c) Specimen 10R (×20). d) Specimen 4L – control (×10). 103

Figure 3.10 - Histological appearance of tendon-bone sections with Masson's Trichrome stain with normal appearance comparing untested controls and fatigued specimens (60 cycles between 60% and 45% of failure displacement) shows a normal appearance. a) Specimen 5L (×20) b) Specimen 3R- control (×10) c) Specimen 5R (×20) d) Specimen 4L – control (×20) e) Specimen 5R (×20) f) Specimen 3R – control (×40). 104

Figure 3.11 - a-b) Calibration of constitutive model parameters for the averaged response of the fatigue tests. a) comparison and coefficient of correlation with all the 3212 data points. b) comparison and coefficient of correlation for the peak points. c) normalized engineering stress-time response of the experimental fatigue test simulation for different materials. Pink curve represents a visco-hyperelastic material including continuous damage, yellow curve represents a visco-hyperelastic material and blue curve an hyperelastic material including continuous damage. 105

Figure 4.1 – Histological appearance of ovine pelvic floor muscle-tendon sections stained with Masson's Trichrome stain. Comparison between an untested control, a), and fatigue-tested specimens (b-c) (60 cycles at between 45% and 60% failure displacement[68]). Fatigued specimens show elongated and deformed muscle fibers (arrows), individual fiber rupture (square) and increased interstitial spaces[68]. 120

Figure 4.2– Superior view of the structure representing the levator ani muscles. a) 3-D geometry of the levator ani muscles, in red, with the pubic bone and symphysis pubis (SP) shown in ivory. The levator muscles attach laterally to the ischial spines and posteriorly to the sacrum, neither of which are shown for simplicity. The outline of the pubovisceral muscle (PVM), the most anterior and caudal portion of the levator ani muscles, is shown

with dashed white lines: it takes origin from the pubic bone on either side of the symphysis pubis (SP) and inserts into the perineal body (not shown) near the midline. The vagina, anal sphincter and remaining portions of the levator ani, including the iliococcygeus, coccygeus, and puborectal muscles (PBR) are not delineated for simplicity. The nodes along the green edges were fixed. b) View of the model levator ani muscle showing fiber directions within the muscle and main dimensions (in mm). Black dotted line shows the hiatal length used to calculate the stretch. 123

Figure 4.3– Finite element model of the fetal head showing the a) occipitofrontal diameter, and b) biparietal diameter with head circumference. All dimensions shown are in mm. 124

Figure 4.4 - Expulsive force placed on the model fetal head during simulated directed pushing. a) Profile of a single 10 seconds push and b) Valsalva-push pattern: three 10 second pushes superposed upon the 90 s uterine contraction. 126

Figure 4.5 - Details of the expulsive force placed on the model fetal head during simulated spontaneous pushing. a) 1-push pattern: one 10 second push superposed upon the 90 s uterine contraction b) Profile of a single 5 second push, c) 3-push pattern: three 5 second pushes superposed upon the 90 s uterine contraction. d) 5-push pattern: five 5 second pushes superposed upon the 90 s uterine contraction. 127

Figure 4.6 - Vertical displacement of the fetal head (mm) with time (s) for the four simulated pushing patterns: 1-push, 3-push, 5-push and Valsalva-push. The pictures below show the right lateral view of the fetal head descent for the 1-push simulation at the starting point, at the end of each contraction, and in the final position. The vertical dashed grey lines represent the end of a contraction (C), labelled numerically along the top of the plot. 129

Figure 4.7 - Right lateral view showing the damage distribution in the pelvic floor muscles at the end of the simulation for the four pushing patterns. The peak damage and critical node location are identified. 129

Figure 4.9 - a) Fiber damage evolution at the critical node for the four simulated pushing patterns, b) Comparison of the fiber maximum damage at the critical node for the simulated pushing patterns, c) Fiber maximum damage at the critical node as a function of the simulations total time, and d) Fiber maximum damage at the critical node as a function of the time spent in active pushing, which is the sum of the duration of the maternal pushes.... 131

Figure 5.1 - Histological appearance of muscle-tendon sections with Masson's Trichrome stain. Comparison between fatigued specimens (60 cycles between 60% and 45% failure displacement [49]) (a-c) and untested control (d). Fatigued specimens show crimped muscle fibers (arrows), individual fiber rupture (circle) and increased interstitial spaces. 147

Figure 5.2 - (a-b) Damage evolution, eq. (5.41), as function of the material parameters Ξ_{maxacc} and C. Damage evolves linearly or nonlinearly, depending on C, until it reaches the maximum value of 1, which can occur faster or slower depending on Ξ_{maxacc}. (c-e) Permanent deformation weighting function (5.44) depends on the material parameters ξ_0, ξ and γ. Depending on ξ, the permanent deformation rate increases faster or slower with the damage variable, and linearly or nonlinearly, depending on γ. 156

Figure 5.3 - a) Uniaxial stretch under force control, b) simple shear under force control, c) cyclic uniaxial stretch under force control, d) uniaxial stretch under displacement control followed by 90º rigid body rotation. a-d1) Evolution of the largest absolute residual of ABAQUS® Newton-Raphson iterative scheme (normalized to the maximum value of each time increment) with the iteration number. a-c2) Evolution of the maximum principal stretch with the principal stretch ratio. d2) Evolution of the maximum principal stretch with time.. 160

Figure 5.4 - Geometry of the dog bone sample (dimensions in mm) with a representation of the applied displacement. For the finite element simulation only 1/8 of the model was defined and meshed, considering symmetry boundary conditions. The fiber direction, m_0, was defined as the direction of the applied displacement. 161

Figure 5.5 - a) Profile of the applied stretch with time. Note that the stretch was only imposed until the last cycle peak, illustrated as the release point. After that point the material was released from any applied displacement/loads and allowed to return to the unloaded state. After the simulation, the new unloaded state occurs for a stretch of 1.08, which represents the permanent deformation. b) Cauchy stresses in the direction of the applied displacement as a function of the stretch. The stresses are the average result of the gauge section finite elements. The energy dissipation due to the irreversible processes is visible due to the hysteresis of the curve. We can also verify the permanent deformation of 1.08 at the end of the test. c) Evolution of the permanent set variable with time (average result of the gauge section finite elements)..... 162

Figure 5.6 - a) Distribution of the fiber stretch λ_f at the simulation starting point and at the end, which is the new unloaded state. b) Permanent stretch λ_p at the end of the simulation. c) Damage variable at the end of the simulation. 163

Figure 5.7- Geometry of the rectangular specimen (dimensions in mm) with a representation of the biaxial applied displacement. For the finite element simulation only 1/8 of the model was defined and meshed, considering symmetry boundary conditions. a) The fiber direction, $m_{0,}$ was defined in the vertical direction. b) fiber direction oriented with an angle of 45º in the x-y plane. 164

Figure 5.8- a) Results for the rectangular specimen with the fibers aligned vertically b) results for the rectangular specimen with the fibers oriented 45º in the x-y plane. Note that the stretch was only imposed until the last peak cycle. After that point the material was released from any applied displacement and allowed to return to the new unloaded state. 1) Cauchy stresses in the x direction $\boldsymbol{\sigma}_{xx}$, as a function of the stretch in the same direction, λ_{xx}. 2) Cauchy stresses in the y direction $\boldsymbol{\sigma}_{yy}$, as a function of the stretch in the same direction λ_{yy}. The stresses are the average within all finite elements. The stretches in b1) and b2) are the average of the top and side nodes, respectively, since in the final unloading stage the specimen becomes distorted due to permanent deformation (see Figure 5.9c). 3) evolution of the permanent set variable λ_p with time (average result of all finite elements)..... 165

Figure 5.9- a) Non-deformed rectangular specimen. b) permanent stretch distribution at the end of the simulation with the fibers vertically aligned. c) permanent stretch distribution at the end of the simulation with the fibers oriented 45º in the x-y plane. 165

Figure 5.10 - Finite element model of the second stage of labor, which includes the pelvic floor muscles in red (C3D8H elements), the fetal head in grey (C3D4 elements) and a rigid surface for the anterior region constraint. 166

Figure 5.11 - Expulsive force placed on the fetal head during the simulated Valsalva directed maternal pushes superposed upon each 90 s uterine contraction. 167

Figure 5.12 - Calibration of the constitutive material parameters for the averaged response of the fatigue tests from Vila Pouca et al[49]. a) Comparison of the numerical and experimental data for all 3212 data points. b) Comparison of the numerical and experimental data (mean $\pm$ SD) for the maximum and minimum peak points. SD: standard deviation; r: absolute error mean..... 168

Figure 5.13 - a) Evolution of the hiatal length (Level 1) stretch value. The green dot indicates the point of complete fetal head expulsion. Following recovery, there is a permanent stretch of 1.03. b) Evolution of the permanent deformation variable λ_p at the critical node. Each contraction is identified by the grey dotted lines. c) Distribution of the permanent deformation variable λ_p on the pelvic floor muscles after the fetal head expulsion. The critical node location, and the peak nodal permanent deformation and Level 1 are identified. 169

List of Tables

Table 1 - Advantages and Disadvantages of selected animal models for pelvic floor research, particularly pelvic organ prolapse (POP)[14,82,85] 7

Table 1.1 - List of the injured muscles and tendons reported by the included observational studies. 41

Table 1.2 - Distribution of the observational studies by country. 43

Table 3.1 - Summary of the testing protocols. 92

Table 3.2 - Constitutive model parameters obtain from the micro-genetic algorithm optimization. 101

Table 4.1- Summary of observational studies that compared maternal and fetal outcomes for directed and spontaneous pushing groups. POPQ: Pelvic Organ Prolapse Quantification 121

Table 4.2 - Calculated expulsive force acting on the fetal head at the peak of the uterine contraction, at the peak of the maternal push, and at the peak when the 2 variables are combined 126

Table 5.1 - Algorithm for the damage accumulation and permanent set evolution. 158

Table 5.2 - Arbitrary material parameters applied to verify quadratic convergence, objectivity, and overall behavior of the constitutive model. 159

Table 5.3 - Material parameters of the hypothetical tissue applied to the dog bone sample.. 161

Table 5.4 - Material parameters of the pelvic floor muscles, calibrated from ovine experimental data [49]. 168

Table B.1 - ARRIVE guidelines checklist and score defined for the evaluation. 191

Table B.2 - Quality evaluation and score of the laboratory studies included in this study. ... 192

Table B.3 - STROBE guidelines checklist and score defined for the evaluation. 193

Table B.4 - Quality evaluation and score of the cohort studies included in this study. 194

Table B.5 - CARE guidelines checklist and score defined for the evaluation. 198

Table B.6 - Quality evaluation and score of the case report studies included in this study. .. 199

Table C.1 - Characteristics of the included laboratory studies. 203

Table D.1 - Characteristics of the included observational studies. 205

Table E.1- Levator ani constitutive model parameters, obtained from the micro-genetic algorithm optimization [134]. 225

Acronyms and Symbols

Acronyms

PVM	Pubovisceral Muscle
MRI	Magnetic Resonance Imaging
TPUS	Transperineal Ultrasound
POP	Pelvic Organ Prolapse
CSA	Cross-Sectional Area
DIC	Digital Image Correlation
HGO	Holzapfel-Gasser-Ogden
MTJ	Musculotendinous Junction
ARRIVE	Animal Research: Reporting In Vivo Experiments
STROBE	Strengthening the Reporting of Observational Studies in Epidemiology
CARE	Case Report Statement and Checklist
PRISMA	Preferred Reporting Items for Systematic Reviews and Meta-Analyses
ACL	Anterior Cruciate Ligament
CBJ	Collagen-Bone Junction
IUP	Intra-Uterine Pressure

Symbols

$(\nabla)_{\mathrm{ich}}$	Isochoric contribution of ∇
$(\nabla)_{\mathrm{vol}}$	Volumetric contribution of ∇
$(\nabla)_{\mathrm{vis}}$	Viscous contribution of ∇
$\overline{(\nabla)}$	Modified contribution of ∇, associated with the isotropic contribution
$(\nabla)_{\mathrm{m}}$	Ground matrix contribution of ∇
$(\nabla)_{\mathrm{f}}$	Fiber contribution of ∇
$(\nabla)_{\mathrm{e}}$	Elastic contribution of ∇
$(\nabla)_{\mathrm{p}}$	Permanent deformation contribution of ∇
$(\nabla)^{\infty}$	∇ at $t \longrightarrow \infty$ responsible for the thermodynamic equilibrium state
$\mathbf{F}$	Deformation gradient
J	Jacobian
$\mathbf{C}$	Right Cauchy-Green deformation tensor
λ_{f}	Fiber stretch
λ_{p}	Permanent stretch
$\mathbf{m}_0$	Fiber direction in the reference configuration
I_1	First Invariant of the deformation
I_4	Pseudo-Invariant of the deformation
$\boldsymbol{\Gamma}_{\alpha}$	Internal variables that characterize the non-equilibrium state of the deformation
$\mathbf{S}$	Second Piola-Kirchhoff stress tensor
$\mathbf{Q}_{\alpha}$	Non-Equilibrium stresses arising from viscous effects
Ψ	Strain energy density function
C_{10}	Stress-like material parameter of $\overline{\Psi_{\mathrm{m}}}$
k_1	Stress-like material parameter of $\overline{\Psi_{\mathrm{f}}}$
k_2	Dimensionless parameter of $\overline{\Psi_{\mathrm{f}}}$
κ	Bulk modulus
α	Viscous relaxation process
τ_{α}	Relaxation times viscous parameters
β_{α}	Free-energy dimensionless viscous parameters
$\mathbb{P}$	Fourth-order projection tensor
$\mathbb{I}$	Fourth-order identity tensor
$\mathbb{C}$	Material fourth-order elasticity tensor
$\boldsymbol{\sigma}$	Cauchy stress tensor
$\mathbb{c}$	Spatial elasticity tensor
D	Continuous damage Variable
$\widehat{\mathrm{D}}$	Non-local continuous damage variable

$\mathrm{D_{max}}$	Weighting parameter of the fatigue damage model
Ξ_t^{acc}	Accumulated equivalent strain
$\Xi_{\mathrm{max}}^{\mathrm{acc}}$	Maximum accumulated equivalent strain
C	Exponent parameter of the fatigue damage model
$\mathrm{k_p}$	Weighting function of the permanent set evolution
ξ_0	Minimum value of the weighting function $\mathrm{k_p}$
ξ	Speed of the permanent deformation rate
γ	Shape of permanent deformation rate evolution
ϕ_{p}	Stretch based criterion for the permanent deformation
λ_{crit}	Critical stretch for permanent deformation
$\otimes$	Tensor Product
:	Tensor Contraction
$\odot$	$-(\star^{-1}\odot\star^{-1}=)_{ijkl} = -\left((\star)_{ik}^{-1}(\star)_{jl}^{-1} + (\star)_{il}^{-1}(\star)_{jk}^{-1}\right)/2$
$\overline{\otimes}$	$\left(\star\,\overline{\otimes}\,\circ\right)_{ijkl} = (\star)_{ik}\otimes(\circ)_{jl}$
$\underline{\otimes}$	$\left(\star\,\underline{\otimes}\,\circ\right)_{ijkl} = (\star)_{il}\otimes(\circ)_{jk}$

Introduction

Anatomy of the female pelvic floor - brief overview

The term pelvic floor comprises all the muscles, connective tissues and organs that fill the opening at the bottom of the bony pelvis[49,53]. The network of muscles supports the bladder, reproductive organs and rectum, and are attached to each other and the bony framework by condensations of fascial tissues[49]. Our daily activities are associated with different abdominal pressures and motions, and the pelvic floor must prevent incontinence and pelvic organ prolapse (i.e. descending or drooping of the organs) while at the same time allowing waste to be eliminated[4]. Although not a daily event, it must also be prepared for childbirth, which includes all the changes during and after pregnancy, besides the vaginal delivery itself [4].

The primary pelvic floor muscles, responsible for structural support, are the levator ani. Together with the coccygeus muscle, they comprise the deep pelvic floor muscles (Figure 1).

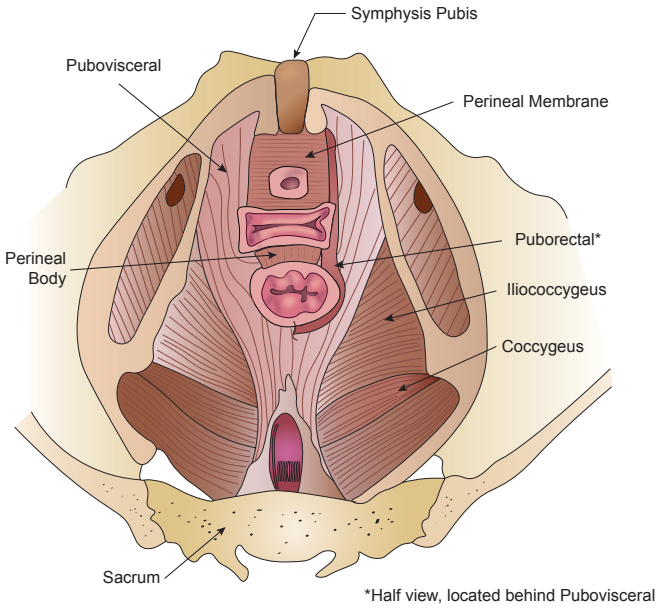

Figure 1 - Schematic view from above of the levator ani muscles (pubovisceral, puborectal and iliococcygeus) and the coccygeus muscles.

The levator ani can be anatomically divided in three components, according to the origin and direction of the muscle fibers: pubovisceral (or pubococcygeal), iliococcygeal and puborectal[4,57]. The coccygeus muscle forms the posterior part of the pelvic diaphragm and since has a different function and origin, it is not part of the levator ani[98]. It originates from the tip of the ischial spine and inserts into the lateral side of the coccyx and lowest part of the sacrum. The pubovisceral muscle originates from the pubic bone and inserts in three regions: perineal body, anal canal and vaginal wall. The iliococcygeal muscle begins at the lateral margin of the pubovisceral muscle and connects with the superior surface of the sacrum and coccyx. The puborectal originates near the perineal membrane, forming a sling behind the rectum and inserts on to the external anal sphincter (for example [4,17,18,32,49,98]).

The opening within the levator ani muscle through which the urethra, vagina and rectum pass is designated urogenital hiatus. The normal baseline activity of the levator ani muscle keeps the urogenital hiatus closed by compressing the vagina, urethra and rectum against the pubic bone[17].

Impact of vaginal delivery on the pelvic floor muscles

During the second stage of labor, which starts after complete dilation (~10cm) is reached, the pelvic floor sustains remarkable changes as the fetus moves progressively through the birth canal. The fetal head induces an extraordinary stretch ratio in the levator ani muscles, particularly in the pubovisceral muscle (PVM), estimated to be between 1.63-3.26[65,84]. Pregnancy induces alterations in the pelvic muscles to facilitate birth, such as larger urogenital hiatus at rest and in straining[97,101] and even increased muscle fiber length by the addition of sarcomeres[3,10]. These alterations have the intention to protect the pelvic floor against the mechanical deformation that happens during a vaginal delivery. Nevertheless, defects in the levator ani muscles are prevalent and have been increasingly documented in the past ~20 years due to the advances in imaging techniques. This increase in documentation is also associated with the discover of the long-term consequences of these type of injuries, which is the development of pelvic floor dysfunctions (i.e urinary and fecal incontinence and pelvic organ prolapse) later in life[15,23,71,104]. As levator ani injuries started to be documented and studied, a significant association was seen between women who sustained these injuries and are affected by a pelvic floor dysfunction[20,22]. So, what was discovered so far regarding levator ani muscle injuries?

In 1943, Gainey H. L.[37] published, most likely one of the first, reports of palpatory assessment of damage of 1000 women delivered by him. He described partial to complete damage of one or more components of the levator ani, being the pubovisceral muscle the most vulnerable. This was manifested by atrophy or detachment of the muscle attachments to the pubic bone. Overall, 31% of patients suffered these injuries. The lack of imaging techniques at the time did not allow the

verification of his conclusions and further studies were not carried on until the past ~20 years. Nevertheless, these advances confirmed his long-forgotten observations.

Using magnetic resonance imaging (MRI), DeLancey et al (2003)[19] identified 20% primiparous women (i.e. women who has given birth once) with a visible defect in the levator ani muscles. Both unilateral and bilateral defects were found, with 18% affecting the PVM and 2% the iliococcygeus muscle. Two types of defects were described, one where the PVM is detached from the origin and one where the muscle might be denervated, but connections to the bone remain. Then, using 3D/4D transperineal ultrasound (TPUS), Dietz and Lanzarone (2005)[25] reported what they called an "avulsion defect", which was when loss of continuity between the PVM and the pelvic sidewall in all volume data sets was found. Between 39 women who deliver vaginally, they found a prevalence of 36%.

One year later, Margulies et al[72] used MRI and found that in 14 patients with complete unilateral defect (i.e complete loss of muscle bulk in one side) the damage was in the PVM. There were missing muscle fibers, that should originate from the pubic bone and insert in the vaginal wall, perineal body and intersphinteric space. At the same time, Kearney et al[56] analyzed MRI of 160 primiparous and 80 nulliparous controls (i.e. women who never gave birth), identifying 18% with PVM defects, 4% what they called minor defects and 14% major defects. In their description, major defects implied bilateral abnormalities, with at least one side presenting a moderate defect or even complete loss of visible PVM on that side.

In 2007, Dietz et al[24] did, which was most likely the first intrapartum diagnosis, presenting a case report where complete absence of the right insertion of the PVM on the inferior pubic ramus was diagnosed during a surgical repair immediately after vaginally delivery. They attempted to reattach the PVM origin, however, in follow-up appointments, MRI showed levator ani thinning and focal defects in the muscle fibers. TPUS was also performed in follow-up and complete absence of the right insertion of the PVM was found, with muscle retraction. These findings were typical of a right-side complete unilateral PVM tear, with no evidence of successful repair. Krofta et al[61] used 3D/4D TPUS on women who had a vaginal delivery with the help of forceps and found a prevalence of PVM defects in 64% of women. This was higher than what has been documented before, highlighting the fact that forceps delivery is a risk factor for levator ani muscle injury. Valsky et al[112] used 3D TPUS on primiparous and nulliparous controls and diagnosed PVM discontinuities and distortion (unilateral or bilateral) in 19% of the primiparous cohort. They also identified large fetal head circumference and prolonged second stage of labor as risk factors.

In 2010, Shek and Dietz[100] applied 4D TPUS on women between 36 and 38 weeks' gestation and 3-4 months after delivery. They hypothesize that minor defects to the PVM portion of the levator ani could cause an irreversible increase in the hiatal area, even if complete disruption of the PVM attachment was not verified. So, they defined the term levator microtrauma for the cases

were an enlargement of 20% of the hiatal area was verified after vaginal delivery. The term levator macrotrauma was defined for complete detachments of the PVM origin as seen using 4D TPUS. 13% of vaginally parous women suffered levator macrotraumas and 29% sustained microtraumas.

In 2012, Chan et al[11] performed 3D TPUS on Chinese primiparous at 35-38 weeks' gestation and 8 weeks postpartum and found PVM injuries in 22%. Durnea et al[30] used 3D TPUS and verified that among the primiparous women, 15% showed signs of partial PVM detachments, 14% complete PVM detachments and 33% of the participants showed also an enlarged levator hiatus, higher than 25 cm. Also in 2015, Miller et al[80] applied MRI at both 7 weeks and 8 months postpartum to evaluate the presence of edema, which is a sign of muscle injury, and the loss of visible muscle, which indicates muscle tear. At 7 weeks postpartum, edema was seen in 90% of the vaginally parous participants and was still evident in 7% after 8 months. Levator ani tears were found in 41% of the participants (12% with unilateral low-grade tear, 19% with bilateral low-grade tear or unilateral high-grade tear and 10% having bilateral high-grade tears) at 7 months postpartum. The tears did not resolve and were still visible at 8 months postpartum. They concluded that torn muscle edges retract from their origin and the resulting gap prohibits healing that would retain muscle volume.

In 2016, Kamisan et al[55] analyzed the application of a birth trainer device in order to verify if it would improve the prevalence of levator ani trauma. The authors used 4D TPUS in the late third trimester and again at 3-6 months postpartum. Among other factors, they analyzed the presence of abnormal PVM attachments and also recovered the term microtrauma from Shek and Dietz[100] to define an hiatal area enlargement of 20%. Overall, abnormal PVM attachment was seen in 13% (bilateral in 4%) and microtrauma in 14% of the participants. The application of the birth trainer did not significantly reduce the prevalence of PVM defects.

In the same year, Da Silva et al[103] attempted to correlate the findings from 3D TPUS with cadaveric observations. They performed the 3D TPUS in 30 cadavers and 36% showed signs of a complete PVM detachment (3% bilateral and 33% unilateral). However, on the cadaveric observations, they verified that the injury caused the PVM to be significantly narrower but still attached to the pubic bone. In 2019, the group[102] performed a similar analysis, but also included histology of the injured PVM attachment. They found that the muscle fibers appeared tortuous with loss of striation in those areas. In the most recent years, injuries to the PVM portion are still being documented, usually diagnosed with 3D/4D TPUS[1,38,59,66,110,117], but also with MRI[90,91].

Of these recent studies, we highlight the work of Lin et al (2019)[66], who reviewed vaginally parous women 20 years after their index births, and 15% still showed signs of complete PVM detachments on TPUS. This once more highlighted the irreversible nature of this injury. Also in 2020, García-Mejido and Sainz[38] found levator ani defects in 25% of the cohort using 3D/4D TPUS. They defined the defects as type I: only the most lateral fibers of the PVM were observed at its insertion; and type II: complete detachment of the PVM from its insertion. 1 year post-

partum, a follow-up analysis showed that 21% of the levator ani defects were resolved, but all of them type I. All the type II defects were visible 1 year postpartum.

To summarize, injuries to the levator ani are visible after vaginal delivery, with a prevalence of 13-41% (excluding the report of Krofta et al[61], who found a prevalence of 64%, but only included forceps vaginal deliveries). Muscle edema is more common, appearing in 51-90% of vaginal deliveries, although it seems to be recoverable if not associated with a higher-degree injury. Without a doubt, the injuries appear more often in the pubovisceral portion of the levator ani, although different designations can be found within the studies, and can be bi-lateral or unilateral. Also, different degrees of injury were observed. Lower-grade injuries, also designated as minor or type I injuries were described at the origin of the PVM as thinning of the muscle, partial detachment, and muscle denervation. In these lower-grade injuries the PVM do not completely lose the attachment to the pubic bone and in some cases, it might be recoverable or partially recoverable. The higher-grade injuries are sometimes themed major or type II injuries and were described as complete detachments of the origin of the PVM accompanied with muscle retraction. Figure 2 shows a schematic representation of these two degrees of injuries.

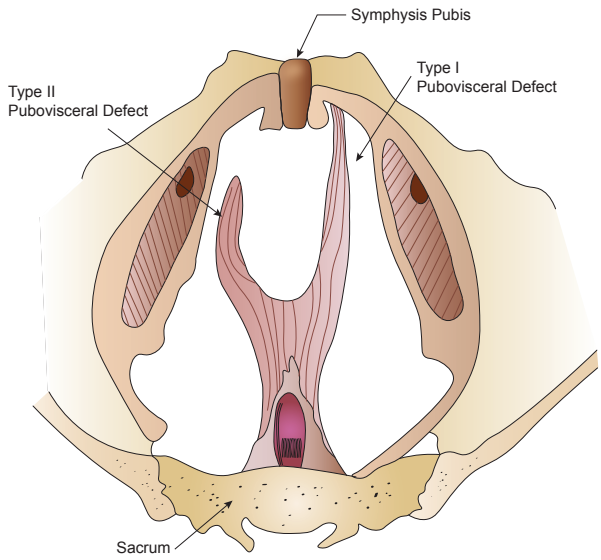

Figure 2 - Schematic view from above of the type I (low-grade or minor) and type II (high grade or major) pubovisceral defect. Puborectal, iliococcygeus and the coccygeus muscles were removed for simplification.

The works from Dietz and colleagues coined the term “avulsion defect” or “levator avulsion” for the high-degree injury. These terms are applied in all the studies from this group and in some cases in studies who based their classification in previous works from Dietz and colleagues. However, we avoided using this term, since an avulsion describes a muscle completely pulled from the bone, sometimes including a bone fragment, and this is not clear from the ultrasounds or MRIs. What Dietz and colleagues describe is a complete detachment from the muscle, a complete tear. So, we applied the term complete PVM detachment or complete PVM tear whenever an “avulsion” was described. All the studies used either MRI or TPUS, which, as stated

before, could not completely characterize the muscle injury. A muscle originates from bone via collagen tissue, what we typically call tendon. So, a tear in a muscle origin can indicate a tear in muscle tissue, collagen tissue, a bone fracture, or a tear in the junctions of these dissimilar tissues. The imaging techniques applied so far could not differentiate the location of the injury, besides being at the PVM origin so, it is not yet understood if the complete PVM detachments occur due to a tear in the PVM, in the collagen tissue that attaches the muscle to the bone, or even if the muscle is completely pulled from the bone.

Another interesting concept discussed in a few studies[55,100] was the idea of micro and macrotrauma. The authors[100] proposed that the enlargement of the hiatal area seen after a vaginal delivery is a direct consequence of microscopic defects in the levator ani and defined that effect as a microtrauma injury. In this degree of injury, no macroscopic tears are visible but there is still a consequence to the levator ani, with the enlargement of its hiatal area.

So, although levator ani injuries have been extensively described and documented over the past ~20 years, there is still a knowledge gap regarding the pathology of this injury. This is relevant in terms of understanding what might be the mechanism of injury. It is natural that the stretching of the PVM due to the passage of the fetal head is the main contributor, however, does the muscle tear by reaching and exceeding the muscle yield stress? Or are there other damage mechanisms involved? Understanding the damage mechanism is crucial to determine the main risk factors of levator ani injury and to implement preventative measures that improve the delivery experience for all women.

Biomechanics of the pelvic floor

As we seen in the previous section, despite the advances in pelvic floor science, there is still a great deal of knowledge gaps. Biomechanics, which can be defined as the study of living organisms through the application of mechanical principles, has become the basic science to solve these clinical problems. The advent of MRI and ultrasounds were crucial, not only to identify the problems as described previously, but also since the images can be used to develop realistic 3-D computational models for mechanical analysis. Animal models, combined with mechanical testing and microscopic imaging techniques are also important tools to have a better understanding of tissue behavior and response to injury. Finally, the onset and evolution of computational methods, including finite element analysis, allowed structural hypothesis to be tested in ways that were not possible before.

Animal models and pelvic floor research

Animal models have been used to improve the understanding of the mechanisms of pelvic floor disorders. They are convenient as they allow for complex experimental design without the

interference of an abundance of co-factors as in the clinical situation. The obstacle with this approach is finding the optimal model for each research question, while consider factors such as cost, availability, facility to handle and keep, among others[82,85]. Particularly for the study of pelvic floor disorders, the challenges arise by the fact that humans are bipedal, have no tail, and in the context of pregnancy and delivery, the fetal head is relatively large compared to the maternal pelvic dimensions, making vaginal delivery more traumatic than in other species. On the other hand, most animals are quadrupeds, with different pelvic floor musculature, including a functional tail[82]. Despite these differences, many quadrupeds, such as cows, pigs, dogs, deer, sheep and even horses develop pelvic floor disorders, and the characteristics and risk factors can be similar to those in humans[14]. A detailed overview of the potential advantages and disadvantages of the different species for pelvic floor research, particularly regarding pelvic floor disorders is presented in Table 1. Examining the different species, rodents and sheep seem the most suitable models for pelvic floor research. Although non-human primates have the most similarities with the human pelvic floor, the high cost and difficulty to handle makes them impractical to work with. Rodents have several advantages and a surprisingly similar pelvic floor. However, they are very small, which can make, for instance, tissue mechanical testing or practice and testing of surgical techniques extra challenging. Sheep have been more extensively studied as an appropriate model for pelvic floor research than pigs and cows. Sheep present spontaneous POP with the same risk factors as humans and a similar pelvic architecture. They also have a moderate cost and are easy to handle, which makes them a promising choice in this field of research.

Table 1 - Advantages and Disadvantages of selected animal models for pelvic floor research, particularly pelvic organ prolapse (POP) [14,82,85]

Species	Advantages	Disadvantages
Rodents	▪ Similarities in the connective tissue components of pelvic support; ▪ Short estrous cycles, making POP development less time intensive to study; ▪ Easy to handle and fewer ethical constraints; ▪ Low-Cost and easy acquisition of subjects; ▪ Genetically manipulated mouse display POP phenotype similar to clinical conditions.	▪ Pelvic floor is oriented horizontally; ▪ Smaller fetal head-to-birth canal ratio than humans; ▪ Different posture and small size; ▪ Slightly different presentations of POP.
Rabbit	▪ Easy to handle; ▪ Low Cost; ▪ Larger size that allows surgical flexibility and higher precision imaging than rodents.	▪ Location variation in reproductive tract; ▪ Different collagen metabolism system; ▪ Different anatomy compared to humans; ▪ Rare spontaneous POP; ▪ Different pelvic floor anatomy.
Sheep	▪ Moderate cost and high availability; ▪ Large animal, suitable for pre-clinical evaluation of gynecological meshes, for example; ▪ Have prolonged labors with relatively large fetuses; ▪ Pelvic architecture has three levels of support, the same as reported in women	▪ Logistic disadvantages regarding space to board and maintain; ▪ The intra-abdominal pressure is more towards the abdominal cavity than to the vaginal orifice, as in humans; ▪ Tail docking can damage the coccygeal support and cause vaginal prolapse.

Table 1 – continued

Species	Advantages	Disadvantages
Sheep	▪ Have levator ani and coccygeus muscles; ▪ Vagina similar in both length, diameter and histology; Similar pathophysiology of POP and risk factors (obesity, high fetal weight, parity, family history of POP, …).	
Cows	▪ Develop POP, with the same risk factors as humans, including inherited factors, estrogenic diets and increases in intra-abdominal pressure; ▪ Relatively easy to handle; ▪ Moderate cost.	▪ Logistic disadvantages regarding space to board and maintain; ▪ Few studies were performed to evaluate the use of cows as a POP animal model.
Pigs	▪ Moderate-low cost; ▪ POP is well documented at estrus (i.e period of sexual receptivity and fertility) and following estrogenic diets; ▪ Suitable to study the effect of diets and hormones on POP; ▪ Anatomy of uterosacral and cardinal ligaments have similar origin and insertions	▪ Few studies were performed to evaluate the use of pigs as a POP animal model.
Non-human Primates (Rhesus macaque, squirrel monkey, baboon)	▪ Histological, hormonal and anatomical similarities to humans; ▪ Similar reproductive cycle, gestation, parturition, large head-to-pelvic outlet ratio and hormonal effects on the pelvic organs; ▪ Levator ani with three distinct muscles, analogous to the iliococcygeus, pubovisceral and puborectalis in humans; ▪ Can develop spontaneous POP.	▪ Cost of maintenance; ▪ Long pregnancy and time to develop spontaneous POP; ▪ Level of expertise needed to handle them; ▪ Higher ethical constraints.

Mechanical testing and microscopic imaging in soft tissues and the pelvic floor

Soft biological tissues have a much more complex behavior compared with common engineering materials. In general, they present a non-linear hyperelastic and viscous behavior, are anisotropic, can grow, shrink, adapt over time, and have the ability to remodel and heal in response to damage[36]. They have passive components that only experience force if they are pulled or pushed by other constituent, or active components, such as muscles, that can independently generate force. This activation can be voluntary, which is the case of skeletal muscles such as the levator ani muscles, or involuntary, which is the case of smooth muscles, such as bladder, vagina, uterus, that contract and relax without though being required. These qualities make the full characterization and testing of soft biological tissues, including the pelvic floor, very challenging. Nevertheless, the established mechanical testing protocols are generally useful for biological tissues, although they often require certain adaptations[2].

To study the passive properties, the tissues are usually dissected and so the tests are performed *ex vivo*. In the pelvic floor, the most common mechanical tests are uniaxial tensile tests (for example [12,67,78,93]), although biaxial[5,16] and stress relaxation tests[86] are also performed. Some new

in vivo approaches have been emerging which can be applied to human specimens, mainly using pressure transducers, imaging methods or a combination of both[68,92,105]. However, these tests use relatively new tools and it is still important to characterize individual tissues using well stablished *ex vivo* tests that provide the baseline data for comparison with the new *in vivo* techniques[95].

Focusing on *ex vivo* tests, the main differences when dealing with soft biological tissues comparatively with engineering materials are: (1) how to obtain and store the specimens before the tests; (2) how to measure cross-sectional area or obtain stress and strain; (3) the need for hydration during tissue preparation and throughout the test; (4) how to appropriately clamp the specimens to the testing machine without inducing damage; and finally, (5) the fact that tissues are usually highly viscoelastic, so are strongly dependent on the strain rate. Each topic is briefly described next.

(1) Specimens for *ex vivo* tests are most commonly obtained from animal models or human cadavers. The best option depends on the purpose of the study; however, animal models might have less ethical constrains, particularly if the tissues are obtained from local farmers markets or butchers and there is no need to maintain and euthanize the animal. A good option regarding animal studies is also to contact different universities and research groups that might be already conducting an experiment with animals. By coordinating with them, tissues that would otherwise go to waste could be applied for other studies. The disadvantage with this approach is to have less control regarding the specimens, and it might not be a viable option for studies with several requirements (age, sex, parity, diet, …). It would be ideal to test tissues immediately following explantation, however, this option is often unavailable. In that case, they must be carefully stored to preserve the mechanical properties. Freezing is the universal method for tissue preservation and although the formation of ice crystals might cause some cell disruption[42], the effect on passive mechanical properties is little to none if the specimens are carefully frozen at least at a temperature below -18º C[35,81,94].

(2) Measure the cross-sectional area (CSA) in soft biological tissues is always a challenge due to their complex geometry and pliability. However, the accuracy of stress depends on an appropriate measurement[2]. There are several techniques that can be applied, both *in vivo* and *in vitro* and they can be destructive, or non-destructive, although the destructive techniques do not allow for subsequent biomechanical testing[40,45]. The non-destructive *in vitro* techniques are the gravimetric method, geometric approximation, laser micrometers, laser reflection systems, linear laser scanner and 3-D scanning. The geometric approximation method is often the most convenient since it is repeatable, convenient, quick and has the lower cost. The CSA of soft tissues is assumed to be round, rectangular or elliptical and it is measured using calipers. More than one measure should be performed to reduce inaccuracy. Nevertheless, this approach can induce some imprecisions, so the results must be interpreted accordingly. The laser and scanning techniques

are usually more reliable, however, are slower, the operations are complicated, more expensive and the equipment's are not so easily available[40].

Measuring strain during the test is also a challenge with soft tissues. Different methods, with different advantages and disadvantages can be applied. Contact extensometers, such as electrical-resistance strain gauges and mechanical, provide high-precision strain measurements in many applications but suffer some practical problems if used in biological tissues[108]. So, non-contact techniques are often applied, using video analysis systems. Typically, high contrast markers are applied to the specimen surface and its motion is tracked using digital video cameras and various digital image processing algorithms able to track marker motions[27,108]. Limitations remain with these methods, the placement of markers can change the tissues ability to deform and create a local defect in the sample[2], for instance if cyanoacrylate glue is used. However, if not appropriately placed, they can move during test, particularly since the specimen must be kept hydrated[108]. Moreover, soft tissues have high deformations, so markers can also deform and rotate, which difficult the motion tracking analysis[27,108].

Markerless strain measurements are optically based methods that uses digital image correlation (DIC) to track the movement of "features" in sequential images[27]. It measures full-field surface strain by comparing level intensity values on the specimen surface[119]. The features are most commonly speckles applied to the surface, for instance by spraying graphite powder or black paint to the surface using an airbrush with a nozzle diameter to yield speckles of 60-100μm[119]. DIC is useful since it captures the strain non-homogeneity in the tissues surface. However, it is technical challenging for soft tissues, mainly due to the high deformations they present. Also, the application of the speckle pattern has similar issues as with the marker's placement. Usually, the speckle is sprayed without using any component, such as glue, to fix it. On one hand, this is the best approach since it does not interfere with the specimen strength and stiffness, however, the high deformation combined with hydration, can move the speckle and correlation is lost[27].

The simpler method of estimating tissue strain, that is commonly reported in the literature, is the clamp-to-clamp. Essentially, the initial clamp-to-clamp distance is measured and as the specimen is elongated during testing, the testing machine measures the movement of one clamp, with respect with the other. So, it is possible to obtain an estimate of strain by dividing the change in length by the initial clamp-to-clamp distance. This method has the lower cost and the less technical challenges. However, it assumes the strain to be homogeneous, which often is not, and can cause strain overestimation. Choosing the appropriate method to measure stress and strain depends on the desired level of accuracy, application, the type of tissue and also of the available technologies in the laboratory[2].

(3) Tissues should be kept appropriately hydrated during preparation and testing to maintain their mechanical properties. If dehydration takes place, stiffness and strength can be

overestimated[83]. The most common hydration medium are saline solutions (i.e. phosphate buffered saline)[75,94], which not only provides hydration, but also protects against variations caused by humidity[94]. The hydration methods are typically spray or immersion bath[2].

(4) Attaching soft tissues to testing systems can be a non-trivial problem. There is no single solution and various techniques have been developed over the years. The two criteria to achieve a good clamping are avoid specimen slippage and failure near the clamps. However, to avoid slippage, one can be tempted to increase clamping pressure, which can cause premature failure. To resolve the issue, the most common approaches are to modify the clamp interface geometry and/or adding additional materials, such as sandpaper or adhesive. Common clamp geometries use serrated rounded off teeth, to ensure a good grip without adding stress concentrations. Cryofixation can also be applied, where the specimen is fixed via circulant coolant, typically liquid nitrogen[34,52]. However, this can only be applied if the specimens are large, so that the temperature at the clamps does not affect the results.

(5) When tissues are highly viscoelastic, the response is history dependent. However, if the specimen is subjected to preconditioning, which in the process of performing cyclic loading within the toe region of the stress-strain curve, the response will reach a steady-state response. This supposedly provides researchers with easily repeatable measurements and it is commonly performed before any biological mechanical test[2,109]. However, the protocols for preconditioning are not standardized and, in some studies, important details of the protocol are often not reported. So, some thought should be taken before applying preconditioning, since it will affect the mechanical response and may induce nonphysiological changes to the tissue[109]. Even in studies where recovery time was allowed, lengthening of the tissues have still been observed and in one investigation, it was seen that even after 30 minutes the portion of the mechanical shift was not recoverable[43]. Depending on the mechanical test, this might not be desirable, and preconditioning might not be performed. In that case, extra care must be taken in defining the strain rate, since the viscoelastic effects will be more prominent. Performing the mechanical tests at smaller strain rates will help minimizing viscoelastic effects.

Besides the mechanical characterization obtained from the mechanical tests, it is often important to analyze soft tissues microstructure. Several imaging techniques and many different types of microscopes have been developed over the years, such as light microscopes, electron microscopes, scanning tunnel microscopes, multiphoton microscopes, among others.[26] When choosing the appropriate imaging method, one must consider the scale of the tissue or feature being investigated, the resolution needed and the required tissue preparation[41]. We briefly overview light microscopy, since it is the relevant method for the following chapters in this work.

Light microscopy is, historically, one of the most powerful tools and it is still the most common microscopy in the world[41,50]. It has the advantage of being extremely versatile in applicability, require minimal training and the images produced are intuitively interpreted. In general, contrast

is provided through the attenuation of light as it passes through the sample and a "shadow" of the image is created. A major limitation of this technique is that often results in low contrast in the samples, so histological stains need to be applied when preparing the sample, which are dyes that bind to specific tissues or cellular components[26,41]. Moreover, it has a relatively low resolving power, which is approximately 0.2µm, allowing a magnification between 1000-1500×. Light microscopy is a designation that includes bright-field, fluorescence, phase-contrast, confocal and polarizing microscopy. In bright-field, the tissue is examined with ordinary light passing through the preparation; in fluorescence, tissue sections are usually irradiated with ultraviolet light and the fluorescent substances appear bright on a dark background; phase-contrast microscopes uses a lens system that produces visible image from transparent objects and it can be used in unstained cell/tissue sections and with living cells; confocal microscopes are similar to bright-field but include features that allow to achieve an high resolution and sharper images and can also capture digital images at a series of focal planes, which can then be used to digitally reconstruct a 3D image; polarizing microscopy allows the recognition of stained and unstained structures of highly organized subunits[79].

For light microscopy it is necessary to prepare the biological samples *a priori*. Although this tissue preparation can change depending on the tissue components and specific microscopy method, in general, the samples go through (a) fixation, (b) dehydration, (c) clearing (d) infiltration (e) embedding, (f) sectioning and (g) histological staining[21,26,41] (Figure 3):

(a) Tissue fixation preserves cells and tissue components by stopping autolysis and putrefaction, so the sample is then "fixed" at a particular point in time. Although it induces some changes in the tissues, such as shrinkage, hardening and color variations, it produces a compromised depiction of features that represent the original tissue[33]. Fixation can be achieved by chemical or physical means. Chemical fixation is achieved by immersing the specimen in the fixative solutions while the physical methods include cryo-preservation (freezing)[21,33]. The most popular fixative solution is formaldehyde (10% neutral buffered formalin), although other aldehydes, alcohols and oxidizing agents can also be used[106,107].

(b) Several methods for tissue dehydration are used, but the most common for light microscopy and electron microscopy is a series of ethanol solutions of increasing alcohol concentration until pure, water-free ethanol is used. This series of increasing concentrations is so that excessive tissue distortion is avoided. Through this process, the water in the specimen is progressively replaced by alcohol[21,79].

(c) Clearing is the process of replacing the alcohol by an organic solvent, miscible with both alcohol and the embedding medium. A common clearing agent is xylene. In cryo-preserved specimens, dehydration and clearing are not necessary[21,79].

(d) The cleared tissue is now be placed in melted histological wax or other supporting material. The most common method is to place the tissue in melted paraffin and in an oven at 52º-60ºC. This evaporates the clearing solvent and promotes infiltration of the tissue with paraffin.[21,79]

(e) Embedding is the process of inserting the specimen in a block of paraffin (or other medium used in the infiltration process) so that it can be clamped to the microtome for section cutting. For paraffin, this is performed in an embedding center, where a mold is filled with melted paraffin. The specimen must be carefully oriented in the mold because its placement will determine the plane of section and so it will impact the visualization of the microstructure. The block must be allowed to harden at room temperature[21,79].

(f) The hardened block with the tissue and the embedding medium is trimmed and placed for sectioning in a microtome or a cryostat. For light microscopy, these are usually between 3-10µm thickness, although electron microscopy requires sections less than 1µm. The sections must be carefully handled and placed in a glass slide for light microscopy[21,79].

(g) There are several histological stains that have been developed to make the various tissue components more visible and distinguishable from one another, for example: Hematoxylin and Eosin (H&E), which stain cell nuclei in blue and remaining basic structures in pink, Masson's trichrome, which stains muscle in red or pink, collagen fibers in blue or green and cell nuclei in black and Sirius red, which stains collagen fibers in red, among others. The stain must be chosen depending on the tissue components and application[21,79].

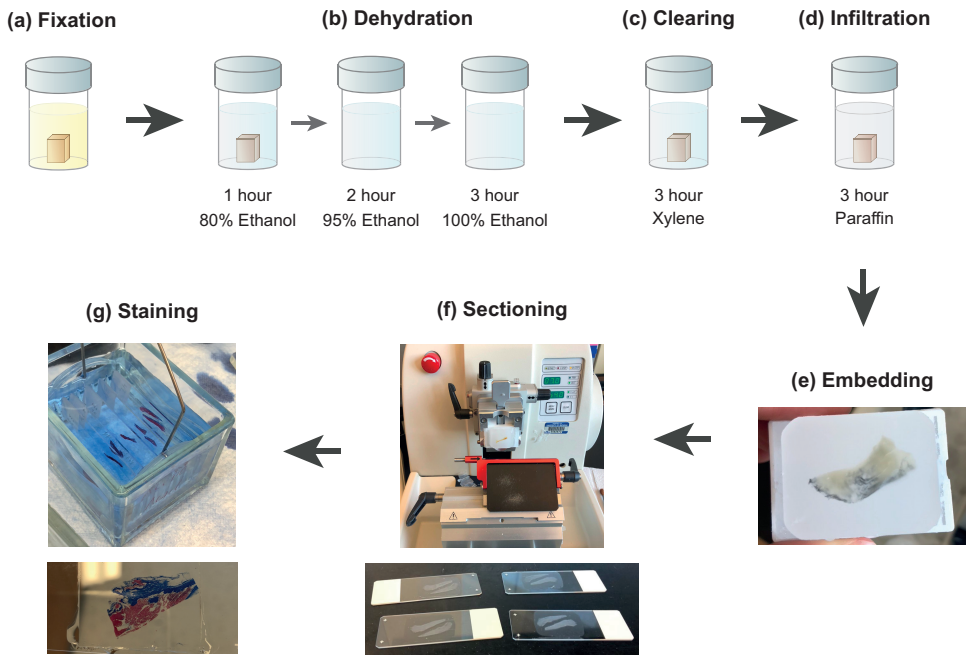

Figure 3 - Schematic representation of the typical steps and timings in tissue processing and histological slide preparation.

Constitutive modeling of soft tissues and the pelvic floor muscles

Constitutive modeling can be understood as the art of describing the mechanical behavior of materials through mathematical models, which are formulated in connection with physical concepts and experimental evidence[73,96] and must always respect mathematical requirements and thermodynamic laws in order to be physically consistent[73]. Constitutive models are based on material parameters and in the context of soft tissues, they should be able to reproduce *in vivo* or *ex vivo* mechanical behavior[73]. So, *in vivo* or *ex vivo* observations must be used to calibrate the values of the constitutive parameters[96]. Generally, different constitutive equations can be applied to describe the same tissue or body. And since soft tissues have a complex behavior, being hyperelastic, anisotropic, viscoelastic, presenting permanent deformation, growth and remodeling, it is always important to analyze what are the key phenomena to answer the research question so that the constitutive equation can be chosen or formulated accordingly[96]. Despite the difficulties in obtaining suitable experimental data, crucial to calibrate the constitutive equations and obtain an accurate representation of the material, the knowledge obtained from the numerical simulations, combined with clinical knowledge, can offer new paradigm for treatment and prevention strategies[62].

Soft tissues typically undergo large deformations, so their mechanical response is characterized by a non-linear stress-strain relationship, which is also associated with an incompressible or quasi-incompressible behavior due to the high water content[73]. Hyperelastic constitutive models, either isotropic or anisotropic, are commonly used to model soft tissues undergoing large deformations[62]. By definition, an hyperelastic material postulates the existence of a strain energy density function, that physically represents the energy stored in the body per unit volume due to deformation. So, hyperelastic constitutive models differentiate themselves in terms of different choices of strain-energy function[73]. Moreover, soft tissues can be affected by inelastic effects such as viscoelasticity, damage and permanent deformation and depending on the application and research question, the consideration of these effects might be necessary. When working with phenomenological constitutive models, it is common to apply a baseline hyperelastic model and then complementing it with inelastic effects models. For instance, a general framework for the description of tissue viscoelasticity is to employ the generalized Maxwell model, which assumes an additive decomposition of the strain energy function into an elastic/in equilibrium contribution, and into an inelastic/nonequilibrium contribution. Since we have this additive decomposition, we can apply the generalized Maxwell model to any hyperelastic model that better suit our application, since the last will only affect the elastic or equilibrium state contribution of the strain energy function. Modeling damage can be extra challenging since the underlying damage mechanisms are still poorly understood and there is not yet a clear definition of what damage is[39]. What is known is that strain-induced local damage

diminishes local tissue stiffness and causes stress softening, also known as Mullins effect[47]. The developed damage models, although can follow different approaches depending on the soft tissue and/or damage mechanism, typically aim to represent this stress-softening and energy dissipation. So, several damage models exist in the literature, from phenomenological models following a continuum damage mechanics approach (for example [6,8,31,46,74,87]) to micromechanical damage models (for example [13,44,63,69]). Contrarily to hyperelastic models, where a few proved are commonly applied, there is still a continuous need for the development of tissue-specific and/or mechanism-specific damage models that better address the clinical application and research question.

Focusing on the female pelvic floor muscles, large deformations occur not only during the second stage of labor, but also during physiological events such as laughing, sneezing or coughing[62]. Commonly hyperelastic constitutive equations for modeling the pelvic floor muscles include the isotropic neo-Hookean and Mooney-Rivlin models and the transversely isotropic Holzapfel-Gasser-Ogden (HGO) and Humphrey and Yin[7,54,62,64,77]. One study incorporated the viscous effects through the generalized Maxwell model[113]. Transversely isotropy is the simplest form of anisotropy, where the material or soft tissue is assumed to be reinforced by one or more family of fibers, each family with a single preferred direction. The stiffness of this material is typically greater along the preferred fiber direction and the response is isotropic orthogonally to that direction[47]. Since the pelvic floor muscles are skeletal muscles, which are typically composed by organized bundles of muscle fibers embedded in a ground substance medium (Figure 4), transversely isotropic models are more appropriate to characterize this material.

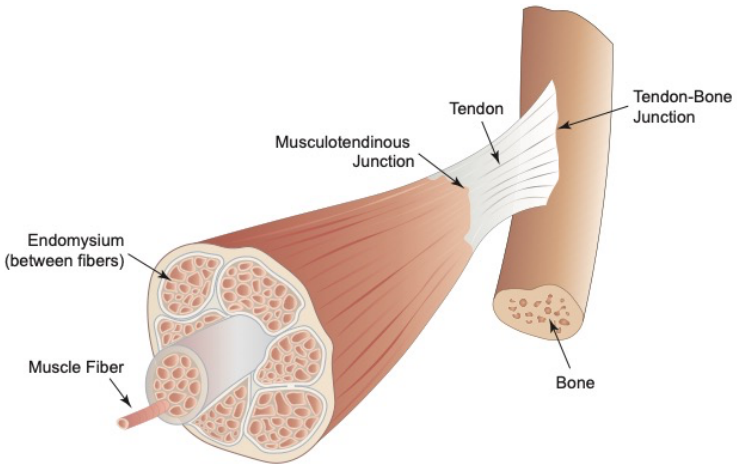

Figure 4 - Schematic construction of a generic skeletal muscle, including its origin or insertion from bone. The muscle is composed of organized bundles muscle fibers involved by the endomysium.

In the context of this work, it is important to introduce a few notions of continuum mechanics, in pair with the transversely hyperelastic HGO model and the generalized Maxwell model for viscoelasticity, although these concepts are described with further detail in the works of Holzapfel et al (for example [47,48,111]).

So, for a continuum body represented in both the reference Ω_0 and current configuration Ω, the mapping $\boldsymbol{\chi}: \Omega_0 \rightarrow \mathbb{R}^3$ defines the motion that transforms, at time *t*, position vectors of the material points $\mathbf{X} \in \Omega_0$ into spatial position vectors in the current configuration, $\mathbf{x} = \boldsymbol{\chi}(\mathbf{X}, t) \in \Omega$. The deformation gradient is then defined as

$$\mathbf{F} = \frac{\partial \boldsymbol{\chi}(\mathbf{X}, t)}{\partial \mathbf{X}} \tag{1}$$

where $J = \det \mathbf{F}$ is the Jacobian of the deformation and represents the volume ratio. The deformation gradient can be multiplicatively decomposed into a dilatational, $\mathbf{F}_{\text{vol}} = J^{\frac{1}{3}}\mathbf{I}$,and distortional (isochoric) part, $\bar{\mathbf{F}} = J^{-\frac{1}{3}}\mathbf{F}$, which is numerically convenient when modeling quasi-incompressible materials such as pelvic floor muscles. Note that $\det \bar{\mathbf{F}} = 1$ and that $J = 1$ is the condition for an isochoric motion. From the deformation gradient, we can write the right Cauchy-Green deformation tensor and its isochoric counterpart as:

$$\mathbf{C} = \mathbf{F}^{\mathrm{T}}\mathbf{F} \tag{2}$$

$$\bar{\mathbf{C}} = \bar{\mathbf{F}}^{\mathrm{T}}\bar{\mathbf{F}} = J^{-\frac{2}{3}}\mathbf{C} \tag{3}$$

If we consider a family of fibers, the preferred direction at point $\mathbf{X} \in \Omega_0$ is defined by the unit vector $\mathbf{m}_0$, $\|\mathbf{m}_0\| = 1$, which in the current configuration gives

$$\mathbf{m} = \mathbf{F}\mathbf{m}_0; \qquad \bar{\mathbf{m}} = \bar{\mathbf{F}}\mathbf{m}_0 \tag{4}$$

So, the stretch in the direction of a fiber family, also designated the fiber stretch, yields:

$$\lambda_{\mathrm{f}} = \|\mathbf{m}\|; \qquad \bar{\lambda}_{\mathrm{f}} = \|\bar{\mathbf{m}}\| \tag{5}$$

We established that we are modeling the pelvic floor muscles as a quasi-incompressible material, and defining also that there are only one family of fibers, we define the following invariants associated with the isochoric deformation as:

$$\bar{\mathrm{I}}_1 = \mathrm{tr}(\bar{\mathbf{C}}) \tag{6}$$

$$\bar{\mathrm{I}}_4 = \mathbf{m}_0 \cdot \bar{\mathbf{C}}\mathbf{m}_0 = \bar{\mathbf{C}} : \mathbf{M}_0 = \bar{\lambda}_{\mathrm{f}}^{\,2}, \quad \mathbf{M}_0 = \mathbf{m}_0 \otimes \mathbf{m}_0 \tag{7}$$

Since the fibers cannot sustain compressive strains, it is important to impose the restriction $\lambda_{\mathrm{f}} \geq 1$.

To describe the viscoelastic effects according to the Generalized Maxwel model, a finite number of internal variables (not accessible to direct observation) is introduced collectively in the reference configuration as $\bar{\boldsymbol{\Gamma}}_\alpha$ with $\alpha = 1, \ldots, w$. The tensorial variables $\bar{\boldsymbol{\Gamma}}_\alpha$ depend on the deformation history and characterize the non-equilibrium state of the deformation process and $w \geq 1$ is the number of relaxation processes associated with the viscoelastic behavior.

Introducing now the strain energy density function, which can be written in a decoupled form according to the volumetric and isochoric decomposition as:

$$\Psi = \Psi_{\text{vol}}^{\infty}(J) + \Psi_{\text{ich}}(\bar{\mathbf{C}}, \mathbf{M}_0, \bar{\mathbf{\Gamma}}_1, \dots, \bar{\mathbf{\Gamma}}_w) \tag{8}$$

and splitting the isochoric contribution even further into a thermodynamic equilibrium state, $\Psi_{\text{ich}}^{\infty}$, and into configurational free energies, $\Upsilon_{\text{ich}\,\alpha}$, responsible for the thermodynamic non-equilibrium state, we have:

$$\Psi_{\text{ich}} = \Psi_{\text{ich}}^{\infty}(\bar{\text{I}}_1, \bar{\text{I}}_4) + \sum_{\alpha=1}^{w} \Upsilon_{\text{ich}\,\alpha}(\bar{\mathbf{C}}, \mathbf{M}_0, \bar{\mathbf{\Gamma}}_\alpha) \tag{9}$$

The HGO model defines the isochoric thermodynamic equilibrium state strain energy function, $\Psi_{\text{ich}}^{\infty}$, considering a further decomposition into a part associated with the isotropic behavior of the ground substance, $\bar{\Psi}_{\text{m}}^{\infty}$, and the family of fibers, $\bar{\Psi}_{\text{f}}^{\infty}$:

$$\bar{\Psi}_{\text{m}}^{\infty} = \text{C}_{10}(\bar{\text{I}}_1 - 3) \tag{10}$$

$$\bar{\Psi}_{\text{f}}^{\infty} = \frac{\text{k}_1}{2\text{k}_2}\{\exp[\text{k}_2(\bar{\text{I}}_4 - 1)^2] - 1\} \tag{11}$$

where C_{10} and k_1 are stress-like material parameters and k_2 is a dimensionless parameter.

The volumetric contribution, $\Psi_{\text{vol}}^{\infty}$, is responsible for establishing the quasi-incompressibility by means of the penalty method, as

$$\Psi_{\text{vol}}^{\infty} = \kappa\left(\frac{J^2 - 1}{2} - \ln(J)\right) \tag{12}$$

where the parameter κ is the bulk modulus.

The stress response can be derived directly from the Clausius-Planck inequality,

$$\mathcal{D}_{\text{int}} = \mathbf{S} : \dot{\mathbf{C}}/2 - \dot{\Psi} \geq 0 \tag{13}$$

which gives the non-negative internal dissipation

$$\mathcal{D}_{\text{int}} = (\mathbf{S} - 2\partial\Psi/\partial\mathbf{C}) : \dot{\mathbf{C}}/2 - \sum_{\alpha=1}^{w} 2\,\partial\Upsilon_{\text{ich}\,\alpha}/\partial\bar{\mathbf{\Gamma}}_\alpha : \dot{\bar{\mathbf{\Gamma}}}_\alpha/2 \geq 0 \tag{14}$$

where $\mathbf{S}$ represents the second Piola-Kirchhoff stress tensor. According to eq. (8)-(11), $\mathbf{S}$ arises in a decoupled form as:

$$\mathbf{S} = \mathbf{S}_{\text{vol}}^{\infty} + \mathbf{S}_{\text{ich}} \tag{15}$$

$$\mathbf{S}_{\text{vol}}^{\infty} = 2\frac{\partial\Psi_{\text{vol}}^{\infty}(J)}{\partial\mathbf{C}} = 2\frac{\partial\Psi_{\text{vol}}^{\infty}(J)}{\partial J}\frac{\partial J}{\partial\mathbf{C}} \tag{16}$$

$$\mathbf{S}_{\text{ich}} = \mathbf{S}_{\text{ich}}^{\infty} + \sum_{\alpha=1}^{w} \mathbf{Q}_{\alpha} \tag{17}$$

$$\mathbf{S}_{\text{ich}}^{\infty} = \mathbf{S}_{\text{m}}^{\infty} + \mathbf{S}_{\text{f}}^{\infty} \tag{18}$$

$$\mathbf{S}_{\text{m}}^{\infty} = J^{-\frac{2}{3}}\mathbb{P} : \bar{\mathbf{S}}_{\text{m}}^{\infty}, \quad \bar{\mathbf{S}}_{\text{m}}^{\infty} = 2\frac{\partial \bar{\Psi}_{\text{m}}^{\infty}(\bar{\mathrm{I}}_1)}{\partial \bar{\mathrm{I}}_1}\frac{\partial \bar{\mathrm{I}}_1}{\partial \bar{\mathbf{C}}} \tag{19}$$

$$\mathbf{S}_{\text{f}}^{\infty} = J^{-\frac{2}{3}}\mathbb{P} : \bar{\mathbf{S}}_{\text{f}}^{\infty}, \quad \bar{\mathbf{S}}_{\text{f}}^{\infty} = 2\frac{\partial \bar{\Psi}_{\text{f}}^{\infty}(\bar{\mathrm{I}}_4)}{\partial \bar{\mathrm{I}}_4}\frac{\partial \bar{\mathrm{I}}_4}{\partial \bar{\mathbf{C}}} \tag{20}$$

$$\mathbf{Q}_{\alpha} = J^{-\frac{2}{3}}\mathbb{P} : \bar{\mathbf{Q}}_{\alpha}, \quad \bar{\mathbf{Q}}_{\alpha} = 2\frac{\partial \Upsilon_{\text{ich}\,\alpha}}{\partial \bar{\mathbf{C}}} \tag{21}$$

$\bar{\mathbf{S}}_{\text{m}}^{\infty}$, $\bar{\mathbf{S}}_{\text{f}}^{\infty}$and $\bar{\mathbf{Q}}_{\alpha}$ are fictious stress tensors, which are projected by the fourth-order material projection tensor, $\mathbb{P} = \mathbb{I} - \frac{1}{3}\mathbf{C}^{-1}\otimes\mathbf{C}$, to derive respectively the deviatoric components $\mathbf{S}_{\text{m}}^{\infty}$, $\mathbf{S}_{\text{f}}^{\infty}$ and $\mathbf{Q}_{\alpha}$.

$\mathbf{Q}_{\alpha}$ are additional internal variables, representing the non-equilibrium stresses arising from the viscous effects. For $t \to \infty$, $\mathbf{S}_{\text{ich}}$ reaches thermodynamic equilibrium, which implies that $\mathbf{Q}_{\alpha} = \mathbf{0}$. These internal variables are governed by evolution equations, that basically define the way the viscoelastic processes evolve:

$$\dot{\mathbf{Q}}_{\alpha} + \frac{\mathbf{Q}_{\alpha}}{\tau_{\alpha}} = \beta_{\alpha}\dot{\mathbf{S}}_{\text{ich}}\,, \quad \mathbf{Q}_{\alpha}^{0+} = \left(J^{-\frac{2}{3}}\mathbb{P} : \mathbf{Q}_{\alpha}\right)\Big|_{t=0^{+}} \tag{22}$$

If a stress-free reference configuration is assumed, $\mathbf{Q}_{\alpha}|_{t=0^{+}} = \mathbf{0}$. Closed-form solutions of the linear equations (22) may be given by the convolution integrals as

$$\dot{\mathbf{Q}}_{\alpha} = \exp\left(\frac{T}{\tau_{\alpha}}\right)\mathbf{Q}_{\alpha}^{0+} + \int_{t=0+}^{t=T} \exp\left[-\frac{(T-t)}{\tau_{\alpha}}\right]\beta_{\alpha}\dot{\mathbf{S}}_{\text{ich}}^{\infty}(t)dt \tag{23}$$

τ_{α} and β_{α} are the viscous material parameters and represent respectively the relaxation times and non-dimensional free-energy factors. Figure 5 shows a possible representation for these parameters and a schematic representation of the decomposition (15) and (17).

These integrals must be solved numerically and assuming a typical subtime interval $[t_n, t_{n+1}]$, with $\Delta t = t_{n+1} - t_n$, and that $\mathbf{S}_{\text{ich}}^{\infty}|_{\text{n}}$, at time t_n, is known, we can reach the recurrence update formula, by means of the mid-point rule, such as:

$$\mathbf{Q}_{\alpha\;n+1} = \boldsymbol{\mathcal{H}}_{\alpha\;n} + \beta_{\alpha}\exp\left(-\frac{\Delta t}{2\tau_{\alpha}}\right)(\mathbf{S}_{\text{ich}}^{\infty})_{n+1} \tag{24}$$

where the history term, $\boldsymbol{\mathcal{H}}_{\alpha\;n}$, yields

$$\boldsymbol{\mathcal{H}}_{\alpha\;n} = \exp\left(-\frac{\Delta t}{2\tau_{\alpha}}\right)\left[\exp\left(-\frac{\Delta t}{2\tau_{\alpha}}\right)\mathbf{Q}_{\alpha\;n} - \beta_{\alpha}(\mathbf{S}_{\text{ich}}^{\infty})_{n}\right] \tag{25}$$

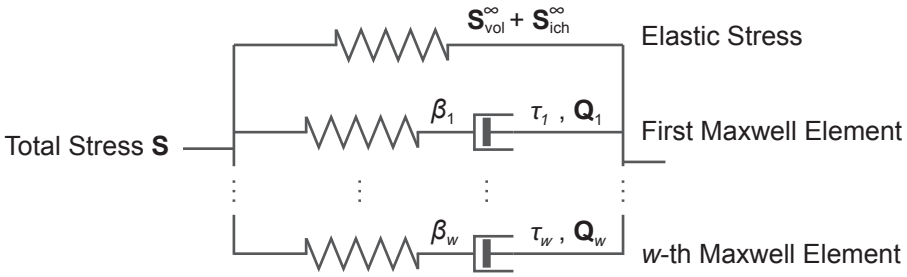

Figure 5 - Schematic model of a viscoelastic material according to the Generalized Maxwell model. The total stress, **S,** decomposes according to (15) and (17). The spring in the first row represents the elastic stress, while each Maxwell element, characterized by a spring in series with a dashpot, represents the non-equilibrium stresses $\mathbf{Q}_{\alpha}$, $_{\alpha=1,\dots,w}$. The material parameters τ_{α} and β_{α} are the mechanical properties of the dashpots and the springs, respectively, and represent the relaxation times and free-energy parameters.

To apply the constitutive model in a finite element context, combined with an iterative solution of the Newton's type, it is necessary to define the elasticity tensor. In the material description, the elasticity tensor can be seen as measurement of the change in stress which results from a change in strain and it is a fourth-order tensor. It decouples with analogy with eq. (8)-(11) and (15)-(20) as:

$$\mathbb{C} = \mathbb{C}^{\infty}_{\mathrm{vol}} + \mathbb{C}_{\mathrm{ich}} \tag{26}$$

$$\mathbb{C}^{\infty}_{\mathrm{vol}} = 2\frac{\partial \mathbf{S}^{\infty}_{\mathrm{vol}}}{\partial \mathbf{C}} = J\tilde{p}\mathbf{C}^{-1}\otimes\mathbf{C}^{-1} - 2Jp\mathbf{C}^{-1}\odot\mathbf{C}^{-1} \tag{27}$$

where $p = \partial\Psi^{\infty}_{\mathrm{vol}}/\partial J$, $\tilde{p} = p + J\,dp/dJ$ and $(\mathbf{C}^{-1}\odot\mathbf{C}^{-1})_{abcd} = \left(\mathbf{C}^{-1}_{ac}\mathbf{C}^{-1}_{bd} + \mathbf{C}^{-1}_{ad}\mathbf{C}^{-1}_{bc}\right)/2$

$$\mathbb{C}_{\mathrm{ich}} = \mathbb{C}^{\infty}_{\mathrm{ich}} + \mathbb{C}_{\mathrm{vis}} \tag{28}$$

with

$$\mathbb{C}^{\infty}_{\mathrm{ich}} = \mathbb{P} : \bar{\mathbb{C}}^{\infty}_{\mathrm{ich}} : \mathbb{P}^{\mathrm{T}} + \frac{2}{3}\mathrm{Tr}\left(J^{-\frac{2}{3}}\overline{\mathbf{S}^{\infty}_{\mathrm{ich}}}\right)\tilde{\mathbb{P}} - \frac{2}{3}(\mathbf{C}^{-1}\otimes\mathbf{S}^{\infty}_{\mathrm{ich}} + \mathbf{S}^{\infty}_{\mathrm{ich}}\otimes\mathbf{C}^{-1}) \tag{29}$$

which is based on the definitions

$$\mathrm{Tr}(\blacksquare) = (\blacksquare):\mathbf{C}\ , \qquad \bar{\mathbf{S}}^{\infty}_{\mathrm{ich}} = \bar{\mathbf{S}}^{\infty}_{\mathrm{m}} + \bar{\mathbf{S}}^{\infty}_{\mathrm{f}}, \qquad \tilde{\mathbb{P}} = \mathbf{C}^{-1}\odot\mathbf{C}^{-1} - \frac{1}{3}\mathbf{C}^{-1}\otimes\mathbf{C}^{-1} \tag{30}$$

$\bar{\mathbb{C}}^{\infty}_{\mathrm{ich}} = \partial\bar{\mathbf{S}}^{\infty}_{\mathrm{ich}}/\partial\bar{\mathbf{C}}$ is the fictitious elasticity tensor and can be obtained for the HGO model as:

$$\bar{\mathbb{C}}^{\infty}_{\mathrm{ich}} = \bar{\mathbb{C}}^{\infty}_{\mathrm{m}} + \bar{\mathbb{C}}^{\infty}_{\mathrm{f}} \tag{31}$$

$$\bar{\mathbb{C}}^{\infty}_{\mathrm{a}} = 4J^{-\frac{4}{3}}\left\{\sum_{\mathrm{b}=1,4}\left(\frac{\partial^2\bar{\Psi}^{\infty}_{\mathrm{a}}}{\partial\bar{\mathrm{I}}_{\mathrm{a}}\partial\bar{\mathrm{I}}_{\mathrm{b}}}\cdot\frac{\partial\bar{\mathrm{I}}_{\mathrm{a}}}{\partial\bar{\mathbf{C}}}\otimes\frac{\partial\bar{\mathrm{I}}_{\mathrm{b}}}{\partial\bar{\mathbf{C}}} + \frac{\partial\bar{\Psi}^{\infty}_{\mathrm{a}}}{\partial\bar{\mathrm{I}}_{\mathrm{a}}}\cdot\frac{\partial^2\bar{\mathrm{I}}_{\mathrm{a}}}{\partial\bar{\mathbf{C}}\partial\bar{\mathbf{C}}}\right)\right\}_{\mathrm{a}=1,4} \tag{32}$$

To condensate the previous equation we defined a numeric index 'a', which allows to reference the invariants $\bar{\mathrm{I}}_1$ and $\bar{\mathrm{I}}_4$. However, in the case of the strain energy components and the fictitious elasticity tensor itself, the index '1' is akin to the ground matrix component 'm' and the index '4' akin with the fibers component 'f'.

Since $\frac{\partial \bar{\mathrm{I}}_1}{\partial \bar{\mathbf{C}}} = \mathbf{I}$ and $\frac{\partial \bar{\mathrm{I}}_1}{\partial \bar{\mathbf{C}}} = \mathbf{m}_0 \otimes \mathbf{m}_0$, eq. (32) simplifies to:

$$\bar{\mathbb{C}}_{\mathrm{m}}^{\infty} = \mathbb{0} \ , \quad \bar{\mathbb{C}}_{\mathrm{f}}^{\infty} = \frac{\partial^2 \bar{\Psi}_{\mathrm{f}}^{\infty}}{\partial \bar{\mathrm{I}}_4 \partial \bar{\mathrm{I}}_4} \cdot \frac{\partial \bar{\mathrm{I}}_4}{\partial \bar{\mathbf{C}}} \otimes \frac{\partial \bar{\mathrm{I}}_4}{\partial \bar{\mathbf{C}}} \tag{33}$$

The viscous contribution, $\mathbb{C}_{\mathrm{vis}}$, is obtained at time t_{n+1} as

$$\mathbb{C}_{\mathrm{vis}} = \mathbb{C}_{\mathrm{ich}}^{\infty} \sum_{\alpha=1}^{w} \beta_{\alpha} \exp\left(-\frac{\Delta t}{2\tau_{\alpha}}\right) \tag{34}$$

Remark: The Generalized Maxwell model for viscoelasticity can be applied as a single process to the isochoric component of the material, as it was defined until this point. In this case, we assume the ground substance and the fibers to have the same viscoelastic behavior. However, we might need to separate the processes and define a viscoelastic behavior for the isochoric ground substance and a different viscoelastic behavior for the fibers. In that scenario, we have internal variables for each component, $\mathbf{Q}_{*\,\alpha}$,$*=$ m, f, obtained similarly from eq. (22)-(25) by replacing $\mathbf{S}_{\mathrm{ich}}^{\infty}$, with $\mathbf{S}_{*}^{\infty}$,$*=$ m, f. For the material elasticity tensor, we will also have a component for each contribution, $\mathbb{C}_{*\,\mathrm{vis}}$,$*=$ m, f, obtained from eq. (34) by substituting $\mathbb{C}_{\mathrm{ich}}^{\infty}$ with $\mathbb{C}_{*}^{\infty}$,$*=$ m, f. Note that different viscoelastic parameters for each contribution can be defined, since we will now have as parameters: $\alpha_*, \beta_{*\,\alpha}$ and $\tau_{*\,\alpha}$, $*=$ m, f

Finally, for finite element implementation, the stress and elasticity tensors are often required in the current configuration. So, to obtain the stress tensor in the current configuration, i.e. the Cauchy stress tensor, $\boldsymbol{\sigma}$, we can apply a push-forward operation to $\mathbf{S}$ as follows:

$$\boldsymbol{\sigma} = J^{-1}\mathbf{F}\mathbf{S}\mathbf{F}^{\mathrm{T}} \tag{35}$$

The push forward operation in the material elasticity tensor, $\mathbb{C}$**,** yields the spatial elasticity tensor, $\mathbb{c}$, as:

$$\mathbb{c}_{abcd} = J^{-1}\mathrm{F}_{ai}\mathrm{F}_{bj}\mathrm{F}_{ck}\mathrm{F}_{dl}\mathbb{C}_{ijkl} \tag{36}$$

In summary, the inputs of the model are the deformation gradient, $\mathbf{F}$, and the material parameters of the transversely hyperelastic HGO model, C_{10}, k_1 and k_2, the volumetric parameter κ and the viscoelastic parameters from the generalized Maxwell model, α, β_{α} and τ_{α}.

Material fatigue – brief description

Material fatigue is one of the most important issues to address in materials science[70], estimated to be responsible for 90% of all mechanical service failures[9]. In short, it can be defined as failure due to repeated loading, where one or more tiny cracks start in the material and grow until complete failure occur [28]. Important research on fatigue was done by August Wöhler around the 1850s and he was considered the founder of fatigue strength research[118]. He performed a series of experimental tests and load measurements in steel, iron and copper specimens and railway axles in real train operations and recognized that a single load application, below the static strength of a structure, did not do any damage to the structure. But if the same load was repeated many times it could induce a complete failure[99,118]. Failure occurred without apparent warning and it was seen as a mysterious phenomenon until the 20th century, causing catastrophic accidents such as bridge collapses, explosion of a pressure vessel, among others[99]. Now it is recognized as a significant problem and has assumed an even greater importance as a result of the increasing use of high-strength materials and the desire for higher performance from these materials[9].

Fatigue damage starts due to inhomogeneities and anisotropy that all materials present at a microscopic level. This inhomogeneity cause nonuniform stresses and regions where the stresses are more severe. Those are usually the locations where fatigue damage starts. The details of the behavior at the microscopic level varies significantly depending on the material. However, a common example of fatigue damage in engineering materials is the development of a small crack due to a microscopic defect such as a void, inclusion, grain boundary or surface scratch, that then grows until it causes failure, sometimes joining other cracks in the process[28]. Nevertheless, fatigue can occur in different forms, and so it has been categorized into two main groups: high-cycle and low-cycle fatigue.

High-cycle fatigue is caused by small elastic strains under a high number of load cycles before failure occur (typically $>10^5$). Fatigue failure is caused mainly by elastic deformation, although plastic deformation can occur at the crack tip[9]. Since high-cycle fatigue is governed by elastic deformation, stresses are usually the most convenient parameter to be used as failure criterion. In high cycle fatigue, the fatigue life of a material indicates the number of cycles to failure at a specified stress level and is characterized by a stress-number of cycles (S-N) curve. It is also common to define the endurance limit of the material, which is the stress bellow which failure does not occur (Figure 6). Some materials do not present an endurance limit, so the stress response continuously decreases with the number of cycles [9,28].

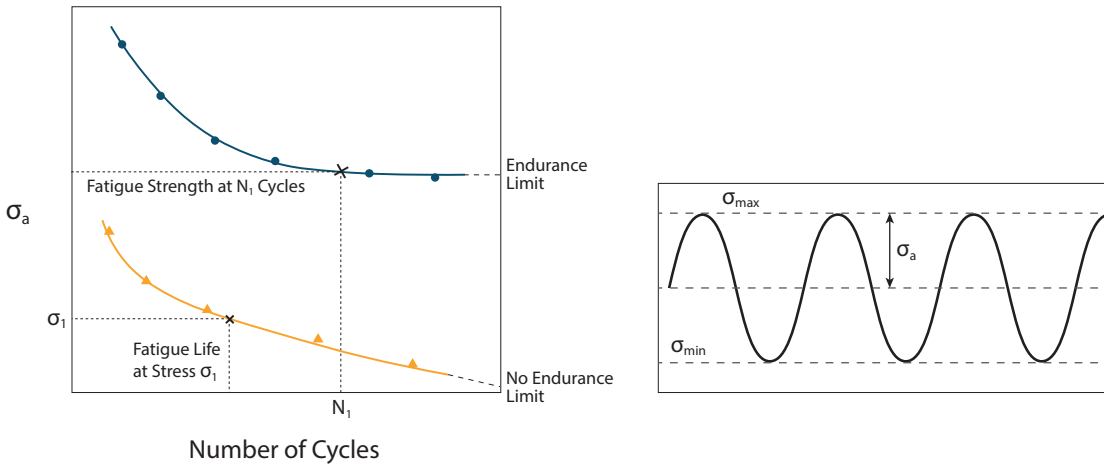

Figure 6 - Typical S-N curve of two materials with and without endurance limit and a common stress cycle used in fatigue testing. $\boldsymbol{\sigma}_a$: Cyclic stress amplitude.

Low-cycle fatigue can be caused by relatively small number of cycles and it is usually accompanied by macroscopic plastic deformation that cannot be neglected and create an hysteresis loop[28]. The material response is more complex, and a strain-based approach is typically applied. Under constant strain amplitude cycles, the material can undergo cyclic softening or cyclic hardening (Figure 7). Cyclic softening leads to decreasing stress peaks with increasing cycles, while cyclic hardening leads to increasing peak stresses with increasing cycles[9].

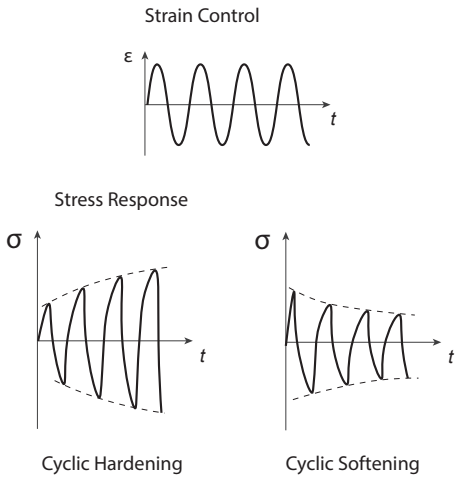

Figure 7 - Strain control test and two possible stress responses, cycle-dependent hardening and softening.

Some authors distinguish the fatigue mechanisms even further, by defining a new group designated as very-low/extreme-low or ultra-low cycle fatigue. However, there is not yet an agreement in defining the limits for low cycle and ultra-low cycle fatigue in terms of number of cycles. Some authors indicate low-cycle fatigue as a phenomena where failure can occur with tens, hundreds and thousands number of cycles[28], whereas others agree that if failure occurs in less than 100 cycles, or if it ranges from several to hundreds of cycles, the damage mechanism is different and should be distinguished as very-low/extremely-low or ultra-low cycle fatigue[29,51,58,76,88,89,114,116].

According to these studies, ultra-low-cycle fatigue is characterized in engineering materials, commonly metals, as very few load reversals that cause large plastic strains leading to a ductile fracture initiation. The damage starts to growth during the first cycle, or just after, so no damage threshold needs to be considered[29]. The underlying microscopic mechanisms of the ductile fracture initiation and propagation are: microvoid nucleation followed by microvoid deformation and finally fracture initiation due to unstable coalescence of microvoids[58,60,114,116].

So, ultra-low-cycle fatigue maybe understood as a transition damage process between the monotonic ductile damage and the low-cycle fatigue and so fatigue damage models in this regime typically involve criteria seen in monotonic ductile models such as void volume fraction, absorbed strain energy density and accumulated plastic strain[88,115].

Thesis outline and specific aims

In this thesis, I set out to address some of the existing gaps in pelvic floor research, exploring the damage mechanism of the levator ani muscles during vaginal delivery by investigating the possibility that low/ultra-low cycle fatigue is involved in its damage process. The hypothesis was developed in Chapter 1 and 2 and tested experimentally in Chapter 3. Then, continuum mechanics combined with finite element techniques were applied and developed to test clinically relevant factors that can influence the risk of levator ani tear. By addressing, testing and evaluating a new damage mechanism during the second stage of labor, I aim to build consciousness regarding material fatigue damage, which can ultimately lead to new techniques in the management of the second stage of labor, that improve the maternal outcomes.

Aim 1 – Material fatigue in the musculoskeletal system

Low-cycle fatigue damage accumulation has been reported at the origin of the anterior cruciate ligament in the knee and thought to be a possible cause for structural failure. Since fatigue is extremely relevant in engineering materials, we aimed to investigate if it could play a bigger role in biological tissues, than what is currently given credit. So, in Chapter 1 I performed a systematic review on musculoskeletal injuries, accessing the incidence, site and mechanism of injury, with the ultimate goal of investigating if material fatigue is a possible damage mechanism in biological tissues.

Aim 2 – Material fatigue due to a difficult labor

Pubovisceral muscle injury, near its origin is known to occur during a difficult vaginal delivery, and it is the major risk factor for the development of pelvic floor disorders later in life. In Chapter 2, I investigated and presented the hypothesis that the pubovisceral muscle can be weakened by an accumulation of microdamage during a difficult labor, involving multiple and forceful pushes.

The aim of this study was to determine whether there is indirect evidence that support this hypothesis.

Aim 3 – Experimental evidence of material fatigue in the levator ani

Chapter 1 and 2 provided indirect evidence to present the hypothesis that the origin of the pubovisceral muscle can be weakened by low-cycle fatigue damage. In Chapter 3, using female sheep as my model species, I experimentally tested this hypothesis. Twenty specimens, analogous to the origin of the pubovisceral muscle, were dissected from female sheep pelvis and subjected to ultimate tensile tests, relaxation and low-cycle fatigue tests. The microstructure of untested control specimens was compared against tested specimens to verify the presence of damage accumulation using light microscopy and histological prepared slices. Therefore, the aim of this Chapter was to experimentally investigate the presence of micro-damage accumulation due to low-cycle fatigue in the origin of the pubovisceral muscle by identifying the signs of micro-damage, the structures where it occurs and possible macroscopic effects.

Aim 4 – Modeling low-cycle fatigue damage

During the second stage of labor, maternal pushes, combined with the uterine contractions, are necessary to facilitate birth. Although there are not specific protocols, it is common for the doctor or midwife to direct these efforts. However, different strategies are often applied, which translates in different loading patterns and a different number of loading cycles. In Chapter 4, I investigate if the type of maternal pushes influences the damage accumulation near the origin of the pubovisceral muscle and if there is a pushing technique that minimizes the risk of tear. To achieve this aim, a biomechanical model of the second stage of labor was developed, including a finite element model of the pelvic floor muscles and the fetal head. A transversely isotropic visco-hyperelastic model including low-cycle fatigue damage was implemented to characterize the behavior of the pelvic floor muscles, calibrated with the experimental data from Chapter 3.

Aim 5 – Modeling permanent deformation

Low-cycle fatigue damage is accompanied of macroscopic permanent deformation in soft tissues. In the pelvic floor muscles, the permanent deformation was identified as an enlargement of the hiatal area after vaginal delivery, which is not recoverable. Besides pubovisceral muscle tear, the enlargement of the hiatal area is also identified as a risk factor for the development of pelvic organ prolapse. In Chapter 5 we developed a constitutive model able to capture the macroscopic permanent deformations due to low-cycle repetitive loading. This constitutive model can provide the necessary framework to study different obstetrical factors that might influence hiatal area enlargement and ultimately contribute to an improved management of the second stage of labor.

References

1. Abdool Z, Lindeque BG, Dietz HP. The impact of childbirth on pelvic floor morphology in primiparous Black South African women: a prospective longitudinal observational study. *Int Urogynecol J*. 2018;29(3):369-375. doi:10.1007/s00192-017-3530-1

2. Abramowitch S, Easley D. Chapter Five - Biomechanical Characterization of Native Pelvic Floor Organs and Tissues. In: Hoyte L, Damaser MBT-B of the FPF, eds. Academic Press; 2016:109-130. doi:https://doi.org/10.1016/B978-0-12-803228-2.00005-2

3. Alperin M, Lawley DM, Esparza MC, Lieber RL. Pregnancy-induced adaptations in the intrinsic structure of rat pelvic floor muscles. *Am J Obstet Gynecol*. 2015;213(2):191.e1-191.e7. doi:10.1016/j.ajog.2015.05.012

4. Ashton-Miller JA, DeLancey JOL. Functional anatomy of the female pelvic floor. *Ann N Y Acad Sci*. 2007;1101:266-296. doi:10.1196/annals.1389.034

5. Becker WR, De Vita R. Biaxial mechanical properties of swine uterosacral and cardinal ligaments. *Biomech Model Mechanobiol*. 2015;14(3):549-560. doi:10.1007/s10237-014-0621-5

6. Begonia MT, Knapp AM, Prabhu RK, Liao J, Williams LN. Shear-deformation based continuum-damage constitutive modeling of brain tissue. *J Biomech*. 2021;117:110260. doi:https://doi.org/10.1016/j.jbiomech.2021.110260

7. Berardi M, Martinez-Romero O, Elías-Zúñiga A, et al. Levator ani deformation during the second stage of labour. *Proc Inst Mech Eng Part H J Eng Med*. 2014;228(5):501-508. doi:10.1177/0954411914533678

8. Calvo B, Peña E, Martins P, et al. On modelling damage process in vaginal tissue. *J Biomech*. 2009;42(5):642-651. doi:https://doi.org/10.1016/j.jbiomech.2008.12.002

9. Campbell FC. *Elements of Metallurgy and Engineering Alloys*. ASM International; 2008.

10. Catanzarite T, Bremner S, Barlow CL, Bou-Malham L, O'Connor S, Alperin M. Pelvic muscles' mechanical response to strains in the absence and presence of pregnancy-induced adaptations in a rat model. *Am J Obstet Gynecol*. 2018;218(5):512.e1-512.e9. doi:10.1016/j.ajog.2018.02.001

11. Chan SSC, Cheung RYK, Yiu AKW, et al. Prevalence of levator ani muscle injury in Chinese women after first delivery. *Ultrasound Obstet Gynecol*. 2012;39(6):704-709. doi:https://doi.org/10.1002/uog.10132

12. Chantereau P, Brieu M, Kammal M, Farthmann J, Gabriel B, Cosson M. Mechanical properties of pelvic soft tissue of young women and impact of aging. *Int Urogynecol J*. 2014;25(11):1547-1553. doi:10.1007/s00192-014-2439-1

13. Christian Gasser T. An irreversible constitutive model for fibrous soft biological tissue: A 3-D microfiber approach with demonstrative application to abdominal aortic aneurysms. *Acta Biomater*. 2011;7(6):2457-2466. doi:https://doi.org/10.1016/j.actbio.2011.02.015

14. Couri BM, Lenis AT, Borazjani A, Paraiso MFR, Damaser MS. Animal models of female pelvic organ prolapse: lessons learned. *Expert Rev Obstet Gynecol*. 2012;7(3):249-260. doi:10.1586/eog.12.24

15. Dannecker C, Lienemann A, Fischer T, Anthuber C. Influence of spontaneous and instrumental vaginal delivery on objective measures of pelvic organ support: assessment with the pelvic organ prolapse quantification (POPQ) technique and functional cine magnetic resonance imaging. *Eur J Obstet Gynecol Reprod Biol*. 2004;115(1):32-38. doi:https://doi.org/10.1016/j.ejogrb.2003.09.047

16. Danso EK, Schuster JD, Johnson I, et al. Comparison of Biaxial Biomechanical Properties of Post-menopausal Human Prolapsed and Non-prolapsed Uterosacral Ligament. *Sci Rep*. 2020;10(1):7386. doi:10.1038/s41598-020-64192-0

17. DeLancey JO. Anatomy. In: Cardozo L, Staskin D, eds. *Textbook of Female Urology and Urogynecology*. 4th Ed. Taylor & Francis Group, LLC.

18. DeLancey JOL. Pelvic Floor Anatomy and Pathology. In: Hoyte L, Damaser M, eds. *Biomechanics*

of the Female Pelvic Floor. Elsevier; 2016.

19. DeLancey JOL, Kearney R, Chou Q, Speights S, Binno S. The appearance of levator ani muscle abnormalities in magnetic resonance images after vaginal delivery. *Obstet Gynecol*. 2003;101(1):46-53. doi:10.1016/S0029-7844(02)02465-1

20. DeLancey JOL, Morgan DM, Fenner DE, et al. Comparison of levator ani muscle defects and function in women with and without pelvic organ prolapse. *Obstet Gynecol*. 2007;109(2 PART 1):295-302. doi:10.1097/01.AOG.0000250901.57095.ba

21. Deng F, Miller J, Swanson T. Histology Revolution: From Inefficient, Two-Dimensional, and Low-Resolution Techniques to High-Throughput, Three-Dimensional and High-Resolution Techniques. *Egypt J Histol*. 2020;43(2):373-379. doi:10.21608/ejh.2019.16977.1168

22. Dietz HP. Pelvic floor trauma in childbirth. *Aust New Zeal J Obstet Gynaecol*. 2013;53(3):220-230. doi:https://doi.org/10.1111/ajo.12059

23. Dietz HP, Bernardo MJ, Kirby A, Shek KL. Minimal criteria for the diagnosis of avulsion of the puborectalis muscle by tomographic ultrasound. *Int Urogynecol J*. 2011;22(6):699-704. doi:10.1007/s00192-010-1329-4

24. Dietz HP, Gillespie AVL, Phadke P. Avulsion of the pubovisceral muscle associated with large vaginal tear after normal vaginal delivery at term. *Aust New Zeal J Obstet Gynaecol*. 2007;47(4):341-344. doi:10.1111/j.1479-828X.2007.00748.x

25. Dietz HP, Lanzarone V. Levator trauma after vaginal delivery. *Obstet Gynecol*. 2005;106(4):707-712. doi:10.1097/01.AOG.0000178779.62181.01

26. Disney CM, Leee PD, Hoyland JA, Sherratt MJ, Bay BK. A review of techniques for visualising soft tissue microstructure deformation and quantifying strain Ex Vivo. *J Microsc*. 2018;272(3):165-179. doi:https://doi.org/10.1111/jmi.12701

27. Doehring TC, Kahelin M, Vesely I. Direct Measurement of Nonuniform Large Deformations in Soft Tissues During Uniaxial Extension. *J Biomech Eng*. 2009;131(6). doi:10.1115/1.3116155

28. Dowling NE. *Mechanical Behavior of Materials: Engineering Methods for Deformation, Fracture, and Fatigue*. 4th Editio. Pearson; 2013.

29. Dufailly J, Lemaitre J. Modeling Very Low Cycle Fatigue. *Int J Damage Mech*. 1995;4(2):153-170. doi:10.1177/105678959500400204

30. Durnea CM, O'Reilly BA, Khashan AS, et al. Status of the pelvic floor in young primiparous women. *Ultrasound Obstet Gynecol*. 2015;46(3):356-362. doi:https://doi.org/10.1002/uog.14711

31. Ehret AE, Itskov M. Modeling of anisotropic softening phenomena: Application to soft biological tissues. *Int J Plast*. 2009;25(5):901-919. doi:https://doi.org/10.1016/j.ijplas.2008.06.001

32. Eickmeyer SM. Anatomy and Physiology of the Pelvic Floor. *Phys Med Rehabil Clin N Am*. 2017;28(3):455-460. doi:10.1016/j.pmr.2017.03.003

33. Eltoum I, Fredenburgh J, Myers R, Grizzle W. Introduction to the Theory and Practice of Fixation of Tissues. *J Histotechnol*. 2001;24:173-190.

34. Firminger CR, Edwards WB. A biomechanical study of clamping technique on patellar tendon surface strain and material properties using digital image correlation. *J Mech Behav Biomed Mater*. 2021;113:104156. doi:https://doi.org/10.1016/j.jmbbm.2020.104156

35. Fischer B, Kurz S, Höch A, Schleifenbaum S. The influence of different sample preparation on mechanical properties of human iliotibial tract. *Sci Rep*. 2020;10(1):14836. doi:10.1038/s41598-020-71790-5

36. Fung Y. *Biomechanics: Mechanical Properties of Living Tissues*. Second Edi. Springer Science & Business Media; 1993.

37. Gainey HL. Post-partum observation of pelvic tissue damage. *Am J Obstet Gynecol*. 1943;45(3):457-466. doi:https://doi.org/10.1016/S0002-9378(43)90528-9

38. García-Mejido JA, Sainz JA. Type of levator ani muscle avulsion as predictor for the disappearance of avulsion. *Neurourol Urodyn*. 2020;39(8):2293-2300. doi:https://doi.org/10.1002/nau.24484

39. Gasser TC. Damage in Vascular Tissues and Its Modeling BT - Material Parameter Identification

and Inverse Problems in Soft Tissue Biomechanics. In: Avril S, Evans S, eds. Springer International Publishing; 2017:85-118. doi:10.1007/978-3-319-45071-1_4

40. Ge X, Zhang L, Xiang G, Hu Y, Lun D. Cross-Sectional Area Measurement Techniques of Soft Tissue: A Literature Review. *Orthop Surg*. 2020;12(6):1547-1566. doi:https://doi.org/10.1111/os.12757

41. Goth W, Lesicko J, Sacks MS, Tunnell JW. Optical-Based Analysis of Soft Tissue Structures. *Annu Rev Biomed Eng*. 2016;18:357-385. doi:10.1146/annurev-bioeng-071114-040625

42. Gottsauner-Wolf F, Grabowski JJ, Chao EY, An KN. Effects of freeze/thaw conditioning on the tensile properties and failure mode of bone-muscle-bone units: a biomechanical and histological study in dogs. *J Orthop Res*. 1995;13(1):90-95. doi:10.1002/jor.1100130114

43. Graf BK, Vanderby R, Ulm MJ, Rogalski RP, Thielke RJ. Effect of preconditioning on the viscoelastic response of primate patellar tendon. *Arthrosc J Arthrosc Relat Surg*. 1994;10(1):90-96. doi:https://doi.org/10.1016/S0749-8063(05)80298-1

44. Hadi MF, Barocas VH. Microscale fiber network alignment affects macroscale failure behavior in simulated collagen tissue analogs. *J Biomech Eng*. 2013;135(2):21026. doi:10.1115/1.4023411

45. Hayes A, Easton K, Devanaboyina PT, Wu J-P, Kirk TB, Lloyd D. A review of methods to measure tendon dimensions. *J Orthop Surg Res*. 2019;14(1):18. doi:10.1186/s13018-018-1056-y

46. Hokanson J, Yazdani S. A constitutive model of the artery with damage. *Mech Res Commun*. 1997;24(2):151-159. doi:https://doi.org/10.1016/S0093-6413(97)00007-4

47. Holzapfel GA. *Nonlinear Solid Mechanics: A Continuum Approach for Engineering*. John Wiley & Sons; 2000.

48. Holzapfel GA, Gasser TC. A viscoelastic model for fiber-reinforced composites at finite strains: Continuum basis, computational aspects and applications. *Comput Methods Appl Mech Eng*. 2001;190(34):4379-4403. doi:https://doi.org/10.1016/S0045-7825(00)00323-6

49. Hoyte L, Damaser M. Magnetic Resonance-Based Female Pelvic Anatomy as Relevant for Maternal Childbirth Injury Simulations. *Ann N Y Acad Sci*. 2007;1101(1):361-376. doi:https://doi.org/10.1196/annals.1389.018

50. Inkson BJ. 2 - Scanning electron microscopy (SEM) and transmission electron microscopy (TEM) for materials characterization. In: Hübschen G, Altpeter I, Tschuncky R, Herrmann H-GBT-MCUNE (NDE) M, eds. Woodhead Publishing; 2016:17-43. doi:https://doi.org/10.1016/B978-0-08-100040-3.00002-X

51. Jia LJ, Ge H. *Ultra-Low-Cycle Fatigue Failure of Metal Structures under Strong Earthquakes.* Springer; 2019.

52. Jiang M, Lawson ZT, Erel V, et al. Clamping soft biologic tissues for uniaxial tensile testing: A brief survey of current methods and development of a novel clamping mechanism. *J Mech Behav Biomed Mater*. 2020;103:103503. doi:https://doi.org/10.1016/j.jmbbm.2019.103503

53. Jing D. Experimental and Theoretical Biomechanical Analyses of the Second Stage of Labor. Doctoral Dissertation, Department of Mechanical Engineering, University of Michigan, Ann Arbor. Published online 2010.

54. Jing D, Ashton-Miller JA, DeLancey JOL. A subject-specific anisotropic visco-hyperelastic finite element model of female pelvic floor stress and strain during the second stage of labor. *J Biomech*. 2012;45(3):455-460. doi:https://doi.org/10.1016/j.jbiomech.2011.12.002

55. Kamisan Atan I, Shek KL, Langer S, et al. Does the Epi-No® birth trainer prevent vaginal birth-related pelvic floor trauma? A multicentre prospective randomised controlled trial. *BJOG An Int J Obstet Gynaecol*. 2016;123(6):995-1003. doi:https://doi.org/10.1111/1471-0528.13924

56. Kearney R, Miller JM, Ashton-Miller JA, DeLancey JOL. Obstetric factors associated with levator ani muscle injury after vaginal birth. *Obstet Gynecol*. 2006;107(1).

57. Kearney R, Sawhney R, DeLancey JOL. Levator ani muscle anatomy evaluated by origin-insertion pairs. *Obstet Gynecol*. 2004;104(1):168-173. doi:10.1097/01.AOG.0000128906.61529.6b

58. Kim Y, Hwang W. High-Cycle, Low-Cycle, Extremely Low-Cycle Fatigue and Monotonic

Fracture Behaviors of Low-Carbon Steel and Its Welded Joint. *Mater (Basel, Switzerland)*. 2019;12(24):4111. doi:10.3390/ma12244111

59. Kimmich N, Birri J, Zimmermann R, Kreft M. Association between the side of levator Ani muscle trauma and fetal position at birth – a prospective observational study TT - Assoziation zwischen der betroffenen Seite der Levatormuskelverletzung und der fetalen Position bei Geburt – eine prospektive O. *Z Geburtshilfe Neonatol*. 2021;225(02):134-139.

60. Kiran R, Khandelwal K. A micromechanical cyclic void growth model for ultra-low cycle fatigue. *Int J Fatigue*. 2015;70:24-37. doi:https://doi.org/10.1016/j.ijfatigue.2014.08.010

61. Krofta L, Otcenasek M, Kasikova E, Feyereisl J. Pubococcygeus-puborectalis trauma after forceps delivery: evaluation of the levator ani muscle with 3D/4D ultrasound. *Int Urogynecol J Pelvic Floor Dysfunct*. 2009;20(10):1175-1181. doi:10.1007/s00192-009-0837-6

62. Kruger JA, Yan X, Li X, Nielsen PMF, Nash MP. Chapter Eighteen - Applications of Pelvic Floor Modeling and Simulation. In: Hoyte L, Damaser MBT-B of the FPF, eds. Academic Press; 2016:367-382. doi:https://doi.org/10.1016/B978-0-12-803228-2.00018-0

63. Li D, Robertson AM. A Structural Multi-Mechanism Damage Model for Cerebral Arterial Tissue. *J Biomech Eng*. 2009;131(10). doi:10.1115/1.3202559

64. Li X, Kruger JA, Nash MP, Nielsen PMF. Anisotropic effects of the levator ani muscle during childbirth. *Biomech Model Mechanobiol*. 2011;10(4):485-494. doi:10.1007/s10237-010-0249-z

65. Lien K-C, Mooney B, DeLancey JOL, Ashton-Miller JA. Levator ani muscle stretch induced by simulated vaginal birth. *Obstet Gynecol*. 2004;103(1):31-40. doi:10.1097/01.AOG.0000109207.22354.65

66. Lin S, Atan IK, Dietz HP, Herbison P, Wilson PD. Delivery mode, levator avulsion and obstetric anal sphincter injury: A cross-sectional study 20 years after childbirth. *Aust New Zeal J Obstet Gynaecol*. 2019;59(4):590-596. doi:https://doi.org/10.1111/ajo.12948

67. Lopez SO, Eberhart RC, Zimmern PE, Chuong C-J. Influence of body mass index on the biomechanical properties of the human prolapsed anterior vaginal wall. *Int Urogynecol J*. 2015;26(4):519-525. doi:10.1007/s00192-014-2525-4

68. Luo J, Smith TM, Ashton-Miller JA, DeLancey JOL. In Vivo Properties of Uterine Suspensory Tissue in Pelvic Organ Prolapse. *J Biomech Eng*. 2014;136(2). doi:10.1115/1.4026159

69. Maceri F, Marino M, Vairo G. Integrated mechanical models for collagenous biostructures at different length scales. *IFAC Proc Vol*. 2012;45(2):1018-1022. doi:https://doi.org/10.3182/20120215-3-AT-3016.00180

70. Machado R, Sencadas V. Advanced techniques for characterizing bioinspired materials. In: Rodrigues L, Mota MBT-BM for MA, eds. Woodhead Publishing; 2017:177-214. doi:https://doi.org/10.1016/B978-0-08-100741-9.00007-3

71. Mant J, Painter R, Vessey M. Epidemiology of genital prolapse: observations from the Oxford Family Planning Association Study. *Br J Obstet Gynaecol*. 1997;104(5):579-585. doi:10.1111/j.1471-0528.1997.tb11536.x

72. Margulies RU, Huebner M, DeLancey JOL. Origin and insertion points involved in levator ani muscle defects. *Am J Obstet Gynecol*. 2007;196(3):251.e1-251.e5. doi:10.1016/j.ajog.2006.10.894

73. Marino M. Constitutive modeling of soft tissues. In: Narayan R, ed. *Encyclopedia of Biomedical Engineering*. Vol 1-3. Elsevier; 2019:81-110. doi:https://doi.org/10.1016/B978-0-12-801238-3.99926-4

74. Martin C, Sun W. Modeling of long-term fatigue damage of soft tissue with stress softening and permanent set effects. *Biomech Model Mechanobiol*. 2013;12(4):645-655. doi:10.1007/s10237-012-0431-6

75. Martin RB, Burr DB, Sharkey NA, Fyhrie DP. *Skeletal Tissue Mechanics*. Second Ed. Springer; 2015.

76. Martinez X, Oller S, Barbu LG, Barbat AH, de Jesus AMP. Analysis of Ultra Low Cycle Fatigue problems with the Barcelona plastic damage model and a new isotropic hardening law. *Int J Fatigue*. 2015;73:132-142. doi:https://doi.org/10.1016/j.ijfatigue.2014.11.013

77. Martins JAC, Pato MP., Pires EB, Natal Jorge RM, Parente MPL, Mascarenhas T. Finite Element Studies of the Deformation of the Pelvic Floor. *Ann N Y Acad Sci*. 2007;1101(1):316-334. doi:https://doi.org/10.1196/annals.1389.019

78. Martins PALS, Filho ALS, Fonseca AMRM, et al. Uniaxial mechanical behavior of the human female bladder. *Int Urogynecol J*. 2011;22(8):991-995. doi:10.1007/s00192-011-1409-0

79. Mescher AL. Histology & Its Methods of Study. In: *Junqueira's Basic Histology*. 14th Ed. Mc Graw Hill Education; 2016.

80. Miller JM, Low LK, Zielinski R, Smith AR, Delancey JOL, Brandon C. Evaluating maternal recovery from labor and delivery: Bone and levator ani injuries. *Am J Obstet Gynecol*. 2015;213(2):188.e1-188.e11. doi:10.1016/j.ajog.2015.05.001

81. Moon DK, Woo SL-Y, Takakura Y, Gabriel MT, Abramowitch SD. The effects of refreezing on the viscoelastic and tensile properties of ligaments. *J Biomech*. 2006;39(6):1153-1157. doi:https://doi.org/10.1016/j.jbiomech.2005.02.012

82. Mori da Cunha MGMC, Mackova K, Hympanova LH, Bortolini MAT, Deprest J. Animal models for pelvic organ prolapse: systematic review. *Int Urogynecol J*. 2021;32(6):1331-1344. doi:10.1007/s00192-020-04638-1

83. Nicolle S, Palierne J-F. Dehydration effect on the mechanical behaviour of biological soft tissues: Observations on kidney tissues. *J Mech Behav Biomed Mater*. 2010;3(8):630-635. doi:https://doi.org/10.1016/j.jmbbm.2010.07.010

84. Parente MPL, Jorge RMN, Mascarenhas T, Fernandes AA, Martins JAC. Deformation of the pelvic floor muscles during a vaginal delivery. *Int Urogynecol J Pelvic Floor Dysfunct*. 2008;19(1):65-71. doi:10.1007/s00192-007-0388-7

85. Patnaik SS, Borazjani A, Brazile B, et al. Chapter Six - Pelvic Floor Biomechanics From Animal Models. In: Hoyte L, Damaser MBT-B of the FPF, eds. Academic Press; 2016:131-148. doi:https://doi.org/10.1016/B978-0-12-803228-2.00006-4

86. Peña E, Calvo B, Martínez MA, et al. Experimental study and constitutive modeling of the viscoelastic mechanical properties of the human prolapsed vaginal tissue. *Biomech Model Mechanobiol*. 2010;9(1):35-44. doi:10.1007/s10237-009-0157-2

87. Peña E, Peña JA, Doblaré M. On the Mullins effect and hysteresis of fibered biological materials: A comparison between continuous and discontinuous damage models. *Int J Solids Struct*. 2009;46(7):1727-1735. doi:https://doi.org/10.1016/j.ijsolstr.2008.12.015

88. Pereira JCR, de Jesus AMP, Xavier J, Correia JAFO, Susmel L, Fernandes AA. Low and ultra-low-cycle fatigue behavior of X52 piping steel based on theory of critical distances. *Int J Fatigue*. 2020;134:105482. doi:https://doi.org/10.1016/j.ijfatigue.2020.105482

89. Pereira JCR, de Jesus AMP, Xavier J, Fernandes AA. Ultra low-cycle fatigue behaviour of a structural steel. *Eng Struct*. 2014;60:214-222. doi:https://doi.org/10.1016/j.engstruct.2013.12.039

90. Pipitone F, Duarte Thibault ME, Gaetke-Udager K, Fenner DE, Swenson CW. Musculoskeletal findings on MRI among postpartum women with persistent pelvic pain. *Int Urogynecol J*. 2021;32(7):1779-1783. doi:10.1007/s00192-020-04441-y

91. Pipitone F, Miller JM, DeLancey JOL. Injury-associated levator ani muscle and anal sphincter ooedema following vaginal birth: a secondary analysis of the EMRLD study. *BJOG An Int J Obstet Gynaecol*. 2021;n/a(n/a). doi:https://doi.org/10.1111/1471-0528.16760

92. van Raalte H, Egorov V. Characterizing female pelvic floor conditions by tactile imaging. *Int Urogynecol J*. 2015;26(4):607-609. doi:10.1007/s00192-014-2549-9

93. Rivaux G, Rubod C, Dedet B, Brieu M, Gabriel B, Cosson M. Comparative analysis of pelvic ligaments: A biomechanics study. *Int Urogynecol J Pelvic Floor Dysfunct*. 2013;24(1):135-139. doi:10.1007/s00192-012-1861-5

94. Rubod C, Boukerrou M, Brieu M, Dubois P, Cosson M. Biomechanical Properties of Vaginal Tissue. Part 1: New Experimental Protocol. *J Urol*. 2007;178(1):320-325. doi:https://doi.org/10.1016/j.juro.2007.03.040

95. Ruiz-Zapata AM, Feola AJ, Heesakkers J, de Graaf P, Blaganje M, Sievert K-D. Biomechanical

Properties of the Pelvic Floor and its Relation to Pelvic Floor Disorders. *Eur Urol Suppl*. 2018;17(3):80-90. doi:https://doi.org/10.1016/j.eursup.2017.12.002

96. Sacco R, Guidoboni G, Mauri AG. Introduction. In: Sacco R, Guidoboni G, Mauri AGBT-ACPBA to M in B and LS, eds. Academic Press; 2019:255-256. doi:https://doi.org/10.1016/B978-0-12-812518-2.00018-4

97. Sanozidis A, Mikos T, Assimakopoulos E, et al. Changes in levator hiatus dimensions during pregnancy and after delivery in nulliparas: a prospective cohort study using 3D transperineal ultrasound. *J Matern Neonatal Med*. 2018;31(11):1505-1512. doi:10.1080/14767058.2017.1319926

98. El Sayed RF. Magnetic Resonance Imaging of the Female Pelvic Floor: Anatomy Overview, Indications, and Imaging Protocols. *Radiol Clin North Am*. 2020;58(2):291-303. doi:10.1016/j.rcl.2019.11.005

99. Schijve J. *Fatigue of Structures and Materials*. 2nd Ed. Springer; 2009.

100. Shek KL, Dietz HP. Intrapartum risk factors for levator trauma. *BJOG An Int J Obstet Gynaecol*. 2010;117(12):1485-1492. doi:10.1111/j.1471-0528.2010.02704.x

101. Shek KL, Kruger J, Dietz HP. The effect of pregnancy on hiatal dimensions and urethral mobility: an observational study. *Int Urogynecol J*. 2012;23(11):1561-1567. doi:10.1007/s00192-012-1795-y

102. Da Silva AS, Asfour V, Digesu GA, Cartwright R, Fernando R, Khullar V. Levator Ani avulsion: The histological composition of this site. A cadaveric study. *Neurourol Urodyn*. 2019;38(1):123-129. doi:10.1002/nau.23847

103. Da Silva AS, Digesu GA, Dell'Utri C, Fritsch H, Piffarotti P, Khullar V. Do ultrasound findings of levator ani "avulsion" correlate with anatomical findings: A multicenter cadaveric study. *Neurourol Urodyn*. 2016;35(6):683-688. doi:10.1002/nau.22781

104. Skoner MM, Thompson WD, Caron VA. Factors associated with risk of stress urinary incontinence in women. *Nurs Res*. 1994;43(5):301-306.

105. Smith TM, Luo J, Hsu Y, Ashton-Miller J, Delancey JO. A novel technique to measure in vivo uterine suspensory ligament stiffness. *Am J Obstet Gynecol*. 2013;209(5):484.e1-484.e7. doi:https://doi.org/10.1016/j.ajog.2013.06.003

106. Srinivasan M, Sedmak D, Jewell S. Effect of Fixatives and Tissue Processing on the Content and Integrity of Nucleic Acids. *Am J Pathol*. 2002;161(6):1961-1971. doi:https://doi.org/10.1016/S0002-9440(10)64472-0

107. Thavarajah R, Mudimbaimannar VK, Elizabeth J, Rao UK, Ranganathan K. Chemical and physical basics of routine formaldehyde fixation. *J Oral Maxillofac Pathol*. 2012;16(3):400-405. doi:10.4103/0973-029X.102496

108. Todros S, Pianigiani S, de Cesare N, Pavan PG, Natali AN. Marker Tracking for Local Strain Measurement in Mechanical Testing of Biomedical Materials. *J Med Biol Eng*. 2019;39(5):764-772. doi:10.1007/s40846-018-0457-z

109. Tonge TK, Murienne BJ, Coudrillier B, Alexander S, Rothkopf W, Nguyen TD. Minimal preconditioning effects observed for inflation tests of planar tissues. *J Biomech Eng*. 2013;135(11):114502. doi:10.1115/1.4025105

110. Turel F, Caagbay D, Dietz HP. Prevalence of maternal birth trauma in Nepali women. *J Ultrasound Med*. 2018;37(12):2803-2809. doi:10.1002/jum.14637

111. Unterberger MJ, Schmoller KM, Wurm C, Bausch AR, Holzapfel GA. Viscoelasticity of cross-linked actin networks: experimental tests, mechanical modeling and finite-element analysis. *Acta Biomater*. 2013;9(7):7343-7353. doi:10.1016/j.actbio.2013.03.008

112. Valsky D V, Lipschuetz M, Bord A, et al. Fetal head circumference and length of second stage of labor are risk factors for levator ani muscle injury, diagnosed by 3-dimensional transperineal ultrasound in primiparous women. *Am J Obstet Gynecol*. 2009;201(1):91.e1-91.e7. doi:10.1016/j.ajog.2009.03.028

113. Vila Pouca MCP, Ferreira JPS, Oliveira DA, Parente MPL, Natal Jorge RM. Viscous effects in

pelvic floor muscles during childbirth: a numerical study. *Int j numer method biomed eng*. 2017;(September):e2927. doi:10.1002/cnm.2927

114. Wang T, Wen J-F, Liao P-P, Zhang X-C, Kim Y-J, Tu S-T. A study of ultra-low cycle fatigue failure based on a fracture strain energy model. *Int J Fatigue*. 2021;146:106149. doi:https://doi.org/10.1016/j.ijfatigue.2021.106149

115. Wen Z. Modeling of ductile fracture in steel structures for monotonic and cyclic loading. Doctoral Degree, Department of Civil Engineering, Carleton University. Published online 2012.

116. Xue L. A unified expression for low cycle fatigue and extremely low cycle fatigue and its implication for monotonic loading. *Int J Fatigue*. 2008;30(10):1691-1698. doi:https://doi.org/10.1016/j.ijfatigue.2008.03.004

117. Youssef A, Salsi G, Cataneo I, et al. Fundal pressure in second stage of labor (Kristeller maneuver) is associated with increased risk of levator ani muscle avulsion. *Ultrasound Obstet Gynecol*. 2019;53(1):95-100. doi:10.1002/uog.19085

118. Zenner H, Hinkelmann K. August Wöhler – founder of fatigue strength research. *Steel Constr*. 2019;12(2):156-162. doi:https://doi.org/10.1002/stco.201900011

119. Zhou B, Ravindran S, Ferdous J, Kidane A, Sutton MA, Shazly T. Using Digital Image Correlation to Characterize Local Strains on Vascular Tissue Specimens. *J Vis Exp*. 2016;(107):e53625. doi:10.3791/53625

Chapter 1

Injuries in muscle-tendon-bone units

A systematic review considering the role of passive tissue fatigue

Injuries in muscle-tendon-bone-units

A systematic review considering the role of passive tissue fatigue

Maria C.P. Vila Pouca[1,2], Marco P.L. Parente[1,2], Renato M. Natal Jorge[1,2], James A. Ashton-Miller[3]

1 Department of Mechanical Engineering, Faculty of Engineering of University of Porto, Porto, Portugal

2 Institute of Science and Innovation in Mechanical and Industrial Engineering, Porto, Portugal

3 Departments of Mechanical and Biomedical Engineering, College of Engineering and School of Kinesiology, University of Michigan, Ann Arbor, Michigan, USA

Published In

The Orthopaedic Journal of Sports Medicine

DOI: https://doi.org/10.1177/23259671211020731

Article Type: Systematic Review

Submitted: March 11, 2021

Accepted: March 25, 2021

Abstract

Background: Low-cycle fatigue damage accumulating to the point of structural failure has been recently reported at the origin of the human anterior cruciate ligament under strenuous repetitive loading. If this can occur in a ligament, low-cycle fatigue damage may also occur in the connective tissue of muscle-tendon units. To this end, we reviewed what is known about how, when, and where injuries of muscle-tendon units occur throughout the body.

Purpose: To systematically review injuries in the muscle-tendon-bone complex; assess the site of injury (muscle belly, musculotendinous junction [MTJ], tendon/aponeurosis, tendon/aponeurosis–bone junction, and tendon/aponeurosis avulsion), incidence, muscles and tendons involved, mechanism of injury, and main symptoms; and consider the hypothesis that injury may often be consistent with the accumulation of multiscale material fatigue damage during repetitive submaximal loading regimens.

Methods: PubMed, Web of Science, Scopus, and ProQuest were searched on July 24, 2019. Quality assessment was undertaken using ARRIVE, STROBE, and CARE (Animal Research: Reporting In Vivo Experiments, Strengthening the Reporting of Observational Studies in Epidemiology, and the Case Report Statement and Checklist, respectively).

Results: Overall, 131 studies met the inclusion criteria, including 799 specimens and 2,823 patients who sustained 3,246 injuries. Laboratory studies showed a preponderance of failures at the MTJ, a viscoelastic behavior of muscle-tendon units, and damage accumulation at the MTJ with repetitive loading. Observational studies showed that 35% of injuries occurred in the tendon midsubstance; 28%, at the MTJ; 18%, at the tendon-bone junction; 13%, within the muscle belly and that 6% were tendon avulsions including a bone fragment. The biceps femoris was the most injured muscle (25%), followed by the supraspinatus (12%) and the Achilles tendon (9%). The most common symptoms were hematoma and/or swelling, tenderness, edema and muscle/tendon retraction. The onset of injury was consistent with tissue fatigue at all injury sites except for tendon avulsions, where 63% of the injuries were caused by an evident trauma.

Conclusions: Excluding traumatic tendon avulsions, most injuries were consistent with the hypothesis that material fatigue damage accumulated during repetitive submaximal loading regimens. If supported by data from better imaging modalities, this has implications for improving injury detection, prevention, and training regimens.

Keywords: muscle injuries; fatigue damage; muscle-tendon-bone injuries; systematic review

1.1. Introduction

The archetypical construction of muscle-tendon-bone units includes a muscle that has an origin and an insertion, a tendon or an aponeurosis that interdigitates with muscle via a musculotendinous junction (MTJ); and an enthesis, where the tendon/aponeurosis inserts into the bone[140,153]. Injuries to muscle-tendon/aponeurosis-bone units are common[115,138] and are known to have two anatomic sites where failure is most likely to occur. These include junctions between tissues with substantial different mechanical properties, such as the tendon/aponeurosis-bone junction and the MTJ[140]. Engineers recognize junctions between dissimilar materials as being locations where mechanical stress concentrates, meaning that these junctions have to sustain higher stresses even when the muscle-tendon/aponeurosis-bone unit is uniformly loaded[153]. When mechanical stress concentrates, it can reach values that lead to failure on a nanoscale. When the loading cycle is repeated, the damage can spread to the microscale and, under certain conditions, result in partial tears on the ultrastructural scale or even in a complete rupture on the macroscopic scale. Such a failure has been reported in muscle near the MTJ[153] as well as in the tendon/ aponeurosis midsubstance[8].

Chen et al recently found molecular, cellular, and ultrastructural evidence of low-cycle fatigue damage accumulation in type I collagen at the origin of the anterior cruciate ligament at its femoral enthesis after repeated submaximal loading[23]. This multiscale finding is significant since this entheseal location is also where the preponderance of anterior cruciate ligament ruptures occurs clinically[166] as well as experimentally under certain forms of large repeated knee loading[83].

Any structure can fail in tension under a single supramaximal loading cycle that exceeds its so-called ultimate tensile strength. However, a characteristic of low-cycle fatigue failure is that the structure can fail under 2 or more tensile loading cycles, each less than the ultimate tensile strength that by itself would not cause failure. In other words, multiscale damage can accumulate in substructures to weaken the structure to the point that it fails upon the next submaximal loading cycle, often without warning. This is the engineering concept of fatigue, also termed material fatigue, which provides an underlying mechanism for describing how damage can accumulate and be driven to propagate across length scales, from the molecular to the ultrastructural, under repetitive submaximal loading exceeding a certain magnitude. This is the mechanistic hypothesis that we consider in this article as underlying many overuse injuries.

The purpose of this work was to systematically review injuries in the muscle-tendon-bone complex to assess the site of injury (muscle belly, MTJ, tendon/aponeurosis, tendon/aponeurosis–bone junction, and tendon/aponeurosis avulsion), incidence, muscles and tendons involved, mechanism of injury, and main symptoms. Hopefully, this work will provide the necessary framework to evaluate our hypothesis that injury may often be consistent with the accumulation of multiscale material fatigue damage during repetitive submaximal loading regimens.

For simplicity, we generalize the term “tendon/ aponeurosis” to “tendon” throughout the Methods and Results sections.

1.2. Methods

1.2.1. Search strategy

A systematic literature search was performed following the PRISMA guidelines[98] (Preferred Reporting Items for Systematic Reviews and Meta-Analyses) on July 24, 2019. The PubMed, Web of Science, Scopus, and ProQuest databases were searched. Only peer-reviewed studies published in full English text between January 1960 and May 2019 were included. The search strings that we employed are listed in Appendix A.

1.2.2. Data extraction

The results from the initial search (citations including title and abstract) were exported to Mendeley Desktop (Version 1.19.4; Elsevier). After removing duplicates, M.V.P. screened all titles and abstracts and excluded records if the title and/or abstract was irrelevant. A full article review was performed for the final inclusion. The references of eligible articles were then screened for relevant studies. Review articles were excluded.

In our definition of injury, we included partial or complete tears, whether of the tendon, the MTJ, the tendon-bone junction, or the muscle belly; tendinopathy, whether in the tendon-bone junction or tendon midsubstance; and tendon avulsions (defined as a complete detachment of the tendon from the bone while containing a small fragment of bone) and MTJ strains if verified using magnetic resonance imaging, computed tomography scans, or surgery. To clarify the term, if a patient sustained bilateral tendon avulsion (or a muscle belly and a tendon tear), the patient was considered to have sustained 2 injuries.

The injury site locations within the muscle-tendon-bone unit were labelled as follows: muscle (M) to refer to midsubstance muscle belly injury, musculotendinous (MTJ) to refer to injuries within the musculotendinous (or myotendinous junction), tendon (T) to refer to intratendinous injuries (within the tendon midsubstance), tendon-bone (TB) to refer to injuries within the tendon-bone interface, and avulsion (AV) to refer to a complete detachment of the tendon that includes a bony fragment. Although tendon-bone injuries and avulsions can occur at the same interface, the failure mechanism is distinct because avulsion failures involve failure within the bone.

The classification of the muscle/tendons was mostly performed using groups of muscle-tendon units—for example, injuries within the proximal or distal tendon of the biceps femoris are classified as a biceps femoris tendon injury. Some exceptions were made. For instance, injuries in the Achilles tendon are so prominent that we decided to separate them from the proximal

injuries of the gastrocnemius unit, so they have their own category. We based our classification according to Netter[100].

To evaluate the possibility of injuries being caused by submaximal repetitive loading (material fatigue), the onset of injury was divided into 2 categories: "evident trauma" and "possible contribution of material fatigue." Evident trauma was chosen in cases of falls, work accidents (eg, crushed shoulders, hands caught in machines), car accidents, recreational sports activities (first time or casual players; eg, skiing and bowling), and professional sports (if the mechanism of injury was a twisting motion of the knee, a tackle in American football, or a forceful hit). Possible contribution of material fatigue was chosen for high school, collegiate, or professional well-trained athletes; avid weightlifters; and people who were actively or previously engaged in sports activities or the military. As such, this category included injuries sustained by those active in sports, whatever their age, where no evident trauma was reported. Particularly in older patients, other factors might be at play, such as degenerative changes attributed to aging. However, in older adults active in sports, age-related changes and material fatigue can be present together. Thus, although we cannot state that the injuries in this category are exclusively caused by material fatigue, we argue that it can play a role.

Baseline data extraction for laboratory studies included number of specimens, type of model, tested muscle, site of injury, and major relevant findings. For observational studies, data included number of participants, country where the study was performed, age of the patients, relevant medical conditions, methods of diagnosis, muscle or tendon injured, site of injury, onset of injury, and main symptoms.

1.2.3. Quality assessment

To access quality and risk of bias, 3 checklists were followed. ARRIVE (Animal Research: Reporting In Vivo Experiments)[77] was used for the laboratory studies. It consists of a 20-item checklist that describes the minimum information that all scientific publications reporting research with animals should include. The observational studies were case reports and cohort studies. The STROBE (Strengthening the Reporting of Observational Studies in Epidemiology)[152] checklist was chosen to evaluate the cohort studies. It consists of 22 items that highlight the essential information to include in observational studies. Eighteen items are common to cohort studies, case-control studies, and cross-sectional studies, and 4 are specific to each of the 3 study designs. CARE (Case Report Statement and Checklist)[46] was followed for case reports. It consists of a 13-item checklist that provides a framework to satisfy the need for completeness and transparency for published case reports.

With the ARRIVE, STROBE, and CARE checklists, a number of points was attributed to each item, depending on how many topics the item covered. For instance, if the item regarding the abstract recommended that the study provide a summary of the background, research objectives,

methods, results, and conclusions, 5 points were attributed to this item. Each study was reviewed, and the items were scored from 0 to the maximum number of points attributed. The points were added for each study and recorded as a percentage. Nonapplicable items were deducted from the maximum possible score in that study. Study quality was assessed via percentage: ≥80%, very good; 50%-80%, good; 30%-50%, fair; and ≤30%, poor. A more extensive description and a table with the score of each study are presented in Appendix B.

1.2.4. Statistical analysis

Statistical analysis was performed using MATLAB (Version R2018a; MathWorks) for injury site and age comparison. One-way analysis of variance was used, and $P = .001$ was the threshold for significance.

Quantitative values are presented as the mean and standard error of the mean unless stated otherwise.

1.3. Results

1.3.1. Search results

The combined search terms yielded 10,686 results: 1,736 from PubMed, 1,592 from Web of Science, 3,999 from Scopus, and 3,359 from ProQuest. Ten additional records were added from other sources. A primary review of titles and abstracts resulted in 258 documents. Of these, 131 studies met the inclusion criteria (Figure 1.1).

In total, 131 studies were included in the final analysis: 11 laboratory studies[‖] and 120 observational studies[¶], of which there were 50 cohort studies and 70 case reports or case series. Of the laboratory studies, 10 were rated as good quality (50%-80%), and 1 was rated as fair (30%-50%). Of the observational cohort studies, 9 were rated as very good quality (80%-100%); 39, good; and 2, fair. Of the case reports or case series, 4 were rated as very good quality; 60, good; and 6, fair. None of the studies was rated as poor quality (≤30%). Details can be found in Appendix B.

Of the laboratory studies (n = 11), 8 used New Zealand White rabbits as a model[#],whereas each of the remaining 3 studies used mice[79], Mongrel dogs[54] and cadaveric human specimens[121]. A total of 799 specimens were tested to evaluate muscle-tendon-bone units of different muscle complexes. The musculotendinous units included the extensor digitorum longus, the tibialis anterior, the rectus femoris, the gastrocnemius, the soleus, and the supraspinatus tendon and

[‖]References [47,48,149,54,59,79,88,104,121,139,143]

[¶]References [1,3,16,137,141,142,144,146,147,150,151,154,155,17,156–165,18,19,21,24–28,5,29–36,38,39,6,40–45,49–52,7,53,55–58,62–66,9,67–69,71–76,78,10,80,81,84–87,89–92,11,93,96,97,99,102,103,105–108,14,109–111,113,116,117,119,122–124,15,126–135]

[#]References [47,48,59,88,104,139,143,149]

muscle. Histologic features were noted in 5 articles[54,59,104,121,143]. The laboratory studies are summarized in Appendix C.

In the observational studies (n = 120), the population was injury specific in 107 studies (analyzed patients with specific injuries or pain in specific sites) and injury/population specific in 13 studies (analyzed athletes with specific injuries). A total of 2,823 patients with injuries in muscle-tendon-bone units were observed: 2,047 from the injury-specific studies and 776 from injury/population–specific studies.

The injured muscle and tendon units are listed in Table 1.1 and the number of studies per country is shown in Table 1.2. From the studies that included age data** the patients were 41.4±13.5 years old (mean ± standard deviation). Observational studies are summarized in Appendix D.

Table 1.1 - List of the injured muscles and tendons reported by the included observational studies.

Quadriceps tendon (QT)	Popliteus tendon (POP)
Rectus Femoris (RF)	Peroneus Longus (PL)
Vastus Medialis (VM)	Peroneus brevis muscle (PB) and tendon (PBT)
Vastus Lateralis (VL)	Infraspinatus muscle (IP) and tendon (IPT)
Vastus Intermedius tendon (VI)	Supraspinatus muscle (SP) and tendon (SPT)
Gluteus Minimus tendon (GMINT)	Teres Minor (TMIN)
Gluteus Medius Tendon (GMEDT)	Subscapularis muscle (SC) and tendon (SCT)
Tensor Fascia Lata (TFL)	Pectoralis major muscle (PM) and tendon (PMT)
Gracilis (GRC)	Biceps Brachii (BB)
Adductor Longus (ADL)	Latissimus Dorsi tendon (LDT)
Quadratus Femoris (QF)	Brachialis (BCH)
Bicep Femoris (BF)	Deltoid (DLT)
Semimembranosus (SM)	Triceps muscle (TR) and tendon (TT)
Semitendinosus (ST)	Teres Major (TMJ)
Triceps Surae (TS)	Flexor Profundus tendon (FPT)
Gastrocnemius (GST)	Flexor Pollicis Longus (FPL)
Achilles tendon (ACT)	Extensor Digitorum (ED)
Extensor Hallucis Longus (EHL)	Extensor Indicis Proprius (EIP)
Tibial Tendon (TT)	Extensor Pollicis Longus (EPL)
Patellar Tendon (PT)	Extensor Digiti Minimi (EDM)

**References 1,3,16,147,150,151,154–160,17,161–165,18,19,21,24–28,5,29–31,33–36,38–40,6,42,44,45,49–53,55,56,7,57,58,62–69,9,71–76,78,80,81,84,10,85–87,89–93,96,97,11,99,102,103,105–110,113,14,116,119,122–124,126–130,15,131–135,137,141,142,144,146

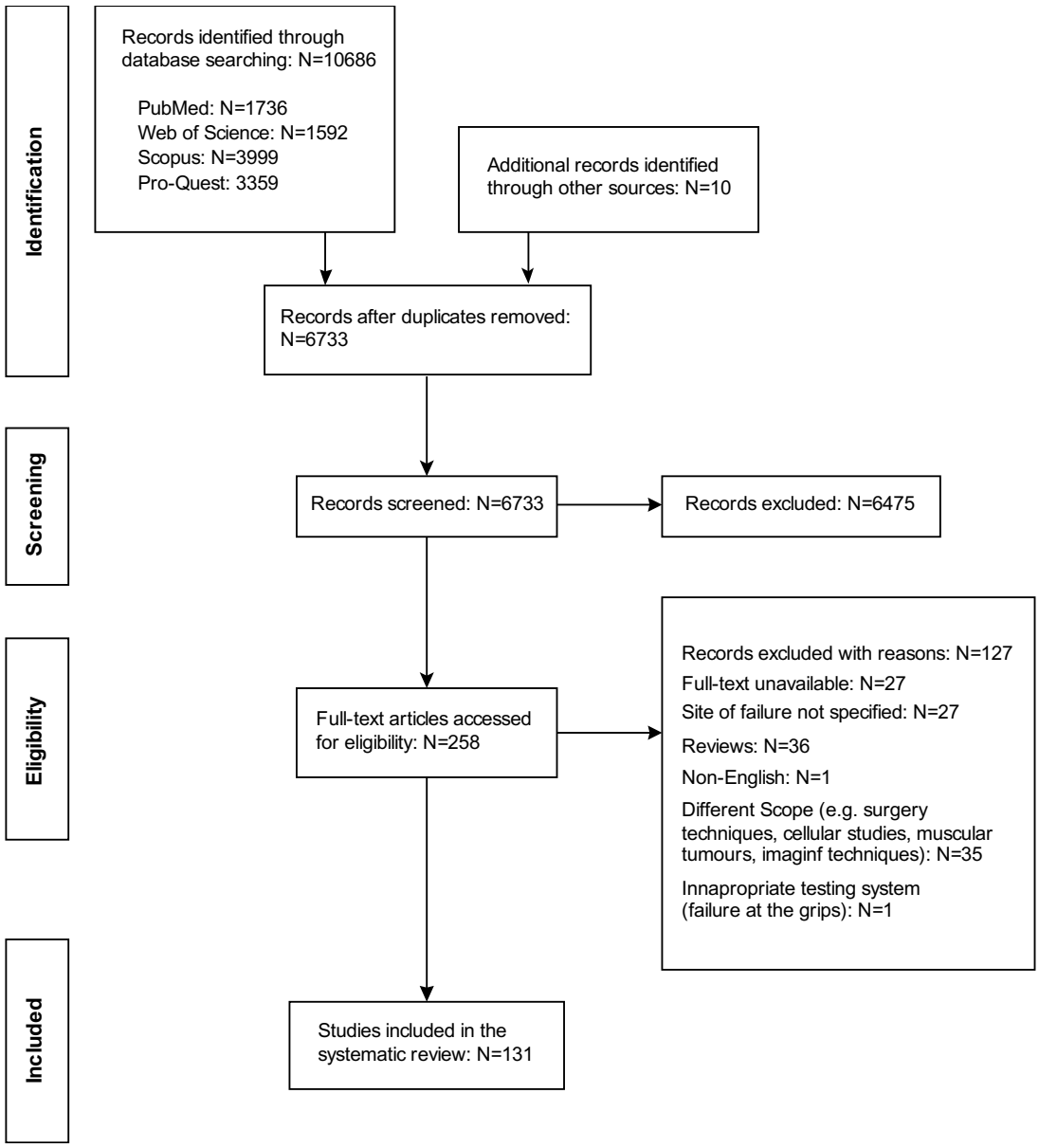

Figure 1.1 - PRISMA flowchart detailing study identification and record screening process[98]. PRISMA, Preferred Reporting Items for Systematic Reviews and Meta-Analyses.

Table 1.2 - Distribution of the observational studies by country.

Countries	No. of Studies
United States of America	55
Japan	10
United Kingdom	10
France	7
Australia	7
Finland	5
Italy	5
Switzerland	4
India	3
Netherlands	3
Turkey	3
Denmark	1
Taiwan	1
Croatia	1
Brazil	1
Canada	1
Serbia	1

1.3.2. Laboratory studies employing mechanical failure tests

Ten studies used animal models, seven in vivo[47,48,88,104,139,143,149] and three in vitro[54,59,79], and one study used cadaveric human specimens[121]. Eight studies used an Instron Testing Instrument (Instron Corp)[††], and 3 used an MTS systems instrument (MTS Bionix 858 Test System; MTS Corp)[54,139,149].

Different muscle groups were tested at different strain rates, but when pulled to failure, the site of injury was at the MTJ in 8 studies (73%),[‡‡] independent of the strain rate. This behavior was verified for muscles with different architectures (extensor digitorum longus, tibialis anterior, rectus femoris, gastrocnemius, the 4 peroneus muscles, and the supraspinatus), whether the muscles were tested passively or actively using electrical stimulation. Failure was seen at the distal MTJ in all specimens in 6 studies[48,59,104,139,143,149] and in 95% of the cases in one study[47]. One article indicated that most failures occurred at the proximal MTJ[79], although the number of specimens was not specified. Failure was confirmed when histologic assessment was performed[54,59,104,143] by areas of fiber rupture, hemorrhage, edema, and acute inflammatory cells being found at the MTJ. One study[121](9%) in cadaveric human specimens (mean age, 62 years; range, 39-83 years) focused on the supraspinatus tendon, without including the muscle and the MTJ. In that study, failure was seen at the tendon-bone interface in 65% of the cases and at the

[††] References [47,48,59,79,88,104,121,143]
[‡‡] References [47,48,54,59,79,104,139,143,149]

tendon midsubstance in 35%. Histology showed thinning of tendon fibers and granulation of the tissue more frequently in the insertion group than in the midsubstance group. One article (9%) did not state the specific injury site[88]. Viscoelastic effects were also demonstrated[139], with a larger ultimate tensile force (peak force at failure) being found at higher strain rates. Material fatigue (damage accumulation that can lead to failure attributed to a submaximal cyclic load) was analyzed in 4 studies[88,104,143,149]

Based on the ultimate tensile properties of control specimens (whether tested via controlled force or displacement), nondisruptive injuries were mechanically caused at a percentage of the failure force or displacement. Nondisruptive injuries at 20% ultimate tensile force did not influence the failure parameters, and the histology showed no differences as compared with the controls. At 30% ultimate tensile force, histology showed areas of fiber rupture and hemorrhage near the MTJ, although the failure parameters were not affected. After a nondisruptive injury at a stretch just before failure, the ultimate tensile force was decreased by 37%; the ultimate tensile displacement, by 21%. Histology then showed incomplete disruption at the MTJ.

1.3.3. Observational studies

From the observational studies, 1 did not specify the injured muscles, referring only to the lower extremities[43]; 2 did not cite the age of the patients [41,43]; and 3 reported just the age range[32,111,117]. Fifteen did not specify the activities at the time of injury[§§] although 2 of those studies[85,156] did differentiate between progressive and traumatic onset. In the 2,823 patients, a total of 3,246 injuries were observed. Age was specified in 2,106 injuries; onset of injury, in 1,772. The activity at the time of injury was sports in 66% of the patients when the onset of injury was indicated. Among other events were falls, working accidents, car accidents, and moving heavy objects. Hematoma and/or swelling were described in 49 (41%) of the studies[‖‖]; retraction of either the muscle or the tendon in 34 (28%)[¶¶]; tenderness in 33 (28%)[##]; edema in 32 (27%)[a]; ecchymosis in 16 (13%)[b]; a mass of soft tissue in 14 (12%)[c]; and hemorrhage in 10 (8%)[d].

[§§] References [33,38,102,135,150,156,162,45,49,56,66,85,87,89,97]

[‖‖] References [6,11,32,34,39,44,51,52,56–58,62,14,65,68,71,74,76,80,81,87,99,103,15,105,108,109,113,116,122–124,126,127,16,132,147,151,154,157–159,163,164,18,19,21,25,31]

[¶¶] References[5,14,62–64,66,67,69,75,80,85,89,18,97,105,108,124,126,135,137,144,146,151,19,156,157,159,164,35,38,44,56–58]

[##] References [3,6,41,62,65,68,72,74,81,86,87,97,10,109,113,116,119,122,124,130,141,142,146,11,147,158,14,21,24,27,29,40]

[a] References[11,19,43,52,56,58,65,66,72,73,81,85,25,92,97,110,111,116,135,144,146,156,162,26,163,165,27–29,32,34,35]

[b] References[16,17,107,123,141,147,158,164,18,33,44,58,68,81,92,105]

[c] References[5,6,96,144,155,158,17,21,24,62,64,69,74,81]

[d] References[14,25,26,29,43,52,111,135,146,165]

1.3.4. Injury site

Of the 3,246 injuries, 1,130 (35%) were within the tendon, 918 (28%) were in the MTJ, 584 (18%) were at the tendon-bone junction, 434 (13%) were within the muscle belly, and 180 (6%) were tendon avulsions (Figure 1.2).

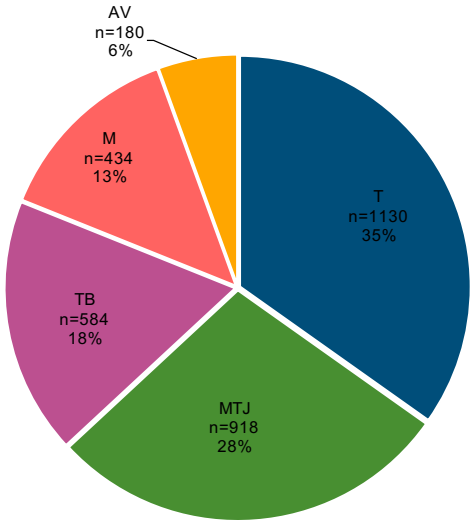

Figure 1.2 - Injury site distribution among the patient cohort (n = 3246). AV, tendon avulsion; M, muscle belly; MTJ, musculotendinous junction; T, tendon; TB, tendon-bone junction.

Patient age was reported for 2,106 injuries. The mean age was 28.5 ± 2.1 years for muscle belly injuries, 32.5 ± 0.8 years for tendon avulsions, 33.7 ± 0.5 years for MTJ injuries, 47.4 ± 0.4 years for tendon injuries, and 51.4 ± 0.5 years for tendon-bone junction injuries. The age of the patients by injury site is displayed in a box-and-whisker plot in Figure 1.3.

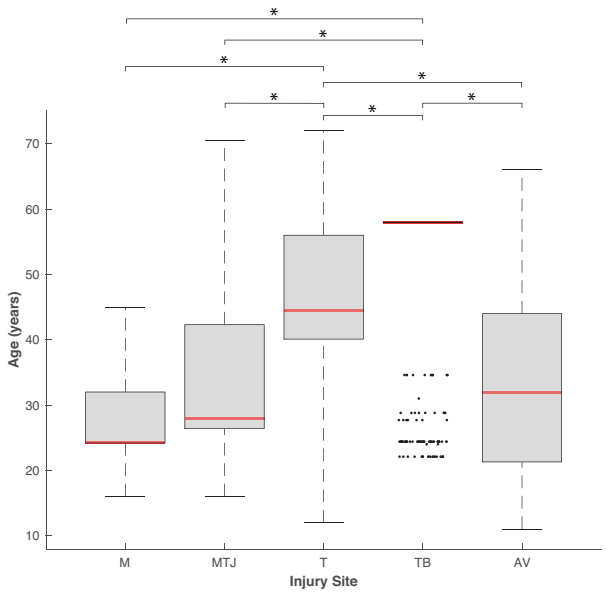

Figure 1.3 - Box-and-whisker plot (median, 25th percentile; range, 75th percentile) of patient age by injury site (n = 2,106). *P < .001. One-way analysis of variance. Dots appearing outside the whisker are outliers (observations numerically distant from the rest of data). AV, tendon avulsion; M, muscle belly; MTJ, musculotendinous junction; T, tendon; TB, tendon-bone junction.

With the exception of age comparisons for MTJ versus avulsions, MTJ versus muscle belly injuries, and avulsions versus muscle belly injuries, all the mean ages were significantly different between injury sites ($P < .001$, 1-way analysis of variance).

Musculoskeletal injuries (with the exception of muscle belly injuries) occur where the muscle originates from the bone (proximal location) and where the muscle inserts into the bone (distal location). In Figure 1.4, we differentiate the injury site (tendon avulsion, tendon, tendon-bone, and MTJ) into proximal and distal locations within each "muscle." Muscle belly injuries were assumed to be in mid-substance, and so they were not included in this analysis, which comprised 2,328 injuries. The primary site of injury was at the distal attachment for all injury sites. Overall, 74% of the injuries occurred at the distal location, and 26% occurred at the proximal location. This was especially marked for tendon injuries, 40% of which occurred at the distal attachment as opposed to 5% at the proximal attachment.

The analysis of onset of injury, divided in the 2 categories (evident trauma and possible contribution of material fatigue), comprised 1,772 injuries. Every one of the injuries categorized into the "possible contribution of material fatigue" group was associated with exercise/sports activity practiced on a regular basis. These sports/exercise injuries (after those with known trauma were excluded) were the ones that we could comfortably include in this category since these activities typically involve repetitive loading. The results by injury site are shown in Figure 1.5. Material fatigue could be involved in the cause of injury at all sites, with the exception of tendon avulsions, where evident trauma was the primary cause of injury.

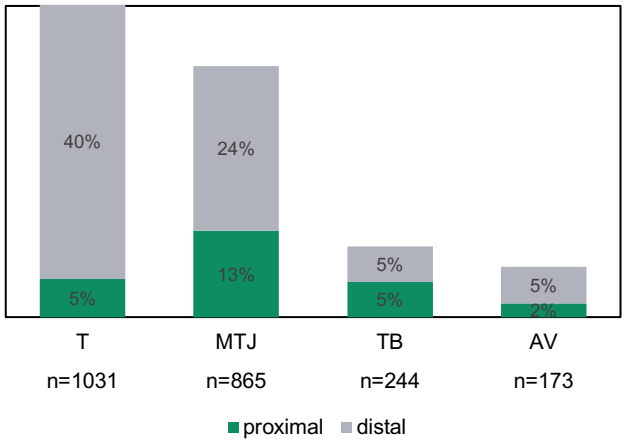

Figure 1.4 - Distribution of proximal and distal locations within each muscle by injury site (n = 2,328). AV, tendon avulsion; MTJ, musculotendinous junction; T, tendon; TB, tendon-bone junction.

1.3.5. Injury muscle/tendon groups

The distribution of injuries by muscle/tendon and injury site is illustrated in Figure 1.6 and included 2,832 injuries. As described in the Methods section, the injuries in this category were primarily grouped by muscle-tendon units, with tendon injuries grouped as proximal and distal

injuries. A few exceptions were made for certain tendons, which were assigned their own category (eg, Achilles tendon).

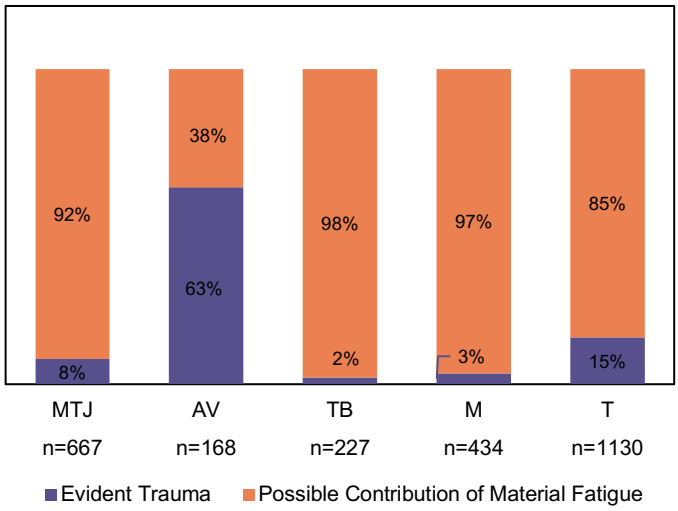

Figure 1.5 - Comparison of onset of injury category by injury sites (n = 1,772). AV, tendon avulsion; M, muscle belly; MTJ, musculotendinous junction; T, tendon; TB, tendon- bone junction.

The biceps femoris was the most commonly injured musculotendinous unit, representing 25.1% of the injuries. Of those, 14.4% were in the MTJ, and 9.7% were in the muscle belly. The highest incidence of MTJ injuries was in the biceps femoris (14.4%); that of tendon midsubstance injuries was in the supraspinatus (11.4%); that of tendon-bone junction injuries was in the patellar tendon (5.0%); that of muscle belly was once again in the biceps femoris (9.7%); and complete tendon avulsions occurred more frequently in the pectoralis major and triceps brachii (1.1%). There were 3 muscle groups more predominantly involved: the hamstring, the quadriceps, and the rotator cuff. From the hamstring group, the biceps femoris was the most frequently injured (25.1%); from the quadriceps group, the rectus femoris was the most injured unit (3.1%); and from the rotator cuff, the supraspinatus was the most prone to injury (11.7%).

The age of the patients at the time of injury was verified for the different muscle/tendon units. This information was not always reported, especially in studies involving injuries in different muscle/tendon groups, since the norm is to provide the mean age of the entire cohort. Nevertheless, of the 3,246 injuries, it was possible to associate age with the muscle-tendon unit in 1,681. Mean and standard error of the mean are presented as well in Figure 1.6. Injuries in the biceps femoris, which was the most commonly injured unit, occurred frequently in young adults (26.3 ± 0.5 years). The muscle units associated with older patients were the deltoid (73.0 ± 1.2 years) and the gluteus medius (68.0 ± 0.7 years), while the popliteus (15.5 ± 4.3 years) and the extensor hallucis longus (16.0 ± 6.1 years) were seen in the younger patients of the cohort. Between muscle groups, hamstring injuries occurred more frequently in younger adults, as did quadriceps injuries, while rotator cuff injuries were more typical in middle-aged patients.

Information regarding injury of the proximal or distal attachments was reported in 2,328 injuries and is shown in Figure 1.7. Regarding specific musculotendinous units, the biceps femoris showed a balanced distribution, with 9.7% at the distal location and 8.6% at the proximal location. However, injury of the other hamstring muscles occurred more frequently at proximal locations. The rotator cuff injuries all occurred at distal locations, as did injuries in the pectoralis major muscle, while in the quadriceps group, they occurred more frequently at proximal locations.

The onset of injury in musculotendinous units was reported in 1,415 injuries analyzed in the categories of evident trauma and possible contribution of material fatigue. The results are shown in Figure 1.8.

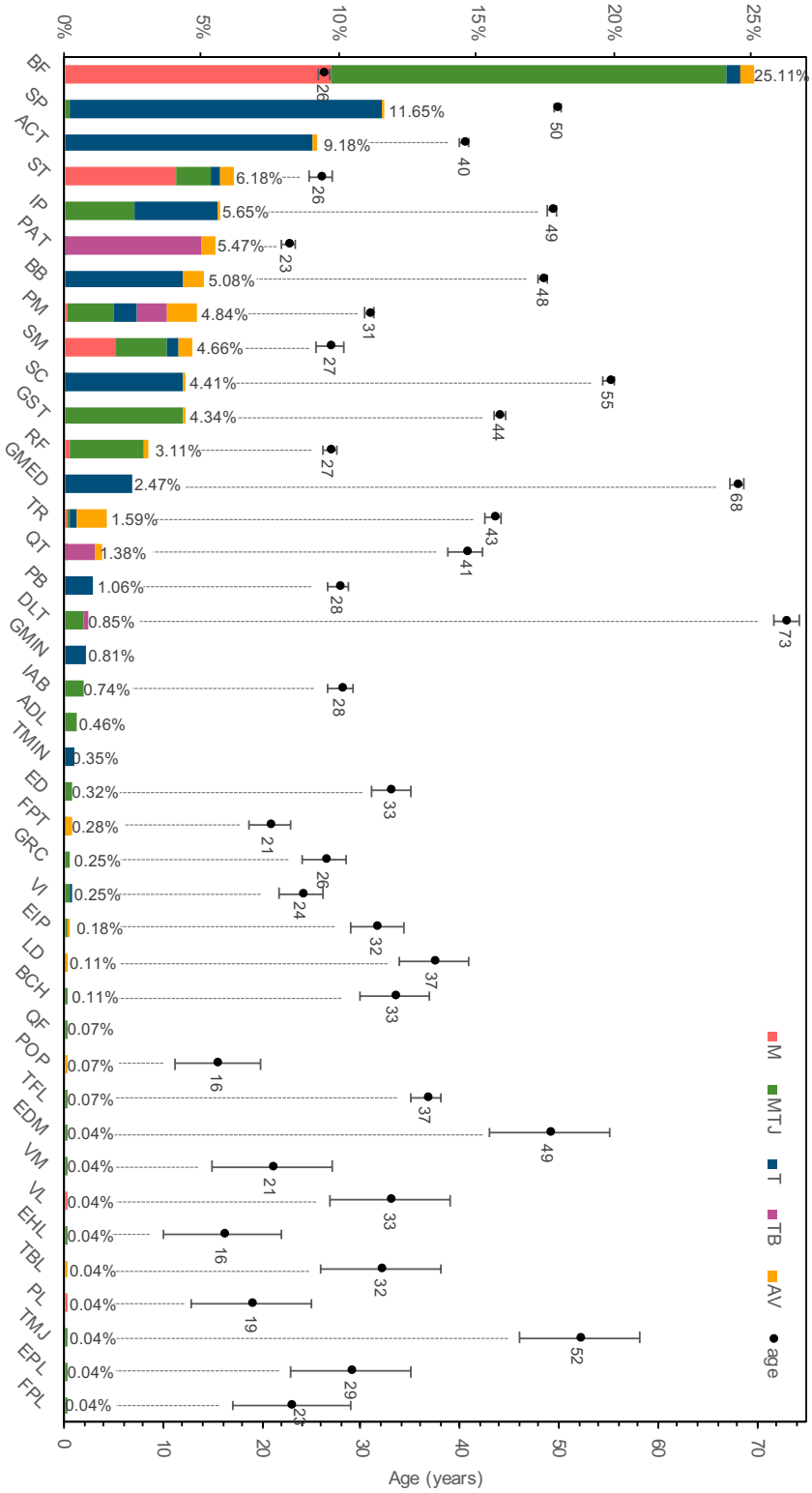

Figure 1.6 - Injury distribution by muscle/tendon and injury site (n = 2,832) and mean ± SEM age by muscle/tendon (n = 2,106). Patient age was not reported for ADL, TMIN, and QF injuries. ACT, Achilles tendon; ADL, adductor longus; AV, tendon avulsion; BB, biceps brachii; BCH, brachialis; BF, biceps femoris; DLT, deltoid; ED, extensor digitorum; EDM, extensor digiti minimi; EHL, extensor hallucis longus; EIP, extensor indicis proprius; EPL, extensor pollicis longus; FPL, flexor pollicis longus; FPT, flexor profundus tendon; GMED, gluteus medius; GMIN, gluteus minimus; GRC, gracilis; GST, gastrocnemius; IAB, internal abdominal; IP, infraspinatus; LD, latissimus dorsi; M, muscle belly; MTJ, musculotendinous junction; PAT, patellar tendon; PB, peroneus brevis; PL, peroneus longus; PM, pectoralis major; POP, popliteus; QF, quadratus femoris; QT, quadriceps tendon; RF, rectus femoris; SC, subscapularis; SM, semimembranosus; SP, supraspinatus; ST, semitendinosus; T, tendon; TB, tendon-bone junction; TBL, tibialis posterior; TFL, tensor fasciae latae; TMIN, teres minor; TMJ, teres major; TR, triceps brachii; VI, vastus intermedius; VL, vastus lateralis; VM, vastus medialis.

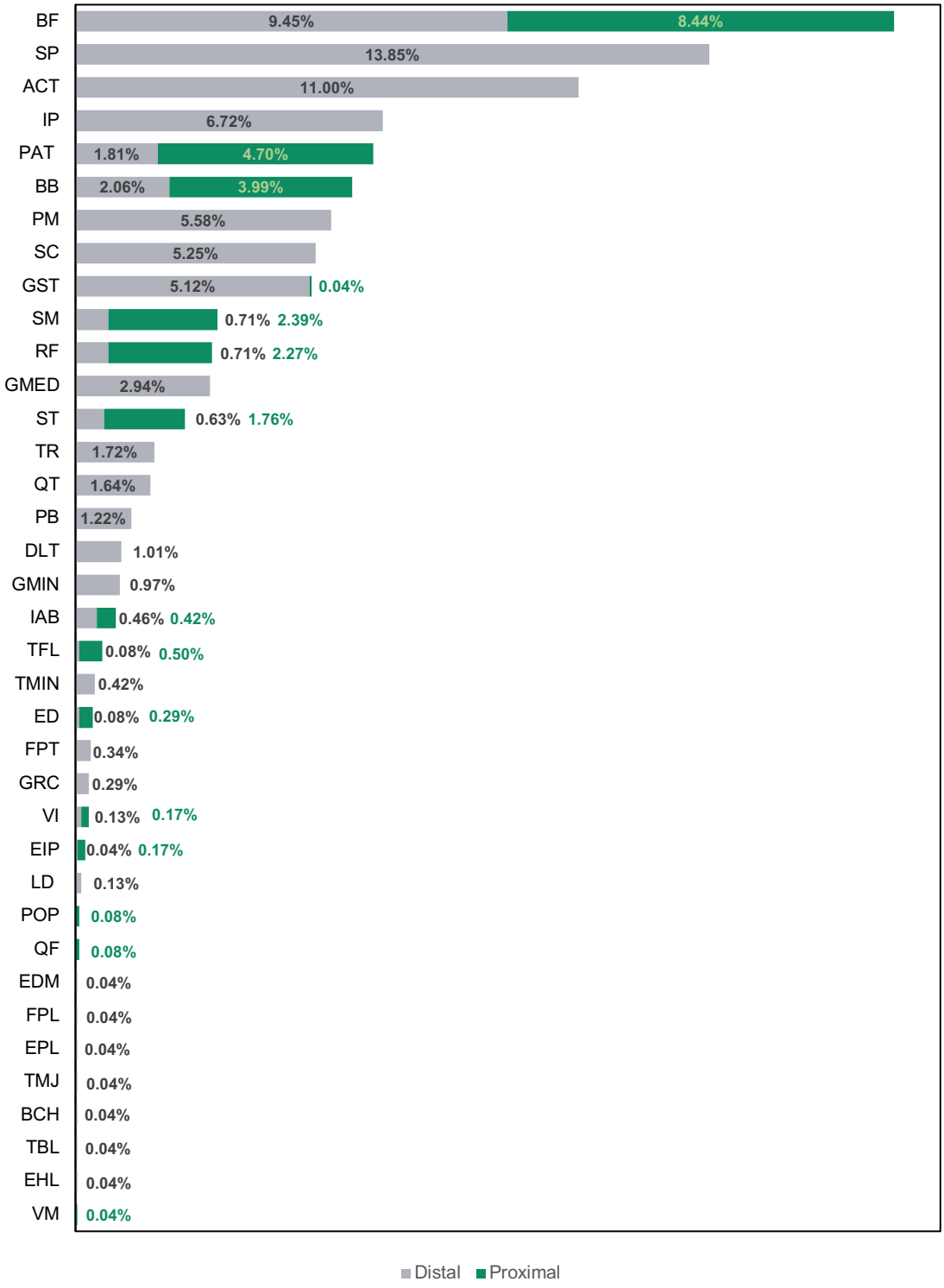

Figure 1.7 - Distribution of injuries by musculotendinous group and proximal and distal locations (n = 2,328). ACT, Achilles tendon; BB, biceps brachii; BCH, brachialis; BF, biceps femoris; DLT, deltoid; ED, extensor digitorum; EDM, extensor digiti minimi; EHL, extensor hallucis longus; EIP, extensor indicis proprius; EPL, extensor pollicis longus; FPL, flexor pollicis longus; FPT, flexor profundus tendon; GMED, gluteus medius; GMIN, gluteus minimus; GRC, gracilis; GST, gastrocnemius; IAB, internal abdominal; IP, infraspinatus; LD, latissimus dorsi; PAT, patellar tendon; PB, peroneus brevis; PM, pectoralis major; POP, popliteus; QF, quadratus femoris; QT, quadriceps tendon; RF, rectus femoris; SC, subscapularis; SM, semimembranosus; SP, supraspinatus; ST, semitendinosus; TBL, tibialis posterior; TFL, tensor fasciae latae; TMIN, teres minor; TMJ, teres major; TR, triceps brachii; VI, vastus intermedius; VM, vastus medialis.

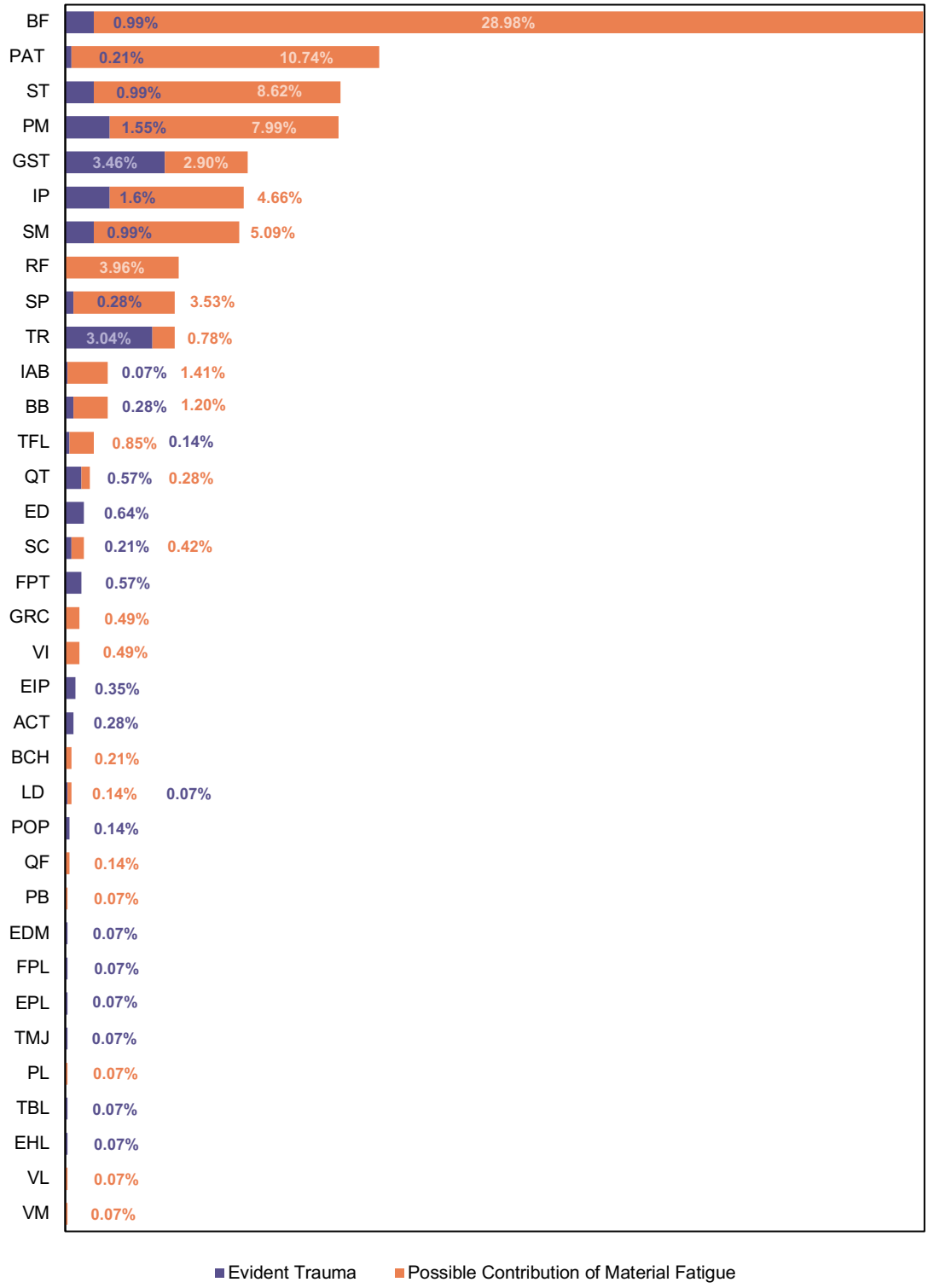

Figure 1.8 - Comparison of onset of injury category (in percentages) by injured muscle/tendon (n = 1,415). ACT, Achilles tendon; BB, biceps brachii; BCH, brachialis; BF, biceps femoris; ED, extensor digitorum; EDM, extensor digiti minimi; EHL, extensor hallucis longus; EIP, extensor indicis proprius; EPL, extensor pollicis longus; FPL, flexor pollicis longus; FPT, flexor profundus tendon; GRC, gracilis; GST, gastrocnemius; IAB, internal abdominal; IP, infraspinatus; LD, latissimus dorsi; PAT, patellar tendon; PB, peroneus brevis; PL, peroneus longus; PM, pectoralis major; POP, popliteus; QF, quadratus femoris; QT, quadriceps tendon; RF, rectus femoris; SC, subscapularis; SM, semimembranosus; SP, supraspinatus; ST, semitendinosus; TBL, tibialis posterior; TFL, tensor fasciae latae; TMJ, teres major; TR, triceps brachii; VI, vastus intermedius; VL, vastus lateralis; VM, vastus medialis.

1.4. Discussion

This review included data from 131 studies, with 799 specimens in laboratory studies and 2,823 patients in observational studies. To the best of our knowledge, this is the largest series of muscle and tendon injuries analyzed since the report of 1,014 cases by Anzel et al[4] in 1959. In the ensuing 60 years, participation in sports has burgeoned, with increased female participation, a broader age range, and many more types of sports. Since sports are now the main cause of musculoskeletal injuries, it is natural that the patterns of these type of injuries may have changed with time. As such, we believe that the present review provides an update on current trends in musculoskeletal injuries.

In the laboratory studies, failure and disruption occurred mainly at the MTJ, independent of strain rate and muscle architecture. Moreover, the site of failure was more commonly the distal attachment, independent of whether the soft tissues of the specimen were gripped via a clamp at the proximal or distal end of the muscle. This supports the muscle-tendon junction being the weakest link of the muscle-tendon unit because tensile-testing machine grips can often induce local failures of their own, owing to artifactual stress concentrations[101].

The behavior of the muscle-tendon unit has been described as viscoelastic[139]. Viscoelasticity has an important functional significance for biological soft tissues because it allows them to stretch more at a constant load (known as creep behavior) as well as to decrease mechanical stresses over time when held at a constant length (known as relaxation behavior). These behaviors help soft tissues withstand larger deformations without injury[2].

Four studies analyzed the influence of repetitive loading[88,104,143,149]. Small nondisruptive injuries caused by a single tensile loading cycle to 30% of failure force were evidenced by microdamage in the MTJ detectable histologically. For larger nondisruptive injuries, the mechanical properties were more severely affected. This implies that repeated activities are a risk factor for musculotendinous tears. Moreover, it suggests that if the movement requires large enough muscle forces, a small number of loading cycles can suffice to disrupt the tissue in a way that partial or even complete failure occurs without warning in an otherwise normal movement.

The observational studies showed that the most common injury site was the tendon substance (35%), followed by the MTJ. These results are not in accordance with the animal studies, which showed a preponderance for failure at the MTJ. This is interesting since midsubstance tendon injuries are mostly described as rare in normal tendons, especially considering that they can withstand higher loads than those the muscle can generate or the bone can sustain[140,148]. However, since tendinopathy was also considered an injury in the tendon midsubstance, this could explain the discrepancy with the laboratory tests, which used tissue from mostly younger/healthier individuals where tissue degeneration and aging effects were not a variable.

Of the reported injuries, 28% were at MTJs, and patients were significantly younger ($P < .001$) than were those with tendon and tendon-bone junction injuries. Only 8% of these injuries were associated with evident trauma, which means that 92% were instigated by a noncontact event and occurred in well-trained athletes. This information, with the fact that in laboratory studies the MTJ showed signs of disruption at submaximal loads[88,104,143,149] strongly suggests that material fatigue damage can play a role in MTJ injuries.

The patients with tendon-bone junction injuries were significantly older ($P < .001$) than were patients with injuries at all the other analyzed sites. This could be indicative that aging and the associated degenerative changes involve the tendon-bone junction besides the tendon itself, weakening the tissue. However, tendon-bone junction injuries, particularly insertional tendinopathies or enthesopathies, have been associated with overuse injury, [12,13,22,37,125] which, as we hypothesized, may be related to material fatigue. Since just 2% of the cases were caused by evident trauma, the degenerative changes can be also be a result of damage accumulation attributed to overuse.

Tendon avulsion was the least common injury, and although it is usually considered the most typical in children and adolescents[94,140], the mean age of these patients was actually 32.5 ± 0.8 years. As such, it should not be exclusively associated with children and adolescents. When the onset of injury was analyzed, 63% of tendon avulsions occurred because of an evident trauma. Moreover, it was the only injury site at which evident trauma was the primary cause of damage, which could explain the older patients with this type of injury. It seems that in cases of traumatic fall, vehicle accidents, and work-related accidents, avulsion fractures can occur independent of age. It is interesting to observe that although tendon-bone junction injuries and tendon avulsions occur in the same interface—with the distinction that in tendon avulsions there is a complete detachment of the tendon with a bony fragment—they seem to have different mechanisms. Not only was the age of the patients significantly different ($P < .001$), but tendon-bone injuries had a low rate of "evident trauma" injuries, although they were the primary cause of tendon avulsions.

When patient results were analyzed by muscle/tendon groups, the hamstring and rotator cuff groups stood out, as did the gastrocnemius, the rectus femoris, and the Achilles and patellar tendon groups. It was confirmed, as described in the literature[28,29,117,134,135,150], that the biceps femoris is the most prone to injury in the hamstring group; the supraspinatus, in the rotator cuff; the Achilles tendon, in the triceps surae; and the rectus femoris, in the quadriceps. It was surprising that the triceps brachii musculotendinous unit represented 1.59% of the injuries. Although not a large proportion, it was not the least injured unit.

It is not clear why certain musculotendinous units are more susceptible to injury at a specific site, the underlying causes being likely multifactorial. Many factors are known to affect the stresses at myofascial junctions, including the relative lengths and widths of the muscle's proximal and distal MTJ[114]; however, it seems that MTJ and muscle belly injuries might be more

common in the lower extremities. A wonderfully illustrative example of a hamstring material fatigue injury is the one recorded in real time at the proximal MTJ of the long head of the biceps femoris in a professional athlete running at 5.4 m/s (or about 80% of an average sprinter speed but less than half Usain Bolt's maximum sprinting speed) up a 15% incline on a treadmill [60]. After appropriately warming up, the athlete had just completed several trials on the treadmill at the same and steeper inclines. The motion capture data showed that the injury occurred during an eccentric contraction of the muscle (when stresses are known to be higher than are isometric values) at the end of a stride, as the muscle decelerated the limb for the next heel contact. Clearly, in this example of constant submaximal speed running, even though the muscle forces were likely substantial, (1) they were still submaximal, (2) they had already been repeated many times within the past hour, and (3) evidently sufficient microdamage had accumulated at the biceps femoris MTJ to weaken it to the point of a partial failure under the submaximal loading. Although the exact anatomic and physiological reason for the failure remains unknown, material fatigue was certainly involved because of the many preceding loading cycles that did not cause injury.

An anatomic feature that makes muscle-tendon units more prone to injury at the tendon is the ratio between the tendon and the muscle cross-sectional area (CSA). For instance, a study reported that in the anterior portion of the supraspinatus, the physiological CSA was measured as 140 ± 44 mm^2 and the tendon CSA was measured as 26.4 ± 11.3 mm^2.[118] This is equivalent to a tendon/muscle CSA ratio of 0.19. In the posterior portion of the supraspinatus, which is much less prone to injury[118], the tendon/muscle ratio was 0.5, meaning that the difference in CSAs was not so accentuated. Since the mechanical stress is defined in terms of force per unit area, a smaller tendon CSA, combined with a large muscle CSA, will increase the stresses in the tendon above those at the muscle or the MTJ for the same force. The higher the mechanical stress, generally the higher the risk for incurring fatigue damage under repetitive submaximal loading.

Aside from the injuries attributed to trauma via a single overload in muscle, tendon, or bone, the results of the present review are consistent with the idea that fatigue damage accumulation may play an important role in musculoskeletal injuries. Although we cannot prove that the observed injuries were caused by material fatigue, we can prove that most of them were not caused by evident trauma. This information, with the fact that sports and exercise activity were the main cause of injury in all of the cases, indicates that material fatigue can be one of the mechanisms of injury, which is supported by the experimental studies. The widely used expression "overuse injury" implicitly acknowledges this damage mechanism but is often associated with specific type of injuries, such as tendinopathies[20,82,95].

In the case of the tendon injuries, where "overuse" is linked clinically to the development of tendinopathy, microdamage has been noted in the form of collagen fibril disruption at 6% strain[136]. Moreover, fatigue resistance decreases with age in the interfascicular matrix and in the fascicules[145]. If the loading is repeated at a high-enough intensity, this damage accumulation can

become severe since tendon and tendon-bone injuries naturally have limited healing potential[70] and there is almost no tissue renewal after complete formation of the tendon[61]. Moreover, the tendon-bone interface is a distinctive and specialized structure that almost never recovers completely to its undamaged state, even after surgical treatment[120].

In the case of muscle injuries, several experimental[88,104,143,149] and even some observational studies[85,156] have presented the idea of repetitive loading causing severe damage in muscle near the MTJ. Since muscles are well known to have an intrinsic capacity to adapt and minor injuries heal spontaneously in healthy adults[112] we believe that the concept of "overuse" is not clinically recognized when associated with muscle or MTJ injuries. However, beyond a certain injury threshold, natural muscle repair can prove insufficient, leading to loss of contractile tissue, fatty degeneration, and fibrotic scar tissue[120]. This penetration is soon halted by the formation of new mini myotendinous junctions with the scar. Although the scar diminishes with time, it is possible that some connective tissue remains[70].

The ability to heal is what distinguishes these tissues from engineering materials, and it can make the difference when dealing with this injury mechanism. Each tissue in the muscle-tendon-bone unit needs its own time to heal, so after the injured tissue type is identified, allowing adequate time to heal is a reasonable prevention strategy. Also, given the cumulative feature of this damage mechanism, it is a possibility that earlier symptoms occur, which happens, for example, with tendinopathies. In the future, this could be used to aid preventive measures by allowing more time to heal. Therefore, it is important to recognize this damage mechanism helps with prevention. We do not exclude other damage mechanisms and factors at play (nutrition, aging, type of training, intensity of training, recovery, etc). Rather, we point out that fatigue damage accumulation is yet another damage mechanism of which to be aware, particularly regarding sports or exercise activity.

Therefore, more research is needed, aided by improved noninvasive imaging methods, to answer the question of how many musculoskeletal structures can accumulate damage owing to too many submaximal loads of a certain intensity being imposed within a given time frame. Although material fatigue failure plays a role in many fields of research[23,153] recognition of this type of mechanism of failure in musculoskeletal injuries should prove beneficial by improving the diagnosis and prevention of such injuries.

Strengths

To our knowledge, this is the only systematic review to focus on all structures composing the muscle-tendon-bone unit and then to assess injury incidence by site and muscular group, age, attachment location, and onset of injury. Four databases were searched using broad search criteria to allow the capture of a wide range of articles. We included laboratory and observational studies, which helped to corroborate trends found in each and together strengthen the conclusions. The

large numbers of studies (n = 131), specimens in laboratory studies (n = 799), and injuries reported in the observational studies (n = 3,246) increase the reliability of the results.

Limitations

Limitations include the screening and evaluation phase being performed by a single person (M.V.P.). However, to provide complete transparency of how the quality of each study was evaluated, an extensive description is presented in Appendix B, which includes the score assigned to each article. Last, while there was an inherent risk of selection bias, we tried to counteract this by including broad search terms and searching in 4 databases.

1.5. Conclusion

While midsubstance tendon injuries were the most common injury, mainly affecting middle-aged patients, MTJ injuries, the second-most frequent injury, affected younger adults. Tendon-bone junction injuries occurred in significantly older patients when compared with all other sites of injury. Tendon avulsion, the least common injury, occurred in young adults. The biceps femoris was the most frequently injured structure, usually at its proximal MTJ, while the second-most injured structure was the midsubstance of the supraspinatus tendon.

With the exception of tendon avulsions, which were primarily linked with evident trauma, most injuries did not seem to be caused by a single traumatic event. This is consistent with our hypothesis that fatigue damage accumulation may play a role, particularly in well-trained athletes, although we recognize that many other factors can be at play. If material fatigue is indeed involved, this has implications for improving injury detection, prevention, and training regimens.

Acknowledgements

The content is solely the responsibility of the authors and does not represent the official views of the US National Institutes of Health. One or more of the authors declared the following potential conflict of interest or source of funding: Research reported in this publication was supported by US Public Health Service awards P30 AG024824, P30AR069620, and R01 AR054821. The authors also acknowledge support from the Portuguese Foundation for Science and Technology under grant SFRH/BD/136213/2018 and funding provided by the Associated Laboratory for Energy, Transports and Aeronautics (Portugal) under project UIDB/50022/2020. AOSSM checks author disclosures against the Open Payments Database (OPD). AOSSM has not conducted an independent investigation on the OPD and disclaims any liability or responsibility relating thereto.

References

1. Äärimaa V, Rantanen J, Heikkilä J, Helttula I, Orava S. Rupture of the pectoralis major muscle. *Am J Sports Med*. 2004;32(5):1256-1262. doi:10.1177/0363546503261137

2. Abramowitch S, Easley D. Chapter Four - Introduction to Classical Mechanics. In: Hoyte L, Damaser MBT-B of the FPF, eds. Academic Press; 2016:89-107. doi:https://doi.org/10.1016/B978-0-12-803228-2.00004-0

3. Andersen E. Triceps tendon avulsion. *Injury*. 1986;17(4):279-280.

4. Anzel SH, Covey KW, Weiner AD, Lipscomb PR. Disruption of muscles and tendons: An analysis of 1,014 cases. *Surgery*. 1959;45(3):406-414. doi:10.5555/uri:pii:0039606059901989

5. Asinger DA, el-Khoury GY. Tensor fascia lata muscle tear: evaluation by MRI. *Iowa Orthop J*. 1998;18:146-149.

6. Aso K, Torisu T. Muscle belly tear of the triceps. *Am J Sports Med*. 1984;12(6):485-487. doi:10.1177/036354658401200614

7. Bach BR, Warren RF, Wickiewicz TL. Triceps rupture:A case report and literature review. *Am J Sports Med*. 1987;15(3):285-289. doi:10.1177/036354658701500319

8. Balius R, Alomar X, Pedret C, et al. Role of the Extracellular Matrix in Muscle Injuries: Histoarchitectural Considerations for Muscle Injuries. *Orthop J Sport Med*. 2018;6(9):2325967118795863-2325967118795863. doi:10.1177/2325967118795863

9. Basic-Jukic N, Juric I, Racki S, Kes P. Spontaneous tendon ruptures in patients with end-stage renal disease. *Kidney Blood Press Res*. 2009;32(1):32-36. doi:10.1159/000201792

10. Bass CJ, Connell DA. Sonographic findings of tensor fascia lata tendinopathy: Another cause of anterior groin pain. *Skeletal Radiol*. 2002;31(3):143-148. doi:10.1007/s00256-001-0459-7

11. Benazzo F, Marullo M, Pietrobono L. Supraspinatus rupture at the musculotendinous junction in a young woman. *J Orthop Traumatol*. 2013;15(3):231-234. doi:http://dx.doi.org/10.1007/s10195-013-0271-x

12. Benjamin M, Kumai T, Milz S, Boszczyk BM, Boszczyk AA, Ralphs JR. The skeletal attachment of tendons - Tendon "entheses." *Comp Biochem Physiol - A Mol Integr Physiol*. 2002;133(4):931-945. doi:10.1016/S1095-6433(02)00138-1

13. Benjamin M, Toumi H, Ralphs JR, Bydder G, Best TM, Milz S. Where tendons and ligaments meet bone: attachment sites ('entheses') in relation to exercise and/or mechanical load. *J Anat*. 2006;208(4):471-490. doi:10.1111/j.1469-7580.2006.00540.x

14. Bianchi S, Martinoli C, Waser NP, Bianchi-Zamorani MP, Federici E, Fasel J. Central aponeurosis tears of the rectus femoris: sonographic findings. *Skeletal Radiol*. 2002;31(10):581-586. doi:10.1007/s00256-002-0559-z

15. Bowers KDJ. Patellar tendon avulsion as a complication of Osgood-Schlatter's disease. *Am J Sports Med*. 1981;9(6):356-359. doi:10.1177/036354658100900603

16. Bunshah JJ, Raghuwanshi S, Sharma D, Pandita A. Triceps tendon rupture: An uncommon orthopaedic condition. *BMJ Case Rep*. 2015;2015. doi:10.1136/bcr-2014-206446

17. Butcher JD, Siekanowicz A, Pettrone F. Pectoralis Major Rupture: Ensuring Accurate Diagnosis and Effective Rehabilitation. *Phys Sportsmed*. 1996;24(3):37.

18. Canovas F, Nicolau F, Bonnel F. Avulsion of the flexor digitorum profundus tendon associated with a chondroma of the distal phalanx. *J Hand Surg Br*. 1998;23(1):130-131.

19. Carrino JA, Chandnanni VP, Mitchell DB, Choi-Chinn K, DeBerardino TM, Miller MD. Pectoralis major muscle and tendon tears: diagnosis and grading using magnetic resonance imaging. *Skeletal Radiol*. 2000;29(6):305-313.

20. Casanova R, And AC, Goepfert AR, Hueppchen NA, Weiss PM, American College of Obstetricians and Gynecologists. *Beckmann and Ling's Obstetrics and Gynecology*. 8th Editio. Philadelphia : Wolters Kluwer; 2019.

21. Cetinkaya E, Aydin CG, Akman YE, et al. A rare knee extensor mechanism injury: Vastus intermedius tendon rupture. *Int J Surg Case Rep*. 2015;14:186-188. doi:10.1016/j.ijscr.2015.07.035

22. Chauvin NA, Ho-Fung V, Jaramillo D, Edgar JC, Weiss PF. Ultrasound of the joints and entheses in healthy children. *Pediatr Radiol*. 2015;45(9):1344-1354. doi:10.1007/s00247-015-3313-0

23. Chen J, Kim J, Shao W, et al. An anterior cruciate ligament failure mechanism. *Am J Sports Med*. 2019;47(9):2067-2076. doi:10.1177/0363546519854450

24. Clay NR. A pulled muscle. Partial avulsion of the extensor indicis proprius tendon following a hyperflexion injury. *Injury*. 1988;19(2):127-128. doi:10.1016/0020-1383(88)90092-7

25. Connell DA, Jhamb A, James T. Side Strain: A Tear of Internal Oblique Musculature. *Am J Roentgenol*. 2003;181(6):1511-1517. doi:10.2214/ajr.181.6.1811511

26. Connell DA, Potter HG, Sherman MF, Wickiewicz TL. Injuries of the pectoralis major muscle: evaluation with MR imaging. *Radiology*. 1999;210(3):785-791. doi:10.1148/radiology.210.3.r99fe43785

27. Cooper ME, Selesnick FH. Partial rupture of the distal insertion of the patellar tendon: A report of two cases in professional athletes. *Am J Sports Med*. 2000;28(3):402-406.

28. Crema MD, Guermazi A, Tol JL, Niu J, Hamilton B, Roemer FW. Acute hamstring injury in football players: Association between anatomical location and extent of injury--A large single-center MRI report. *J Sci Med Sport*. 2016;19(4):317-322. doi:http://dx.doi.org/10.1016/j.jsams.2015.04.005

29. Cross TM, Gibbs N, Houang MT, Cameron M. Acute Quadriceps Muscle Strains: Magnetic Resonance Imaging Features and Prognosis. *Am J Sports Med*. 2004;32(3):710-719. doi:10.1177/0363546503261734

30. Depalma MJ, Perkins RH. Patellar Tendinosis: Acute Patellar Tendon Rupture and Jumper's Knee. *Phys Sportsmed*. 2004;32(5):41-45.

31. DeRoos WK, Zeeman RJ. A flexor tendon rupture in the palm of the hand. *J Hand Surg Am*. 1991;16(4):663-665.

32. DeSmet AA, Best TM. MR imaging of the distribution and location of acute hamstring injuries in athletes. *AJR Am J Roentgenol*. 2000;174(2):393-399. doi:10.2214/ajr.174.2.1740393

33. DeWaal Malefijt MC, Beeker TW. Avulsion of the triceps tendon in secondary hyper parathyroidism: A case report. *Acta Orthop*. 1987;58(4):434-435. doi:10.3109/17453678709146376

34. Dürig M, Schuppisser JP, Gauer EF, et al. Spontaneous rupture of the gastrocnemius muscle. *Injury*. 1977;9(2):143-145. doi:10.1016/0020-1383(77)90009-2

35. Entwisle T, Ling Y, Splatt A, Brukner P, Connell D. Distal Musculotendinous T Junction Injuries of the Biceps Femoris: An MRI Case Review. *Orthop J Sport Med*. 2017;5(7):2325967117714998. doi:10.1177/2325967117714998

36. Evans NA, Bowrey DJ, Newman GR. Ultrastructural analysis of ruptured tendon from anabolic steroid users. *Injury*. 1998;29(10):769-773. doi:10.1016/S0020-1383(98)00183-1

37. Fan L, Xu B, Liu N, Wang L. Histopathological changes in patellar tendon enthesis of rabbit induced by electrical stimulation intensity. *J Orthop Sci Off J Japanese Orthop Assoc*. 2020;25(2):344-348. doi:10.1016/j.jos.2019.04.007

38. Farley TE, Neumann CH, Steinbach LS, Jahnke AJ, Petersen SS. Full-thickness tears of the rotator cuff of the shoulder: diagnosis with MR imaging. *AJR Am J Roentgenol*. 1992;158(2):347-351. doi:10.2214/ajr.158.2.1729796

39. Farrar EL 3rd, Lippert FG 3rd, Farrar III EL, Lippert III FG. Avulsion of the triceps tendon. *Clin Orthop Relat Res*. 1981;No. 161(161):242-246.

40. Ferretti A, Ippolito E, Mariani P, Puddu G. Jumper's knee. *Am J Sports Med*. 1983;11(2):58-62. doi:10.1177/036354658301100202

41. Ferretti A, Puddu G, Mariani PP, Neri M. The natural history of jumper's knee. Patellar or quadriceps tendonitis. *Int Orthop*. 1985;8(4):239-242. doi:10.1007/bf00266866

42. Fitzpatrick D, Cagle P, Flatow E. Isolated Teres Major Rupture: A case report with a suggested dedicated imaging protocol and review of the literature. *J Radiol Case Rep*. 2016;10(4):31-36.

doi:10.3941/jrcr.v10i4.2674

43. Fleckenstein JL, Weatherall PT, Parkey RW, Payne JA, Peshock RM. Sports-related muscle injuries: evaluation with MR imaging. *Radiology*. 1989;172(3):793-798. doi:10.1148/radiology.172.3.2772190

44. Floor S, Van Der Veen AH, Devilee RJ. Two patients with a complete proximal rupture of the hamstring. *Arch Orthop Trauma Surg*. 2010;130(4):523-526. doi:10.1007/s00402-009-0950-5

45. Freccero DM, Berkowitz MJ. The relationship between tears of the peroneus brevis tendon and the distal extent of its muscle belly: an MRI study. *Foot ankle Int*. 2006;27(4):236-239. doi:10.1177/107110070602700402

46. Gagnier JJ, Riley D, Altman DG, Moher D, Sox H, Kienle G. The CARE guidelines: consensus-based clinical case reporting guideline development. *Dtsch Arztebl Int*. 2013;110(37):603-608. doi:10.3238/arztebl.2013.0603

47. Garrett WEJ, Nikolaou PK, Ribbeck BM, Glisson RR, Seaber A V. The effect of muscle architecture on the biomechanical failure properties of skeletal muscle under passive extension. *Am J Sports Med*. 1988;16(1):7-12. doi:10.1177/036354658801600102

48. Garrett WEJ, Safran MR, Seaber A V, Glisson RR, Ribbeck BM. Biomechanical comparison of stimulated and nonstimulated skeletal muscle pulled to failure. *Am J Sports Med*. 1987;15(5):448-454. doi:10.1177/036354658701500504

49. Gaskin CM, Anderson MW, Choudhri A, Diduch DR. Focal partial tears of the long head of the biceps brachii tendon at the entrance to the bicipital groove: MR imaging findings, surgical correlation, and clinical significance. *Skeletal Radiol*. 2009;38(10):959-965. doi:http://dx.doi.org/10.1007/s00256-009-0720-z

50. Gidwani S, Bircher MD. Avulsion injuries of the hamstring origin - A series of 12 patients and management algorithm. *Ann R Coll Surg Engl*. 2007;89(4):394-399. doi:10.1308/003588407X183427

51. Giuffre BM, Lisle DA. Case Report: Tear of the distal biceps branchii tendon: A new method of ultrasound evaluation. *Australas Radiol*. 2005;49(5):404-406. doi:http://dx.doi.org/10.1111/j.1440-1673.2005.01469.x

52. Godoy IRB, Martinez-Salazar EL, Simeone FJ, Bredella MA, Palmer WE, Torriani M. MRI of pectoralis major tears: association between ancillary findings and tear severity. *Skeletal Radiol*. 2018;47(8):1127-1135. doi:http://dx.doi.org/10.1007/s00256-018-2893-9

53. Goodier D, Maffulli N, Good CJ, Good J. Tibial tuberosity avulsion associated with patellar tendon avulsion. *Acta Orthop Belg*. 1994;60(2):336-338.

54. Gottsauner-Wolf F, Grabowski JJ, Chao EY, An KN. Effects of freeze/thaw conditioning on the tensile properties and failure mode of bone-muscle-bone units: a biomechanical and histological study in dogs. *J Orthop Res*. 1995;13(1):90-95. doi:10.1002/jor.1100130114

55. Gruel JB. Isolated avulsion of the popliteus tendon. *Arthroscopy*. 1990;6(2):94-95.

56. Gyftopoulos S, Rosenberg ZS, Schweitzer ME, Bordalo-Rodrigues M. Normal anatomy and strains of the deep musculotendinous junction of the proximal rectus femoris: MRI features. *AJR Am J Roentgenol*. 2008;190(3):W182-6. doi:10.2214/AJR.07.2947

57. Hart ES. Acute Quadriceps Tendon Rupture. *Orthop Nurs*. 2013;32(1):53-54.

58. Hasegawa K, Schofer JM. Rupture of the Pectoralis Major: A Case Report and Review. *J Emerg Med*. 2010;38(2):196-200. doi:10.1016/j.jemermed.2008.01.025

59. Hasselman CT, Best TM, Seaber A V, Garrett WEJ. A threshold and continuum of injury during active stretch of rabbit skeletal muscle. *Am J Sports Med*. 1995;23(1):65-73. doi:10.1177/036354659502300111

60. Heiderscheit BC, Hoerth DM, Chumanov ES, Swanson SC, Thelen BJ, Thelen DG. Identifying the time of occurrence of a hamstring strain injury during treadmill running: A case study. *Clin Biomech*. 2005;20(10):1072-1078. doi:https://doi.org/10.1016/j.clinbiomech.2005.07.005

61. Heinemeier KM, Schjerling P, Heinemeier J, Magnusson SP, Kjaer M. Lack of tissue renewal in human adult Achilles tendon is revealed by nuclear bomb (14)C. *FASEB J*. 2013;27(5):2074-2079.

doi:10.1096/fj.12-225599

62. Henry JC, Scerpella TA. Acute traumatic tear of the latissimus dorsi tendon from its insertion: A case report. *Am J Sports Med*. 2000;28(4):577-579.

63. Hertel R, Lambert SM. Supraspinatus rupture at the musculotendinous junction. *J shoulder Elb Surg*. 1998;7(4):432-435.

64. Hughes C 4th, Hasselman CT, Best TM, Martinez S, Garrett WEJ. Incomplete, intrasubstance strain injuries of the rectus femoris muscle. *Am J Sports Med*. 1995;23(4):500-506. doi:10.1177/036354659502300422

65. Huri G, Dubin JM, Ozgonen K, Kaya D, Doral MN. A unique rectus femoris injury in an adolescent professional soccer player: A case report. *JBJS Case Connect*. 2014;4(4). doi:10.2106/JBJS.CC.M.00290

66. Ilaslan H, Iannotti JP, Recht MP. Deltoid muscle and tendon tears in patients with chronic rotator cuff tears. *Skeletal Radiol*. 2007;36(6):503-507. doi:10.1007/s00256-007-0279-5

67. Irmola T, Heikkilä JT, Orava S, Sarimo J. Total proximal tendon avulsion of the rectus femoris muscle. *Scand J Med Sci*. 2007;17(4):378-382. doi:http://dx.doi.org/10.1111/j.1600-0838.2006.00564.x

68. Jaiswal A, Kacchap ND, Tanwar YS, Kumar D, Kumar B. Rupture of the triceps tendon – A case series. *Chinese J Traumatol - English Ed*. 2016;19(4):235-238. doi:10.1016/j.cjtee.2016.06.006

69. Jansen JA, Cormier S, Patel J V. Acute rectus femoris rupture at the distal musculotendinous junction in a football player: A case report and surgical technique. *Curr Orthop Pract*. 2012;23(4):390-392. doi:10.1097/BCO.0b013e31825b2249

70. Järvinen TAH, Järvinen TLN, Kääriäinen M, Kalimo H, Järvinen M. Muscle injuries: biology and treatment. *Am J Sports Med*. 2005;33(5):745-764. doi:10.1177/0363546505274714

71. Kameyama M, Shiraishi T. Traumatic rupture of the extensor digitorum communis and extensor digiti minimi at the musculotendinous junction associated with volar dislocation of the distal radioulnar joint--a case report. *Hand Surg*. 2000;5(2):165-168.

72. Kankaya Y, Oruç M, Uysal A, Koçer U. Multiple Closed flexor Tendon Avulsions From Their Insertions by a High-energy Explosion. *J Hand Surg Am*. 2006;31(6):663-664. doi:10.1016/j.jhsb.2006.07.014

73. Karjalainen PT, Soila K, Aronen HJ, et al. MR imaging of overuse injuries of the Achilles tendon. *AJR Am J Roentgenol*. 2000;175(1):251-260. doi:10.2214/ajr.175.1.1750251

74. Kawashima M, Sato M, Torisu T, Himeno R, Iwabuchi A. Rupture of the pectoralis major. Report of 2 cases. *Clin Orthop Relat Res*. 1975;(109):115-119. doi:10.1097/00003086-197506000-00015

75. Khiami F, Tavassoli S, De Ridder Baeur L, Catonné Y, Sariali E. Distal partial ruptures of triceps brachii tendon in an athlete. *Orthop Traumatol Surg Res*. 2012;98(2):242-246. doi:10.1016/j.otsr.2011.09.022

76. Kibuule LK, Fehringer E V. Distal triceps tendon rupture and repair in an otherwise healthy pediatric patient: A case report and review of the literature. *J Shoulder Elb Surg*. 2007;16(3):e1-e3. doi:10.1016/j.jse.2006.06.002

77. Kilkenny C, Browne WJ, Cuthill IC, Emerson M, Altman DG. Improving Bioscience Research Reporting: The ARRIVE Guidelines for Reporting Animal Research. *PLOS Biol*. 2010;8(6):e1000412.

78. Kim TK, Rauh PB, McFarland EG. Partial tears of the subscapularis tendon found during arthroscopic procedures on the shoulder: A statistical analysis of sixty cases. *Am J Sports Med*. 2003;31(5):744-750.

79. Law DJ, Caputo A, Tidball JG. Site and mechanics of failure in normal and dystrophin-deficient skeletal muscle. *Muscle Nerve*. 1995;18(2):216-223. doi:10.1002/mus.880180211

80. Lempainen L, Sarimo J, Mattila K, Heikkilä J, Orava S. Distal tears of the hamstring muscles: Review of the literature and our results of surgical treatment. *Br J Sports Med*. 2007;41(2):80-83. doi:10.1136/bjsm.2006.031211

81. Levine JW, Savoie III FH. Traumatic rupture of the latissimus dorsi. *Orthopedics*. 2008;31(8):799. doi:10.3928/01477447-20080801-14

82. Lian Ø, Scott A, Engebretsen L, Bahr R, Duronio V, Khan K. Excessive Apoptosis in Patellar Tendinopathy in Athletes. *Am J Sports Med*. 2007;35(4):605-611. doi:10.1177/0363546506295702

83. Lipps DB, Wojtys EM, Ashton-Miller JA. Anterior cruciate ligament fatigue failures in knees subjected to repeated simulated pivot landings. *Am J Sports Med*. 2013;41(5):1058-1066. doi:10.1177/0363546513477836

84. Lukac D, Jakovljevic DK, Klasnja A, Drapsin M, Slavic D, Karan V. Ultrasonographic evaluation of the ruptured medial head of gastrocnemius muscle . *Rev Bras Med do Esporte*. 2016;22(5):381-385. doi:10.1590/1517-869220162205158755

85. Lunn J V, Castellanos-Rosas J, Tavernier T, Barthelemy R, Walch G. A novel lesion of the infraspinatus characterized by musculotendinous disruption, edema, and late fatty infiltration. *J shoulder Elb Surg*. 2008;17(4):546-553. doi:10.1016/j.jse.2007.11.016

86. Maehara H, Sakaguchi Y. Avulsion Fracture of the Medial Head of the Gastrocnemius Muscle: A Case Report. *J Bone Jt Surg - Ser A*. 2004;86(2):373-375. doi:10.2106/00004623-200402000-00024

87. Maffulli N. The clinical diagnosis of subcutaneous tear of the Achilles tendon: A prospective study in 174 patients. *Am J Sports Med*. 1998;26(2):266-270.

88. Mair SD, Seaber A V, Glisson RR, Garrett WE, Garrett Jr. WE. The role of fatigue in susceptibility to acute muscle strain injury. *Am J Sports Med*. 1996;24(2):137-143. doi:10.1177/036354659602400203

89. Makridis KG, Lequesne M, Bard H, Djian P. Clinical and MRI results in 67 patients operated for gluteus medius and minimus tendon tears with a median follow-up of 4.6 years. *Orthop Traumatol Surg Res*. 2014;100(8):849-853. doi:10.1016/j.otsr.2014.08.004

90. Mansat P, Frankle MA, Cofield RH. Tears in the subscapularis tendon: Descriptive analysis and results of surgical repair. *Jt Bone Spine*. 2003;70(5):342-347. doi:10.1016/S1297-319X(03)00044-7

91. Mechrefe AP, Walsh EF, DiGiovanni CW. Anterior tibial tendon avulsion with distal tibial fracture entrapment: case report. *Foot ankle Int*. 2006;27(8):645-647. doi:10.1177/107110070602700816

92. Mellado JM, Calmet J, Giné J, Saurí A. Pectoralis major muscle and tendon tears: Report of two cases with surgical correlation and postoperative follow-up. *Eur J Radiol Extra*. 2004;50(3):101-104. doi:10.1016/j.ejrex.2004.03.005

93. Menz P, Nettle WJ. Closed rupture of the musculotendinous junction of extensor hallucis longus. *Injury*. 1989;20(6):378-381.

94. Micheli LJ, Fehlandt AFJ. Overuse injuries to tendons and apophyses in children and adolescents. *Clin Sports Med*. 1992;11(4):713-726.

95. Millar NL, Hueber AJ, Reilly JH, et al. Inflammation is Present in Early Human Tendinopathy. *Am J Sports Med*. 2010;38(10):2085-2091. doi:10.1177/0363546510372613

96. Miller WA. Rupture of the musculotendinous juncture of the medial head of the gastrocnemius muscle. *Am J Sports Med*. 1977;5(5):191-193. doi:10.1177/036354657700500505

97. Miranda MO, Bureau NJ. Supraspinatus Myotendinous Junction Injuries: MRI Findings and Prevalence. *AJR Am J Roentgenol*. 2019;212(1):W1-W9. doi:10.2214/AJR.18.19776

98. Moher D, Liberati A, Tetzlaff J, Altman DG, Group TP. Preferred Reporting Items for Systematic Reviews and Meta-Analyses: The PRISMA Statement. *PLOS Med*. 2009;6(7):e1000097.

99. Naito K, Homma Y, Morita M, Mogami A, Obayashi O. Triceps tendon avulsion: a case report and discussion about the olecranon ossification nucleus. *Eur J Orthop Surg Traumatol*. 2013;23 Suppl 2:S193-6. doi:10.1007/s00590-012-1127-4

100. Netter FH, 1906-1991. *Atlas of Human Anatomy*. 6th Editio. Saunders/Elsevier; 2014.

101. Ng BH, Chou SM, Krishna V. The Influence of Gripping Techniques on the Tensile Properties of Tendons. *Proc Inst Mech Eng Part H J Eng Med*. 2005;219(5):349-354. doi:10.1243/095441105X34239

102. Nimityongskul P, Montague WL, Anderson LD. Avulsion fracture of the tibial tuberosity in late

adolescence. *J Trauma - Inj Infect Crit Care*. 1988;28(4):505-509. doi:10.1097/00005373-198804000-00015

103. Nishida Y, Tsukushi S, Yamada Y, Hosono K, Ishiguro N. Brachialis Muscle Tear Mimicking an Intramuscular Tumor: A Report of Two Cases. *J Hand Surg Am*. 2007;32(8):1237-1241. doi:10.1016/j.jhsa.2007.06.002

104. Noonan TJ, Best TM, Seaber A V, Garrett WEJ. Identification of a threshold for skeletal muscle injury. *Am J Sports Med*. 1994;22(2):257-261. doi:10.1177/036354659402200217

105. Ohashi K, El-Khoury GY, Albright JP, Tearse DS. MRI of complete rupture of the pectoralis major muscle. *Skeletal Radiol*. 1996;25(7):625-628.

106. Panni AS, Tartarone M, Maffulli N. Patellar tendinopathy in athletes. Outcome of nonoperative and operative management. *Am J Sports Med*. 2000;28(3):392-397. doi:10.1177/03635465000280031901

107. Pedret C, Balius R, Barcelo P, et al. Isolated tears of the gracilis muscle. *Am J Sports Med*. 2011;39(5):1077-1080. doi:10.1177/0363546510394436

108. Pina A, Garcia I, Sabater M. Traumatic avulsion of the triceps brachii. *J Orthop Trauma*. 2002;16(4):273-276. doi:10.1097/00005131-200204000-00010

109. Pitts RT, Garner HW, Ortiguera CJ. Pectoralis major avulsion in a skeletally immature wrestler: A case report. *Am J Sports Med*. 2010;38(5):1034-1037. doi:10.1177/0363546509351559

110. Pochini A de C, Ejnisman B, Andreoli C V, et al. Pectoralis major muscle rupture in athletes: A prospective study. *Am J Sports Med*. 2010;38(1):92-98. doi:10.1177/0363546509347995

111. Pomeranz SJ, Heidt RSJ. MR imaging in the prognostication of hamstring injury. Work in progress. *Radiology*. 1993;189(3):897-900. doi:10.1148/radiology.189.3.8234722

112. Qazi TH, Duda GN, Ort MJ, Perka C, Geissler S, Winkler T. Cell therapy to improve regeneration of skeletal muscle injuries. *J Cachexia Sarcopenia Muscle*. 2019;10(3):501-516. doi:https://doi.org/10.1002/jcsm.12416

113. Rajasekhar C, Kakarlapudi TK, Bhamra MS. Avulsion of the triceps tendon. *Emerg Med J*. 2002;19(3):271-272.

114. Rehorn MR, Blemker SS. The effects of aponeurosis geometry on strain injury susceptibility explored with a 3D muscle model. *J Biomech*. 2010;43(13):2574-2581. doi:https://doi.org/10.1016/j.jbiomech.2010.05.011

115. Renström P, Hach T. Insertional Tendinopathy in Sports. In: Maffulli N, Renstrom P, Leadbetter WB, eds. *Tendon Injuries*. Springer-Verlag London; 2005:70-85. doi:10.1007/b137778

116. Rochman R, SanGiovanni TP, Uribe JW. Muscle belly tears of the peroneal muscles: A case report. *Foot Ankle Int*. 2006;27(12):1159-1160. doi:10.1177/107110070602701227

117. Roe M, Murphy JC, Gissane C, Blake C. Hamstring injuries in elite Gaelic football: an 8-year investigation to identify injury rates, time-loss patterns and players at increased risk. *Br J Sports Med*. 2018;52(15):982-988. doi:10.1136/bjsports-2016-096401

118. Roh MS, Wang VM, April EW, Pollock RG, Bigliani LU, Flatow EL. Anterior and posterior musculotendinous anatomy of the supraspinatus. *J Shoulder Elb Surg*. 2000;9(5):436-440. doi:10.1067/mse.2000.108387

119. Rose PS, Frassica FJ. Atraumatic bilateral patellar tendon rupture: A case report and review of the literature. *J Bone Jt Surg*. 2001;83(9):1382-1386.

120. Rothrauff BB, Tuan RS. Cellular therapy in bone-tendon interface regeneration. *Organogenesis*. 2014;10(1):13-28. doi:10.4161/org.27404

121. Sano H, Ishii H, Yeadon A, Backman DS, Brunet JA, Uhthoff HK. Degeneration at the insertion weakens the tensile strength of the supraspinatus tendon: a comparative mechanical and histologic study of the bone-tendon complex. *J Orthop Res*. 1997;15(5):719-726. doi:10.1002/jor.1100150514

122. Schache AG, Koulouris G, Kofoed W, Morris HG, Pandy MG. Rupture of the conjoint tendon at the proximal musculotendinous junction of the biceps femoris long head: A case report. *Knee Surgery, Sport Traumatol Arthrosc*. 2008;16(8):797-802. doi:10.1007/s00167-008-0517-y

123. Shah S, Montgomery W, Bastidas M. A unique myotendinous avulsion injury of the achilles tendon.

Curr Orthop Pract. 2009;20(4):464-466. doi:10.1097/BCO.0b013e31819cadf1

124. Sharma P, Vijayargiya M, Tandon S, Gaur S. Triceps tendon avulsion: a rare injury. *Ethiop J Health Sci*. 2014;24(1):97-99. doi:10.4314/ejhs.v24i1.14

125. Shaw HM, Benjamin M. Structure-function relationships of entheses in relation to mechanical load and exercise. *Scand J Med Sci Sports*. 2007;17(4):303-315. doi:10.1111/j.1600-0838.2007.00689.x

126. Sherman OH, Snyder SJ, Fox JM. Triceps tendon avulsion in a professional body builder. A case report. *Am J Sports Med*. 1984;12(4):328-329. doi:10.1177/036354658401200415

127. Shields CL, Ashby ME. Diagnosis in patellar tendon avulsion. *J Natl Med Assoc*. 1975;67(3):231-232.

128. Sierra RJ, Weiss NG, Shrader MW, Steinmann SP. Acute triceps ruptures: Case report and retrospective chart review. *J Shoulder Elb Surg*. 2006;15(1):130-134. doi:10.1016/j.jse.2005.01.004

129. Silder A, Heiderscheit BC, Thelen DG, Enright T, Tuite MJ. MR observations of long-term musculotendon remodeling following a hamstring strain injury. *Skeletal Radiol*. 2008;37(12):1101-1109. doi:10.1007/s00256-008-0546-0

130. Simonet WT, Saylor III HL, Sim L. Abdominal wall muscle tears in hockey players. *Int J Sports Med*. 1995;16(2):126-128. doi:10.1055/s-2007-972978

131. Singh RK, Pooley J. Complete rupture of the triceps brachii muscle. *Br J Sports Med*. 2002;36(6):467. doi:http://dx.doi.org/10.1136/bjsm.36.6.467

132. Smith JH. Avulsion of a profundus tendon with simultaneous intraarticular fracture of the distal phalanx—Case report. *J Hand Surg Am*. 1981;6(6):600-601. doi:10.1016/S0363-5023(81)80141-4

133. Sollender JL, Rayan GM, Barden GA. Triceps tendon rupture in weight lifters. *J shoulder Elb Surg*. 1998;7(2):151-153.

134. Sonnery-Cottet B, Edwards TB, Noel E, Walch G. Rotator cuff tears in middle-aged tennis players: Results of surgical treatment. *Am J Sports Med*. 2002;30(4):558-564.

135. Speer KP, Lohnes J, Garrett WEJ. Radiographic imaging of muscle strain injury. *Am J Sports Med*. 1993;21(1):89-95; discussion 96. doi:10.1177/036354659302100116

136. Stauber T, Blache U, Snedeker JG. Tendon tissue microdamage and the limits of intrinsic repair. *Matrix Biol*. 2020;85-86:68-79. doi:https://doi.org/10.1016/j.matbio.2019.07.008

137. Street CC, Burks RT. Chronic complete hamstring avulson causing foot drop: A case report. *Am J Sports Med*. 2000;28(4):574-576. doi:10.1177/03635465000280042201

138. Sullivan JC, Best TM. Injury of the Musculotendinous Junction. In: Maffulli N, Renstrom P, Leadbetter WB, eds. *Tendon Injuries*. Springer-Verlag London; 2005:63-69. doi:10.1007/b137778

139. Sun J-SS, Tsuang Y-HH, Liu T-KK, Hang Y-SS, Cheng C-KK. Failure sites and peak tensile forces of the composite triceps surae muscle by passive extension in the rabbit. *Clin Biomech*. 1994;9(5):310-314. doi:10.1016/0268-0033(94)90044-2

140. Tadros AS, Huang BK, Pathria MN. Muscle-Tendon-Enthesis Unit. *Semin Musculoskelet Radiol*. 2018;22(03):263-274. doi:10.1055/s-0038-1641570

141. Takami H, Takahashi S, Ando M, Kabata K. Rupture of the flexor pollicis longus tendon at the musculotendinous junction in a bowler. *Arch Orthop Trauma Surg*. 1998;117(4-5):277-278.

142. Takami H, Takahashi S, Ando M, Suzuki K. Traumatic rupture of the extensor tendons at the musculotendinous junction. *J Hand Surg Am*. 1995;20(3):474-477. doi:10.1016/S0363-5023(05)80110-8

143. Taylor DC, Dalton JDJ, Seaber A V, Garrett WEJ. Experimental muscle strain injury. Early functional and structural deficits and the increased risk for reinjury. *Am J Sports Med*. 1993;21(2):190-194. doi:10.1177/036354659302100205

144. Temple HT, Kuklo TR, Sweet DE, Gibbons CL, Murphey MD. Rectus femoris muscle tear appearing as a pseudotumor. *Am J Sports Med*. 1998;26(4):544-548. doi:10.1177/03635465980260041301

145. Thorpe CT, Riley GP, Birch HL, Clegg PD, Screen HRC. Fascicles and the interfascicular matrix show decreased fatigue life with ageing in energy storing tendons. *Acta Biomater*. 2017;56:58-64. doi:https://doi.org/10.1016/j.actbio.2017.03.024

146. Tiger E, Mayer DP, Glazer R. Complete avulsion of the triceps tendon: MRI diagnosis. *Comput Med Imaging Graph*. 1993;17(1):51-54. doi:10.1016/0895-6111(93)90074-W

147. Toczylowski HM, Balint CR, Steiner ME, Boardman M, Scheller Jr. AD. Complete rupture of the distal biceps brachii tendon in female patients: A report of 2 cases. *J Shoulder Elb Surg*. 2002;11(5):516-518. doi:10.1067/mse.2002.126617

148. Towers JD, Russ E V, Golla SK. Biomechanics of Tendons and Tendon Failure. *Semin Musculoskelet Radiol*. 2003;07(01):59-66. doi:10.1055/s-2003-41085

149. Tsuang Y-H, Sun J-S, Chen I-H, et al. The effects of cyclic stretching on tensile properties of the rabbit's skeletal muscle. *Clin Biomech (Bristol, Avon)*. 1998;13(1):48-53.

150. Tung GA, Yoo DC, Levine SM, Brody JM, Green A. Subscapularis Tendon Tear: Primary and Associated Signs on MRI. *J Comput Assist Tomogr*. 2001;25(3):417-424.

151. Valente M, Mancuso F, Alecci V. Isolated rupture of biceps femoris tendon. *Musculoskelet Surg*. 2013;97(3):263-266. doi:10.1007/s12306-011-0171-2

152. Vandenbroucke JP, von Elm E, Altman DG, et al. Strengthening the Reporting of Observational Studies in Epidemiology (STROBE): Explanation and Elaboration. *PLOS Med*. 2007;4(10):e297.

153. VanDusen K, Larkin L. Muscle-tendon interface. In: *Regenerative Engineering of Musculoskeletal Tissues and Interfaces*. ; 2015:409-429. doi:10.1016/B978-1-78242-301-0.00017-3

154. Vastamäki M, Brummer H, Solonen KA. Avulsion of the distal biceps brachii tendon. *Acta Orthop*. 1981;52(1):45-48. doi:10.3109/17453678108991757

155. Wagner JR, Cooney WP. Rupture of the triceps muscle at the musculotendinous junction: a case report. *J Hand Surg Am*. 1997;22(2):341-343. doi:10.1016/S0363-5023(97)80175-X

156. Walch G, Nove-Josserand L, Liotard J-P, Noel E. Musculotendinous infraspinatus ruptures: an overview. *Orthop Traumatol Surg Res*. 2009;95(7):463-470. doi:10.1016/j.otsr.2009.06.004

157. Wang Y-C, Jeng C-M, Shen P-W, et al. Pectoralis major muscle tear diagnosed with magnetic resonance imaging and ultrasound - A case report. *Tzu Chi Med J*. 2005;17(6):441-444+456.

158. Warme WJ, Whitaker DC. Pectoralis major tendon avulsion from rappelling. *Mil Med*. 2004;169(2):151-154. doi:10.7205/milmed.169.2.151

159. Weishaupt D, Schweitzer ME, Morrison WB. Injuries to the distal gastrocnemius muscle: MR findings. *J Comput Assist Tomogr*. 2001;25(5):677-682.

160. Wenger DR. Avulsion of the Profundus Tendon Insertion in Football Players. *Arch Surg*. 1973;106(2):145-149. doi:10.1001/archsurg.1973.01350140013006

161. White GM, Riley Jr. LH. Isolated avulsion of the subscapularis insertion in a child. A case report. *J Bone Jt Surg - Ser A*. 1985;67(4):635-636. doi:10.2106/00004623-198567040-00021

162. Williams BD, Schweitzer ME, Weishaupt D, et al. Partial tears of the distal biceps tendon: MR appearance and associated clinical findings. *Skeletal Radiol*. 2001;30(10):560-564. doi:10.1007/s002560100397

163. Winblad JB, Escobedo E, Hunter JC. Brachialis Muscle Rupture and Hematoma. *Radiol Case Reports*. 2008;3(4):251. doi:10.2484/rcr.v3i4.251

164. Yoon MY, Koris MJ, Ortiz JA, Papandrea RF. Triceps avulsion, radial head fracture, and medial collateral ligament rupture about the elbow: A report of 4 cases. *J Shoulder Elb Surg*. 2012;21(2):e12-e17. doi:10.1016/j.jse.2011.06.017

165. Yoshioka H, Anno I, Niitsu M, Takahashi H, Matsumoto K, Itai Y. MRI of muscle strain injuries. *J Comput Assist Tomogr*. 1994;18(3):454-460.

166. Zantop T, Brucker PU, Vidal A, Zelle BA, Fu FH. Intraarticular rupture pattern of the ACL. *Clin Orthop Relat Res*. 2007;454:48-53. doi:10.1097/BLO.0b013e31802ca45b

Chapter 2

Pelvic floor muscle injury during a difficult labor

Can tissue fatigue damage play a role?

Pelvic floor muscle injury during a difficult labor

Can tissue fatigue damage play a role?

Maria C.P. Vila Pouca[1,2], Marco P.L. Parente[1,2], Renato M. Natal Jorge[1,2], John O.L. DeLancey[3,] James A. Ashton-Miller[4]

1 Department of Mechanical Engineering, Faculty of Engineering of University of Porto, Porto, Portugal

2 Institute of Science and Innovation in Mechanical and Industrial Engineering, Porto, Portugal

3 Department of Obstetrics and Gynecology, University of Michigan Medical School, Ann Arbor, Michigan, USA

4 Departments of Mechanical and Biomedical Engineering, College of Engineering and School of Kinesiology, University of Michigan, Ann Arbor, Michigan, USA

Published In

International Urogynecology Journal

DOI: https://doi.org/ 10.1007/s00192-021-05012-5

Article Type: Clinical Opinion

Submitted: August 2, 2021

Accepted: October 12, 2021

Abstract

Pubovisceral muscle (PVM) injury during a difficult vaginal delivery leads to pelvic organ prolapse later in life. If one could address how and why the muscle injury originates, one might be able to better prevent these injuries in the future.

In a recent review we concluded that many atraumatic injuries of the muscle-tendon unit are consistent with it being weakened by an accumulation of passive tissue damage during repetitive loading. While the PVM can tear due to a single overstretch at the end of the second stage of labor we hypothesize that it can also be weakened by an accumulation of microdamage and then tear after a series of submaximal loading cycles. We conclude that there is strong indirect evidence that low cycle fatigue of PVM passive tissue is a possible mechanism of its proximal failure. This has implications for finding new ways to better prevent PVM injury in the future.

Keywords: difficult vaginal delivery; repetitive pushing; material fatigue; pelvic muscle injury

2.1. Introduction

Pelvic floor muscle injury occurs in 13 to 41% of the women who deliver vaginally[17,29], usually during a first birth[24]. The injury often involves the proximal pubovisceral muscle (PVM) near its origin from the pubic bone[17] (Figure 2.1). The PVM is a critical portion of the levator ani muscle complex that helps to hold the pelvic floor closed and support the pelvic organs; it is sometimes also called the pubococcygeal muscle. PVM injuries have been associated with the development of pelvic organ prolapse[6] later in life, significantly affecting women's quality of life[9], and often resulting in the need for surgery. Unfortunately, this surgery has a failure rate of approximately 30%[2], so preventing the injury in the first place would be desirable. This raises the following question addressed in this paper: What do we know about injuries of the muscle-tendon unit in other parts of the body and how might this help inform our understanding of birth induced injury?

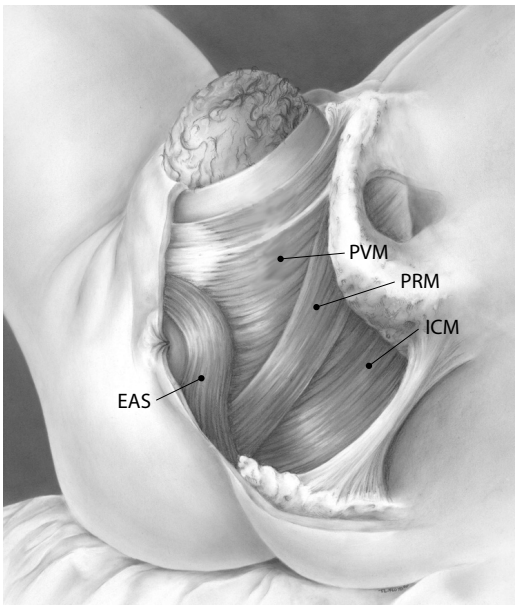

Figure 2.1 - A left inferior view illustrating the pubovisceral muscle (PVM), which originates behind the pubic bone and forms the most distal portion of the levator ani muscle. It is particularly stretched late in the second stage of labor as the fetal head is driven by strong 2-3 maternal pushes, at three minutes intervals, through the birth canal to crown. EAS: External anal sphincter; ICM: iliococcygeal muscle; PRM: Puborectal muscle; ©DeLancey.

A recent systematic review of 3,246 musculoskeletal injuries (including partial or complete tears, whether in the tendon, the musculotendinous junction, the tendon-bone junction, or the muscle belly; tendinopathy, whether in the tendon-bone junction or tendon midsubstance; tendon avulsions, defined as a complete detachment of the tendon from the bone while containing a small fragment of bone and musculotendinous strains if verified using magnetic resonance imaging, computed tomography scans, or surgery) found 35% of the injuries within the tendon, 28% in the musculotendinous junction, 18% at the tendon-bone interface, 13% within the muscle belly and 6% tendon avulsions that included a bony fragment[38]. There was an age effect in that the mean

ages at injury were 29 years for the muscle belly, 33 years for tendon avulsion, 34 years for musculotendinous junction, 47 years for tendon mid-substance injuries and 51 years for tendon-bone interface. Only 13% of all injuries were linked to evident trauma such as a fall, a work or car accident, or sports injuries sustained during collisions or tackles involving high tensile loading rates: 63% were tendon avulsion injuries, 15% being tendon mid-substance injuries, 8% musculotendinous junction injuries, 3% muscle belly injuries and 2% being tendon-bone junction injuries. Since the preponderance, 87%, of injuries were not associated with evident trauma and occurred in well-trained athletes (professional, collegiate and high-schoolers) and people previously or currently actively engaged in sports activity, we have argued in Vila Pouca et al [38] that many of these atraumatic injuries may therefore be due to passive tissue fatigue failure: namely repeated sub-maximal loading cycles causing an accumulation of microdamage that progressively weakens the passive tissue in the muscle-tendon unit until it fails under a normal sub-maximal loading cycle.

The reason for this proposition is that microdamage accumulation, in the form of collagen unravelling has been demonstrated at the origin of a passive, Type 1 collagen structure, the anterior cruciate ligament (ACL), following repetitive sub-maximal loading [4], and in the form of collagen denaturation when a tendon reaches its yield point [14,42]. Microdamage accumulation under repetitive loading has also been reported at the musculotendinous junction of rabbit leg muscles (for example [25]) and it has led to complete structural failure of tendon *in vitro* (for example [26]) as well as *in vivo*[1]. These examples of damage mechanisms weakening a tensile structure under repetitive sub-maximal loads until it fails are consistent with the phenomenon of low-cycle tissue fatigue[e] whereby, in biological tissue, the rate of damage accumulation exceeds the rate at which the tissue can repair itself.

What is the mechanism of low cycle tissue fatigue[f]? It is widely known in material science that when a large enough tensile load is applied to a structure, the structure will fail in one loading cycle due to the stress or strain in the material exceeding that which it can withstand without failing (Figure 2.2). In low-cycle tissue fatigue[f], however, two or more sub-maximal loading cycles, neither of which are intense enough to induce failure by themselves, cause a sufficient number of defects to appear, coalesce and accumulate with each cycle so as to weaken the material to the extent that it fails (tears) partially or even completely under the next sub-maximal cycle (Figure 2.3). An additional characteristic of low cycle fatigue behavior is that the lower the load being applied repetitively, the greater the number of loading cycles the structure will withstand before failing, and vice versa[16]. Let us say the second stage of labor lasts, say, two hours in

[e] Note: The term tissue 'fatigue' in this context has nothing to do with muscle fatigue which is a completely different physiological process adversely affecting the ability of muscle to generate contractile force.

[f] For the purpose of this paper, as we shall see, the 'low' in low cycle fatigue refers to between 2 to 120 loading cycles.

nullipara[11], and a maternal push is timed to coincide with the uterine contraction every 3 minutes[12] this would require up to 40 pushes by the nullipara. If coached, the maternal push can be performed up to 2-3 times per contraction[10], which would require up to 80-120 pushes by the nullipara. Any structure that fails under 2 to 120 loading cycles due to an accumulation of microdamage weakening can be described as failing due to low cycle material fatigue[g].

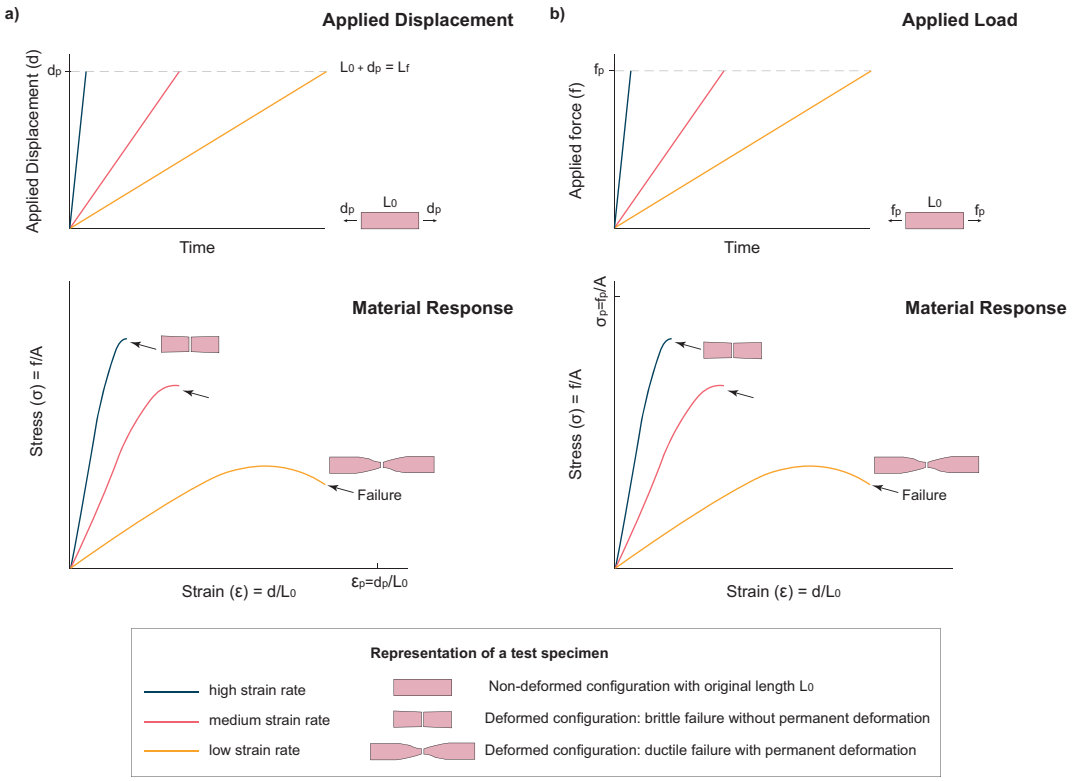

Figure 2.2 - Schematic illustration showing the relationship between material stress[h] and strain[i] as a tissue fails under an applied displacement **(a)** or applied load **(b)** load in a single loading cycle at each of three loading rates. The top row at left is the case when a linearly increasing displacement is applied to the material, at right **(b)** is the case when the same material is loaded instead by a linearly increasing tensile force. In the top row of **(a)** and **(b)** the three different curves in each plot are for a high strain rate (blue), a medium strain rate (pink) and a low strain rate (yellow). The lower panels for **a)** and **b)** show the corresponding relationships between the tensile stress induced in the tissue and its strain. Note the effect of loading rate on the value of the tensile stress at failure (indicated by the arrow): the lower the rate of loading, the lower the stress, but the longer the length at which the material fails.

If, as we have described above, low cycle fatigue can occur in a highly organized, fibrous structure as specialized as the ACL, as well as at the origin and insertion of leg muscles, we hypothesize that low-cycle fatigue can also occur at or near the origin of the PVM during a difficult labor. The right and left PVM are the last pelvic floor muscles to be engaged by the fetal head late in labor and, more importantly, they are the portion of the pelvic floor muscles that are

[g] As opposed to the high cycle fatigue failure found in many engineering materials after millions of loading cycles.

[h] Stress is defined as force divided by the cross-sectional area of the material carrying that force. It can be thought of as a normalized measure of force.

[i] Strain is defined as the change in length of the material divided by its original length.

stretched more than any other pelvic floor muscles[3]. The PVM of the nullipara have never been called upon before to resist a tensile force or elongation of the magnitude induced by the fetal head as it elongates the muscle every three minutes towards the end of the second stage of labor (Figure 2.1) and despite the protective adaptations that occur during pregnancy in preparation for childbirth, it is still subjected to an extraordinary loading. Therefore, the aim of the present paper was to determine whether there is indirect evidence that would support the hypothesis of low cycle fatigue causing PVM failures during a difficult or long labor of the type described by Tracy et al[35].

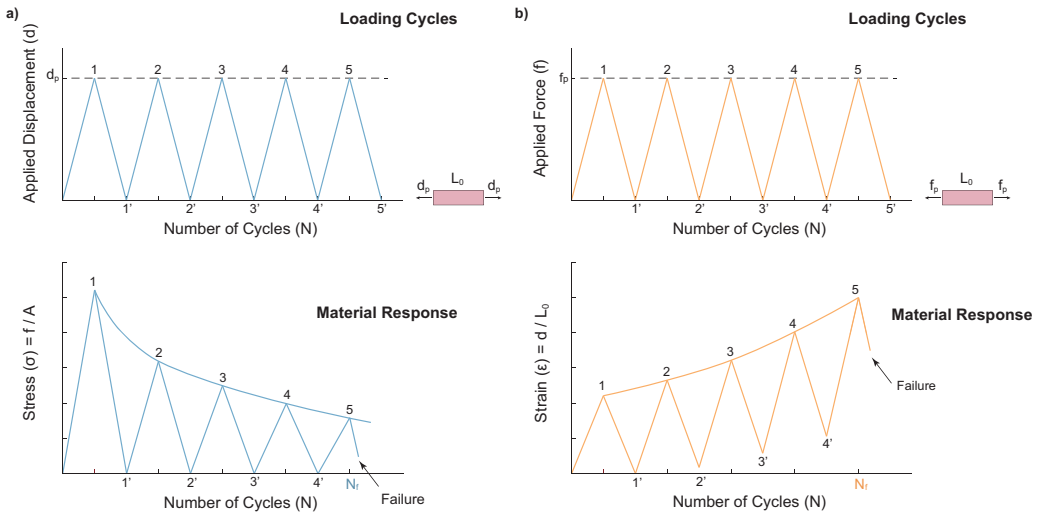

Figure 2.3 - Schematic representation of how low cycle fatigue can cause the failure of a soft tissue material subjected to cyclic sub-maximal stretch loading. **(a)** A cyclic linear increase and decrease in stretch is applied with the peak value less than the value that would cause failure in the first cycle. The lower figure shows the time course of the failure occurring at a lower stress than the peak stress induced by the first loading cycle, due to an accumulation of microdamage in the tissue. **(b)** A cyclic linear increase and decrease in tensile force is instead applied to the same material, with the peak force value being less than that required to cause failure in the first cycle. The lower panel shows the time course of the peak tensile strain induced by each loading cycle until failure occurs during the fifth loading cycle due to an accumulation of microdamage. Pushing during the second stage of labor loads the pelvic floor tissue most closely to the example shown at right in **(b)**.

2.2. What distinguishes muscle/ligament origins and insertions?

The origin and insertion of tendons and ligaments are known to be highly developed regions of transition between these strong, flexible structures and the more rigid bone to which they attach. Since tendon and ligament share a similar hierarchical structure, with highly aligned collagen fibrils, fibers, fiber bundles and fascicles, the interfaces between tendon or ligament and bone have been described as indistinguishable[23]. So, we shall here term them as the “collagen-bone junction (CBJ)”.

The CBJ, also known in some cases as an enthesis, can be fibrous or fibrocartilaginous in nature (Figure 2.4). A fibrous CBJ is characterized by dense fibrous tissue at the interface with perforating mineralized collagen fibers and a structure that becomes ever more mineralized as

one nears the bone[28]. Other CBJ have fibrocartilage interposed between the collagen tissue and the bone, such as occurs in the anterior cruciate ligament, thereby creating a continuous gradient in mechanical properties, such as the elastic modulus, from uncalcified collagen to calcified bone[28].

Muscles are typically connected to their tendons via finger-like projections of muscle fascicles which interdigitate with collagen tissues[37].

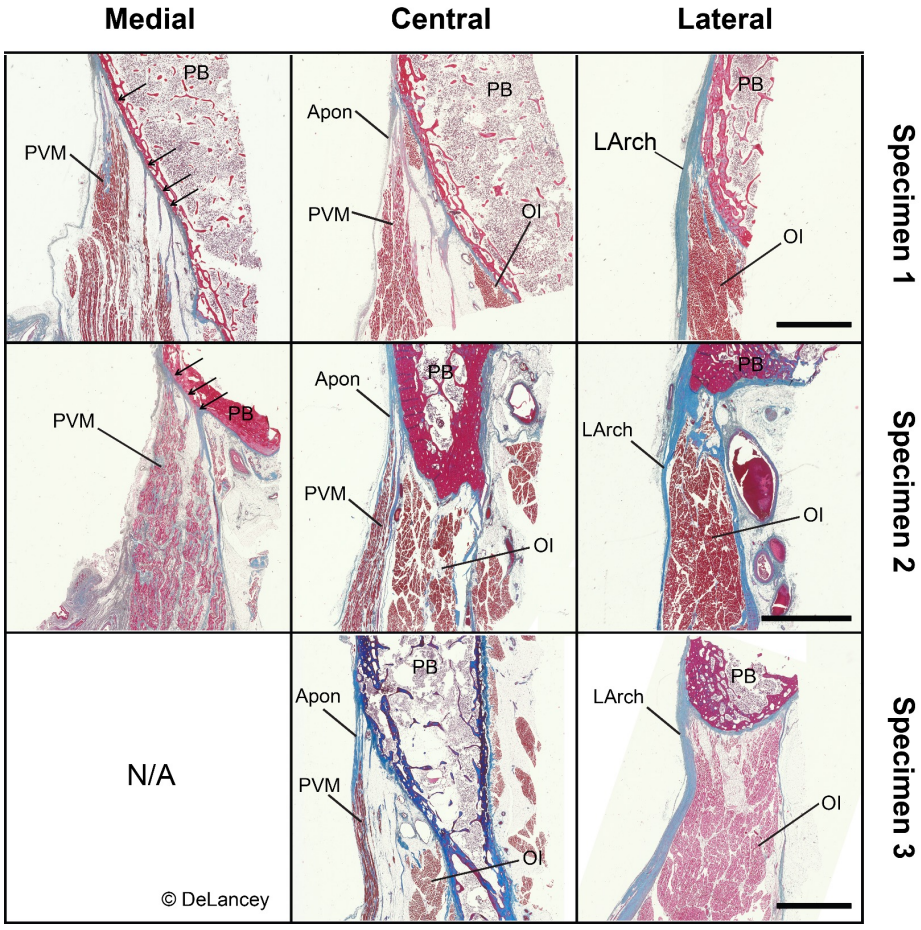

Figure 2.4 - Examples of medial, central and lateral region histology of the pubic origin of the PVM. Each row is from a different donor. Histological images showing the pubic origin of the levator ani from medial (column 1), central (column 2), and lateral (column 3) areas with the orientation picture below. All samples shown are stained in Masson's trichrome, and scale bars are 5mm for each row of images. Medial: The medial levator ani muscle fibers originate from multiple slips attaching in an enthesis to the pubis; oblique interface between the pubic bone (PB) and the levator ani muscle (LA) can also be observed. The thickness of the LA is greater than in other areas. N/A denotes missing data due to a technical issue during harvesting process. Central: The central portion originates from the PB in a single aponeurotic attachment, which is noticeably thinner than medial portion. The obturator internus muscle (OI) can be seen lateral to the LA. Lateral: The levator arch (LArch) appears as a dense blue connective tissue attaching to the PB and forming the lateral margin of the pubic origin of the LA. Note that relative preponderance of the three portions varies by individual. ©DeLancey

Muscle and ligament origins and insertions characteristically include junctions between dissimilar connective tissues, the active muscle on the one hand, and the passive collagenous

connective tissue on the other, each having significantly different tensile material properties. From an engineering point of view, the locations where dissimilar materials interdigitate are typically locations where mechanical stresses concentrate[j]. In other words these junctions sustain higher stresses even when the whole muscle-tendon unit is uniformly loaded, making them more prone to damage[37]. This fact logically makes muscle origins and insertions a region of interest as a potential site for damage to accumulate at and this could eventually accumulate to the point of causing musculoskeletal injury.

2.3. Characteristics of the origin of the pubovisceral muscle

The PVM arises bilaterally from the pubic bone as a thin parallel fibered muscle which thickens to attach, more centrally and caudally, to the perineal body, the vaginal wall, and anal intersphincteric groove[2].

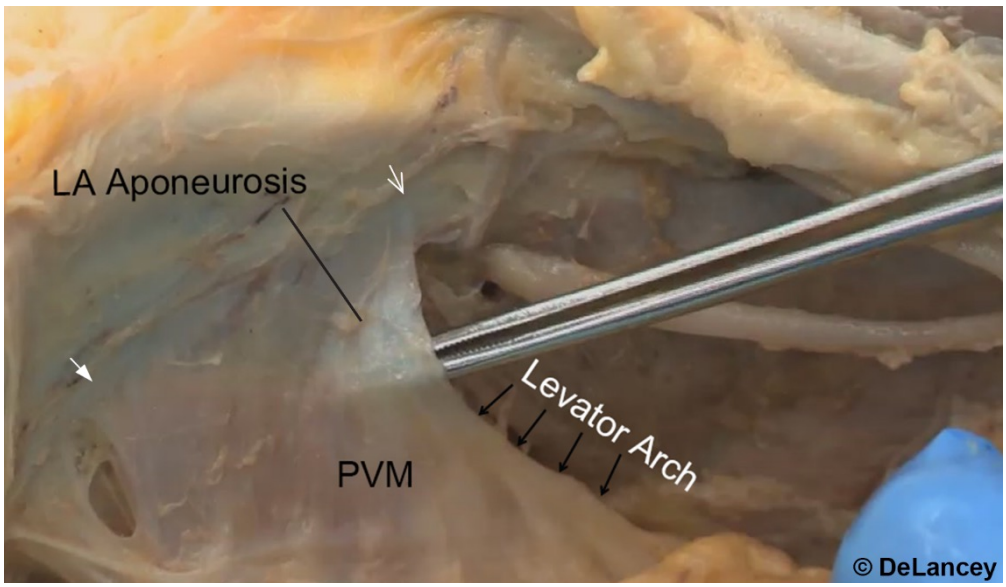

Figure 2.5 - Characteristic features of the origin of the right pubovisceral muscle (PVM). Medial and central portions attach to the pubic bone by an aponeurosis, while the lateral portion attaches to the levator arch (a.k.a arcus tendineus fascia pelvis). Laterally the structure is thin enough to visualize the forceps placed under it for demonstration purposes. ©DeLancey

Its origin on the dorsal aspect of the pubic ramus is long and thin, almost eyebrow shaped (Figure 2.5) ,with the thicker region located more medially, then thinning and extending laterally about 30 mm[8]. In the medial and central portions, a fibrous aponeurosis of thin passive collagenous tissue arises from the synovium over the bone, shorter in the medial region and longer in the central region, to attach to the pubovisceral muscle fibers[8]. The lateral portion of the origin

[j] Examples of this effect can be seen, for instance, when placing a human hair under too much tension. It then has a tendency to fail at the root, not in mid-shaft. Another example are the suture points from surgical repairs. Different techniques have been developed to reduce the stress concentration between the tissue and the stitches in order to reduce the risk of skin tearing.

attaches to the ventral portion of the arcus tendinous levator ani (levator arch) that originates from the pubic bone about a centimeter lateral to the pubic symphysis, and passes medial to the obturator fascia to insert on the ischial spine, the latter serving as the nominal boundary between the PVM and iliococcygeal portions of the pelvic floor muscle[8].

2.4. Is there evidence of low-cycle fatigue damage occurring in soft tissues?

Passive connective tissues, consisting principally of Type 1 collagen, are known to exhibit low-cycle fatigue damage under repetitive strenuous loading. As we have noted in the Introduction, molecular, cellular and ultrastructural evidence of low-cycle fatigue damage accumulation has been demonstrated in the Type 1 collagen of the femoral enthesis of anterior cruciate ligament after repeated sub-maximal loading[4]. This has been observed clinically[41] as well as experimentally under large repetitive sub-maximal knee loading cycles[15]. Likewise, in tendon, another passive connective tissue structure also with a high Type 1 collagen content, microdamage in the form of collagen fibril disruption has been reported at only 6% strain[k] [32]. In addition, the resistance to fatigue damage is known to decrease with age, both in the interfascicular matrix and in the fascicles[34], a fact that might be important in understanding why older nullipara have a significantly higher PVM injury risk[7]. So, if a Type 1 collagen structure with the generous cross-sectional dimensions of ligaments or tendons can accumulate fatigue damage under repetitive strenuous loading, it seems reasonable that heavily loaded sheet-like structures, such as aponeuroses and fascia connecting the PVM to adjacent structures can also exhibit an accumulation of microdamage. It is noteworthy that passive structures like a ligament or tendon are not the only structures to exhibit fatigue damage under repetitive loading.

In striated muscle, for example, damage accumulation near the musculotendinous junction has also been reported under repetitive submaximal loading, with histology showing areas of fiber rupture and hemorrhage near the musculotendinous junction[20] and even incomplete disruption following a strenuous cyclic loading history[33]. Recently, the microdamage accumulation in the muscle has been described as a disruption in the myofibrils, whereby sarcomeres lose their structural integrity[34]. So, active structures such as striated muscle can also exhibit low-cycle fatigue damage as well.

Finally, it well known that even semi-rigid materials like bone can also accumulate fatigue damage, causing the bone to be susceptible to stress-fractures[39], a phenomenon that has recently been shown to occur in the pubic bone during a delivery[17].

So, in summary, there is strong evidence in the literature that passive collagenous structures such as ligament and tendon, active structures such as muscle, and even bone can all accumulate

[k] Defined as change in length over the original length

microdamage under repetitive sub-maximal loading. Moreover, the mechanism of fatigue damage seems similar in these structures in that damage starts in the microstructure, progressing under continued strenuous loading cycles to larger length scales of organization until it can affect the macroscopic properties or even cause structural failure. This is consistent with fatigue damage seen in engineering materials, where the first signs of fatigue damage are microscopic imperfections or flaws that can grow into macroscopic cracks under repeated loading, these in turn can propagate to a critical size until the structure partially or even completely fails [16]. The main difference with the engineering materials, is that biological tissues have the ability to heal, grow and remodel. So, if the rate of damage accumulation is less than the rate at which the tissue can repair itself in a timely manner, it would not be prejudicial. In fact, it could even be beneficial if the microdamage triggers metabolic and structural adaptations that, to reverse it, cause muscle or tendon growth[5] consistent with Davis's law. However, a combination of high sub-maximal loads, many repetitions and/or short recovery times, will eventually lead to irreversible microdamage progression which in turn can cause irreversible macroscopic defects thereby weakening the tissue to cause partial or even complete failure.

In engineering materials, ultrasound is routinely used to detect signs of microdamage accumulation so action can be taken to avert a disastrous failure. For biological tissues, scanning acoustic microscopy (SAM) can provide high-quality microscopy of tissues and cells comparable with light microscopy without the need for staining[18] as well as provide data on the elasticity of tissues, thereby measuring mechanical alterations[19]. The marked advantage of SAM is the ability to inspect the sample subsurfaces layer by layer simultaneously with good penetrating power of the ultrasonic waves while scanning the material surface, for detecting micro defects[40]. The disadvantage is that it still requires flat ~10-15μm samples[18]; however, with the advent of better imaging modalities, it might be possible to develop preventative screening for biological tissues and find the threshold for detrimental or irreversible microdamage accumulation.

2.5. Can the origin of the pubovisceral muscle be susceptible to low-cycle fatigue damage in a difficult vaginal birth?

In the second stage of labor of a typical vaginal birth it is known that spontaneous uterine contractions occur approximately every 3 min, increasing the pressure near the fetal head from 2.6 kPa to 8.5 kPa. Maternal pushes (occurring 2-3 times per uterine contraction if instructed) are added to facilitate the fetus expulsion, increasing this pressure to 19 kPa [3]. This gives expulsive forces on the fetal head of 24 N at rest, of 74 N at the peak of uterine contraction and of 101 N at the peak of each maternal push (considering and fetal cross-sectional area of 9.2 cm^2). So, at peak, this gives a combined effort of 175 N. In case of maternal exhaustion, when the women can no longer make progress, vacuum device is applied to the fetal head for an additional traction force

of 113 N, typically up to four pulls, or if obstetric forceps have to be used, the additional traction force can reach 200 N[3]. Besides these forces, the fetal head induces extraordinary maternal tissue stretch, which many studies have shown to be especially large in the PVM portion of the pelvic floor. So, despite the pregnancy induced alterations in the pelvic floor to facilitate birth, levator ani injuries are prevalent after vaginal delivery.

Magnetic resonance images (MRI) taken weeks after a difficult delivery in nullipara showed pubic bone edema in 66% of the cases, pubic bone fracture in 29%, muscle edema in 90% and low-grade or greater tear in the pubovisceral muscle in 41%[17]. Months later, MRIs of the same women showed the edema to have subsided, but the previously torn PVM was no longer visible at its normal attachment site on one or both sides[17]. This edema is evidence of injury and the ensuing reparative process. Shek and Dietz[29] hypothesize that minor defects to the PVM portion of the levator ani could cause an irreversible increase in the hiatal area and called this a 'microtrauma' injury. 4D Transperineal ultrasound (TPUS) was performed between 36 and 38 weeks gestation and 3-4 months after vaginal delivery and found a complete detachment of the PVM in 13% of the cohort and an irreversible enlargement >20% of the hiatal area on Valsalva in 29% [29]. Despite the term 'microtrauma', the authors actually describe phenomenon consistent with low-cycle fatigue, such as microdamage and permanent/plastic deformation. Recently, Da Silva et al[30,31] attempted to correlate the findings of TPUS with cadaveric observations and verified that injuries showing a complete detachment of the PVM under TPUS (also designated as "avulsion" in the literature) were truly still attached to the pubic bone, although appearing significantly narrower. Histology performed on the cadaveric PVMs showed tortuous muscle fibers and loss of striation, which interestingly is also consistent with the hypothesis of microdamage accumulation, despite the lack of a complete tear. These are only a small percentage of the studies reporting levator ani injuries after a vaginal delivery which, despite being extensive reported, still have poorly understood pathomechanics. Nevertheless, these results demonstrate just how strenuous the pelvic floor tissue and pubic bone loading is during birth, as well as showing the proximal PVM to be a region that is commonly injured in a difficult delivery. Exactly where in the PVM it is injured is still unknown – is it where the aponeurosis attaches to the bone, the aponeurosis itself, the junction between the aponeurosis and the muscle, or the muscle itself?

What can we learn from studying injury sites in musculotendinous units elsewhere in the body? Our review[38] showed that bony avulsions and collagen-bone junction injuries are typically linked to older individuals. Since the age of first time mothers most commonly ranges from 24 - 29 years old (data from 37 developed countries of Europe, East Asia and USA[27]), this makes the aponeurosis, musculotendinous junction, or muscle belly the most likely injury locations in younger women. MRI obtained after difficult first time deliveries shows signs of edema at the origin of the pubovisceral muscle[17], which makes it more likely that an aponeurosis avulsion or musculotendinous junction occurred. In our review of muscle-tendon injuries in other parts of the

body, avulsion injuries were frequently linked with an evident trauma[38] would certainly be consistent with the kind of injury sustained during an instrumented delivery with forceps when the head is often delivered by a single pull lasting a few seconds during which the applied traction force can reach 200 N [21]. But in the case of a difficult non-instrumented delivery, it could typically involve more than one stretch of the PVM at the end of second stage of labor. For the same reason, the rate of loading is an order of magnitude slower, for example, than a single fall onto an outstretched arm, which is a frequent cause of triceps brachii tendon avulsions in a tenth of a second [22]. The strains and loads acting on the pelvic floor are very significant, however the pelvic floor is relatively prepared for childbirth, so it is not expected that the strains and loads normally exceed the ultimate failure strain and/or stress[m] without an instrumented delivery. An injury can happen, and in that case the injury would occur due to that single forceful load exceeding the ultimate failure properties of the tissues. However, in a typical labor, it is more likely that as the mother pushes hard every three minutes to deliver the fetal head [12], causing high but sub-maximal strains (which in the caudal part of the PVM, can reach to three times its original length [13]), microdamage starts to develop from the start, quickly progresses and eventually causes a partial or even complete failure, given that there is no time for any damage to be repaired.

Thus, we postulate that a prolonged or difficult second stage of labor, involving multiple and forceful pushes, can cause damage to accumulate at the weakest link of the proximal PVM, most likely the aponeurosis itself, or the junction between it and the muscle. In some cases, the damage accumulation can mean that a forceful push that ordinarily would not cause injury if it were the only push, can cause a complete tear because of the recent repetitive history of large sub-maximal loads in a structure that on day-to-day activity, is never called upon to withstand such large repeated loading cycles.

This argument does not preclude the possibility that a single forceful push, on its own, and without low-cycle fatigue, could tear the PVM from the bone, its CBJ or even the muscle belly, due to the extraordinary stretch required (*vide supra*) exceeding the ultimate strain in and/or stress in the structure. Rather, this paper augments the "single push" failure mode by adding a second mechanism of PVM failure: namely low cycle fatigue failure of the PVM after repetitive submaximal pushes. If future studies confirm this second possibility, it should lead to new ways of preventing this injury in the labor and delivery room during a difficult birth. Given that these tissues are viscoelastic[35,36], there is a tradeoff: making each push long enough to maximize tissues stretch during each push in order to facilitate fetal head descent, but not inducing maternal exhaustion with too lengthy or strenuous pushing, and knowing that too strenuous pushing near the end of labor increases the risk of partial or even complete material fatigue of the PVM. Given

[m] Maximum stress or strain that the material can withstand without failing.

these factors, it might prove fruitful to identify the optimal pushing strategy, building on the work of Lien et al[12].

2.6. Conclusions

1) Evidence from musculoskeletal injuries elsewhere in the body point to the aponeurosis or the musculotendinous junction as being the weak links in pelvic muscle placed under large repetitive loading in young women of childbearing age.

2) This supports our hypothesis that the PVM may accumulate sufficient microdamage during the multiple forceful pushes near the end of the second stage of labor to weaken the tissue to the point of a partial or complete tear of the structure during the next push.

3) The clinical significance of these observations is that minimizing the number or intensity of such loading cycles during a vaginal birth would reduce the risk of irreversible PVM injuries, especially if the loading rate can be reduced to allow time for tissue viscoelastic behavior to aid in tissue elongation.

Acknowledgements

Authors gratefully acknowledge the support from Fundação para a Ciência e Tecnologia (Portugal) under grant SFRH/BD/136213/2018, the funding provided by LAETA (Portugal), under project UIDB/50022/2020 and the U.S. Public Health Service grants 5P30AG024824-15, RC2 DK122379-01 and 5R01AR054821-09.

References

1. Andarawis-Puri N, Flatow EL. Tendon fatigue in response to mechanical loading. *J Musculoskelet Neuronal Interact*. 2011;11(2):106-114.

2. Ashton-Miller JA, DeLancey JOL. Functional anatomy of the female pelvic floor. *Ann N Y Acad Sci*. 2007;1101:266-296. doi:10.1196/annals.1389.034

3. Ashton-Miller JA, DeLancey JOL. On the biomechanics of vaginal birth and common sequelae. *Annu Rev Biomed Eng*. 2009;11(1):163-176. doi:10.1146/annurev-bioeng-061008-124823.On

4. Chen J, Kim J, Shao W, et al. An anterior cruciate ligament failure mechanism. *Am J Sports Med*. 2019;47(9):2067-2076. doi:10.1177/0363546519854450

5. Cheng AJ, Jude B, Lanner JT. Intramuscular mechanisms of overtraining. *Redox Biol*. 2020;35:101480. doi:https://doi.org/10.1016/j.redox.2020.101480

6. DeLancey JOL. What's new in the functional anatomy of pelvic organ prolapse? *Curr Opin Obstet Gynecol*. 2016;28(5):420-429. doi:10.1097/GCO.0000000000000312

7. Kearney R, Miller JM, Ashton-Miller JA, DeLancey JOL. Obstetric factors associated with levator ani muscle injury after vaginal birth. *Obstet Gynecol*. 2006;107(1).

8. Kim J, Betschart C, Ramanah R, Ashton-Miller JA, DeLancey JOL. Anatomy of the pubovisceral muscle origin: Macroscopic and microscopic findings within the injury zone. *Neurourol Urodyn*. 2015;34(8):774-780. doi:10.1002/nau.22649

9. Laganà AS, La Rosa VL, Rapisarda AMC, Vitale SG. Pelvic organ prolapse: the impact on quality of life and psychological well-being. *J Psychosom Obstet Gynecol*. 2018;39(2):164-166. doi:10.1080/0167482X.2017.1294155

10. Lee N, Gao Y, Lotz L, Kildea S. Maternal and neonatal outcomes from a comparison of spontaneous and directed pushing in second stage. *Women and Birth*. 2019;32(4):e433-e440. doi:https://doi.org/10.1016/j.wombi.2018.10.005

11. Leveno KJ, Nelson DB, McIntire DD. Second-stage labor: how long is too long? *Am J Obstet Gynecol*. 2016;214(4):484-489. doi:https://doi.org/10.1016/j.ajog.2015.10.926

12. Lien K-C, DeLancey JOL, Ashton-Miller JA. Biomechanical analyses of the efficacy of patterns of maternal effort on second-stage progress. *Obstet Gynecol*. 2009;113(4):873-880. doi:10.1097/AOG.0b013e31819c82e1

13. Lien K-C, Mooney B, DeLancey JOL, Ashton-Miller JA. Levator ani muscle stretch induced by simulated vaginal birth. *Obstet Gynecol*. 2004;103(1):31-40. doi:10.1097/01.AOG.0000109207.22354.65

14. Lin AH, Allan AN, Zitnay JL, Kessler JL, Yu SM, Weiss JA. Collagen denaturation is initiated upon tissue yield in both positional and energy-storing tendons. *Acta Biomater*. 2020;118:153-160. doi:https://doi.org/10.1016/j.actbio.2020.09.056

15. Lipps DB, Wojtys EM, Ashton-Miller JA. Anterior cruciate ligament fatigue failures in knees subjected to repeated simulated pivot landings. *Am J Sports Med*. 2013;41(5):1058-1066. doi:10.1177/0363546513477836

16. Milella PP. *Fatigue and Corrosion in Metals*. 1st ed. (Milella PP, ed.). Springer-Verlag Mailand; 2013. doi:10.1007/978-88-470-2336-9

17. Miller JM, Low LK, Zielinski R, Smith AR, Delancey JOL, Brandon C. Evaluating maternal recovery from labor and delivery: Bone and levator ani injuries. *Am J Obstet Gynecol*. 2015;213(2):188.e1-188.e11. doi:10.1016/j.ajog.2015.05.001

18. Miura K. Application of scanning acoustic microscopy to pathological diagnosis. In: Stanciu S, ed. *Microscopy and Analysis*. ; 2016:381–403.

19. Miura K, Fukushi Y. Scanning acoustic microscopy imaging of cellular structural and mechanical alterations from external stimuli. *Heliyon*. 2021;7(8):e07847. doi:https://doi.org/10.1016/j.heliyon.2021.e07847

20. Noonan TJ, Best TM, Seaber A V, Garrett WEJ. Identification of a threshold for skeletal muscle injury. *Am J Sports Med*. 1994;22(2):257-261. doi:10.1177/036354659402200217

21. Pearse WH. Electronic recording of forceps delivery. *Am J Obstet Gynecol*. 1963;86(1):43-51. doi:https://doi.org/10.1016/0002-9378(63)90075-9

22. Pina A, Garcia I, Sabater M. Traumatic avulsion of the triceps brachii. *J Orthop Trauma*. 2002;16(4):273-276. doi:10.1097/00005131-200204000-00010

23. Rothrauff BB, Tuan RS. Cellular therapy in bone-tendon interface regeneration. *Organogenesis*. 2014;10(1):13-28. doi:10.4161/org.27404

24. Samuelsson E, Ladfors L, Lindblom BG, Hagberg H. A prospective observational study on tears during vaginal delivery: occurrences and risk factors. *Acta Obstet Gynecol Scand*. 2002;81(1):44-49.

25. Sassmannshausen G, Mair SD. Musculotendinous injuries about the athletically active middle-aged knee. *Sports Med Arthrosc*. 2003;11(2):107-111. doi:10.1097/00132585-200311020-00004

26. Schechtman H, Bader DL. In vitro fatigue of human tendons. *J Biomech*. 1997;30(8):829-835. doi:https://doi.org/10.1016/S0021-9290(97)00033-X

27. Schmidt L, Sobotka T, Bentzen JG, Nyboe Andersen A. Demographic and medical consequences of the postponement of parenthood. *Hum Reprod Update*. 2012;18(1):29-43. doi:10.1093/humupd/dmr040

28. Sevivas N, França G, Oliveira N, et al. Biomaterials for Tendon Regeneration BT - Muscle and Tendon Injuries: Evaluation and Management. In: Canata GL, d'Hooghe P, Hunt KJ, eds. Springer Berlin Heidelberg; 2017:131-143. doi:10.1007/978-3-662-54184-5_13

29. Shek KL, Dietz HP. Intrapartum risk factors for levator trauma. *BJOG An Int J Obstet Gynaecol*. 2010;117(12):1485-1492. doi:10.1111/j.1471-0528.2010.02704.x

30. Da Silva AS, Asfour V, Digesu GA, Cartwright R, Fernando R, Khullar V. Levator Ani avulsion: The histological composition of this site. A cadaveric study. *Neurourol Urodyn*. 2019;38(1):123-129. doi:10.1002/nau.23847

31. Da Silva AS, Digesu GA, Dell'Utri C, Fritsch H, Piffarotti P, Khullar V. Do ultrasound findings of levator ani "avulsion" correlate with anatomical findings: A multicenter cadaveric study. *Neurourol Urodyn*. 2016;35(6):683-688. doi:10.1002/nau.22781

32. Stauber T, Blache U, Snedeker JG. Tendon tissue microdamage and the limits of intrinsic repair. *Matrix Biol*. 2020;85-86:68-79. doi:https://doi.org/10.1016/j.matbio.2019.07.008

33. Taylor DC, Dalton JDJ, Seaber A V, Garrett WEJ. Experimental muscle strain injury. Early functional and structural deficits and the increased risk for reinjury. *Am J Sports Med*. 1993;21(2):190-194. doi:10.1177/036354659302100205

34. Thorpe CT, Riley GP, Birch HL, Clegg PD, Screen HRC. Fascicles and the interfascicular matrix show decreased fatigue life with ageing in energy storing tendons. *Acta Biomater*. 2017;56:58-64. doi:https://doi.org/10.1016/j.actbio.2017.03.024

35. Tracy P V, Wadhwani S, Triebwasser J, et al. On the variation in maternal birth canal in vivo viscoelastic properties and their effect on the predicted length of active second stage and levator ani tears. *J Biomech*. 2018;74:64-71. doi:10.1016/j.jbiomech.2018.04.019

36. Tracy P V, Wineman AS, Orejuela FJ, Ramin SM, DeLancey JOL, Ashton-Miller JA. A constitutive model description of the in vivo material properties of lower birth canal tissue during the first stage of labor. *J Mech Behav Biomed Mater*. 2018;79:213-218. doi:https://doi.org/10.1016/j.jmbbm.2017.12.025

37. VanDusen K, Larkin L. Muscle-tendon interface. In: *Regenerative Engineering of Musculoskeletal Tissues and Interfaces*. ; 2015:409-429. doi:10.1016/B978-1-78242-301-0.00017-3

38. Vila Pouca MCP, Parente MPL, Natal Jorge RM, Ashton-Miller JA. Injuries in muscle-tendon-bone units: a systematic review considering the role of passive tissue fatigue. *Orthop J Sport Med*. 2021;9(8). doi:DOI: 10.1177/23259671211020731

39. Yeni YN, Fyhrie DP. Fatigue damage-fracture mechanics interaction in cortical bone. *Bone*. 2002;30(3):509-514. doi:https://doi.org/10.1016/S8756-3282(01)00696-2

40. Yu H. Scanning acoustic microscopy for material evaluation. *Appl Microsc*. 2020;50(1):25. doi:10.1186/s42649-020-00045-4

41. Zantop T, Brucker PU, Vidal A, Zelle BA, Fu FH. Intraarticular rupture pattern of the ACL. *Clin Orthop Relat Res*. 2007;454:48-53. doi:10.1097/BLO.0b013e31802ca45b

42. Zitnay JL, Jung GS, Lin AH, et al. Accumulation of collagen molecular unfolding is the mechanism of cyclic fatigue damage and failure in collagenous tissues. *Sci Adv*. 2020;6(35):eaba2795. doi:10.1126/sciadv.aba2795

Chapter 3

Investigating the birth-related caudal maternal pelvic floor muscle injury

The consequences of low cycle fatigue damage

Investigating the birth-related caudal maternal pelvic floor muscle injury

The consequences of low cycle fatigue damage

Maria C.P. Vila Pouca[1,2], Marco P.L. Parente[1,2], Renato M. Natal Jorge[1,2], James A. Ashton-Miller[3]

1 Department of Mechanical Engineering, Faculty of Engineering of University of Porto, Porto, Portugal
2 Institute of Science and Innovation in Mechanical and Industrial Engineering, Porto, Portugal
3 Departments of Mechanical and Biomedical Engineering, College of Engineering and School of Kinesiology, University of Michigan, Ann Arbor, Michigan, USA

Published In

Journal of the Mechanical Behavior of Biomedical Materials
DOI: https://doi.org/10.1016/j.jmbbm.2020.103956

Submitted: May 5, 2020
Accepted: June 24, 2020

Abstract

Background: One of the major causes of pelvic organ prolapse is pelvic muscle injury sustained during a vaginal delivery. The most common site of this injury is where the pubovisceral muscle takes origin from the pubic bone. We hypothesized that it is possible for low-cycle material fatigue to occur at the origin of the pubovisceral muscle under the large repetitive loads associated with pushing during the second stage of a difficult labor.

Purpose: The main goal was to test if the origin of the pubovisceral muscle accumulates material damage under sub-maximal cyclic tensile loading and identify any microscopic evidence of such damage.

Methods: Twenty origins of the ishiococcygeous muscle (homologous to the pubovisceral muscle in women) were dissected from female sheep pelvises. Four specimens were stretched to failure to characterize the failure properties of the specimens. Thirteen specimens were then subjected to relaxation and subsequent fatigue tests, while three specimens remained as untested controls. Histology was performed to check for microscopic damage accumulation.

Results: The fatigue stress-time curves showed continuous stress softening, a sign of material damage accumulation. Histology confirmed the presence of accumulated microdamage in the form of kinked muscle fibers and muscle fiber disruption in the areas with higher deformation, namely in the muscle near the musculotendinous junction.

Conclusions: The origin of ovine ishiococcygeous muscle can accumulate damage under sub-maximal repetitive loading. The damage appears in the muscle near the musculotendinous junction and was sufficient to negatively affect the macroscopic mechanical properties of the specimens.

Keywords: fatigue, pelvic muscle injury, microscopic damage, pubovisceral muscle, histology, tissue fatigue damage.

3.1. Introduction

Pelvic organ prolapse, a serious and common condition, adversely affects quality of life, particularly in older women[18,29,55]. The lifetime risk of needing prolapse surgery ranges between 1 in 10 to 1 in 5 women, with over 300, 000 surgeries being performed for this condition in the U.S. every year[17,53]. Unfortunately, the surgery has a failure rate of approximately 30%[4], so preventing prolapse in the first place would be desirable. To that end, mechanistic insights are needed into the injury mechanism(s). Pelvic floor muscle injury occurs most frequently during the first vaginal birth and has been identified as one of the major causes for pelvic organ prolapse[30,45]. Moreover, a characteristic site of injury has been identified with magnetic resonance imaging to be the origin of the pubovisceral muscle from the pubic bone[12–14,34].

Most muscles originate from bone via a tendon or an aponeurosis that itself interdigitates with muscle fibers and fascicles called the musculotendinous junction (MTJ), with their other end inserting onto a bone at an enthesis where the tendon/aponeurosis inserts into the bone[47,50]. Injuries to bone-tendon/aponeurosis-muscle units are common and tend to occur at the tendon/aponeurosis-bone junction or at the musculotendinous junction[47]. From a mechanical point of view, junctions between dissimilar materials are well known to be regions of mechanical stress concentration, not only due to the different material properties, but also because these regions are usually accompanied by a change in cross-sectional area; this means that if the whole unit is uniformly loaded these junctions have to sustain higher stresses, making them more prone to tear[50]. In the human, the pubovisceral muscle originates bilaterally from the dorsal aspect of the pubic bone via an aponeurosis on either side of the pubic symphysis[26,27].

Low cycle fatigue failure can occur in soft connective tissues. For example, sub-maximal repetitive loading has been demonstrated to cause failure of the origin of the human anterior cruciate ligament (ACL), a highly organized connective tissue structure within the knee, in less than 100 loading cycles[33]. Recently, Chen et al[9] found molecular, cellular and ultrastructural evidence of low-cycle fatigue damage accumulation at the origin of the ACL, more specifically at its femoral enthesis, following cyclic sub-maximal loading. So, if low-cycle material fatigue can occur at the origin of the ACL, we reasoned that low-cycle material fatigue could also occur at the origin of the pubovisceral muscle during the second stage of a difficult vaginal delivery, when it can be stretched to at least 3 times its original length every 3 min over a 3 h period[32,41]. The concept of low cycle material fatigue is that a structure can fail under two or more repetitive sub-maximal loading cycles that would not, by themselves, cause failure. This occurs because in each loading cycle there is a microscopic damage accumulation that weakens the structure, making it more prone to fail with the increase of damage accumulation.

At the origin of the ACL the damage accumulation occurs at the femoral enthesis, the ligament-bone junction, and the ligament, as in tendon, consists primarily of collagen type I[3,54].

Moreover, there are a considerable number of studies that have shown fatigue damage accumulation in tendons and collagenous structures at the fiber and fibril level[5,16,46,48,51,52,56]. With these considerations our working hypothesis was that the origin of the pubovisceral muscle could accumulate microscopic damage at the tendon-bone interface under repetitive sub-maximal loading with the number of loading cycles being equivalent to that experienced during a difficult vaginal delivery. Our alternative hypotheses were that damage accumulation could occur in a different site, or that no evidence of fatigue damage accumulation would occur.

To test our hypothesis, we performed low-cycle fatigue tests on ovine specimens using a test protocol of 60 cycles to 60% failure displacement and analyzed the behavior of the stretch-stress curves. We also examined histological sections of the specimens in a search for evidence of damage accumulation. The tests were performed on the origin of the ishiococcygeous muscle from female mature sheep, which is the structure most analogous to the origin of the pubovisceral muscle in women.

Once we had obtained the mechanical properties of the ishiococcygeous muscle origin, we developed a constitutive model for fatigue damage that was incorporated into a visco-hyperelastic material model. Using a micro-genetic algorithm, we calibrated the material parameters for the averaged response of the stress-time curve of our fatigue tests. This is important for the development of realistic finite element models, which are highly dependent on defining the appropriate constitutive laws and also defining the appropriate material parameters [8]. Finally, to explore how the results might apply to humans, we developed a simplified finite element model of the origin of the pubovisceral muscle using our visco-hyperelastic material model that included fatigue damage.

3.2. Materials and methods

3.2.1. Animal model of the origin of the pubovisceral muscle

While there is no perfect substitute for human specimens, using animal models in research has become a common alternative since they provide significantly improved access to tissue and there are fewer ethical constraints[2,11].

In this study we decided to choose sheep as an animal model for the origin of the pubovisceral muscle. This choice was made because they represent an established reproductive model for humans, have prolonged labor with relatively large fetuses, spontaneously develop prolapse, have similar pelvic muscles anatomy and were more available than other large models such as primate[2].

The human pelvic floor muscles, or levator ani, can be subdivided in the puborectal, pubovisceral (also known as pubococcygeal) and iliococcygeus muscles. The human pubovisceral muscle originates from the pubic bone on either side of the pubic symphysis and inserts into the perineal body, vaginal wall and the anal canal[25]. In sheep, the levator ani appears as a uniform

muscle[6,49], and is designated as the ishiococcygeous if one follows the terminology of Basset, E.G [6]. Our dissections confirmed that the ovine ishiococcygeous originates from the ishium and fans out from the origin to insert into the vaginal wall, anal canal and tail bones (Figure 3.1b), consistent with Basset, E.G.[6] (Figure 3.1a). Although there are some dissimilarities, we conclude that the origin of the ovine ishiococcygeous muscle is the most homologous structure to the origin of the pubovisceral muscle in humans.

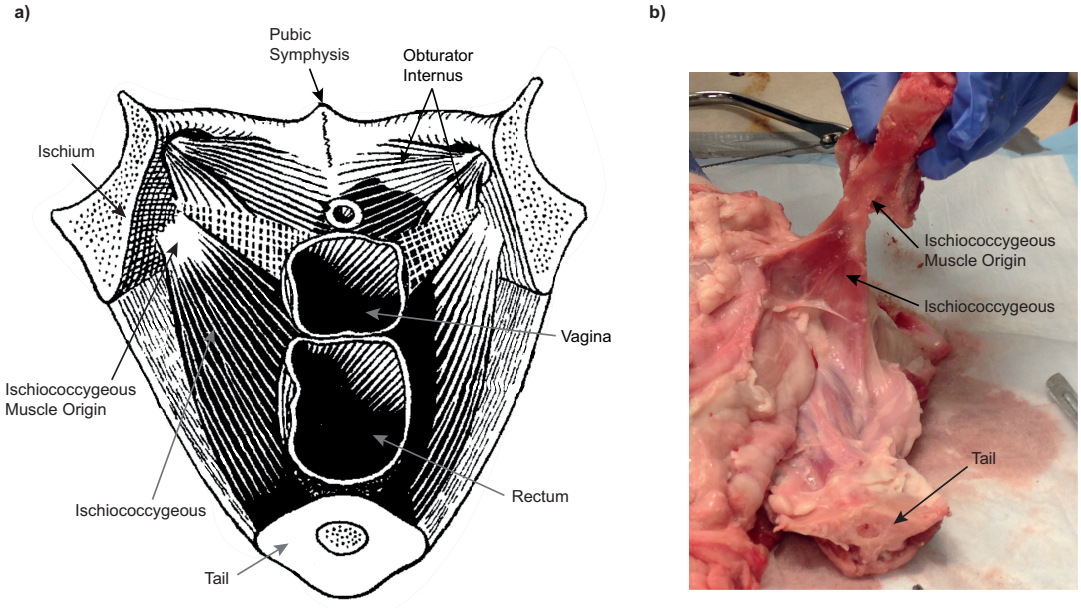

Figure 3.1 - Superior view of the ovine pelvic floor. **a)** schematic representation showing the origin and insertion of the ishiococcygeous muscle, adapted from Basset. E.G[6]. **b)** posterolateral image showing the origin of the left ishiococcygeous muscle (pubic bone already trimmed at the proximal end) and the muscle fanning out and inserting onto to vaginal wall, anal canal, and coccygeal bone of tail.

3.2.2. Specimens procurement and preparation

Ten pelvises from female skeletally mature nulliparous sheep were collected thereby providing 20 specimens of the origin of pubovisceral muscle. Age and weight were provided for eight pelvises and the longitudinal and cross-sectional dimensions of the pelvic cavity were measured for all specimens. The breed of the animals was not provided. Two fresh pelvises, obtained from the Michigan State University Meat laboratory, were double bagged and stored in the Biomechanics Research Lab at the University of Michigan at –20°C. Eight pelvises were provided by the University of Minnesota's Experimental Surgical Services and sent to the University of Michigan via dry ice shipments.

The pelvises were kept frozen at –20°C for between 3 and 68 days (mean 28 ± 16 days). Each pelvis was thawed in their bags to room temperature overnight for dissection the next day. After mostly blunt dissection was used to identify the ischococcygeal muscle, a scalpel was used to free the insertions of the muscle at the vagina, anal canal and coccygeal bone. The ischocyccygeal muscle takes origin immediately posterior to the obturator foramen from the posteromedial aspect

of the inferior ischium at its junction with the pubic bone. As such, the muscle origin and underlying bone were excised *en bloc* from the adjacent pelvic bone by using a bone saw and pruning shears to divide the ischia ventral to the origin and the pubic bone posterior to the origin (Figure 3.1). The paired left and right pubovisceral specimens were then kept in a sealed container in a refrigerator for the mechanical tests to be performed the following day. Prior to the mechanical tests, the specimens were thawed to room temperature. A 1x Phosphate-buffered saline (PBS) was used to fully hydrate the tissues. Then, to avoid a muscle tear caused by grips, the distal end of the muscle specimen was adhered between two pieces of ripstop nylon (64 gsm) using cyanoacrylate glue. In all the specimens, the ripstop ended 15 mm from the MTJ. To ensure a proper grip at the bone end of the specimen, the bone was trimmed and flattened using a DREMEL® equipped with a flush cut blade. During the preparation, the specimens were kept hydrated by frequently spraying PBS solution or keeping them covered with a Kimwipe soaked in 1x PBS. Figure 3.2 shows a specimen prior to the mechanical test, before and after preparation with a digital caliper showing the scale in mm. Specimens were designated '1' through '10' according to each pelvis, with an 'L' or 'R' for left or right origin, respectively. So, a reference to specimen '1R' and '1L' means they both belong to the same pelvis (No. 1) and are the right and left ishiococcygeous origin, respectively.

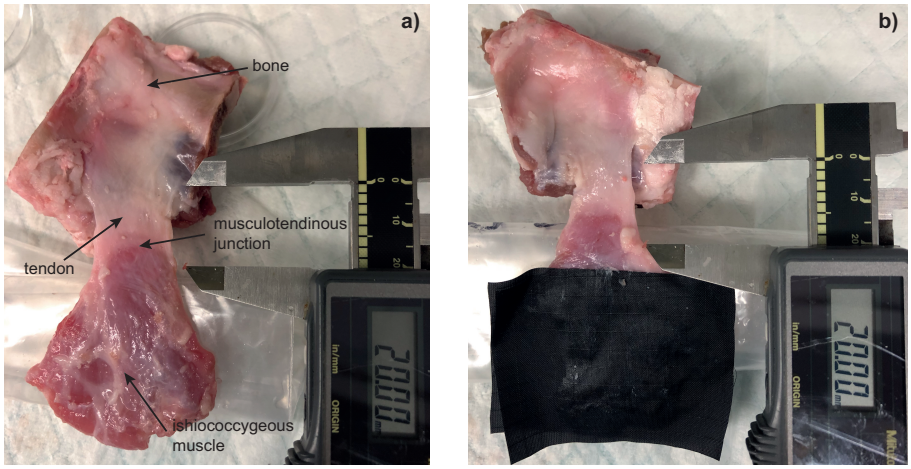

Figure 3.2 - An anterolateral view of the ischiococcygeus muscle specimen after dissection: **a)** prior to preparation the medial surface of the (left) pubic bone can be seen at top with the bony origin (white collagenous tissue) of the muscle visible to the left of the small rectangular-shaped piece of clear skin tape (which itself lies over where the obturator foramen would normally be, the ischiococcygeus tendon with undisturbed margins, the MTJ and muscle proper below; **b)** after preparation consisting of adhering the ripstop nylon to both side of the muscle to within 15 mm of the MTJ. The jaws of the digital caliper serve as a 20 mm scale.

3.2.3. Experimental design and protocol

This study was divided in two parts. In the first part, ultimate tensile tests were performed, to characterize the failure mechanical properties of the muscle-tendon-bone unit. In the second part, relaxations and fatigue tests were performed respectively at 35% and 60% of the failure

displacement. Three specimens were used for the ultimate tensile tests and 16 specimens for relaxation and fatigue tests. Of these 16 specimens, 3 samples were not tested in order to remain as untested controls. One specimen was discarded due to tear at the grips during the ultimate tensile test. The controls were randomly selected from among the 16 specimens using a custom Matlab® program.

Custom design clamps were chosen to grip the specimens, however, to completely avoid slippage, an abrasive sandpaper was also glued via double-sided adhesive tape to each grip. The sandpaper made direct contact proximally with the bone, and for the other grip contact with the ripstop nylon. An ADMET eXpert 4500 MicroTest system (Resolution 0.001N) with MTESTQuattro (version 5) controller and a 100 lbf load cell (WMC-100, Interface) was the equipment used for all the tests. Figure 3.3 shows the specimen inserted in the setup and ready for testing.

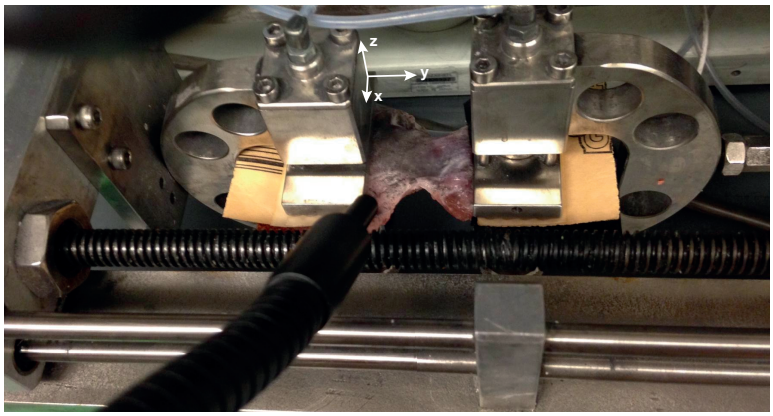

Figure 3.3 - Specimen inserted in the setup, hydrated with PBS, and ready for testing**.**

The ultimate tensile tests were performed under displacement control while the specimens were stretched to failure at a displacement rate of 0.1 mm/s. It was decided not to precondition the specimens since it changes the stress-strain response of the tissues [10]. Force-displacement data were acquired at a rate of 0.5 s^{-1}. Failure properties were obtained at the peak of the force displacement curve: the mean force to failure and mean displacement to failure were calculated from the results of all samples. The mean displacement to failure served as the failure 'baseline' for the relaxation and fatigue tests.

The relaxation and fatigue tests were performed under displacement control. For the relaxation tests, the specimens were stretched up to 35% failure displacement at 10 mm/s and then the same displacement was maintained for 1000 s. Force-displacement data were acquired at 0.01 s^{-1} during the first 10 seconds, at 0.1 s^{-1} between 10 and 100 sec, and at 1 s^{-1} for the remaining 900 seconds. At the end of the relaxation test the specimen was taken back to the initial position and allowed to rest for 20 min in the setup. Then, the fatigue test was carried out. A preload of 0.7 N was initially applied to take up the slight slack caused by the relaxation test. The specimen was then

cyclically stretched between 60% and 45% of the failure displacement for 60 cycles at a rate of 0.1 mm/s. This is approximately one loading-unloading cycle every 53 s resulting in a fatigue test with a duration of 53 min. This duration corresponds with the mean length of a second stage of labor of 54.4 ± 23.6 min[28]. The 60% failure displacement was chosen because during vaginal birth the levator ani hiatus has an estimated stretch ratio of 1.62–3.76[23] and we wanted to stretch the specimens to a large deformation, but one that still lay in the sub-maximal range. Moreover, we predicted that the specimen would have permanent deformation so, to avoid compression in the unloading stage, we decided to unload to 45% failure displacement instead of unloading to the initial position. Force-displacement data were acquired at a rate of 1 s^{-1}. Two cameras Point Grey GRAS-50S5M-C acquired a picture per second during the test. Testing protocols are summarized in Table 3.1.

Throughout the mechanical tests, the sample was kept hydrated by regularly spraying 1x PBS. Samples' initial cross-sectional area was assumed to be a rectangle and both the thickness and the width were measured at the MTJ using the digital caliper with a resolution of 0.01 mm. A minimum of three measurements were performed for each dimension. For the stress calculation, force was divided by initial and non-deformed cross-sectional area. So, throughout the manuscript, the plotted stresses are engineering stresses, also known as first Piola-Kirchhoff stresses, and represent force in the current configuration divided by area in the non-deformed reference configuration. The stretch can be defined as L_f/L_i, where L_f is the final and L_i the initial grip-to-grip distance.

Table 3.1 - Summary of the testing protocols.

Procedure 1: Uniaxial Tensile Tests (N=3)
▪ Uniaxial Tension in the y-direction up to failure: displacement control, rate 0.1mm/s
Procedure 2: Relaxation and Fatigue Tests (N=13)
▪ Stress relaxation in the y-direction at 35% failure displacement: rate 10mm/s stretch, 1000s holding
▪ Rest 20 min in the initial position
▪ Preload 0.7N
▪ Uniaxial tension in the y-direction up to 60% failure displacement, unload to 45% failure displacement: displacement control, 60 cycles, rate 0.1mm/s

3.2.4. Digital image correlation

Digital image correlation was used to track a speckle pattern on a sequence of images obtained from the fatigue tests in order to calculate the displacement or strain field on the surface of the specimen. To create the speckle pattern, one surface of the specimen was sprayed with graphite powder. which was applied with a squeeze bulb pump. The outlet had a net in order to sift through smaller and more consistent speckle sizes for use. Digital image correlation was performed using the software Vic-3D 7.

3.2.5. Permanent deformation

As referred in section 3.2.2, the distance from the MTJ to the ripstop nylon was originally set to 15 mm. After the fatigue tests, the same distance was remeasured using a digital caliper in all the specimens in order to provide an estimate of the permanent deformation due to the submaximal cyclic loading.

3.2.6. Microscopic damage assessment

A histological evaluation was performed to assess if there was damage accumulation in the specimens subjected to cyclic loading at a submaximal level. We were aware that the freeze/thaw process, to which all specimens were subjected to, can affect the appearance of the muscle's microscopic structure, with loss of striation, loss of intracellular staining and formation of ice crystals[19]. As such, the analysis between the controls and tested specimens was made with those artifacts in mind when assessing any true mechanical damage.

Due to the size of each sample it was necessary to divide it in two, one part including the muscle-tendon and the other, the tendon-bone (Figure 3.4) in order to fit within the histology slide cassettes. Tendon-muscle sections were again divided in two so that one part was sliced in the y-z plane and the other in the y-x plane (Figure 3.4). Tendon-bone sections were only sliced in the y-z plane. The specimens were fixed immediately after the fatigue test in 10% Formalin for 3–4 days. In the case of each control, the specimen was kept hydrated with 1xPBS during the testing phase of the contralateral specimen and both specimens were fixed at the same time.

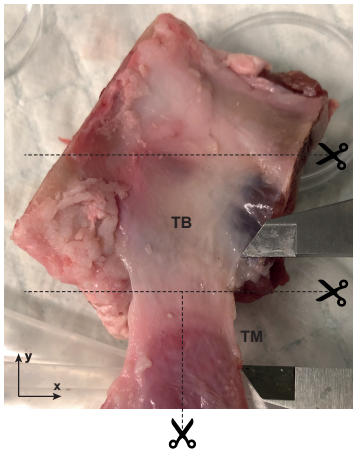

Figure 3.4 - Illustration showing how ischiococcygeal muscle specimens were divided (dashed lines with scissor logo) for histological evaluation: Tendon-Bone (TB) and Tendon-Muscle (TM) sections. Tendon-Bone samples were sliced with the microtome in the y-z plane. Tendon-Muscle samples were divided in two, according to the figure, and one section was sliced in the y-x plane while the second was sliced in the y-z plane.

After fixation, the samples were rinsed under running tap water for 20 min and then transferred to 70% Ethanol. The tendon-muscle samples were then ready for the paraffin processing procedure: 1 h in 80% ethanol, 2 h in 95% ethanol, 3 h in 100% ethanol, 3 h in xylene and 3 h in paraffin. Tendon-bone samples had to be decalcified using 20% EDTA, the decalcification being

checked regularly using a FaxitronTM X-Ray Specimen Radiography System. After decalcification, the tendon-bone specimens were submitted to the same paraffin processing procedure as the tendon-muscle specimens. The next step was to embed the samples in paraffin, which was performed using a Leica HistoCore Arcadia embedding center. A Leica RM2255 microtome was then used to section 5 µm slices of all samples. Samples were stained with Masson's Trichrome and observed on a Nikon E800 light microscope. The Masson's Trichrome stain allowed us to distinguish between muscle cells and collagen fibers, which are stained red and blue, respectively. Cell nuclei stained black.

3.2.7. Constitutive modeling and finite element simulation

Based on our experimental evidence, presented in section 3.3.1-3.3.3, we assumed a transversely isotropic response and considered the viscoelastic behavior. We chose to apply and develop a phenomenological material model since they tend to have a simpler implementation, which makes them more robust and computationally efficient than the complex multi-scale models, and often conduct to similar macroscopic results. Multi-scale models have the advantage that the material parameters have generally a straightforward relationship to with structural features[35], however, depending the desired application they are not always necessary. Moreover, multi-scale models are computationally more expensive and tend to have a greater number of material parameters which complicate any real application. We considered the Holzapfel-Gasser-Ogden (HGO)[22] model for the hyperelastic behavior, paired with the generalized Maxwell-model for the viscous effects[20,21] and a phenomenological fatigue damage material model, whose law of evolution was developed in this work. So, the complete material model is transversely isotropic visco-hyperelastic, including a continuous damage model.

Since the high water content causes soft tissues to be incompressible or quasi-incompressible[35], we applied a penalty function for the volumetric contribution to assure incompressibility. The complete strain energy function can be represented in a decoupled form as:

$$\Psi = \Psi_{vol} + [(1 - D_m) \cdot (\bar{\Psi}_m + \bar{\Psi}_m^{vsc})] + [(1 - D_f) \cdot (\bar{\Psi}_f + \bar{\Psi}_f^{vsc})] \quad (3.1)$$

where Ψ_{vol} is the volumetric contribution, $\bar{\Psi}_m$ is the isochoric matrix contribution, $\bar{\Psi}_f$ the isochoric collagen fibers contribution, $\bar{\Psi}_m^{vsc}$ and $\bar{\Psi}_f^{vsc}$ are the viscous contributions associated respectively with the ground matrix and with the collagen fibers. D_* $\left(0 < D_* < 1\ _{*=m,f}\right)$ are the continuous damage variables affecting each isochoric contribution of the strain energy. The index m, f refer respectively to the ground matrix and collagen fibers contributions or material parameters. The specific contributions can be defined as:

$$\Psi_{\mathrm{vol}} = \kappa\left(\frac{J^2-1}{2} - \ln(J)\right) \tag{3.2}$$

$$\bar{\Psi}_{\mathrm{m}} = C_{10}(\bar{I}_1 - 3) \tag{3.3}$$

$$\bar{\Psi}_{\mathrm{f}} = \frac{k_1}{2k_2}\{\exp[(\bar{I}_4 - 1)^2] - 1\} \tag{3.4}$$

$$\bar{\Psi}_{*}^{\mathrm{vsc}} = \sum_{\alpha=1}^{m} \gamma_{*\alpha}(\bar{\mathbf{C}}, \bar{\boldsymbol{\Gamma}}_{\alpha}) \qquad {}_{*=\mathrm{m,f}} \tag{3.5}$$

where $J = \det \mathbf{F}$ is a measure of the volume variation, being $\mathbf{F}$ the deformation gradient. $\mathbf{C} = \mathbf{F}^{\mathrm{T}}\mathbf{F}$ is the right Cauchy-Green deformation tensor and $\bar{\mathbf{C}} = J^{-2/3}\mathbf{C}$ is the isochoric right Cauchy-Green deformation tensor, associated with the volume preserving deformation of the material. $\bar{I}_1 = \mathrm{trace}(\bar{\mathbf{C}})$ is the first invariant of the of the isochoric Cauchy-Green tensor and $\bar{I}_4 = \bar{\lambda}_{\mathrm{f}}^{\,2} = \mathbf{m}_0 \cdot \bar{\mathbf{C}}\,\mathbf{m}_0$ is a pseudo-invariant arising directly from the anisotropy that is equal to the square of the stretch $\bar{\lambda}_{\mathrm{f}}$ in the fiber direction $\mathbf{m}_0$. $\gamma_{*\alpha}$ are scalar-valued functions that may be seen as a dissipative potential and $\bar{\boldsymbol{\Gamma}}_{\alpha}$ are tensorial variables, akin $\bar{\mathbf{C}}$, and characterize the viscoelastic isochoric response of the material. $\alpha = 1,2, \ldots m$ represents the number of viscoelastic processes, denoted by the number of parallel elements in the Maxwell model. Each Maxwell element can be represented by a spring in series with a dashpot. The spring represents the solid behavior and is characterized by a free energy parameter $\beta_{*\alpha}$ $_{*=\mathrm{m,f}}$ and the dashpot characterizes the viscous behavior and is function of a relaxation time $\tau_{*\alpha}$ $_{*=\mathrm{m,f}}$. The material parameters of this constitutive model are: C_{10} for the ground matrix contribution, k_1 and. k_2 for the fiber contribution, $\alpha = 1,2, \ldots m$, $\beta_{*\alpha}$ $_{*=\mathrm{m,f}}$ and $\tau_{*\alpha}$ $_{*=\mathrm{m,f}}$ for the viscous contribution and κ, which is the bulk modulus, for the volumetric contribution. Since we wanted to guarantee incompressibility, we defined the bulk modulus to a very high value, κ =100000, which was sufficient to guarantee that $J = 1$ and $\Psi_{\mathrm{vol}} = 0$. More details concerning the transversely isotropic material model and the generalized Maxwell model for viscoelasticity can be found elsewhere[20–22].

The novelty of this constitutive model is the continuous damage model, which was developed using the concept of accumulated equivalent strain Ξ_t^{acc}, as defined by Peña, et al 2009[42]. This allows for a continuous damage accumulation within the whole strain history of the deformation process[42]. It can be represented as:

$$\Xi_t^{acc} = \int_0^t \left|\frac{\mathrm{d}\bar{\Psi}(\mathbf{C})}{\mathrm{d}s}\right| ds \tag{3.6}$$

Which gives a simple equation of evolution:

$$\frac{\mathrm{d}\Xi_t^{acc}}{\mathrm{d}t} = \left|\frac{\mathrm{d}\bar{\Psi}(\mathbf{C})}{\mathrm{d}t}\right| \tag{3.7}$$

The damage propagation and accumulation was defined using a modification of Lemaitre and Plumtree nonlinear cumulative expression[39], in which the ratio between the number of cycles and the number of cycles to fatigue failure was replaced with the ratio between the accumulated equivalent strain and its maximum value. We also added a parameter, D_{max}, which allows one to control the weight of the damage variable. This parameter was added mostly due to numerical problems that often arise when performing a complex simulation with a damage material model. If the damage variable evolves to be equal to 1 in all the isochoric strain energy contributions, even if only in one finite element, the simulation stops since there is no stiffness in that finite element. This indicates that there is a tear in that region, but it can bring the simulation to an abrupt and early halt. To overcome this problem, we can now define the maximum amount of damage with the D_{max} parameter. Even if we are expecting a complete tear, we can set it to be almost equal to 1 and complete the simulation. In our case, we decided to be more conservative and set the maximum damage of the ground matrix to 0.9, since no complete tear was observed in the specimens (see section 3.3).

$$D_{*} = D_{max\,*}\left\{1 - \left(1 - \frac{\Xi_{t\,*}^{acc}}{\Xi_{max\,*}^{acc}}\right)^{1/C_{*}}\right\}_{*=m,f} \tag{3.8}$$

The maximum value of the accumulated equivalent strain Ξ_{max}^{acc}, the exponent C and the weight parameter D_{max} ($0 < D_{max} \leq 1$) are the damage model material parameters.

One interesting aspect about this law of evolution is that despite its simplicity, we can consider a linear or nonlinear evolution just by controlling the parameter C. If C<1 the evolution is nonlinear and faster in the earlier deformation stages, for C=1 the evolution is linear, and for C>1 it is again nonlinear but slower in the initial deformation stages and faster closer to the tearing point. For this reason, it is a versatile damage law that can be applied to different materials.

The criteria for damage evolution can be represented as:

$$\dot{\Xi}_{t}^{acc} = \begin{cases} \dfrac{d\bar{\Psi}}{dt}, & \dot{\Xi}_{t}^{acc} \geq 0 \\ 0, & \dot{\Xi}_{t}^{acc} < 0 \end{cases} \tag{3.9}$$

To calibrate the constitutive material parameters (with exception of $D_{max\,*}$), a micro-genetic algorithm was developed using MATLAB® integrated with Python and ABAQUS® finite element software. Succinctly, the micro-genetic algorithm generates randomly a micro population of nine elements. Afterwards, the fitness of each element is analyzed, and the fittest element is carried on to the next generation. The remaining elements go through a tournament selection strategy in which the winner elements become parents to the next generation. To develop the next generation, these parents suffer a crossover to create the elements of the next generation. After this, the convergence of the population is checked and if there is no diversity, the micro-population is restarted randomly, with exception of the fittest element, which is always carried to the next

generation. In this work, the elements of the population were the constitutive model parameters and the fitness of each element was evaluated using a least squares evaluation function, F_e, between the experimental data and the solution from the numerical software ABAQUS®, in which our material model was implemented via user-defined subroutine UMAT:

$$F_e = \sqrt{\sum_{i=1}^{n} \frac{\left(P_i^e - P_i^\Psi\right)^2}{n-2}} \tag{3.10}$$

n is the number of considered experimental points and P_i^e and P_i^Ψ are respectively the engineering stresses in the direction of the applied stretch from the experimental data and from the numerical simulation in ABAQUS®.

The simulation was performed to replicate the experimental protocol of the fatigue experimental tests, including the 60 cycles and 3212 experimental points. The geometrical model used to calibrate the parameters is presented in Figure 3.5 and it is a simplification of our average specimen. Only 1/8 of the specimen was modelled since we applied symmetry boundary conditions. The mesh consists in 224 eight-node brick elements (C3D8). The bottom elements were clamped to simulate the grip in the experimental test. The fibers were assumed to have a principal direction, which was defined in the direction of the applied stretch. The variable used to compare with the experimental data was the engineering stress in the direction of the applied load. We decided to use an averaged response of all the finite elements in the geometrical model, since our experimental data corresponds also to an averaged response of the complete specimen. Since we calibrated the material parameters from all the contributions (hyperelastic, viscoelastic and damage) simultaneously, the constitutive model is able to capture the overall behavior, thereby overcoming the inconsistency that might occur with the Generalized Maxwell model for viscoelasticity[44].

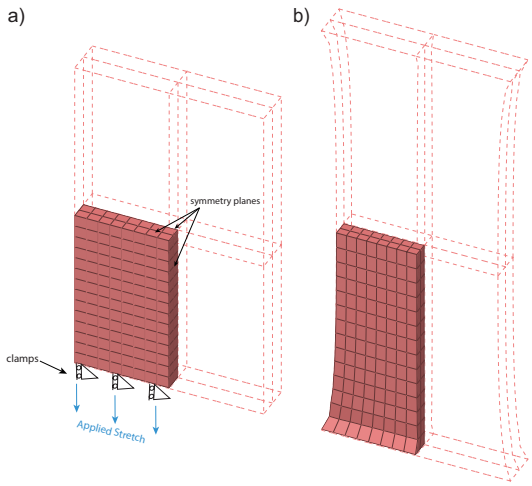

Figure 3.5 - Finite Element model for the simulation of the experimental fatigue tests integrated in the micro-genetic algorithm for the calibration of the constitutive model parameters. The finite element model consists in a simplification of 1/8 of the averaged specimen. Representation of the boundary conditions and direction of the applied stretch. **a)** initial configuration **b)** deformed configuration at the peak displacement.

To evaluate the fitting, we calculated the coefficient of determination and the absolute error mean. The coefficient of determination can be obtained as:

$$R^2 = 1 - \frac{S_{res}}{S_{tot}} \tag{3.11}$$

where $S_{res} = \sum_{i=1}^{n}\left(P_i^e - P_i^\Psi\right)^2$ is the sum of the squares of the residuals with the experimental data values and $S_{tot} = \sum_{i=1}^{n}\left(P_i^e - \overline{P_i^e}\right)^2$ is the total sum of squares, with the mean of the experimental data $\overline{P_i^e}$, and n is the number of data points.

The absolute error mean can be defined as:

$$\bar{r} = \frac{\sum_{i=1}^{n}\left|P_i^e - P_i^\Psi\right|}{n} \tag{3.12}$$

where $\sum_{i=1}^{n}\left|P_i^e - P_i^\Psi\right|$ is the sum of the absolute differences between the experimental data and the numerical values and n is the number of data points.

The coefficient of determination is widely used, and varies between 0 and 1, being 1 the optimal value. The mean absolute error allows to quantitatively analyze the differences and, when compared with the resolution of the experimental measurements, can also be a tool to test the fitting. In our work, since we are analyzing engineering stresses, the resolution can be obtained dividing the force resolution by the area resolution. According to the ADMET specifications, the force resolution is 0.001N, and due to the digital caliper used in the area measurements, area resolution is 0.01mm^2. As such, the resolution of the engineering stresses is 0.1 MPa.

After calibrating the constitutive model parameters, we decided to use the finite element model to better understand the response of our specimen and its material properties. As presented in sections 3.3.2 and 3.3.3, the specimen has a visco-hyperelastic behavior and shows signs of material damage. As such, applying the same simulation used for calibrating the material parameters, we compare the response considering the complete constitutive model, with a response including only a viscoelastic behavior and including only the continuous damage model. This helps one understand the effect of each contribution.

3.3. Results

The longitudinal length (approximate distance between pubic symphysis and coccyx) and cross-sectional width (approximate distance between the obturators) were measured in all pelvises to be 11.85±1.86mm and 10.13±3.14mm, respectively. The weight and age of the sheep was provided in the 8 pelvises (16 specimen) used for the relaxation and fatigue tests and were 83.3±8.2Kg and 1 year 10 months±7 months, respectively.

The mean width of all the specimens at the MTJ was 14.89±2.63mm, the thickness was 3.07±0.57mm and the initial grip-to-grip distance 25.72±6.24mm.

3.3.1. Ultimate tensile tests

The average results of the force-displacement curve are illustrated in Figure 3.6a. Using the averaged response, the ultimate tensile displacement was 17.1±2.4mm and the ultimate tensile force 79.8±8.8N. Normalizing, the ultimate tensile stretch was 1.97±0.45 and the ultimate tensile engineering stress 2.1±0.2 MPa.

3.3.2. Relaxation tests

In the relaxation tests, the specimens were stretched 6 mm (35% failure displacement) and the displacement was maintained during 1,000 s. The normalized engineering stress-time curve of the experiments and its averaged response is illustrated in Figure 3.6b. The normalized engineering stress is the current stress divided by the peak stress. At the end of the 1,000s there was an 81±3.8% stress relaxation.

3.3.3. Fatigue tests

The fatigue tests consisted in 60 cycles of stretching the specimen until 10.3mm (60% failure displacement) and return the position until 7.7mm (45% failure displacement). The averaged response of the engineering stress-stretch curve and the engineering stress-time curve is illustrated in Figure 3.6c-d. Due to the amount of data in these graphics, we decided to present only the mean response. All the specimens presented visible permanent deformation after the fatigue tests, yet no macroscopic failure was visible.

The strain distribution in one example specimen, obtained from the digital image correlation, is illustrated in Figure 3.7. It shows the evolution of the strain field during the fatigue test. Each picture captures the specimen during a loading peak cycle, specifically during the 1st, 20th, 40th and 60th peak cycle. The averaged measured permanent deformation was 7.37±2.20mm, which in terms of stretch corresponds to 1.49±0.15.

3.3.4. Histologic assessment

Figure 3.8 illustrates muscle-tendon sections from both control and tested specimens. All the pictures were obtained from the muscle portion approximately 5-15mm from the MTJ. Compared to the untested controls, it is possible to see significant fiber disruption and increase in the interstitial spaces in the specimens stretch at 60% failure displacement for 60 cycles. Figure 3.8f and g) illustrate individual fiber disruption occurring adjacent to apparently normal muscle fibers. Figure 3.8d and h) show kinked and distorted muscle fibers, which we take as one sign of cumulative damage.

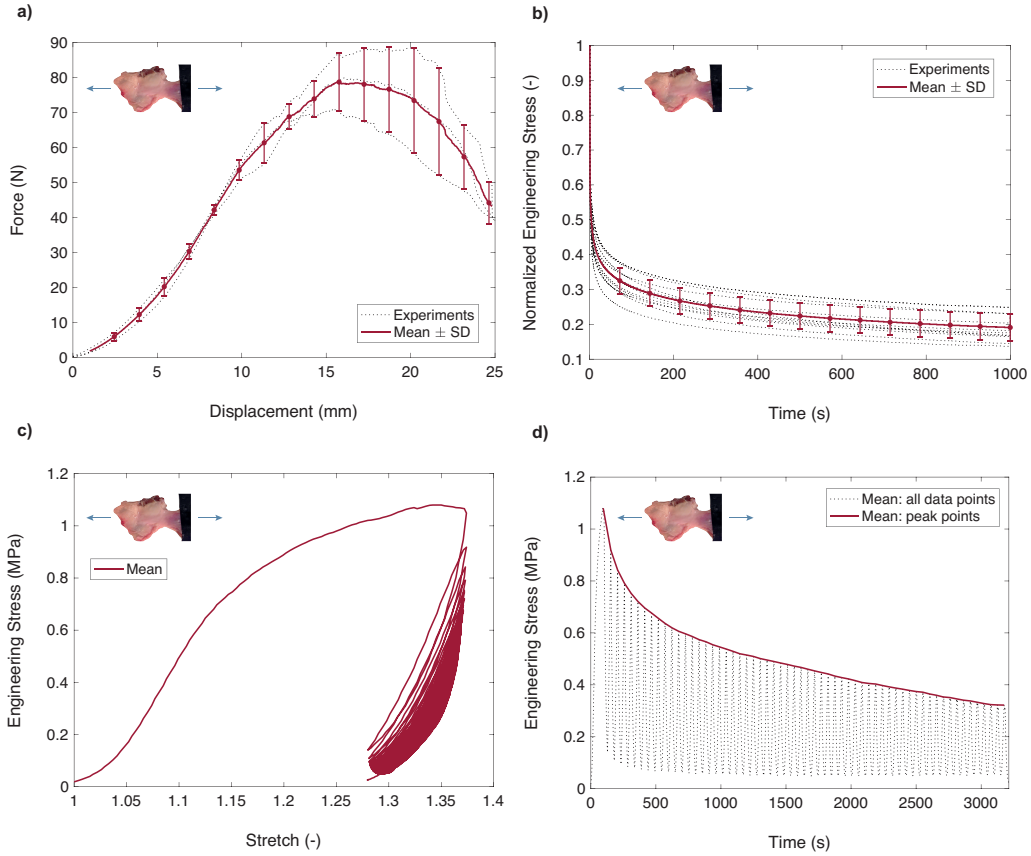

Figure 3.6 - Force-displacement curves from the ultimate tensile tests (dashed lines). **a)** Averaged response: mean ± SD (standard deviation) (solid line). **b)** Averaged response of the relaxation tests: normalized engineering stress (current stress/peak stress) of all the experiments (dashed lines). Averaged response: mean ± SD (solid line). **c-d)** Averaged response of the fatigue tests **c)** engineering stress-grip to grip stretch **d)** engineering stress-time.

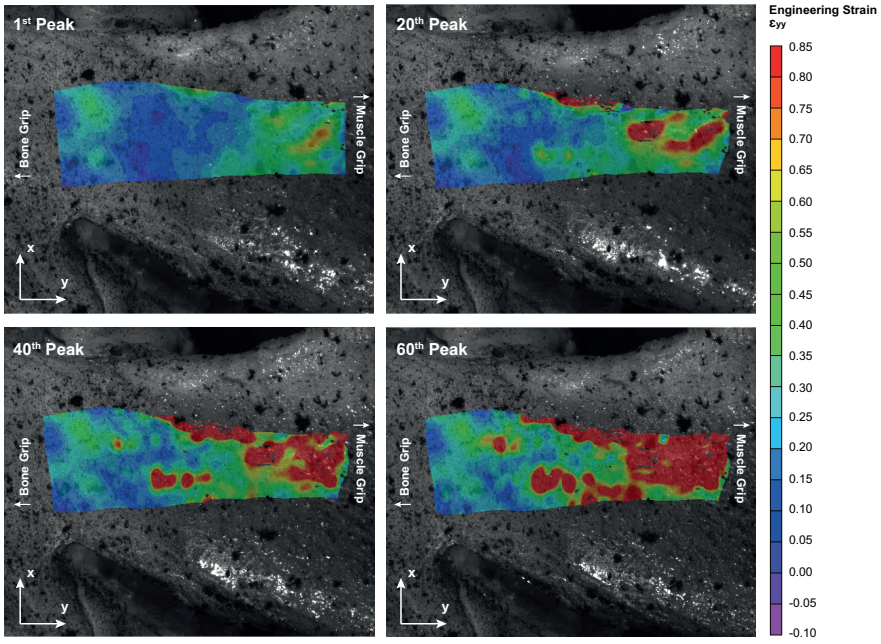

Figure 3.7 - Evolution of the engineering strain εyy distribution throughout the fatigue test in specimen 6R.

Figure 3.9 shows sections from muscle-tendon specimens at the MTJ. Figure 3.9a-b show muscle fibers attaching to the collagen fibers from the tendon. Although the two sections are from tested specimens, both collagen and muscle fibers show a normal appearance. Figure 3.9c-d show an area of just collagen fibers, being d) a control specimen. Although collagen fibers seem to be more crimped in the untested specimen, there are no evident signs of damage in the collagen tissue.

Finally, Figure 3.10 shows structures from tendon-bone specimens. No signs of damage are visible in the muscle fibers (Figure 3.10a) in the collagen fibers (Figure 3.10c) or in the tendon-bone junction (Figure 3.10e).

3.3.5. Calibration of constitutive parameters

Using the micro-genetic algorithm, we calibrated the constitutive parameters to capture the visco-hyperelastic behavior, including the fatigue damage that we obtained from the experimental tests. Figure 3.11a and b compares the calibrated constitutive model from section 3.2.7 with the fatigue experimental data. We were more interested in capturing the stress decrease due to the viscoelastic behavior and due to the fatigue continuous damage, as such, we were more focused in capturing correctly the peak values in each loading cycle. Looking at all the data points in Figure 3.11a the coefficient of correlation is 0.891, not as good as when we focus only on the peak points (Figure 3.11b) which is 0.912. Moreover, the mean absolute error considering all the 3,212 data points was 0.051 MPa, while considering only the peak points it was 0.027 MPa. Since both absolute errors are lower than the precision of the stress calculation, which is 0.1 MPa (see section 3.2), we believe our correlation is sufficient to capture the behavior of the material. The calibrated material parameters are presented in Table 3.2.

Table 3.2 - Constitutive model parameters obtain from the micro-genetic algorithm optimization.

Hyperelastic Parameters	**Viscoelastic Parameters**	**Continuous Damage Parameters**
$C_{10} = 0.14$ MPa	$\beta_{m,f\,1} = 5.08\ (-)$	$D_{max\,m} = 0.9\ (-)$
$k_1 = 0.05$ MPa	$\tau_{m,f\,1} = 33.59$ s	$\Xi^{acc}_{max\,m} = 4.07$ MPa
$k_2 = 0.23\ (-)$	$\beta_{m,f\,2} = 0.79(-)$	$C_m = 1.65\ (-)$
	$\tau_{m,f\,2} = 44.14$ s	$D_{max\,f} = 1.0\ (-)$
		$\Xi^{acc}_{max\,f} = 2.25$MPa
		$C_f = 0.27\ (-)$

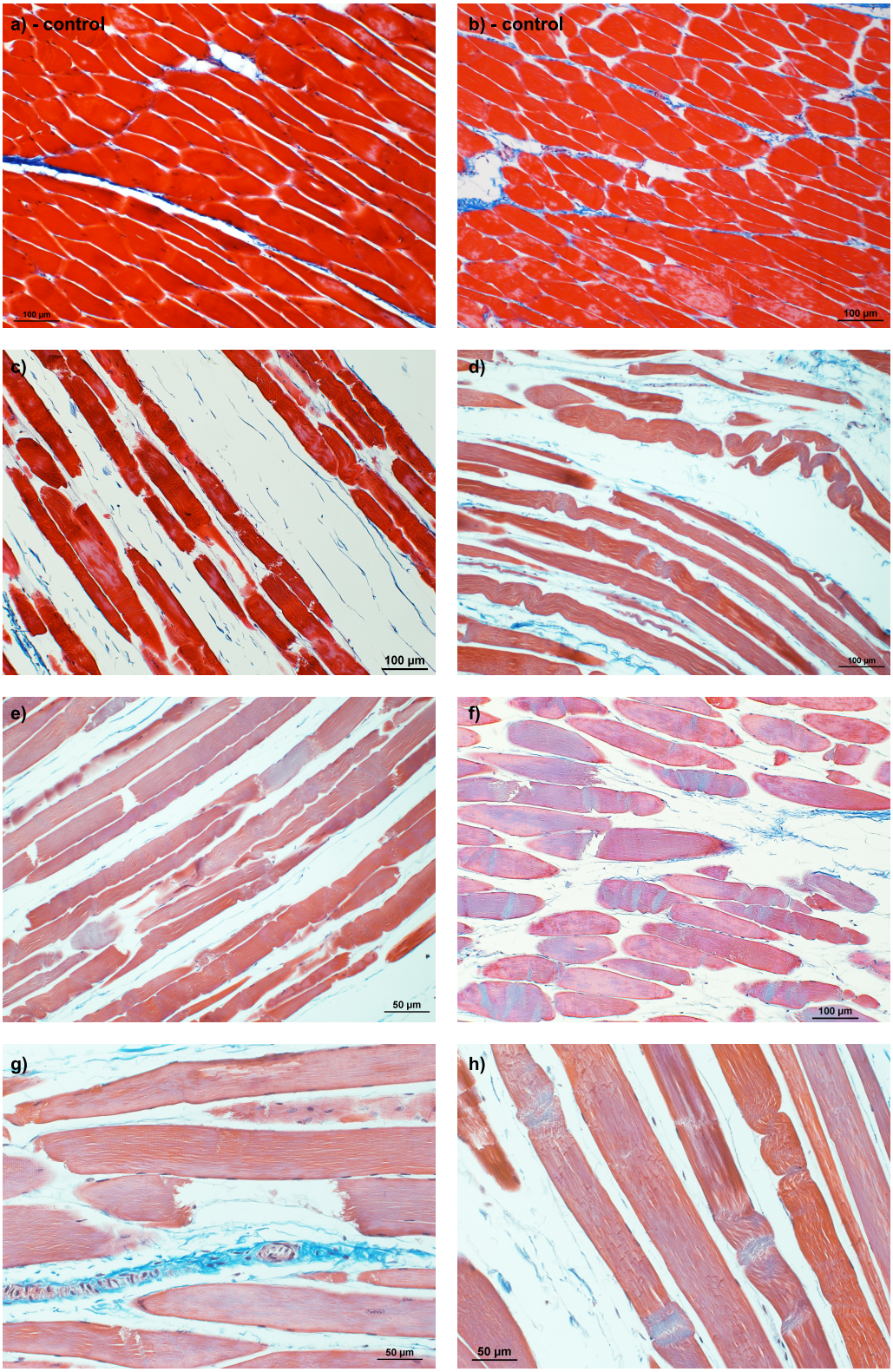

Figure 3.8 - Histological appearance of muscle-tendon sections with Masson's Trichrome stain. Comparison between untested controls **(a-b)** and fatigued specimens **(c-h)** (60 cycles between 60% and 45% of failure displacement). Fatigued specimens show kinked muscle fibers, individual fibers disruption and increase in interstitial spaces. **a)** Specimen 4L – control (~5 – 10mm of MTJ, ×10) **b)** Specimen 4L – control (~10 – 15mm of MTJ, ×10) **c)** Specimen 5R (~10 – 15 mm of MTJ, ×10) **d)** Specimen 10L (~10 – 15mm of MTJ, × 10) **e)** Specimen 10R (~10 – 15mm of MTJ, ×10). **f)** Specimen 5L (~10-15mm of MTJ, ×10) **g)** Specimen 10L (~10 – 15mm of MTJ, ×20) **h)** Specimen 10L (~5 – 10mm of MTJ, ×20).

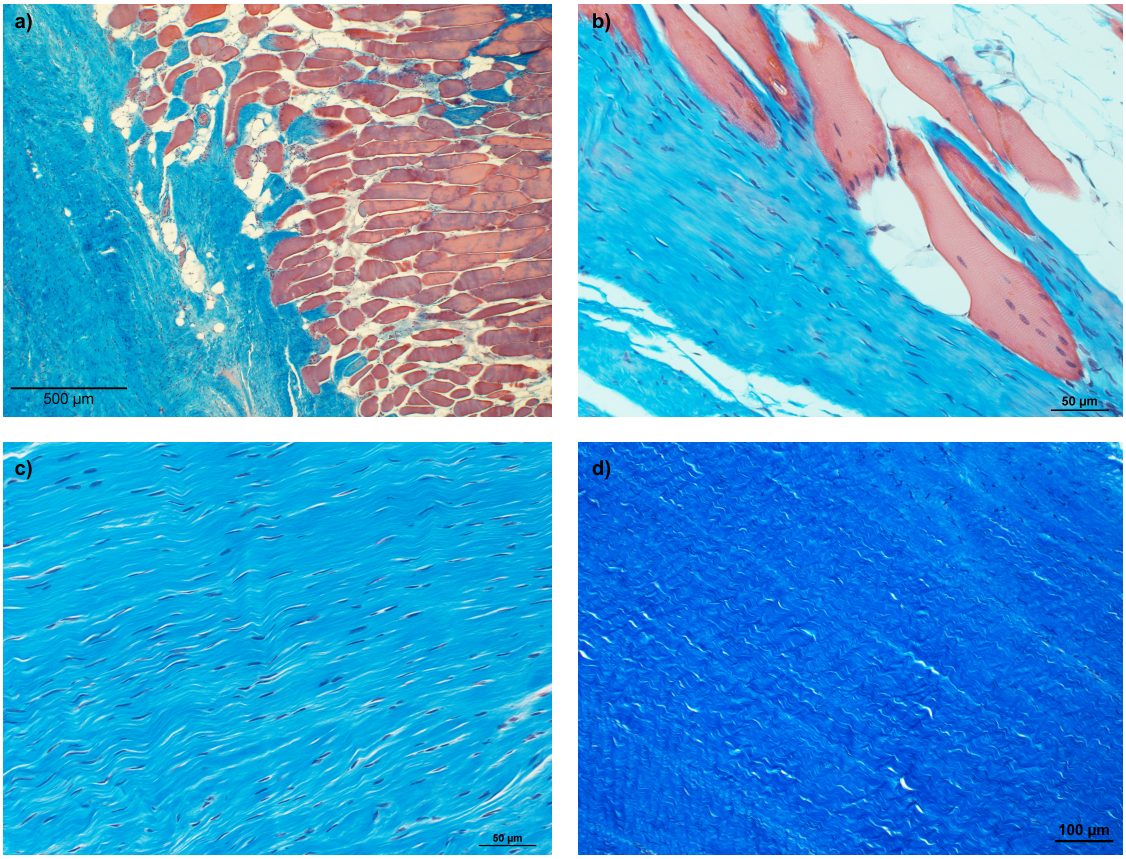

Figure 3.9 - Histological appearance of muscle-tendon sections at the MTJ with Masson's Trichrome stain. Collagen and muscle fibers with normal appearance in the MTJ and in the collagen fibers. **a)** Specimen 9L (×4). **b)** Specimen 10L (×20). **c)** Specimen 10R (×20). **d)** Specimen 4L – control (×10).

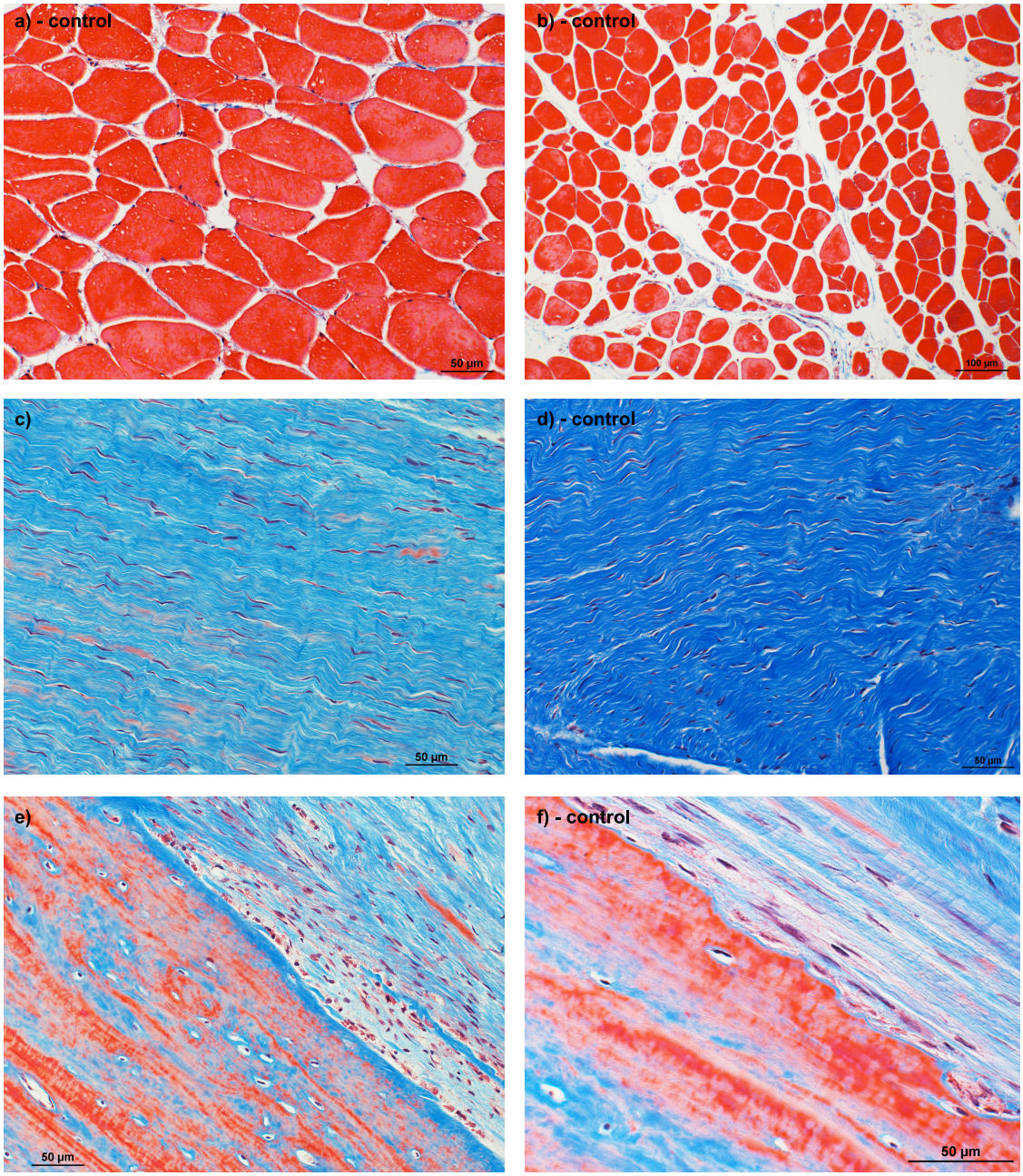

Figure 3.10 - Histological appearance of tendon-bone sections with Masson's Trichrome stain with normal appearance comparing untested controls and fatigued specimens (60 cycles between 60% and 45% of failure displacement) shows a normal appearance. **a)** Specimen 5L (×20) **b)** Specimen 3R- control (×10) **c)** Specimen 5R (×20) **d)** Specimen 4L – control (×20) **e)** Specimen 5R (×20) **f)** Specimen 3R – control (×40).

3.3.6. Numerical analysis and interpretation of the specimen behavior

In this section we used the geometrical and material model described in section 3.2.7 to better interpret the experimental results from the fatigue tests and the overall mechanical behavior of the specimen. We performed a simulation of the fatigue tests using the complete constitutive model with the calibrated parameters described in Table 3.2, but also for a material that is only visco-hyperelastic, without damage, and one that is only hyperelastic including damage. The purpose was to analyze separately the effects of viscoelasticity and the effects of material damage on the response of the biological materials.

Figure 3.11c shows the normalized engineering stress-time response for the three materials. The stress was normalized dividing by the peak value of each curve, which allows for a better comparison of the results. We can see that viscoelasticity is responsible for most of the energy dissipation in the first loading cycles. However, after approximately 10 loading cycles it reaches an almost equilibrium state, and the stress softening occurs mostly due to the continuous damage model. Combining both models, we have the solution that most approaches our experimental data. This confirms that our specimen has a characteristic behavior of a visco-hyperelastic material and that the 60 cycles at 60% failure displacement were sufficient to cause material damage.

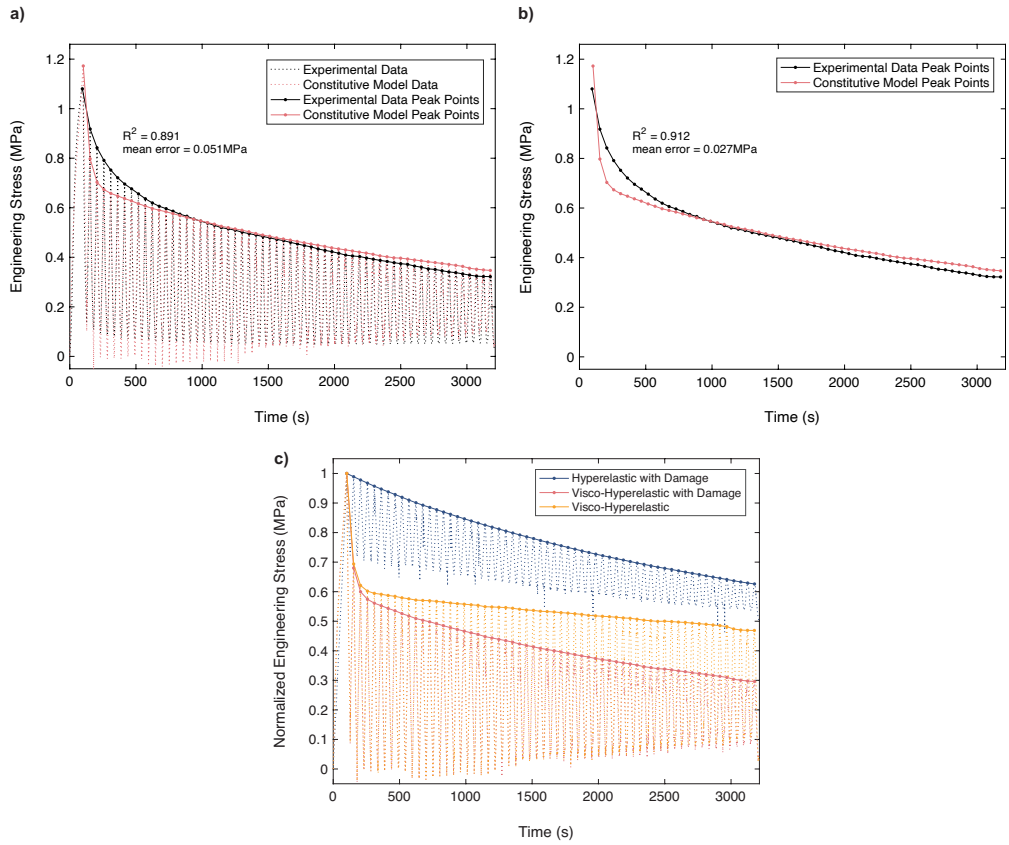

Figure 3.11 - a-b) Calibration of constitutive model parameters for the averaged response of the fatigue tests. **a)** comparison and coefficient of correlation with all the 3212 data points. **b)** comparison and coefficient of correlation for the peak points. **c)** normalized engineering stress-time response of the experimental fatigue test simulation for different materials. Pink curve represents a visco-hyperelastic material including continuous damage, yellow curve represents a visco-hyperelastic material and blue curve an hyperelastic material including continuous damage.

3.4. Discussion

We believe that this is the first study investigating the biomechanical properties of the origin of the most caudal pelvic floor muscle, the ovine ishiococcygeous muscle, which serves as a homolog to the origin of the pubovisceral muscle in humans[6]. The primary finding of this research is that the origin of the ishiococcygeous muscle can accumulate low cycle fatigue damage under sub-maximal repetitive loading. This was observable not only in the stress-time curves but also in the microscopic analysis performed afterwards. The significance of the most caudal pelvic floor muscle is that in both the sheep and human, this muscle is the muscle that has to stretch the most in order to allow the fetal head to pass out of the birth canal, and it is the most likely to suffer a stretch-related injury.

As expected, the material behavior of the specimen was nonlinear and hyperelastic. This can be seen by the force-displacement curve from the ultimate tensile tests since the specimen was highly deformable and the relation between force and displacement was nonlinear (Figure 3.6a). We did not find data in the literature for the failure properties of the origin of the pubovisceral muscle in humans or animal models. However, there is *ex-vivo* data on human vaginal tissue, that has been reported to fail at a stress of 2.1–3.5 MPa and a stretch of 1.30–1.33[15,36] and also on human pelvic ligaments, with the uterosacral ligament reportedly failing at a stress of 6.3 MPa and a stretch of 1.59[37] and the round ligaments at a stress of 4.3 MPa and a stretch of 1.77[37]. There is also one study that reports *ex-vivo* failure of a segment of human levator ani at a stress of approximately 0.24 MPa and a stretch of 1.37[40]. Although these are different structures, it gives a baseline for the order of magnitude of the failure parameters of biological tissues in the pelvic region. We obtained a failure stress of 2.2 MPa and a failure stretch of 1.97, which is of the same order of magnitude of values found in the literature for tissues in the pelvic region providing some face validity.

The relaxation test allowed us to see that the origin of the ishiococcygeous muscle is highly viscoelastic since there is a significant stress relaxation when maintaining the same displacement for 1000 s. In fact, we obtained an 81% decrease of the stresses after the 1000 s (Figure 3.6b). Viscoelasticity is extremely important for biological tissues, but most especially for tissues in the female pelvis, since it allows tissues to withstand larger deformations with less damage[1]. This is particularly important during childbirth since it is the relaxation of the vagina and other pelvic floor tissues over time that allow further dilatation as labor progresses [24].

The mechanical effect captured from the fatigue tests confirms both the nonlinear hyperelastic and viscoelastic behavior. During the first cycle there is a significant hysteresis, which indicates a substantial energy dissipation. Over time the effects of hysteresis diminish, but not to an equilibrium state. This equilibrium state means that over time a steady state would be reached in

the response of the tissue, typically in 10–20 cycles, if there was no damage to the material[1,38]. However, it can be seen in the stress-stretch curve and in the stress-time curve that our material does not reach a steady state in the 60 cycles (Figure 3.6c and d). This indicates that there is continuous energy dissipation for which material damage is responsible. Besides the indication of damage due to the energy dissipation seen in the stretch-time curves, we also observed macroscopically that the specimen exhibited permanent deformation after the fatigue tests. However, no macroscopic tears were visible during and after the test. So, what might be responsible?

The histological analysis took our findings to another level. It confirmed the presence of damage at the microscopic scale and showed the weakest regions of the bone-tendon-muscle unit that constitutes the origin of the ishiococcygeous muscle. The main findings were individual muscle fiber rupture and kinked muscle fibers that occurred in the muscle in an approximately 5–15 mm region of the MTJ (Figure 3.9). Importantly, neither the MTJ nor the tendon-bone sections showed any apparent sign of damage (Figure 3.10). Moreover, we could not identify obvious signs of damage in the collagen fibers, although compared with the untested controls, fatigued specimens did seem to have less crimped collagen fibers (Figure 3.9c and d, Figure 3.10c and d). This is consistent with the results from the strain distribution obtained through the speckle pattern (Figure 3.7) that shows engineering strains of approximately 0.85 in the muscle and musculotendinous region, but only 0.15–0.45 in the tendon and tendon-bone region for the same globally applied stretch. So, we rejected our working hypothesis and instead accepted one of the alternatives hypothesis, namely that the accumulation of damage occurred at a different site than the tendon-bone junction. In particular, we verified accumulation of damage in the muscle fibers near the MTJ.

To have a better understanding of the characteristic behavior of our specimen, we developed and implemented a visco-hyperelastic material model including continuous damage. Using the finite element software ABAQUS® and the user-defined subroutine UMAT, we were able to simulate the fatigue test mimicking our experimental protocol. We included the material having a visco-hyperelastic behavior because of the experimental fatigue curves that we obtained. We were able to confirm that behavior by performing the same simulation considering only an hyperelastic material with continuous damage and a visco-hyperelastic material without damage. We saw that the viscoelasticity is responsible for the major energy loss in the first 3–4 cycles (Figure 3.11c). This is a defense mechanism of soft biological tissues, since for the same applied stretch, the stresses decrease, allowing tissues to withstand larger deformations with less damage. On the other hand, the continuous stress softening that is observed throughout the remaining loading cycles does not occur due to viscoelasticity. Comparing the purely visco-hyperelastic material with the visco-hyperelastic material including continuous damage, we can see that after 3–4 cycles the stresses continue to significantly decrease for the material where damage is

considered. For the visco-hyperelastic material without damage, there are only minor decreases, because the material reaches an equilibrium. However, this stress softening that is associated with continuous damage is not a defense mechanism as it occurs with viscoelasticity. On the contrary, it occurs because the repetitive loading causes material damage accumulation capable of affecting the microscopic-scale mechanical properties of the material. In other words, it weakens the material, making it more prone to tear due to a load that in an undamaged state would not be enough to cause failure.

Numerous studies have been focused on the effects of cyclic loading in collagen fibers and collagen fibrils, reporting signs of accumulated damage as kinked patterns in the collagen fibers and fiber disruption[5,16,46,51,52]. According to Fung, D.T et al.[16], initial fatigue loading lengthens the collagen fibers from a crimped to an uncrimped state. Continued loading causes stretching of a local population of collagen fibers into their plastic range of deformation, causing the formation of kinked deformation patterns. Further loading leads to rupture of the plastically deformed collagen fibers. However, only the tendon or other collagenous structures were being tested in those studies. Here, we included the complete muscle origin and show that the weakest region in the passive ishiococcygeous muscle is the muscle near the MTJ. The collagen fibers showed significant less deformation and after the 60 loading cycles they only appear to be less crimped than the untested controls. This is consistent with the initial fatigue loading phase postulated by Fung, D.T et al.[16]. One interesting fact is that cyclic loading seems to affect the muscle fibers in a similar way than the collagen fibers, since we could see in the histological analysis that the muscle fibers are deformed into their plastic range, which caused kinked muscle fibers and fiber disruption.

The present study has several limitations. First, our specimens came from non-pregnant sheep and since it is expected that pregnant pelvic tissues are more compliant[43], the amount of damage may have been overestimated in this study if one is considering the second stage of labor. Secondly, this was an *in vitro* study of passive inert muscle and the muscle-tendon-bone unit may behave differently *in vivo*, especially given that active contractions can occur. With active contractions the muscle and collagen fiber stress would be expected to increase[7], so considering this aspect, our present observations of the extent of damage accumulation may be conservative. Thirdly, we froze the specimens once, which might have had some influence on the tissues[19], although we bore that in mind when studying the histological sections. Fourthly, we saw with the speckle pattern that the strain distribution is not the same throughout the specimen, so interpretation of the engineering stress-strain curves needs to take that into account. In effect, they represent an averaged overall behavior of the bone-tendon-muscle unit. Fifthly, the digital image correlation software did not work over the duration of the experiment for all the specimens, so we did not obtain the strain field throughout the fatigue experiment in the 13 tested specimens. We believe this happened since we have a high deformation and a long experiment, which caused

the software to lose correlation of the speckle points as the experiment progressed in some of the specimens. In the future we plan to test beforehand better ways to apply the speckle pattern in order to overcome this problem. Lastly, from a structural point of view the part of the ishciococcygeal muscle that is the closest homolog to the human pubovisceral muscle is the part that inserts onto the sheep lateral vagina, in a similar manner that the pubovisceral muscle inserts onto the human perineal body and lateral vagina. Hence it might be fruitful in the future to focus on the mechanical behavior of this subdivision of the muscle (i.e., the medial- most of the two 'TM' specimens visible on the right side of Figure 3.4).

Nevertheless, we believe this study is the first to characterize biomechanically the origin of the ishiococcygeous muscle, a homologous structure to the origin of the pubovisceral muscle in humans. It showed that the complete bone-tendon-muscle origin exhibits a nonlinear and highly viscoelastic behavior, even in a non-pregnant state. The weakest region is the muscle near the MTJ, which is the material that has the highest deformation for the same applied stretch. When cyclically stretched at a sub-maximal displacement, it is capable of accumulating damage at a microscopic level, which weakens the material. The evidence of damage accumulation included kinked muscle fibers and muscle fiber disruption in the areas with higher deformation, namely in the muscle near the MTJ. We also developed a material constitutive model, applicable in ABAQUS® finite element software, that was able to capture the stress softening due to viscoelasticity and the continuous damage. This can be useful for testing more complex loading scenarios that occur during the second stage of labor.

We believe that this work can guide future studies on the origin of the pubovisceral muscle. Future work should be focused on verifying our findings in pregnant tissues and in human specimens, if possible. This is an important topic since the origin of the pubovisceral muscle is commonly torn, sometimes completely so, during a difficult vaginal delivery; it is never repaired because the surgical risk outweighs any benefit. Understanding the behavior of the weakest region of the bone-tendon-muscle unit is important in helping to improve the management of injury afterwards. But even more important is the urgent need to prevent the injury in the first place. If our results are corroborated by others, understanding that the muscle can accumulate damage with repetitive large loading cycles, which can weaken the region and make it prone to tear, could lead to a change and standardization in the management of labor. Currently, there are different pushing techniques that lead to different pushing patterns that cause different numbers of pubovisceral muscle loading cycles during the second stage of labor[31].

This is the first study to show the possibility of fatigue damage accumulating at the origin of the last pelvic floor muscle engaged by the fetal head during delivery, namely the ishiococcygeous muscle in sheep, which corresponds to the pubovisceral muscle in humans, the muscle that undergoes the greatest stretch at the end of the second stage of delivery. Although further studies

are needed, we hope that our findings trigger additional research in this area that can ultimately lead to designing an improved management of labor, with better outcomes for the mother.

3.5. Conclusions

Our findings showed that the origin of the ishiococcygeous muscle from mature sheep, a muscle that is homologous to the pubovisceral muscle in humans, can accumulate damage at the microscopic level due to a sub-maximal repetitive loading of only 60 cycles at 60% failure displacement. This damage accumulation was seen in the muscle from 5 to 15 mm from the MTJ. Evidence of damage was the presence of kinked muscle fibers, indicating permanent deformation, and individual muscle fiber rupture. Although there was not sufficient data to confirm this, it is possible that the first stage of fatigue is the permanent deformation of muscle fibers, which cause the fiber kinking. With the continuity of the loading cycles those kinked fibers eventually tear. Besides the microscopic evidence of damage, the 60 cycles at 60% failure displacement were sufficient to affect the mechanical properties of the specimen, as seen by the continued energy dissipation in the stress-time curve.

This work showed that the weakest region in the bone-tendon-muscle unit of the ovine ishiococcygeous muscle origin to be the muscle near the MTJ, and that muscle can accumulate damage due to a repetitive sub-maximal loading that negatively affects its mechanical properties.

Acknowledgements

Research reported in this publication was supported by U.S. Public Health Service awards P30 AG024824 and P30 AR069620. The content is solely the responsibility of the authors and does not represent the official views of the U.S. National Institutes of Health. Authors also acknowledge the support from the Portuguese Foundation for Science and Technology (FCT) under grant SFRH/BD/136213/2018 and under the research project UIDB/50022/2020.

The authors thank the University of Michigan Department of Orthopedic Surgery Histology Core and Carol Whitinger for training the first author in the paraffin embedder, microtome and tissue staining and also for performing the initial paraffin processing and bone decalcification of our samples. We thank Professor Susan V. Brooks for teaching us how to interpret the histological images of muscle and tendon. We also thank the University of Michigan Soft Tissues Research Lab, directed by Professor Ellen M. Arruda, for making available the tensile test machine and the digital image correlation equipment and Andrea Poli for helping with the design and performance of the experimental tests. For providing the specimens used in this work, we thank the Meat Laboratory of the Michigan State University and the Experimental Surgical Services from the University of Minnesota. Finally, we thank Professor John O.L. DeLancey for consultations and help with the first sheep pelvis dissection.

References

1. Abramowitch S, Easley D. Chapter Four - Introduction to Classical Mechanics. In: Hoyte L, Damaser MBT-B of the FPF, eds. Academic Press; 2016:89-107. doi:https://doi.org/10.1016/B978-0-12-803228-2.00004-0

2. Abramowitch SD, Feola A, Jallah Z, Moalli PA. Tissue mechanics, animal models, and pelvic organ prolapse: A review. *Eur J Obstet Gynecol Reprod Biol*. 2009;144:S146-S158. doi:https://doi.org/10.1016/j.ejogrb.2009.02.022

3. Alshomer F, Chaves C, Kalaskar DM. Advances in Tendon and Ligament Tissue Engineering: Materials Perspective. Bandyopadhyay A, ed. *J Mater*. 2018;2018. doi:http://dx.doi.org/10.1155/2018/9868151

4. Ashton-Miller JA, DeLancey JOL. Functional anatomy of the female pelvic floor. *Ann N Y Acad Sci*. 2007;1101:266-296. doi:10.1196/annals.1389.034

5. Baldwin SJ, Kreplak L, Lee JM. Characterization via atomic force microscopy of discrete plasticity in collagen fibrils from mechanically overloaded tendons: Nano-scale structural changes mimic rope failure. *J Mech Behav Biomed Mater*. 2016;60:356-366. doi:10.1016/j.jmbbm.2016.02.004

6. Bassett EG. The anatomy of the pelvic and perineal regions of the ewe. *Aust J Zool*. 1965;13(2):201-242.

7. Brooks S V, Zerba E, Faulkner JA. Injury to muscle fibres after single stretches of passive and maximally stimulated muscles in mice. *J Physiol*. 1995;488(2):459-469. doi:10.1113/jphysiol.1995.sp020980

8. Budday S, Sommer G, Birkl C, et al. Mechanical characterization of human brain tissue. *Acta Biomater*. 2017;48:319-340. doi:https://doi.org/10.1016/j.actbio.2016.10.036

9. Chen J, Kim J, Shao W, et al. An anterior cruciate ligament failure mechanism. *Am J Sports Med*. 2019;47(9):2067-2076. doi:10.1177/0363546519854450

10. Cheng S, Clarke EC, Bilston LE. The effects of preconditioning strain on measured tissue properties. *J Biomech*. 2009;42(9):1360-1362. doi:https://doi.org/10.1016/j.jbiomech.2009.03.023

11. Couri BM, Lenis AT, Borazjani A, Paraiso MFR, Damaser MS. Animal models of female pelvic organ prolapse: lessons learned. *Expert Rev Obstet Gynecol*. 2012;7(3):249-260. doi:10.1586/eog.12.24

12. DeLancey JOL, Kearney R, Chou Q, Speights S, Binno S. The appearance of levator ani muscle abnormalities in magnetic resonance images after vaginal delivery. *Obstet Gynecol*. 2003;101(1):46-53. doi:10.1016/S0029-7844(02)02465-1

13. DeLancey JOL, Sørensen HC, Lewicky-Gaupp C, Smith TM. Comparison of the puborectal muscle on MRI in women with POP and levator ani defects with those with normal support and no defect. *Int Urogynecol J*. 2012;23(1):73-77. doi:10.1007/s00192-011-1527-8

14. Dietz HP, Gillespie AVL, Phadke P. Avulsion of the pubovisceral muscle associated with large vaginal tear after normal vaginal delivery at term. *Aust New Zeal J Obstet Gynaecol*. 2007;47(4):341-344. doi:10.1111/j.1479-828X.2007.00748.x

15. Ferreira JPS, Rynkevic R, Martins PALS, et al. Predicting the mechanical response of the vaginal wall in ball burst tests based on histology. *J Biomed Mater Res Part B Appl Biomater*. 2019;n/a(n/a). doi:10.1002/jbm.b.34534

16. Fung DT, Wang VM, Laudier DM, et al. Subrupture tendon fatigue damage. *J Orthop Res*. 2009;27(2):264-273. doi:10.1002/jor.20722

17. Gao Y, Zhao Z, Yang Y, Zhang M, Wu J, Miao Y. Diagnostic value of pelvic floor ultrasonography for diagnosis of pelvic organ prolapse: a systematic review. *Int Urogynecol J*. 2020;31(1):15-33. doi:10.1007/s00192-019-04066-w

18. Ghetti C, Skoczylas LC, Oliphant SS, Nikolajski C, Lowder JL. The Emotional Burden of Pelvic Organ Prolapse in Women Seeking Treatment: A Qualitative Study. *Female Pelvic Med Reconstr Surg*. 2015;21(6):332-338. doi:10.1097/SPV.0000000000000190

19. Gottsauner-Wolf F, Grabowski JJ, Chao EY, An KN. Effects of freeze/thaw conditioning on the tensile properties and failure mode of bone-muscle-bone units: a biomechanical and histological study in dogs. *J Orthop Res*. 1995;13(1):90-95. doi:10.1002/jor.1100130114

20. Holzapfel GA. *Nonlinear Solid Mechanics: A Continuum Approach for Engineering*. John Wiley & Sons; 2000.

21. Holzapfel GA, Gasser TC. A viscoelastic model for fiber-reinforced composites at finite strains: Continuum basis, computational aspects and applications. *Comput Methods Appl Mech Eng*. 2001;190(34):4379-4403. doi:https://doi.org/10.1016/S0045-7825(00)00323-6

22. Holzapfel GA, Gasser TC, Ogden RW. A new constitutive framework for arterial wall mechanics and a comparative study of material models. *J Elast Phys Sci solids*. 2000;61(1):1-48. doi:10.1023/A:1010835316564

23. Hoyte L, Damaser MS, Warfield SK, et al. Quantity and distribution of levator ani stretch during simulated vaginal childbirth. *Am J Obstet Gynecol*. 2008;199(2):198.e1-5. doi:10.1016/j.ajog.2008.04.027

24. Jing D, Ashton-Miller JA, DeLancey JOL. A subject-specific anisotropic visco-hyperelastic finite element model of female pelvic floor stress and strain during the second stage of labor. *J Biomech*. 2012;45(3):455-460. doi:https://doi.org/10.1016/j.jbiomech.2011.12.002

25. Kearney R, Sawhney R, DeLancey JOL. Levator ani muscle anatomy evaluated by origin-insertion pairs. *Obstet Gynecol*. 2004;104(1):168-173. doi:10.1097/01.AOG.0000128906.61529.6b

26. Kim J, Betschart C, Ramanah R, Ashton-Miller JA, DeLancey JOL. Anatomy of the pubovisceral muscle origin: Macroscopic and microscopic findings within the injury zone. *Neurourol Urodyn*. 2015;34(8):774-780. doi:10.1002/nau.22649

27. Kim J, Ramanah R, DeLancey JOL, Ashton-Miller JA. On the anatomy and histology of the pubovisceral muscle enthesis in women. *Neurourol Urodyn*. 2011;30(7):1366-1370. doi:10.1002/nau.21032

28. Koyucu RG, Demirci N. Effects of pushing techniques during the second stage of labor: A randomized controlled trial. *Taiwan J Obstet Gynecol*. 2017;56(5):606-612. doi:https://doi.org/10.1016/j.tjog.2017.02.005

29. Laganà AS, La Rosa VL, Rapisarda AMC, Vitale SG. Pelvic organ prolapse: the impact on quality of life and psychological well-being. *J Psychosom Obstet Gynecol*. 2018;39(2):164-166. doi:10.1080/0167482X.2017.1294155

30. de Leeuw JW, Struijk PC, Vierhout ME, Wallenburg HC. Risk factors for third degree perineal ruptures during delivery. *BJOG*. 2001;108(4):383-387.

31. Lien K-C, DeLancey JOL, Ashton-Miller JA. Biomechanical analyses of the efficacy of patterns of maternal effort on second-stage progress. *Obstet Gynecol*. 2009;113(4):873-880. doi:10.1097/AOG.0b013e31819c82e1

32. Lien K-C, Mooney B, DeLancey JOL, Ashton-Miller JA. Levator ani muscle stretch induced by simulated vaginal birth. *Obstet Gynecol*. 2004;103(1):31-40. doi:10.1097/01.AOG.0000109207.22354.65

33. Lipps DB, Wojtys EM, Ashton-Miller JA. Anterior cruciate ligament fatigue failures in knees subjected to repeated simulated pivot landings. *Am J Sports Med*. 2013;41(5):1058-1066. doi:10.1177/0363546513477836

34. Margulies RU, Huebner M, DeLancey JOL. Origin and insertion points involved in levator ani muscle defects. *Am J Obstet Gynecol*. 2007;196(3):251.e1-251.e5. doi:10.1016/j.ajog.2006.10.894

35. Marino M. Constitutive modeling of soft tissues. In: Narayan R, ed. *Encyclopedia of Biomedical Engineering*. Vol 1-3. Elsevier; 2019:81-110. doi:https://doi.org/10.1016/B978-0-12-801238-3.99926-4

36. Martins P, Lopes Silva-Filho A, Rodrigues Maciel da Fonseca AM, et al. Biomechanical properties of vaginal tissue in women with pelvic organ prolapse. *Gynecol Obstet Invest*. 2013;75(2):85-92. doi:10.1159/000343230

37. Martins P, Silva-Filho AL, Fonseca AMRM, et al. Strength of round and uterosacral ligaments: a biomechanical study. *Arch Gynecol Obstet*. 2013;287(2):313-318. doi:10.1007/s00404-012-2564-3

38. Meyers MA, Chawla KK. *Mechanical Behaviour of Materials*. Cambridge University Press; 2009.

39. Milella PP. *Fatigue and Corrosion in Metals*. 1st ed. (Milella PP, ed.). Springer-Verlag Mailand; 2013. doi:10.1007/978-88-470-2336-9

40. Nagle AS, Barker MA, Kleeman SD, Haridas B, Mast TD. Passive biomechanical properties of human cadaveric levator ani muscle at low strains. *J Biomech*. 2014;47(2):583-586. doi:10.1016/j.jbiomech.2013.11.033

41. Parente MPL, Jorge RMN, Mascarenhas T, Fernandes AA, Martins JAC. Deformation of the pelvic floor muscles during a vaginal delivery. *Int Urogynecol J Pelvic Floor Dysfunct*. 2008;19(1):65-71. doi:10.1007/s00192-007-0388-7

42. Peña E. Computational aspects of the numerical modelling of softening, damage and permanent set in soft biological tissues. *Comput Struct*. 2014;130:57-72. doi:https://doi.org/10.1016/j.compstruc.2013.10.002

43. Rynkevic R, Martins P, Hympanova L, Almeida H, Fernandes AA, Deprest J. Biomechanical and morphological properties of the multiparous ovine vagina and effect of subsequent pregnancy. *J Biomech*. 2017;57:94-102. doi:https://doi.org/10.1016/j.jbiomech.2017.03.023

44. Samadi-Dooki A, Voyiadjis GZ. A fully nonlinear viscohyperelastic model for the brain tissue applicable to dynamic rates. *J Biomech*. 2019;84:211-217. doi:https://doi.org/10.1016/j.jbiomech.2019.01.007

45. Samuelsson E, Ladfors L, Lindblom BG, Hagberg H. A prospective observational study on tears during vaginal delivery: occurrences and risk factors. *Acta Obstet Gynecol Scand*. 2002;81(1):44-49.

46. Silver FH, Jaffe M, Shah RG. 11 - Structure and behavior of collagen fibers. In: Bunsell ARBT-H of P of T and TF (Second E, ed. *The Textile Institute Book Series*. Woodhead Publishing; 2018:345-365. doi:https://doi.org/10.1016/B978-0-08-101272-7.00011-0

47. Tadros AS, Huang BK, Pathria MN. Muscle-Tendon-Enthesis Unit. *Semin Musculoskelet Radiol*. 2018;22(03):263-274. doi:10.1055/s-0038-1641570

48. Torp S B, Friedman B. Effects of Age and of mechanical deformation on the ultrastructure of tendon. In: *Proceedings of the Colston Conference*. University of Bristol; 1974:223-250.

49. Urbankova I, Vdoviakova K, Rynkevic R, et al. Comparative Anatomy of the Ovine and Female Pelvis. *Gynecol Obstet Invest*. 2017;82(6):582-591. doi:10.1159/000454771

50. VanDusen K, Larkin L. Muscle-tendon interface. In: *Regenerative Engineering of Musculoskeletal Tissues and Interfaces*. ; 2015:409-429. doi:10.1016/B978-1-78242-301-0.00017-3

51. Veres SP, Harrison JM, Lee JM. Repeated subrupture overload causes progression of nanoscaled discrete plasticity damage in tendon collagen fibrils. *J Orthop Res*. 2012;31(5):731-737. doi:10.1002/jor.22292

52. Veres SP, Lee JM. Designed to fail: A novel mode of collagen fibril disruption and its relevance to tissue toughness. *Biophys J*. 2012;102(12):2876-2884. doi:10.1016/j.bpj.2012.05.022

53. Wilkins MF, Wu JM. Lifetime risk of surgery for stress urinary incontinence or pelvic organ prolapse. *Minerva Ginecol*. 2017;69(2):171-177. doi:10.23736/S0026-4784.16.04011-9

54. Woo SL, Fisher MB, Feola AJ. Contribution of Biomechanics to Management of Ligament and Tendon Injuries. *Mol cell Biomech*. 2008;5(1):49-68.

55. Zielinski R, Miller J, Low LK, Sampselle C, Delancey JOL. The relationship between pelvic organ prolapse, genital body image, and sexual health. *Neurourol Urodyn*. 2012;31(7):1145-1148. doi:10.1002/nau.22205

56. Zuskov A, Freedman BR, Gordon JA, Sarver JJ, Buckley MR, Soslowsky LJ. Tendon Biomechanics and Crimp Properties Following Fatigue Loading Are Influenced by Tendon Type and Age in Mice. *J Orthop Res*. 2020;38(1):36-42. doi:10.1002/jor.24407

Chapter 4

On the management of maternal pushing during the second stage of labor

A biomechanical study considering passive tissue fatigue damage accumulation

On the management of maternal pushing during the second stage of labor

A biomechanical study considering passive tissue fatigue damage accumulation

Maria C.P. Vila Pouca[1,2], João P.S. Ferreira[1,2], Marco P.L. Parente[1,2], Renato M. Natal Jorge[1,2], James A. Ashton-Miller[3]

1 Department of Mechanical Engineering, Faculty of Engineering of University of Porto, Porto, Portugal

2 Institute of Science and Innovation in Mechanical and Industrial Engineering, Porto, Portugal

3 Departments of Mechanical and Biomedical Engineering, College of Engineering and School of Kinesiology, University of Michigan, Ann Arbor, Michigan, USA

Published In:

American Journal of Obstetrics and Gynecology

DOI: https://doi.org/10.1016/j.ajog.2022.01.023

Article Type: Original Research

Submitted: July 8, 2021

Accepted: January 31, 2022

Abstract

Background: During the second stage of labor, the maternal pelvic floor muscles undergo repetitive stretch loading as uterine contractions and strenuous maternal pushes combined to expel the fetus, and it is not uncommon that these muscles sustain a partial or complete rupture. It has recently been demonstrated that soft tissues, including the anterior cruciate ligament and connective tissue in sheep pelvic floor muscle, can accumulate damage under repetitive physiological (submaximal) loads. It is well known to material scientists that this damage accumulation can not only decrease tissue resistance to stretch but also result in a partial or complete structural failure. Thus, we wondered whether certain maternal pushing patterns (in terms of frequency and duration of each push) could increase the risk of excessive damage accumulation in the pelvic floor tissue, thereby inadvertently contributing to the development of pelvic floor muscle injury.

Objective: This study aimed to determine which labor management practices (spontaneous vs directed pushing) are less prone to accumulate damage in the pelvic floor muscles during the second stage of labor and find the optimum approach in terms of minimizing the risk of pelvic floor muscle injury.

Study Design: We developed a biomechanical model for the expulsive phase of the second stage of labor that includes the ability to measure the damage accumulation because of repetitive physiological submaximal loads. We performed 4 simulations of the second stage of labor, reflecting a directed pushing technique and 3 alternatives for spontaneous pushing.

Results: The finite element model predicted that the origin of the pubovisceral muscle accumulates the most damage and so it is the most likely place for a tear to develop. This result was independent of the pushing pattern. Performing 3 maternal pushes per contraction, with each push lasting 5 seconds, caused less damage and seemed the best approach. The directed pushing technique (3 pushes per contraction, with each push lasting 10 seconds) did not reduce the duration of the second stage of labor and caused higher damage accumulation.

Conclusion: The frequency and duration of the maternal pushes influenced the damage accumulation in the passive tissues of the pelvic floor muscles, indicating that it can influence the prevalence of pelvic floor muscle injuries. Our results suggested that the maternal pushes should not last longer than 5 seconds and that the duration of active pushing is a better measurement than the total duration of the second stage of labor. Hopefully, this research will help to shed new light on the best practices needed to improve the experience of labor for women.

Keywords: finite element method; low-cycle fatigue failure; management of labor; pelvic floor muscle; vaginal delivery; second stage of labor; maternal pushes

4.1. Introduction

Human vaginal delivery is a complex event, often involving a tight fit between the fetus and birth canal, and never without risk. Maternal pelvic floor damage in the form of partial or complete tears of the levator ani muscles is still occurring, especially in first-time mothers during a difficult delivery[60]. This injury has been well documented whether to the left, right, or both pubovisceral muscles (PVMs) near their origin on either side of the pubic symphysis, with a prevalence ranging between 13% and 41%[14,16–18,26,41,42,58]. Lying near vital structures in a relatively inaccessible location deep within the pelvis, these injuries are not amenable to surgical repair. Women with this injury are at an increased risk of developing pelvic floor disorders later in life[34] including pelvic organ prolapse and urinary incontinence, both of which can significantly affect the quality of life and require surgery[4,8,34]. As such, there is room for improving the management of labor to provide more satisfactory outcomes for the mother.

Recently, it has been shown that highly specialized collagenous tensile structures, such as the anterior cruciate ligament (ACL), can tear under repetitive submaximal loading [6,37,70]. With each loading cycle, such as landing from a strenuous jump, the origin of the ACL showed accumulation of microdamage at the collagen fibril and fiber levels[15], suggesting that microdamage can accumulate there and, if allowed to continue, can eventually cause a complete structural failure. Although the ACL can, of course, rupture under a single supramaximal load, it can also fail under a series of submaximal loads that in isolation would never cause failure. This type of injury is called a material fatigue failure. Motivated by these results, we performed a systematic review of the musculoskeletal literature[67] and found that repetitive submaximal loading was reported at the musculotendinous junction of rabbit leg muscles, with histologically detectable microdamage accumulation[40,44,62,65]. From observational studies, indirect evidence suggested material fatigue failure as a possible damage mechanism in the tendon and at the musculotendinous junction[67]. This is because several nonimpact and nontraumatic injuries were reported within a cohort represented by professional and recreational athletes or people strongly engaged in sports activities, where strenuous repetitive movements are often performed without adequate rest.

Based on both the ACL data[6,37,70] and indirect evidence found on our systematic review[67], we developed a laboratory study to test the hypothesis that damage could accumulate at the origin of the PVM because of repetitive submaximal loadings. Using sheep as an animal model, we applied 60 loading cycles at a 60% ultimate displacement[n] and found microdamage in the muscle, near the musculotendinous junction injury, in the form of elongated and crimped muscle fibers and individual muscle fiber rupture (Figure 4.1). No visible tear was seen macroscopically; however, there was a visible permanent deformation in all specimens, averaging approximately 50% strain.

[n] Ultimate displacement is the applied displacement that will cause the material to tear.

Moreover, this damage accumulation was sufficient to affect the mechanical properties, in the absence of a complete tear, as captured by the strain-stress response[68].

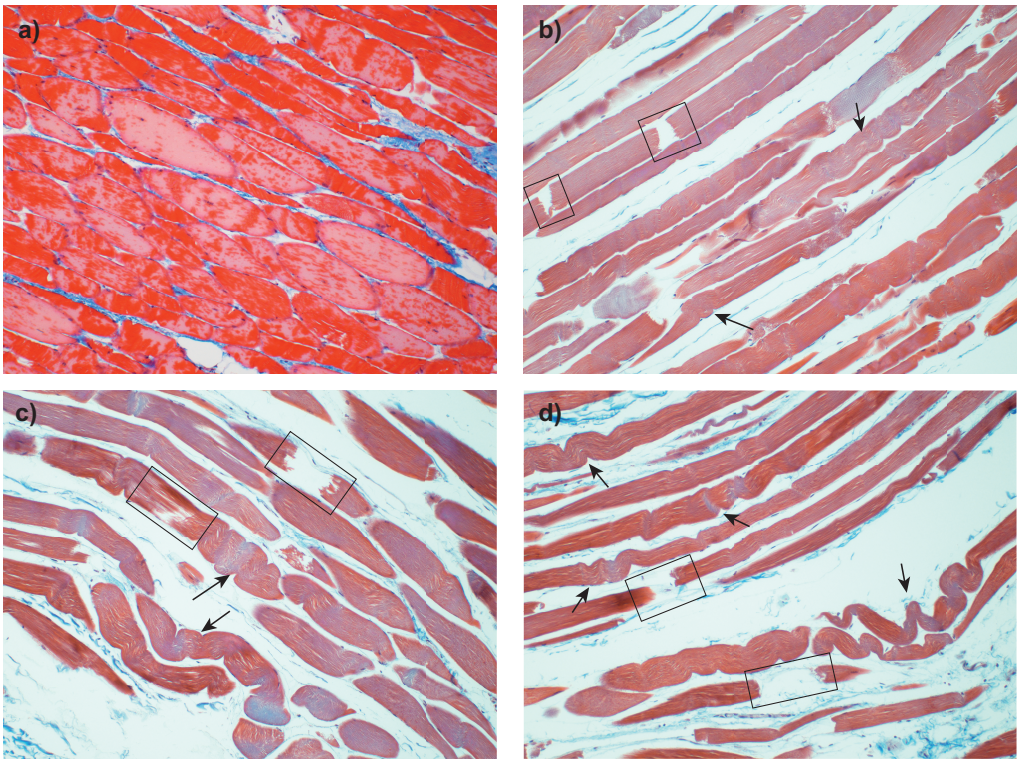

Figure 4.1 – Histological appearance of ovine pelvic floor muscle-tendon sections stained with Masson's Trichrome stain. Comparison between an untested control, **a)**, and fatigue-tested specimens **(b-c)** (60 cycles at between 45% and 60% failure displacement[68]). Fatigued specimens show elongated and deformed muscle fibers (arrows), individual fiber rupture (square) and increased interstitial spaces[68].

During vaginal delivery, the second stage of labor commences during complete cervical dilation after which active maternal pushing can be used to augment each uterine contraction to facilitate the delivery[12]. It is a common practice for the midwife or clinician to direct these efforts by instructing the mother when to begin the "active" stage of labor and thereupon to inhale deeply and to push with a closed glottis for 10 seconds, 2 to 3 times during each uterine contraction. This extended use of the Valsalva maneuver was popularized in the 1950s to accelerate the second stage of labor to avoid the need for forceps, which were in common use at the time[32]. A popular alternative method is spontaneous pushing, which is carried out naturally by the woman according to her desire to push down progressively. There is no deep breathing, and it starts only when the full uterine contraction is well established[3,32]. Generally, 3 to 5 pushes occur near the peak uterine contraction for 3 to 5 seconds with approximately 2-second breathing between efforts[3,20,53,56], although 1 bigger push near the peak of the contraction is also used[35]. Despite the directed pushing being the most common, it is not yet clear what the best pushing technique is. A summary of several studies that compare maternal and fetal outcomes for directed pushing and spontaneous pushing groups is shown in Table 4.1. Overall, these studies have suggested that spontaneous pushing is not detrimental, although it seemed to cause longer mean second stages of labor.

However, it is not clear whether directed pushing is detrimental or not, with some studies showing no substantial differences and other studies finding unfavorable outcomes. All these studies involved small sample sizes, which limited the generalizability of the results. Finally, in a review including 21 studies comparing spontaneous vs directed pushing, Lemos et al[33] concluded that "there is no conclusive evidence to support or refute any specific style" and that "further properly well-designed randomized controlled trials, addressing clinically important maternal and neonatal outcomes are required to add evidence-based information to the current knowledge."

Table 4.1- Summary of observational studies that compared maternal and fetal outcomes for directed and spontaneous pushing groups. POPQ: Pelvic Organ Prolapse Quantification

	Study Design	**Number of Participants**	**Main Outcomes**
Schaffer et al[56]	Randomized trial	128	▪ Directed pushing negatively impacted the first urge to void, bladder capacity and POPQ point Bp
Araujo et al[3]	Clinical trial	62	▪ No significant difference was found in maternal and neonatal outcomes ▪ Spontaneous method decreased maternal anxiety
Yeates and Roberts[73]	Pilot study	10	▪ No difference between the mean duration of the second stage of labor nor in the infants' Apgar scores ▪ Perineal integrity was preserved in the spontaneous pushing group
Paine and Tinker[47]	Clinical Trial	30	▪ No differences were found between spontaneous and directed pushing
Sampselle and Hines[55]	Retrospective study	39	▪ Women who used spontaneous pushing were more likely to have intact perineum's and less likely to have episiotomies and second or third degree lacerations
Thomson[63]	Randomized controlled trial	32	▪ Spontaneous group had significantly longer mean second stages of labor ▪ Directed pushing group had a negative correlation between the length of the second stage and the venous blood pH. No association was found in the Spontaneous group ▪ Longer second stages of labor seem disadvantageous to the fetus in the directed pushing group but not in the spontaneous pushing group.
Barnett and Humenick[5]	Pilot study	10	▪ Longer mean second stages of labor for the spontaneous pushing group ▪ Significant differences in the mean venous umbilical blood pH, with the spontaneous group having a higher mean value
Koyucu and Demirci[30]	Randomized prospective study	80	▪ No statistical significance in the mean pelvic-perineal pain scores, Apgar scores, fetal deceleration, incidence of episiotomy and perineal-cervical lacerations. ▪ Significantly higher duration of the second stage of labor in the spontaneous group ▪ Significantly higher rate of decline in Hb levels in the directed pushing group ▪ Significantly higher urethral straining angle scores in the directed pushing groups

We demonstrated earlier that the most commonly injured structure in the levator ani muscles has the potential to accumulate fatigue damage under repeated submaximal loading cycles consistent with the combination of the uterine contraction augmented by strenuous maternal

pushing [67–69]. Thus, we wondered whether certain maternal pushing patterns could influence the prevalence of PVM tears. Our goal was to analyze the results of 4 different pushing methods to determine whether there is optimum management for labor that reduces the chance of a PVM tear because of material fatigue. A biomechanical approach was chosen to test this idea. Several finite element methods of the second stage of labor have already been developed to analyze factors, such as the pelvic floor strain[36,49], episiotomy[45,46], fetal head flexion[48], duration of the second stage of labor[66], fetal presentation[50] and fetal head molding[43]. These models were developed to answer specific research questions, simplifying factors that do not strongly impact each research question. As such, material properties, such as viscoelastic effects, were often neglected[36,45,46,48,49] (with exception of Vila Pouca et al[66] and Moura et al[43] who included viscoelastic effects to be able to analyze the influence of the duration of the second stage of labor). Moreover, none of these models included the ability to cyclically accumulate damage, an effect we have recently demonstrated can occur in collagenous and muscular tissues[67,68]. This is the main difference between the previous work and the finite element model applied in this work as it, for the first time, includes this ability to cyclically accumulate damage. In addition, it also includes viscoelasticity. Although an engineering approach inherently simplifies the problem, it also has the advantage of eliminating unwanted factors, which helps to achieve a baseline understanding of the problem. Moreover, it is a tool that can be used to better define the methodology of future clinical trials by helping to establish a more insightful hypothesis. The main questions we addressed were as follows: “Does the duration and frequency of maternal pushing influence the accumulation of damage near the origin of the PVM?” and “What frequency and duration of the maternal pushes minimize the risk of PVM tear?”

In light of our recent findings[67–69], our working hypothesis was that the maternal pushes influence PVM damage accumulation and that shorter pushes may be beneficial for the mother.

4.2. Material and methods

To achieve our goal, we developed a simplified finite element model of the second stage of labor during vaginal delivery. It incorporated 3-dimensional (3D) geometric models of the pelvic floor muscles and fetus and a user-defined material model to better reproduce pelvic floor muscle behavior. Different maternal pushing profiles were simulated to find the optimal management of labor concerning maternal pelvic floor health. The simulations were performed using ABAQUS® finite element software (version 2018; Dassault Systèmes) with an implicit solver (ABAQUS®/Standard).

4.2.1. Geometry model and Boundary Conditions

The 3D finite element model of the levator ani muscles was created on the basis of a geometric data point set acquired from a female cadaver measurement by Janda et al[24]. The creation of this geometry is described in Parente et al[49]. Briefly, the geometric point set was used to define a 3D surface, which was extruded to define a volumetric 3D finite element mesh. For the thickness, a constant value of 2 mm was assumed[49]. Figure 4.2a shows this geometric model, which includes the levator ani muscles modeled as 1 structure. A schematic representation of the PVM is shown in Figure 4.2a with highlighted edges (in green) that were fixed. The main dimensions are described in Figure 4.2b along with the fiber directions of the model, which were defined on the basis of the literature[25]. We noted that the area of the model hiatus was set to 32 cm^2 at the initial stage of the simulation (corresponding to the beginning of the second stage of labor) to be representative of pregnancy-induced changes and complete dilation by the beginning of the second stage of labor. This value ranged between 15 and 57 cm^2, which was reported in late pregnancy[59,72].

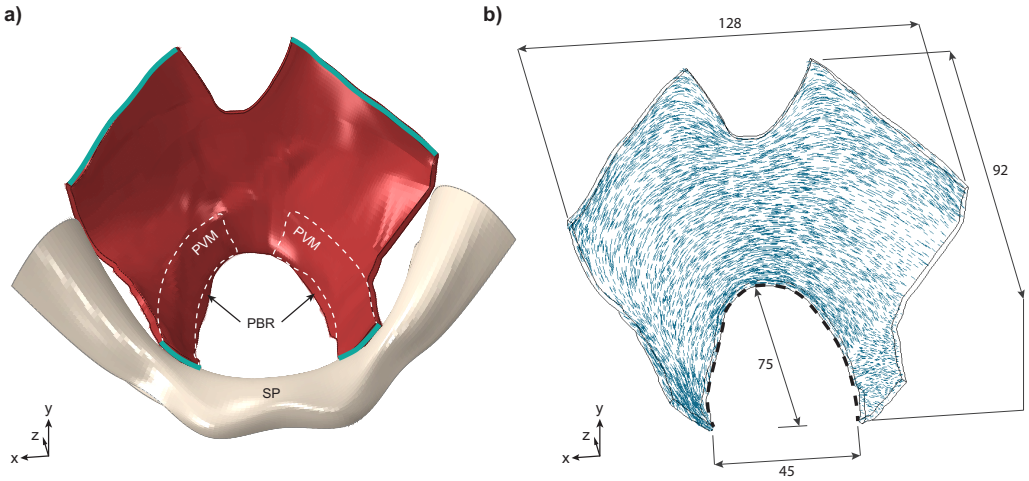

Figure 4.2– Superior view of the structure representing the levator ani muscles. **a)** 3-D geometry of the levator ani muscles, in red, with the pubic bone and symphysis pubis (SP) shown in ivory. The levator muscles attach laterally to the ischial spines and posteriorly to the sacrum, neither of which are shown for simplicity. The outline of the pubovisceral muscle (PVM), the most anterior and caudal portion of the levator ani muscles, is shown with dashed white lines: it takes origin from the pubic bone on either side of the symphysis pubis (SP) and inserts into the perineal body (not shown) near the midline. The vagina, anal sphincter and remaining portions of the levator ani, including the iliococcygeus, coccygeus, and puborectal muscles (PBR) are not delineated for simplicity. The nodes along the green edges were fixed. **b)** View of the model levator ani muscle showing fiber directions within the muscle and main dimensions (in mm). Black dotted line shows the hiatal length used to calculate the stretch.

Figure 4.3 shows the finite element model of the fetal head, which was obtained by a simplification of the model described by Parente et al[49]. This simplification removed intricate details in the fetal head, such as the nose, which often caused numeric problems without being relevant to the simulations. Despite these simplifications, the main dimensions were maintained and represent a 50th percentile full-term fetus[29], with a cross-sectional area of 9199 mm^2.

The initial position of the head was assumed as a vertex presentation with occiput anterior. The fetus descent was defined by the uterine and maternal forces, applied to a fetal head reference node. The head flexion, applied to the same reference node, was added so that the smallest head diameter was presented in the birth canal at all instances. Regarding the fetal boundary conditions, all displacements were free throughout the simulation. The lateral and transversal constraints were imposed by the rigid surface representing the pubic bone and pelvic floor muscles. Except for head flexion concerning the X-axis (Figure 4.3), all other rotations were otherwise fixed. Please refer to the Appendix E for further details on the finite element meshes.

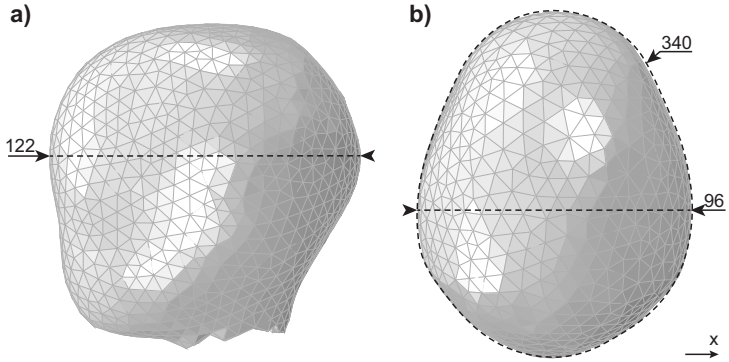

Figure 4.3– Finite element model of the fetal head showing the a) occipitofrontal diameter, and b) biparietal diameter with head circumference. All dimensions shown are in mm.

4.2.2. Material models

The material model for the levator ani muscles incorporated several realistic properties, such as transverse isotropy, visco-hyperelasticity, and the ability to weaken (accumulate damage) because of repetitive submaximal loading[o]. In contrast, the fetal head and "pubic bone" surface, not so critical to the biomechanical model in terms of material properties, were simplified to increase computational efficiency. The fetal head was modeled as a hyperelastic material as the outer layer with a rigid interior. Hyperelasticity is a feature of all soft tissues, including the levator ani, as they can deform significantly. The "pubic bone" surface was modeled as an almost rigid elastic material with very high stiffness. Details on these material models can be found below, and in the Appendix E.

Levator ani muscles

A transversely isotropic visco-hyperelastic model, including cumulative damage with nonlocal averaging, was used to simulate the levator ani muscle behavior. The transversely isotropic

[o] Transverse isotropy occurs when the material stiffness is directionally dependent, which is the case for muscular tissues because of the presence of the fibers. Viscohyperelasticity describes the materials that have a nonlinear force-displacement behavior and time-dependent (viscous) properties. These materials have a force response to strain that, importantly, depends on the strain rate: faster strain rates induce higher forces, whereas lower strain rates induce smaller forces. Moreover, they can "relax": particularly, if subjected to the same strain over some time, the stresses (force per unit area) developed initially decrease over time. Besides these properties, the material model incorporates a cumulative damage model: when submaximal loading cycles are performed, there is damage accumulation in the material, which negatively impacts its mechanical properties by weakening the material.

hyperelastic behavior was captured by the Holzapfel-Gasser-Ogden (HGO) model[23] and viscoelastic behavior by the generalized Maxwell model, as described by Holzapfel and Gasser[22]. These phenomenological models were chosen as they are relatively simple to implement (eg, compared with complex multiscale models) and have a reasonable number of material parameters (as the relationship between stress and strain was empirically modeled from the experimental observation). The HGO and generalized Maxwell model, although initially developed to characterize the behavior of arteries[22,23], are robust and have been successfully applied to several soft biological tissues[19,57]. Moreover, the fatigue damage was simulated using a phenomenological model, whose evolution equation was previously developed on the basis of experimental evidence[68]. Briefly, the damage accumulation is a function of the energy required to deform the material, which accumulates as the material suffers several deformations (loading cycles). As such, if the material deforms significantly, the energy required to deform it will be higher as will the damage accumulation. However, if a smaller deformation is applied several times, the energy required to deform will be the sum of the energy required for each deformation, also causing a considerable damage accumulation. The damage accumulation is measured quantitatively in the muscle fibers by the damage variable $\widehat{D_{f1}}$ $\left(0 \leq \widehat{D_{f1}} \leq 1\right)$, with $\widehat{D_{f1}} = 0$ representing the undamaged state and $\widehat{D_{f1}} = 1$ a complete failure. This damage variable will affect the stress response, mimicking the effect of reduced mechanical integrity observed experimentally, as $\widehat{D_{f1}}$ approaches 1. In a previous work, these material models proved capable to capture the behavior of sheep pelvic floor muscle tissue, under repetitive submaximal loading[68].

Further details and equations regarding the constitutive model can be found in the Appendix E with a table showing the material parameters used.

Fetal Head

The hyperelastic part of the fetal head was modeled following the Neo-Hookean law (equation (E.3) in the Appendix E). The parameter was obtained from the literature[10], C_{10}=0.13 MPa, to represent a skin-like behavior.

Pubic Bone Surface

The surface that constrains the fetal head, the "pubic bone," was modeled with a Young modulus of 1000 MPa and a Poisson coefficient of 0.25.

4.2.3. Maternal pushing

Rempen and Kraus[52] measured the uterine pressure near the fetal head in 44 spontaneous deliveries with a vertex presentation. The results showed that the basal pressure averages 2.6 kPa and that a uterine contraction increased it to an average of 8.5 kPa[4,52]. A maternal push added an average of 10.5 kPa, thereby increasing the total pressure to 19 kPa at the peak of the uterine

contraction[4,52]. These intrauterine pressures apply an expulsive force on the fetal head that can be calculated by multiplying each pressure by the fetal head cross-sectional area[4]. The fetal head cross-sectional area is calculated in section 4.2.1, and the resulting peak forces are listed in Table 4.2.

Table 4.2 - Calculated expulsive force acting on the fetal head at the peak of the uterine contraction, at the peak of the maternal push, and at the peak when the 2 variables are combined

Peak Uterine Contraction (N)	74
Peak Maternal Push (N)	101
Peak Uterine Contraction + Maternal Push (N)	175

To simulate directed pushing, three 10-second maternal pushes were added to the uterine contraction profile, according to the literature[7,21,30,32,35,51,53]. As a key feature of the directed pushing can be seen as extended use of the Valsalva maneuver[32], we defined this pushing profile throughout the paper as the Valsalva-push pattern.

We assumed the volitional maternal effort would take 1 second to ramp up and 1 second to decrease (Figure 4.4a). The profile of the combined efforts is shown in Figure 4.4b.

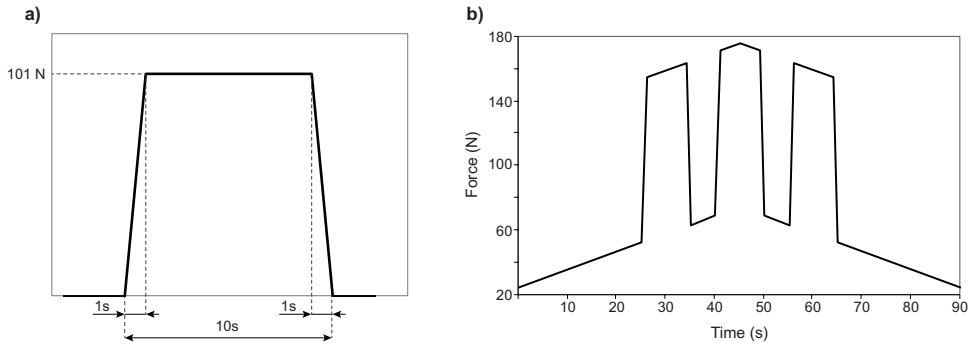

Figure 4.4 - Expulsive force placed on the model fetal head during simulated directed pushing. **a)** Profile of a single 10 seconds push and **b)** Valsalva-push pattern: three 10 second pushes superposed upon the 90 s uterine contraction.

When spontaneously pushing, women reportedly push powerfully 1 time as the contraction reaches its peak[35] or perform 3 to 5 smaller pushes (each lasting for 3–5 seconds with a 2-second interval) [3,20,53,56]. As such, we decided to standardize 3 possible spontaneous pushes, analyzing their effects separately. First, we tested the possible scenario of women pushing powerfully 1 time as the contraction reaches its peak. This is the designated 1-push pattern (Figure 4.5a), with 1 powerful maternal push lasting 10 seconds (Figure 4.4a) superposed symmetrically over the peak of the uterine contraction; moreover, for the remaining analyses, a shorter volitional maternal effort lasting 5 seconds was defined, with the profile represented in Figure 4.5b. As it is reported that women spontaneously perform between 3 and 5 smaller pushes, we tested separately the extremes and defined the 3-push pattern (Figure 4.5c), with three 5 seconds pushes superposed on the uterine contraction and the 5-push pattern (Figure 4.5d), with five 5-second pushes superposed on the uterine contraction.

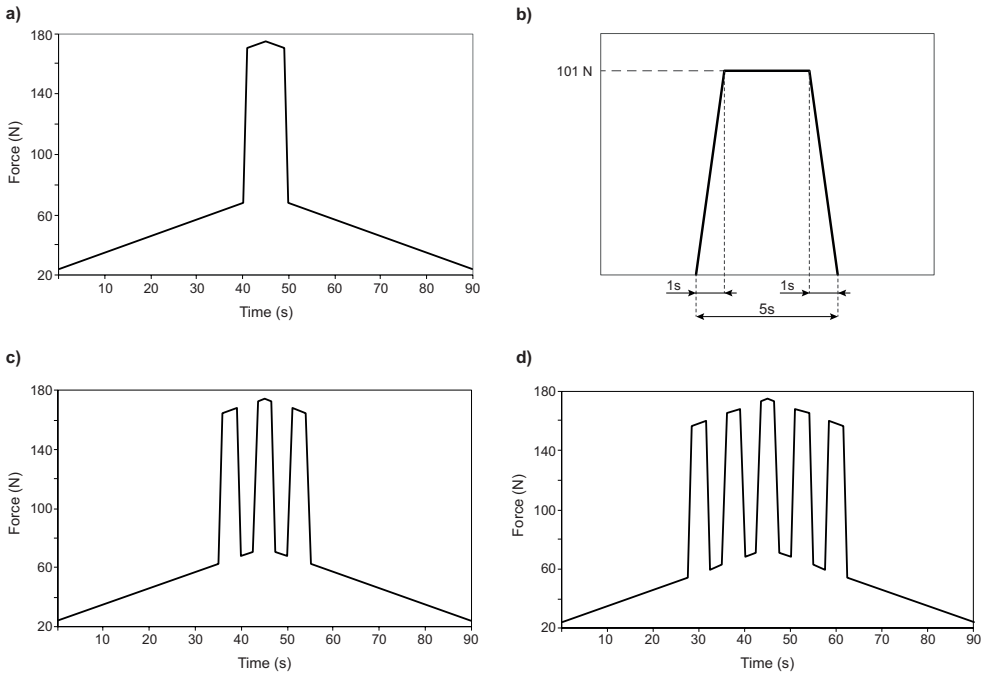

Figure 4.5 - Details of the expulsive force placed on the model fetal head during simulated spontaneous pushing. **a)** 1-push pattern: one 10 second push superposed upon the 90 s uterine contraction **b)** Profile of a single 5 second push, **c)** 3-push pattern: three 5 second pushes superposed upon the 90 s uterine contraction. **d)** 5-push pattern: five 5 second pushes superposed upon the 90 s uterine contraction.

4.2.4. Biomechanical model evaluation

To evaluate the complete biomechanical model, we analyzed the following parameters:

(1) The evolution of the vertical displacement of the fetal head: measured at the same reference node in the 4 simulations and plotted against time. This vertical displacement is useful for comparing the fetal descent between the 4 simulated pushing patterns; however, it does not correlate with any obstetrical measurements. We ended the simulations after the complete passage of the fetal head, which coincided with a vertical displacement of 153 mm.

(2) The stretch ratio of the hiatus contour: the contour of the hiatus was chosen (Figure 2, B: black dotted line) as it was shown to sustain the highest stretches.40 The stretch ratio (λ) was calculated by dividing the current length by the initial length: $\lambda = L/L_0$. This parameter can be related to strain, ε , as: $\varepsilon = \lambda - 1$.

(3) The distribution of the damage variable in the muscle fibers, $\widehat{D_{\mathrm{f1}}}$: This distribution is color coded as follows red: $1 \leq \widehat{D_{\mathrm{f1}}} < 0.8$, orange: $0.8 < \widehat{D_{\mathrm{f1}}} \leq 0.45$, yellow: $0.45 < \widehat{D_{\mathrm{f1}}} \leq 0.35$, green: $0.35 < \widehat{D_{\mathrm{f1}}} \leq 0.1$ and blue $\widehat{D_{\mathrm{f1}}} \leq 0.1$. We defined a risk qualitative scale as follows: red areas represent 'Critical' risk, since the muscle fiber mechanical properties are affected up to 100% (complete tear), orange areas are 'High' risk, yellow areas are 'Noteworthy' risk, green areas are 'Moderate' risk and blue areas are 'Low' risk.

(4) The damage evolution at the critical location, which is the node of maximum predicted damage. We chose this approach instead of averaging around a set of nodes because a nonlocal averaging is already performed to reduce mesh dependency (Appendix E provides further details).

(5) The maximum damage at the critical location as a function of the total time of the simulation.

(6) The maximum damage at the critical location as a function of the time spent in active pushing. This time was measured by counting the number of maternal pushes performed and multiplying by their duration.

4.3. Results

The maximum stretch ratio was 1.87 for the 1-push and 5-push patterns, 1.83 for the Valsalva-push pattern, and 1.80 for the 3-push pattern. As the difference among the 4 simulations is merely the applied maternal pushes, it was expected to result in similar values of muscle stretches.

Figure 4.6 shows the vertical displacement of the fetal head with time for the 4 simulated pushing patterns. The spontaneous 3-push, 5-push, and the Valsalva-push patterns needed 4 complete contractions and reached the end in the first half of the 5th contraction. The spontaneous 1-push pattern took longer to reach the final stage, which occurred in the initial stage of the 6th contraction. Overall, the progress of the fetal head was similar. We can see that in the initial stage of each contraction, when the forces are slowly increasing, the fetal head did not descend. Descent only occurred when the maternal pushes were initiated. Moreover, one can see that the fetal head did not continuously advance but retreated briefly during the unloading and resting phases of the maternal push and during the uterine contraction resting phase. For the pushing patterns involving more than one maternal push, this effect was seen occurring more than once in a contraction, whereas the spontaneous 1-push pattern had a smoother pattern of fetal advance.

Figure 4.7 shows the damage distribution at the end of the simulation for the 4 simulated pushing patterns, with the location of the maximum value pinpointed. The critical risk location did not differ with the pushing patterns, consistently being near the right lateral origin of the PVM. The critical node is the point where the maximum damage was recorded, and this was the same for the 1-push, 3-push, and Valsalva-push patterns. The critical node of the 5-push pattern lay slightly (1.6 mm) further away from the other simulations' critical nodes. Thus, the maximum location site was virtually the same for all tested pushing patterns.

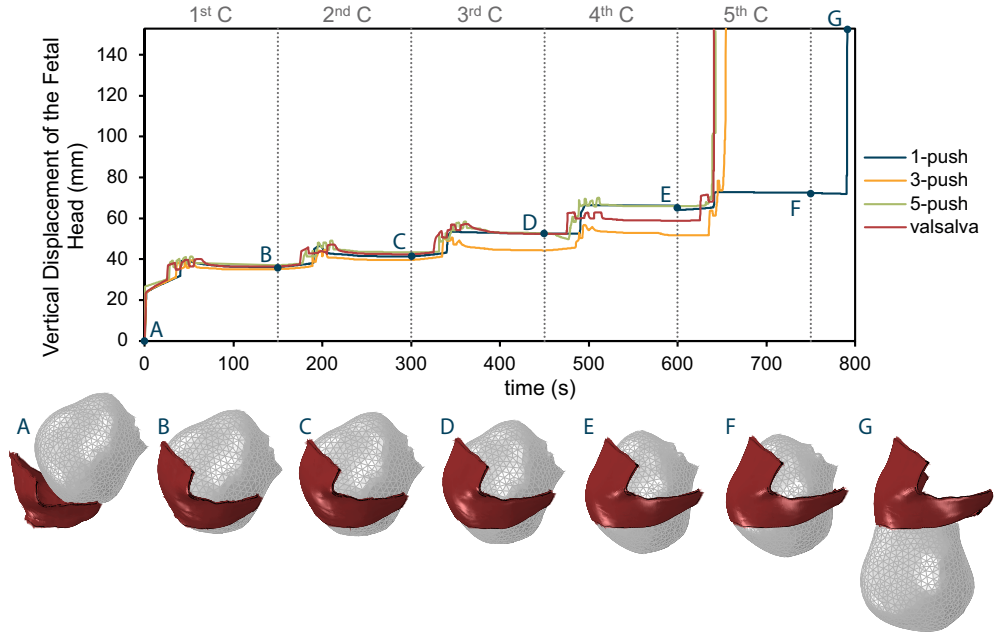

Figure 4.6 - Vertical displacement of the fetal head (mm) with time (s) for the four simulated pushing patterns: 1-push, 3-push, 5-push and Valsalva-push. The pictures below show the right lateral view of the fetal head descent for the 1-push simulation at the starting point, at the end of each contraction, and in the final position. The vertical dashed grey lines represent the end of a contraction (C), labelled numerically along the top of the plot.

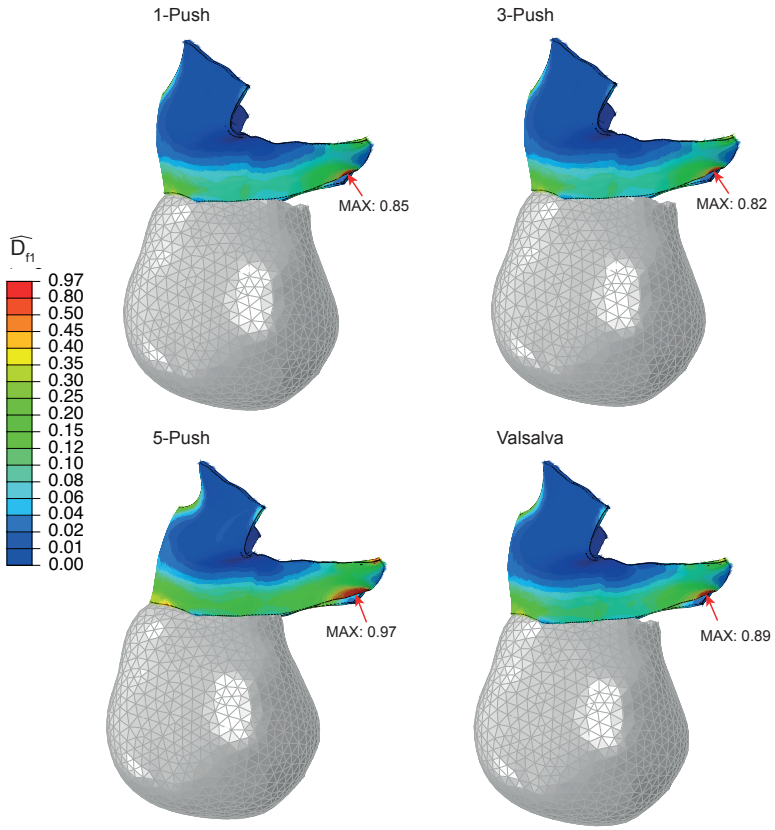

Figure 4.7 - Right lateral view showing the damage distribution in the pelvic floor muscles at the end of the simulation for the four pushing patterns. The peak damage and critical node location are identified.

Figure 4.8 shows a quantitative view of the distribution shown in Figure 4.7. The boxplot includes the muscle fiber damage values predicted for every node of the pelvic floor muscles, grouping the values by the categories defined in the Materials and Methods section (critical, high, noteworthy, moderate, and low). The 5-push pattern has more critical, high, noteworthy, and moderate areas than the other pushing patterns, indicating that it is the pushing pattern that is predicted to cause the highest amount of damage accumulation. Moreover, it is followed by the Valsalva-push pattern. The 1-push pattern led to a similar damage distribution to the 3-push pattern, although more moderate-risk areas exist in the 1-push and more low-risk areas exist in the 3-push pattern.

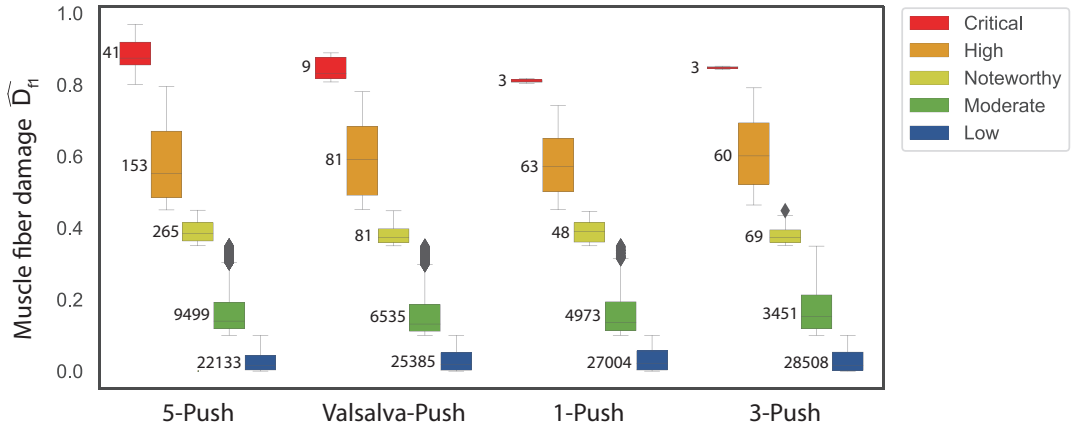

Figure 4.8 –Boxplot grouping the pelvic floor nodal muscle fiber damage values at the end of the simulation for each category (Critical, High, Noteworthy, Moderate and Low) and for the four pushing patterns. Numbers inside the graph area are the number of nodes in each category. Critical: $1 \leq \widehat{D_{f1}} < 0.8$, High: $0.8 < \widehat{D_{f1}} \leq 0.45$, Noteworthy: $0.45 < \widehat{D_{f1}} \leq 0.35$, Moderate: $0.35 < \widehat{D_{f1}} \leq 0.1$ and Low $0 \leq \widehat{D_{f1}} \leq 0.1$

Figure 4.9a shows the fatigue damage evolution at the critical node during each uterine contraction. For easier comparison, Figure 4.9b shows the critical node maximum value, reached at the end of the simulation. The Valsalva-push and 5-push patterns showed faster damage evolution and higher maximum values. The 3-push pattern induced the least maximum damage of all tested pushing patterns, although the damage accumulated faster than with the spontaneous 1-push pattern in almost all uterine contractions. Figure 4.9c and d shows an attempt to verify which time measurement is the better assessment of high-risk labor, in terms of maternal tissue damage. We can see that the simulation total time does not influence the maximum tissue damage Figure 4.9c), whereas the time spent in active pushing seems to exert some influence (Figure 4.9d). However, we did not have enough data to confirm if there was a correlation between the time spent in active pushing and the maximum tissue damage.

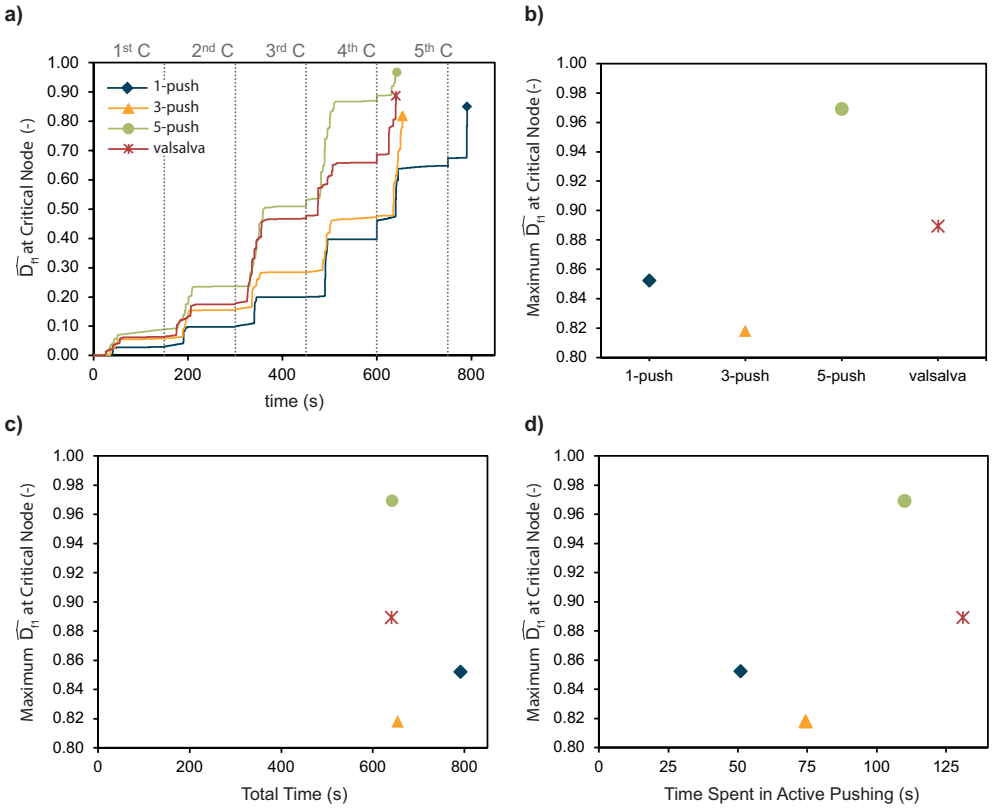

Figure 4.9 - a) Fiber damage evolution at the critical node for the four simulated pushing patterns, **b)** Comparison of the fiber maximum damage at the critical node for the simulated pushing patterns, **c)** Fiber maximum damage at the critical node as a function of the simulations total time, and **d)** Fiber maximum damage at the critical node as a function of the time spent in active pushing, which is the sum of the duration of the maternal pushes.

4.4. Discussion

4.4.1. Principal findings

Our simulations demonstrated that maternal pushing efforts can influence the damage accumulation in the pelvic floor muscles. For all 4 maternal pushing patterns, the region with the most damage accumulation was near the origin of the PVM, which is in agreement with where the tears have been reported to occur using different imaging modalities[18,31,41,42]. The pushing pattern that minimized damage was, for each uterine contraction, 3 maternal pushes lasting 5 seconds. Performing the maternal effort for more than 5 seconds did not shorten the second stage of labor and caused more damage accumulation. The same happened when more than 3 pushes per contraction were performed.

4.4.2. Results in the context of what is known

This work allowed a quantitative view of the effect of vaginal delivery on regions of pelvic floor muscle that were under a remarkable degree of stretch, whichever maternal pushing pattern was used. The degree of tissue-stretch for all pushing patterns was above 1.8, which represented strains above 80%. This value mainly depended on the geometries of both the fetal head and

pelvic floor, which explains why it was similar across the 4 simulations. Moreover, it was dependent on the degree of flexion of the fetal head, which was kept consistent across the 4 scenarios. However, as there was a different progression of the fetal head in each case, this caused slight differences in the degree of tissue strain calculated in the 4 scenarios. Our muscle stretch ratio results were consistent with published values that range from 1.64 to 3.26[36,49].

The predicted duration of the second stage of labor was similar for the 4 pushing patterns, ranging between 10 and 13 minutes. A systematic review that included 208,000 normal labors found the median durations for nulliparous women to range from 14 to 66 minutes (95th percentiles, 65–138 minutes) and multiparous women to range from 6 to 12 min (95th percentiles, 58–76 minutes)[1]. Although our results were shorter than the typical labor, they were still within the reported range, particularly for multiparous women. Moreover, our second stage of labor ended after the passage of the fetal head, and not the fetus, which would slightly increase our predicted second stage of labor duration.

All pushing patterns took the tissue to a critical point, with maximum damage values above 0.8, at the same location of the maximum damage as to where tears have been reported to occur in the literature[18,31,41,42]. One can argue that the differences were not substantial enough to conclude; however, this was also in agreement with the literature[3,21,30]. It may be one of the reasons that there is no consensus on the optimum pushing style from an injury standpoint, as there has not been a considerable difference in published studies (see section 4.1). However, we can still answer our working hypothesis as the type of maternal pushing style did result in different damage accumulations and different maximum critical damage values. Regarding the second part of our hypothesis, which was that the smaller pushes are beneficial for the mother, the answer was not so straightforward. We found that the spontaneous 3-push pattern caused the least damage and the 5-push pattern was the riskiest. Hence, it seems that the frequency exerts an important influence and that more than 3 pushes per contraction is substantially detrimental without shortening the duration of the second stage of labor. In contrast, performing only 1 push per contraction might also not be adequate, because it lengthened the duration of the expulsion stage of the second stage of labor and the damage values were still higher than the 3-push pattern. Thus, we concluded that 3-pushes per contraction is the best approach, but each push should be less than 10 seconds. Maintaining each maternal push for a 10-second duration (Valsalva-push pattern) did not bring any benefits in terms of the duration of labor and caused more tissue damage than the 3-push pattern, for which each push lasted 5 seconds. From a broader perspective, as women do not breathe during the maternal push, reducing the maternal push to 5 seconds can help counteract the reduced fetal oxygenation and mean cerebral oxygen concentrations associated with directed pushing with approximately 10-second maternal pushes[2,11]. Moreover, shorter

maternal pushes may be beneficial if we consider muscle fatigue[p] and maternal exhaustion. The peak force in a volitional push can only be maintained for 2 seconds, after which the force will decline over time[71]. As such, maintaining the effort for 3 to 5 seconds will be more efficient from the point of view of maintaining a high expulsion force. Importantly, if the maternal pushes are performed for shorter periods, the intervening muscle recovery intervals are longer, helping to reduce the risk of maternal exhaustion[9,38]. Another interesting aspect of our results was that the total duration of the second stage of labor does not influence the maternal pelvic floor tissue damage. Although a prolonged second stage of labor is usually a factor to avoid, in terms of maternal injuries, it was not predicted to have an impact, and it might even be better than other management styles that cause a shorter stage of labor (ie, the 1-push pattern caused a longer simulated labor but showed less damage than the Valsalva-push and 5-push patterns). Although we do not have enough data to support this theory, our results did suggest that a better measurement for maternal risk is the time spent in active pushing, which is already well discussed in the literature[39].

4.4.3. Clinical implications

There is currently no consensus as to the optimum pushing style for the management of the second stage of labor. Medical professionals usually favor the directed coaching (Valsalva-push pattern), although there is no evidence that it is the best approach. In contrast, the World Health Organization recommended that women in the expulsive phase of the second stage of labor should be supported to follow their natural desire to push as it helps them to feel more confident and in charge[3]. Although focused on the maternal outcomes only, this study suggested that the goal should not be to shorten the second stage of labor but rather to provide conditions for the mother to sustain less damage to the pelvic floor with less risk of exhaustion. This has immediate implications for directed pushing, which, this work suggested, should be reevaluated to consider damage accumulation in the pelvic floor muscles. At least in terms of damage accumulation, the model suggests that women might benefit from a new, more flexible, coached pushing approach that reduces the active pushing time.

As this engineering approach did not allow us to consider geometric maternal and fetal variability, we chose the standard geometries of a gynecoid pelvis and a 50th percentile fetal head. The size of the fetal head is directly related to the imposed strain, so larger fetal heads have the potential to accumulate damage at a faster rate. A non-gynecoid pelvis is known to be associated

[p] Note that muscle fatigue is a completely different process than the material fatigue discussed in this paper. Muscle fatigue is the decrease in the muscle's ability to actively develop a sustained contractile force over time, as well as when such contractions are repeated after rest intervals that prove insufficient for complete recovery of the muscle; it can result in a state of physical exhaustion. Material fatigue is a phenomenon in which structures fail when subjected to cyclic loading due to the progressive accumulation of damage at a microscopic level.

with a higher risk of labor complications, so if, as a consequence, the second stage of labor involves a higher number of maternal pushes, this would be riskier in terms of damage accumulation and tissue injury. As for the critical locations in those differently shaped pelvises, because of the large report of injuries at the origin of the PVM by different research groups, it is reasonable to assume it is most likely the critical location as well (although other levator ani muscles and pubic bone injuries have been reported to occur, although with lower incidence[42]).

Regarding the positioning of the fetus, it was shown by Parente et al[50] that an occiput posterior presentation increases the degree of muscle strain. Hence, if in each maternal push the degree of muscle strain is higher, the damage accumulation in each contraction will also be higher. As such, an occiput posterior presentation can also be considered a riskier presentation in terms of material fatigue damage.

4.4.4. Research implications

We believe our study provided a visualization of the underlying mechanisms, present in the pelvic floor muscles during the second stage of labor. Unfortunately, it is beyond the scope of this article to verify the model damage predictions in vivo. However, magnetic resonance imaging already has been shown to be effective for visualizing the inflammation in the PVMs following a difficult labor,7 so higher resolution imaging could indeed be used to verify that the inflammation starts in the critical damage zones predicted by this study. These findings could undergird a clinical trial informed by these results to try to reduce the risk of these injuries in the future. In particular, we believe the outcomes of these 3 groups should be compared: directed pushing with 3 pushes per contraction lasting 10 seconds (Valsalva-push pattern), directed pushing pattern with 3 pushes per contraction lasting 5 seconds (3-push pattern), and a spontaneous pushing where the mother would be told to push when she feels the need to do so. Using G-Power and methodology described in the literature[27], we estimated that the total sample size should be between 108 (effect size, 0.305; confidence level, 95%; power, 80%) and 420 (effect size, 0.152; confidence level, 95%; power, 80%). The effect sizes were obtained considering 3 of the results of maximum damage as means (0.82, 0.89, and 0.97) and equal individual standard deviations of 0.2 and 0.4. To better access maternal damage accumulation, the analyzed maternal outcomes must include follow-up appointments to assess hiatal area enlargement or other evidence of irrecoverable damage, besides levator ani tears. A clinical trial of this sort would differ from what is currently in the literature as it would compare different approaches for the directed pushing, with the potential to find a better approach for the maternal pushing style.

4.4.5. Strengths and limitations

The strengths of our approach included the use of a well-characterized material behavior for the pelvic floor muscles, which incorporated visco-hyperelasticity, muscle fiber directions, and, for

the first time, the ability to accumulate damage under repetitive submaximal loading. Although simplified, the geometric models were based on human data. The complete biomechanical model was able to identify the weakest region of the pelvic floor during the second stage of labor, and that region is in agreement with where the literature reports tears.

Limitations of our study included the simplified bowl-shaped pelvic floor geometry having a single hiatus. Moreover, we did not consider the resting pelvic floor geometry changing with age from that of a valley to more of a bowl shape[61] or that the levator plate straightens in late pregnancy[54]. In the future, it would be better to start the model with a pelvic floor geometry measured from a pregnant woman with both the genital and levator hiatuses represented. Nevertheless, we believe the simplifications we used would not affect the qualitative results from the four comparisons that we made. The second limitation concerned the material parameters used to describe pelvic floor tissue behavior, which were obtained from experimental data from nonpregnant ovine pelvic floor muscles[68]. This decision was made because of the lack of any human experimental pelvic floor data regarding low-cycle damage accumulation, thereby pointing out a current knowledge gap. Further studies are needed to characterize the damage accumulation in human pelvic floor tissue in pregnant individuals (see below). Hence, quantitatively, our results must be viewed with care because of a possible overestimation of stress levels (as material parameters came from nonpregnant individuals, with less compliant tissues compared with pregnant). Nevertheless, as we compared 4 pushing patterns while keeping the remaining conditions constant (ie, geometry and material properties), we believe that qualitatively our results were valid and our conclusions would hold for different geometries and material properties. The third limitation was that we did not consider the effect of muscle fatigue[p] in the simulations, specifically the decrease in the peak contractile force that happens in a maximum isometric muscle contraction over time in addition to the decrease in peak force whenever isometric muscle contractions are repeated after intervening rest intervals[38]. A fourth limitation was that although viscoelastic properties were included, we did not consider the effect of the large interindividual differences in levator viscoelastic properties that have been measured during labor[64]; these could affect the propensity for tissue injury. The fifth limitation was that we did not include the perineal body in our finite element model, which was shown to be protective[13], and so it could potentially lessen the damage accumulation in the levator ani. Minor limitations included the fact that we did not differentiate between muscle fibers and collagenous fibers in carrying the load through the ground substance of the pelvic floor muscle material, although the model-predicted locations of maximum damage were the origin of the PVM, where it connects to the pubic bone via an aponeurosis[28].

4.4.6. Conclusions

Fatigue damage accumulation was a possible PVM failure mode during the repetitive loading caused by the strenuous maternal pushing characteristic of the second stage of labor. Maternal pushing style influenced the risk of damage accumulation in the passive tissues of the PVM. Although the critical damage location did not differ across pushing styles, that location was confirmed to lie near the origin of the PVM. The optimal pushing style was 3-pushes per uterine contraction, maintaining each push for 5 seconds. That pattern caused the least amount of damage to the PVM without increasing the duration of the second stage of labor. We could not ascertain whether it is better to achieve that pushing pattern via directed or spontaneous pushing, but, if directed, the model suggests that women should sustain a push for shorter than 10 seconds.

Acknowledgements

Authors acknowledge the support from the Portuguese Foundation of Science under grant SFRH/BD/136213/2018 and under the research project UIDB/50022/2020. The funding sources were not involved in preparing the manuscript and conducting the research.

References

1. Abalos E, Oladapo OT, Chamillard M, et al. Duration of spontaneous labour in 'low-risk' women with 'normal' perinatal outcomes: A systematic review. *Eur J Obstet Gynecol Reprod Biol*. 2018;223:123-132. doi:10.1016/j.ejogrb.2018.02.026

2. Aldrich CJ, D'Antona D, Spencer JA, et al. The effect of maternal pushing on fetal cerebral oxygenation and blood volume during the second stage of labour. *Br J Obstet Gynaecol*. 1995;102(6):448-453. doi:10.1111/j.1471-0528.1995.tb11316.x

3. Araujo AE, Delgado A, Maia JN, et al. Efficacy of spontaneous pushing with pursed lips breathing compared with directed pushing in maternal and neonatal outcomes : a clinical trial. *Authorea*. Published online 2020:1-11. doi:10.22541/au.160278519.95490262/v1

4. Ashton-Miller JA, DeLancey JOL. On the biomechanics of vaginal birth and common sequelae. *Annu Rev Biomed Eng*. 2009;11(1):163-176. doi:10.1146/annurev-bioeng-061008-124823.On

5. Barnett MM, Humenick SS. Infant Outcome in Relation to Second Stage Labor Pushing Method. *Birth*. 1982;9(4):221-229. doi:https://doi.org/10.1111/j.1523-536X.1982.tb01667.x

6. Beaulieu ML, Carey GE, Schlecht SH, Wojtys EM, Ashton-Miller JA. On the heterogeneity of the femoral enthesis of the human ACL: microscopic anatomy and clinical implications. *J Exp Orthop*. 2016;3(1):14. doi:10.1186/s40634-016-0050-8

7. Bloom SL, Casey BM, Schaffer JI, McIntire DD, Leveno KJ. A randomized trial of coached versus uncoached maternal pushing during the second stage of labor. *Am J Obstet Gynecol*. 2006;194(1):10-13. doi:https://doi.org/10.1016/j.ajog.2005.06.022

8. Boyles SH, Weber AM, Meyn L. Procedures for pelvic organ prolapse in the United States, 1979-1997. *Am J Obstet Gynecol*. 2003;188(1):108-115. doi:https://doi.org/10.1067/mob.2003.101

9. Buckthorpe M, Pain MTG, Folland JP. Central fatigue contributes to the greater reductions in explosive than maximal strength with high-intensity fatigue. *Exp Physiol*. 2014;99(7):964-973. doi:https://doi.org/10.1113/expphysiol.2013.075614

10. Buttin R, Zara F, Shariat B, Redarce T, Grangé G. Biomechanical simulation of the fetal descent without imposed theoretical trajectory. *Comput Methods Programs Biomed*. 2013;111(2):389-401. doi:10.1016/j.cmpb.2013.04.005

11. Caldeyro-Barcia R. The Influence of Maternal Bearing-down Efforts during Second Stage on Fetal Well-being. *Birth*. 1979;6(1):17-21. doi:https://doi.org/10.1111/j.1523-536X.1979.tb01298.x

12. Casanova R, And AC, Goepfert AR, Hueppchen NA, Weiss PM, American College of Obstetricians and Gynecologists. *Beckmann and Ling's Obstetrics and Gynecology*. 8th Editio. Philadelphia : Wolters Kluwer; 2019.

13. Cechova H, Kalis V, Havelkova L, et al. Finite element modeling of maximum stress in pelvic floor structures during the head expulsion (FINESSE) study. *Int Urogynecol J*. 2021;32(7):1997-2003. doi:10.1007/s00192-021-04769-z

14. Chan SSC, Cheung RYK, Yiu AKW, et al. Prevalence of levator ani muscle injury in Chinese women after first delivery. *Ultrasound Obstet Gynecol*. 2012;39(6):704-709. doi:https://doi.org/10.1002/uog.10132

15. Chen J, Kim J, Shao W, et al. An anterior cruciate ligament failure mechanism. *Am J Sports Med*. 2019;47(9):2067-2076. doi:10.1177/0363546519854450

16. DeLancey JOL, Kearney R, Chou Q, Speights S, Binno S. The appearance of levator ani muscle abnormalities in magnetic resonance images after vaginal delivery. *Obstet Gynecol*. 2003;101(1):46-53. doi:10.1016/S0029-7844(02)02465-1

17. DeLancey JOL, Sørensen HC, Lewicky-Gaupp C, Smith TM. Comparison of the

puborectal muscle on MRI in women with POP and levator ani defects with those with normal support and no defect. *Int Urogynecol J*. 2012;23(1):73-77. doi:10.1007/s00192-011-1527-8

18. Dietz HP, Gillespie AVL, Phadke P. Avulsion of the pubovisceral muscle associated with large vaginal tear after normal vaginal delivery at term. *Aust New Zeal J Obstet Gynaecol*. 2007;47(4):341-344. doi:10.1111/j.1479-828X.2007.00748.x

19. Ferreira JPS, Parente MPL, Jabareen M, Jorge RMN. A general framework for the numerical implementation of anisotropic hyperelastic material models including non-local damage. *Biomech Model Mechanobiol*. 2017;16(4):1119-1140. doi:10.1007/s10237-017-0875-9

20. Hanson L. Second-stage labor care: challenges in spontaneous bearing down. *J Perinat Neonatal Nurs*. 2009;23(1):31. doi:10.1097/JPN.0b013e318196526b

21. Hofmeyr GJ, Singata-Madliki M. The second stage of labor. *Best Pract Res Clin Obstet Gynaecol*. 2020;67:53-64. doi:https://doi.org/10.1016/j.bpobgyn.2020.03.012

22. Holzapfel GA, Gasser TC. A viscoelastic model for fiber-reinforced composites at finite strains: Continuum basis, computational aspects and applications. *Comput Methods Appl Mech Eng*. 2001;190(34):4379-4403. doi:https://doi.org/10.1016/S0045-7825(00)00323-6

23. Holzapfel GA, Gasser TC, Ogden RW. A new constitutive framework for arterial wall mechanics and a comparative study of material models. *J Elast Phys Sci solids*. 2000;61(1):1-48. doi:10.1023/A:1010835316564

24. Janda S, van der Helm FCT, de Blok SB. Measuring morphological parameters of the pelvic floor for finite element modelling purposes. *J Biomech*. 2003;36(6):749-757. doi:10.1016/s0021-9290(03)00008-3

25. Jing D. Experimental and Theoretical Biomechanical Analyses of the Second Stage of Labor. Doctoral Dissertation, Department of Mechanical Engineering, University of Michigan, Ann Arbor. Published online 2010.

26. Kamisan Atan I, Shek KL, Langer S, et al. Does the Epi-No® birth trainer prevent vaginal birth-related pelvic floor trauma? A multicentre prospective randomised controlled trial. *BJOG An Int J Obstet Gynaecol*. 2016;123(6):995-1003. doi:https://doi.org/10.1111/1471-0528.13924

27. Kang H. Sample size determination and power analysis using the G*Power software. *J Educ Eval Health Prof*. 2021;18:17. doi:10.3352/jeehp.2021.18.17

28. Kim J, Betschart C, Ramanah R, Ashton-Miller JA, DeLancey JOL. Anatomy of the pubovisceral muscle origin: Macroscopic and microscopic findings within the injury zone. *Neurourol Urodyn*. 2015;34(8):774-780. doi:10.1002/nau.22649

29. Kiserud T, Piaggio G, Carroli G, et al. *The World Health Organization Fetal Growth Charts: A Multinational Longitudinal Study of Ultrasound Biometric Measurements and Estimated Fetal Weight*. Vol 14.; 2017. doi:10.1371/journal.pmed.1002220

30. Koyucu RG, Demirci N. Effects of pushing techniques during the second stage of labor: A randomized controlled trial. *Taiwan J Obstet Gynecol*. 2017;56(5):606-612. doi:https://doi.org/10.1016/j.tjog.2017.02.005

31. Krofta L, Otcenasek M, Kasikova E, Feyereisl J. Pubococcygeus-puborectalis trauma after forceps delivery: evaluation of the levator ani muscle with 3D/4D ultrasound. *Int Urogynecol J Pelvic Floor Dysfunct*. 2009;20(10):1175-1181. doi:10.1007/s00192-009-0837-6

32. Lee N, Gao Y, Lotz L, Kildea S. Maternal and neonatal outcomes from a comparison of spontaneous and directed pushing in second stage. *Women and Birth*. 2019;32(4):e433-e440. doi:https://doi.org/10.1016/j.wombi.2018.10.005

33. Lemos A, Amorim MMR, Dornelas de Andrade A, de Souza AI, Cabral Filho JE, Correia JB. Pushing/bearing down methods for the second stage of labour. *Cochrane Database*

Syst Rev. 2017;(3). doi:10.1002/14651858.CD009124.pub3

34. Leombroni M, Buca D, Liberati M, et al. Post-partum pelvic floor dysfunction assessed on 3D rotational ultrasound: a prospective study on women with first- and second-degree perineal tears and episiotomy. *J Matern neonatal Med Off J Eur Assoc Perinat Med Fed Asia Ocean Perinat Soc Int Soc Perinat Obstet*. 2021;34(3):445-455. doi:10.1080/14767058.2019.1609932

35. Lien K-C, DeLancey JOL, Ashton-Miller JA. Biomechanical analyses of the efficacy of patterns of maternal effort on second-stage progress. *Obstet Gynecol*. 2009;113(4):873-880. doi:10.1097/AOG.0b013e31819c82e1

36. Lien K-C, Mooney B, DeLancey JOL, Ashton-Miller JA. Levator ani muscle stretch induced by simulated vaginal birth. *Obstet Gynecol*. 2004;103(1):31-40. doi:10.1097/01.AOG.0000109207.22354.65

37. Lipps DB, Wojtys EM, Ashton-Miller JA. Anterior cruciate ligament fatigue failures in knees subjected to repeated simulated pivot landings. *Am J Sports Med*. 2013;41(5):1058-1066. doi:10.1177/0363546513477836

38. Looft JM, Herkert N, Frey-Law L. Modification of a three-compartment muscle fatigue model to predict peak torque decline during intermittent tasks. *J Biomech*. 2018;77:16-25. doi:10.1016/j.jbiomech.2018.06.005

39. Low LK, Zielinski R, Tao Y, Galecki A, Brandon CJ, Miller JM. Predicting birth-related levator ani tear severity in primiparous women: evaluating maternal recovery from labor and delivery (EMRLD study). *Open J Obstet Gynecol*. 2014;4(6):266-278. doi:10.4236/ojog.2014.46043

40. Mair SD, Seaber A V, Glisson RR, Garrett WE, Garrett Jr. WE. The role of fatigue in susceptibility to acute muscle strain injury. *Am J Sports Med*. 1996;24(2):137-143. doi:10.1177/036354659602400203

41. Margulies RU, Huebner M, DeLancey JOL. Origin and insertion points involved in levator ani muscle defects. *Am J Obstet Gynecol*. 2007;196(3):251.e1-251.e5. doi:10.1016/j.ajog.2006.10.894

42. Miller JM, Low LK, Zielinski R, Smith AR, Delancey JOL, Brandon C. Evaluating maternal recovery from labor and delivery: Bone and levator ani injuries. *Am J Obstet Gynecol*. 2015;213(2):188.e1-188.e11. doi:10.1016/j.ajog.2015.05.001

43. Moura R, Borges M, Vila Pouca MCP, et al. A numerical study on fetal head molding during labor. *Int j numer method biomed eng*. 2021;37(1):e3411. doi:https://doi.org/10.1002/cnm.3411

44. Noonan TJ, Best TM, Seaber A V, Garrett WEJ. Identification of a threshold for skeletal muscle injury. *Am J Sports Med*. 1994;22(2):257-261. doi:10.1177/036354659402200217

45. Oliveira DA, Parente MPL, Calvo B, Mascarenhas T, Jorge RMN. A biomechanical analysis on the impact of episiotomy during childbirth. *Biomech Model Mechanobiol*. 2016;15(6):1523-1534. doi:10.1007/s10237-016-0781-6

46. Oliveira DA, Parente MPL, Calvo B, Mascarenhas T, Jorge RMN. The management of episiotomy technique and its effect on pelvic floor muscles during a malposition childbirth. *Comput Methods Biomech Biomed Engin*. 2017;20(11):1249-1259. doi:10.1080/10255842.2017.1349762

47. Paine LL, Tinker DD. The effect of maternal bearing-down efforts on arterial umbilical cord pH and length of the second stage of labor. *J Nurse Midwifery*. 1992;37(1):61-63. doi:10.1016/0091-2182(92)90023-v

48. Parente M, Natal Jorge RM, Mascarenhas T, Fernandes AA, Silva-Filho AL. Computational modeling approach to study the effects of fetal head flexion during vaginal delivery. *Am J Obstet Gynecol*. 2010;203(3):217.e1-217.e6. doi:10.1016/j.ajog.2010.03.038

49. Parente MPL, Jorge RMN, Mascarenhas T, Fernandes AA, Martins JAC. Deformation of

the pelvic floor muscles during a vaginal delivery. *Int Urogynecol J Pelvic Floor Dysfunct*. 2008;19(1):65-71. doi:10.1007/s00192-007-0388-7

50. Parente MPL, Jorge RMN, Mascarenhas T, Fernandes AA, Martins JAC. The influence of an occipito-posterior malposition on the biomechanical behavior of the pelvic floor. *Eur J Obstet Gynecol Reprod Biol*. 2009;144:S166-S169. doi:https://doi.org/10.1016/j.ejogrb.2009.02.033

51. Polnaszek BE, Cahill AG. Evidence-based management of the second stage of labor. *Semin Perinatol*. 2020;44(2):151213. doi:10.1016/j.semperi.2019.151213

52. Rempen A, Kraus M. *Pressures on the Fetal Head during Normal Labor*. Vol 19.; 1991. doi:10.1515/jpme.1991.19.3.199

53. Roberts JE. The "push" for evidence: management of the second stage. *J Midwifery Womens Health*. 2002;47(1):2-15. doi:10.1016/s1526-9523(01)00233-1

54. Routzong MR, Rostaminia G, Moalli PA, Abramowitch SD. Pelvic floor shape variations during pregnancy and after vaginal delivery. *Comput Methods Programs Biomed*. 2020;194:105516. doi:https://doi.org/10.1016/j.cmpb.2020.105516

55. Sampselle CM, Hines S. Spontaneous pushing during birth. Relationship to perineal outcomes. *J Nurse Midwifery*. 1999;44(1):36-39. doi:10.1016/s0091-2182(98)00070-6

56. Schaffer JI, Bloom SL, Casey BM, McIntire DD, Nihira MA, Leveno KJ. A randomized trial of the effects of coached vs uncoached maternal pushing during the second stage of labor on postpartum pelvic floor structure and function. *Am J Obstet Gynecol*. 2005;192(5):1692-1696. doi:https://doi.org/10.1016/j.ajog.2004.11.043

57. Sharifimajd B, Thore CJ, Stålhand J. Simulating uterine contraction by using an electro-chemo-mechanical model. *Biomech Model Mechanobiol*. 2016;15(3):497-510. doi:10.1007/s10237-015-0703-z

58. Shek KL, Dietz HP. Intrapartum risk factors for levator trauma. *BJOG An Int J Obstet Gynaecol*. 2010;117(12):1485-1492. doi:10.1111/j.1471-0528.2010.02704.x

59. Shek KL, Kruger J, Dietz HP. The effect of pregnancy on hiatal dimensions and urethral mobility: an observational study. *Int Urogynecol J*. 2012;23(11):1561-1567. doi:10.1007/s00192-012-1795-y

60. Sheng Y, Liu X, Low LK, Ashton-Miller JA, Miller JM. Association of pubovisceral muscle tear with functional capacity of urethral closure: evaluating maternal recovery from labor and delivery. *Am J Obstet Gynecol*. 2020;222(6):598.e1-598.e7. doi:https://doi.org/10.1016/j.ajog.2019.11.1257

61. Swenson CW, Masteling M, DeLancey JO, Nandikanti L, Schmidt P, Chen L. Aging effects on pelvic floor support: a pilot study comparing young versus older nulliparous women. *Int Urogynecol J*. 2020;31(3):535-543. doi:10.1007/s00192-019-04063-z

62. Taylor DC, Dalton JDJ, Seaber A V, Garrett WEJ. Experimental muscle strain injury. Early functional and structural deficits and the increased risk for reinjury. *Am J Sports Med*. 1993;21(2):190-194. doi:10.1177/036354659302100205

63. Thomson AM. Pushing techniques in the second stage of labour. *J Adv Nurs*. 1993;18(2):171-177. doi:https://doi.org/10.1046/j.1365-2648.1993.18020171.x

64. Tracy P V, Wadhwani S, Triebwasser J, et al. On the variation in maternal birth canal in vivo viscoelastic properties and their effect on the predicted length of active second stage and levator ani tears. *J Biomech*. 2018;74:64-71. doi:10.1016/j.jbiomech.2018.04.019

65. Tsuang Y-H, Sun J-S, Chen I-H, et al. The effects of cyclic stretching on tensile properties of the rabbit's skeletal muscle. *Clin Biomech (Bristol, Avon)*. 1998;13(1):48-53.

66. Vila Pouca MCP, Ferreira JPS, Oliveira DA, Parente MPL, Natal Jorge RM. Viscous effects in pelvic floor muscles during childbirth: a numerical study. *Int j numer method biomed eng*. 2017;(September):e2927. doi:10.1002/cnm.2927

67. Vila Pouca MCP, Parente MPL, Natal Jorge RM, Ashton-Miller JA. Injuries in muscle-tendon-bone units: a systematic review considering the role of passive tissue fatigue.

Orthop J Sport Med. 2021;9(8). doi:DOI: 10.1177/23259671211020731

68. Vila Pouca MCP, Parente MPL, Natal Jorge RM, Ashton-Miller JA. Investigating the birth-related caudal maternal pelvic floor muscle injury: The consequences of low cycle fatigue damage. *J Mech Behav Biomed Mater*. 2020;110:103956. doi:https://doi.org/10.1016/j.jmbbm.2020.103956

69. Vila Pouca MCP, Parente MPL, Natal Jorge RM, DeLancey JO., Ashton-Miller JA. Pelvic floor muscle injury during a difficult labor. Can tissue fatigue damage play a role? *Int J Urogynecology*. 2022;(33):211-220.

70. Wojtys EM, Beaulieu ML, Ashton-Miller JA. New perspectives on ACL injury: On the role of repetitive sub-maximal knee loading in causing ACL fatigue failure. *J Orthop Res*. 2016;34(12):2059-2068. doi:10.1002/jor.23441

71. Wood DD, Fisher DL, Andres RO. Minimizing fatigue during repetitive jobs: optimal work-rest schedules. *Hum Factors*. 1997;39(1):83-101. doi:10.1518/001872097778940678

72. Wu E, Kuehl TJ, Gendron JM, White W, Yandell PM. Pelvic floor changes in the first term pregnancy and postpartum period. *Int Urogynecol J*. 2021;32(7):1897-1905. doi:10.1007/s00192-020-04456-5

73. Yeates DA, Roberts JE. A comparison of two bearing-down techniques during the second stage of labor. *J Nurse Midwifery*. 1984;29(1):3-11. doi:https://doi.org/10.1016/0091-2182(84)90324-0

Chapter 5

Modeling permanent deformation during low-cycle fatigue

Application to the pelvic floor muscles during labor

Modeling permanent deformation during low-cycle fatigue

Application to the pelvic floor muscles during labor

Maria C.P. Vila Pouca[1,2], Pedro P.M.A. Areias[3,4], Serdar Göktepe[5], James A. Ashton-Miller[6], Renato M. Natal Jorge[1,2], Marco P.L. Parente[1,2]

1 Department of Mechanical Engineering, Faculty of Engineering of University of Porto. Porto, Portugal
2 Institute of Science and Innovation in Mechanical and Industrial Engineering (INEGI). Porto, Portugal
3 Department of Mechanical Engineering, Superior Technical Institute, University of Lisbon. Lisboa, Portugal
4 Mechanical Engineering Institute (IDMEC), Superior Technical Institute. Lisboa, Portugal
5 Department of Civil Engineering, Middle East Technical University. Ankara, Turkey.
6 Departments of Mechanical and Biomedical Engineering, College of Engineering and School of Kinesiology, University of Michigan. Ann Arbor, Michigan, USA

Submitted to:
Journal of the Mechanics of Physics of Solids
Article Type: Original Research

Submitted: January 7, 2022
Current Status: Under review

Abstract

Low cycle fatigue (between two to hundreds of cycles) is associated with large permanent strains and the development of microdamage that can start as soon as the first cycle. It has been identified as a possible damage mechanism in the anterior cruciate ligament and recently was evaluated as a potential damage mechanism at the origin of the pubovisceral muscle (a pelvic floor muscle) near the end of labor. The purpose of this work is to provide a numerical framework that incorporates the effects of permanent deformation due to low-cycle fatigue. Based on experimental evidence, we hypothesize that the microdamage accumulation due to repetitive sub-maximal loading continuously induces macroscopic permanent deformations that adversely affect the tissue mechanical properties and thereby cause stress softening. The constitutive model is suitable for 3D finite element analysis. The model was first tested against simple numerical examples, where quadratic convergence and objectivity were verified. Next, we applied the approach to a human vaginal delivery, employing a transversely isotropic visco-hyperelastic baseline model. It demonstrated the potential of this numerical framework for simulating permanent deformation in pelvic floor muscles during birth. With robust experimental data, this can be an important tool to analyze the obstetrical risk factors for the pelvic floor permanent deformation associated with the development of pelvic organ prolapse later in life.

Keywords: low-cycle fatigue; permanent deformation; finite element method; user defined subroutine; pelvic floor injury.

5.1. Introduction

Soft biological tissues are known to be highly nonlinear, which makes the prediction of their behaviors an open issue, particularly beyond the hyperelastic region. These tissues are anisotropic[23] and can be interpreted as fiber reinforced composites[12] which exhibit viscoelastic behavior[15], stress softening[5,38] and permanent deformation[11,38]. Despite the material complexity, several constitutive models have been proposed over the years to characterize hyperelastic, anisotropic, viscoelastic[23–25] and stress softening behaviors through damage models[5,22] and to a lesser extent, permanent set[16,35,40,42,52]. Most damage and permanent set models are based on the maximum strain energy at a given time, characterizing failure by a single overload, and only a few[35,52] are able to capture material fatigue. We previously developed a damage model[49] that captures the stress softening particularly from low-cycle fatigue, a failure mode found at the origin of the anterior cruciate ligament[8,33,51] and recently also found to be at the origin of the sheep pubovisceral muscle[49]. The stress softening occurs due to a continuous damage buildup that starts at the nano/micro scales, as revealed experimentally[8,49]. In the origin of the sheep 'pubovisceral' muscle, a pelvic floor muscle, the damage buildup was seen closer to the musculotendinous junction in the form of elongated and crimped muscle fibers and even individual muscle fiber rupture (Figure 5.1). This translated into a visible stress softening and a permanent stretch of almost 1.5[49].

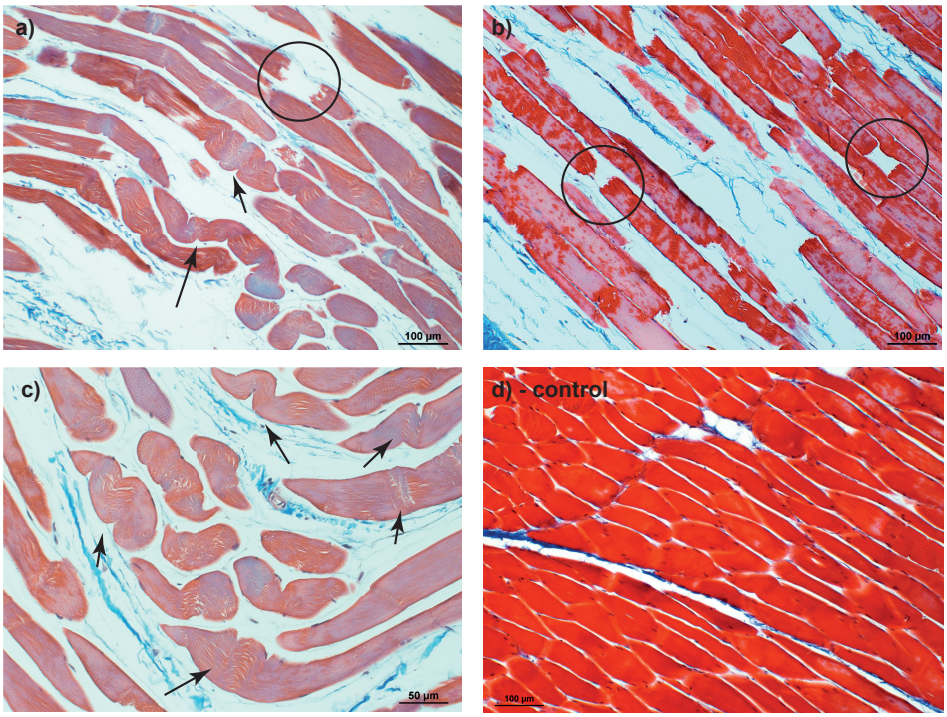

Figure 5.1 - Histological appearance of muscle-tendon sections with Masson's Trichrome stain. Comparison between fatigued specimens (60 cycles between 60% and 45% failure displacement [49]) **(a-c)** and untested control **(d)**. Fatigued specimens show crimped muscle fibers (arrows), individual fiber rupture (circle) and increased interstitial spaces.

Therefore, the goal of the present work is to further evolve our damage model[49] to capture, not only the stress softening, but also the permanent deformation due to low-cycle fatigue. Specifically, we hypothesize that the buildup of microstructural changes (i.e., elongated and crimped fibers) due to a repetitive sub-maximal loading, continuously induces a macroscopic permanent deformation that affects the mechanical properties so as to cause stress softening.

The motivation for this work is the pelvic floor muscle injury that can occur during a difficult vaginal delivery. Although not frequently mentioned when discussing motherhood, it is estimated that between 13 and 41% of women who deliver vaginally[37,43] sustain some degree of pelvic muscle injury, particularly during their first delivery. These injuries not only complicate post-partum recovery but are also associated with the development of pelvic floor disorders later in life[10]. These injuries cannot be safely treated surgically post-partum[2] and the sequelae, like prolapse, can have a significant impact on a woman's quality of life[28]. So, it would be better to prevent these injuries in the first place if we better understood the mechanism of injury. Recently, we focused on the low-cycle fatigue damage mechanism (~80-120 cycles), which we believe may play a causal role in these pelvic floor muscle injuries[48–50]. In a difficult second stage of labor, which may last ~2 h[31], women experience uterine contractions approximately every three minutes[32]. Near the end these are to be associated with strong maternal pushes performed between 1 to 5 times per uterine contraction depending on the coaching strategy[1,20,30,32]. Such strenuous pushes apply significant repetitive loads to the pelvic floor structures. We previously argued[48,49] that this repetitive loading causes microdamage to accumulate and can even ultimately lead to a complete failure of the most susceptible structures. However, even if a complete failure does not occur, the microdamage accumulation can induce permanent deformation in the pelvic muscle or neighboring structure, which is not completely recovered after delivery. This phenomenon has been reported as a significant increase in the postpartum genital hiatus area[7,13,17,26,34,43–45] which gynecologists widely recognize upon vaginal examination of a parous individual. In addition, a significant correlation has been found between the area of the pelvic floor hiatus and pelvic organ prolapse[43], the latter being a herniation of the anterior and/or posterior vagina through the enlarged genital hiatus that often requiring surgical repair. So, we reason that the microdamage accumulation could cause two forms of pelvic floor injury: (i) permanent deformation that leads to an increase in the hiatal area and subsequently contributes to pelvic organ prolapse, and (ii) complete deterioration of the microstructure, which cause a partial or complete tear of muscle and/or passive tissue during labor, thereby contributing to the development of pelvic organ prolapse. With this motivation in mind, the goal of this paper was to develop a computational framework that can be used to analyze the first form of injury. In order to do so, we developed a constitutive model that incorporates the stress softening due to the permanent deformation driven by low-cycle fatigue damage. This constitutive model is implemented into the finite element software ABAQUS® in order to easily be applicable to study more complex scenarios. We believe

this can provide a baseline framework to study several obstetrical factors that might influence the permanent deformation and the hiatal area increase, ultimately leading to an optimized management of the second stage of labor in the case of difficult deliveries.

Therefore, the goal of the present work is to further evolve our damage model[49] to capture, not only the stress softening, but also the permanent deformation due to low-cycle fatigue. Specifically, we hypothesize that the buildup of microstructural changes (i.e., elongated and crimped fibers) due to a repetitive sub-maximal loading, continuously induces a macroscopic permanent deformation that affects the mechanical properties so as to cause the stress softening.

The motivation for this work is the pelvic floor muscle injury that can occur during a difficult vaginal delivery. Although not frequently mentioned when discussing motherhood, it is estimated that between 13 and 41% of women who deliver vaginally[37,43] sustain some degree of pelvic muscle injury, particularly during their first delivery. These injuries not only complicate post-partum recovery but are also associated with the development of pelvic floor disorders later in life[10]. These injuries cannot be safely treated surgically post-partum[2] and the sequelae like prolapse have a significant impact on a woman's quality of life[28]. So, it would be better to prevent these injuries in the first place if we better understood the mechanism of injury. Recently, we focused on the low-cycle fatigue damage mechanism (~80-120 cycles), which we believe may play a causal role in these pelvic floor muscle injuries[48–50]. In a difficult second stage of labor, which may last ~2 h[31], women experience uterine contractions approximately every three minutes[32]. Near the end these are to be associated with strong maternal pushes performed between 1 to 5 times per uterine contraction depending on the coaching strategy[1,20,30,32]. Such strenuous pushes apply significant repetitive loads to the pelvic floor structures. We previously argued[48,49] that this repetitive loading causes microdamage to accumulate and can even ultimately lead to a complete failure of the most susceptible structures. However, even if a complete failure does not occur, the microdamage accumulation can induce permanent deformation in the pelvic muscle or neighboring structure, which is not completely recovered after delivery. This phenomenon has been reported as a significant increase in the postpartum genital hiatus area[7,13,17,26,34,43–45] which gynecologists widely recognize upon vaginal examination of a parous individual. In addition, a significant correlation have been found between the area of the pelvic floor hiatus and pelvic organ prolapse[43], which is a herniation of the anterior and/or posterior vagina through the enlarged genital hiatus that often requires surgical repair. So, in our understanding, the microdamage accumulation can cause two forms of pelvic floor injury: (1) permanent deformation that leads to an increase in the hiatal area and subsequently contributes to pelvic organ prolapse, and (2) complete deterioration of the microstructure, which cause a partial or complete tear of muscle and/or passive tissue during labor, thereby contributing to the development of pelvic organ prolapse. With this motivation in mind, the goal of this paper was to develop a computational framework that can be used to analyze the first form of injury. In order to do so, we developed a

constitutive model that incorporates the stress softening due to the permanent deformation driven by low-cycle fatigue damage. This constitutive model is implemented into a finite element software (ABAQUS®) via the user-defined subroutine (UMAT) in order to easily be applicable to study more complex scenarios. We believe this can provide a baseline framework to study the several obstetrical factors that might influence the permanent deformation and the hiatal area increase, ultimately leading to an optimized management of the second stage of labor in the case of difficult deliveries.

5.2. Material and methods

The constitutive model outlined in this section is defined for a material point, and so it can be applied to solve general boundary-value problems by applying the finite element method. We implemented the material model via the user defined subroutine UMAT an ABAQUS®/Implicit subroutine that allows the implementation of complex constitutive models in that commercial finite element software.

5.2.1. Kinematics

For a continuum body in the reference configuration Ω_0, the mapping $\boldsymbol{\chi} : \Omega_0 \rightarrow \mathbb{R}^3$ transforms a material point in the reference configuration $\mathbf{X} \in \Omega_0$, to a position in the deformed configuration, $\mathbf{x} \in \Omega$, at time *t*. As such, $\boldsymbol{\chi}$ is a vector field designed as motion, carrying points in the reference configuration to places in the current configuration. The total deformation gradient $\mathbf{F}$ is defined as

$$\mathbf{F} = \frac{\partial \boldsymbol{\chi}(\mathbf{X}, t)}{\partial \mathbf{X}}, \tag{5.1}$$

with $J = \det \mathbf{F} > 0$ representing the Jacobian of the transformation.

In the scenario of incompressibility or quasi-incompressibility, it is computational convenient to perform a multiplicative decomposition of the deformation gradient into a volumetric part $\mathbf{F}_{\mathrm{vol}}$ and an isochoric part $\bar{\mathbf{F}}$, such as

$$\bar{\mathbf{F}} = J^{-\frac{1}{3}}\mathbf{F}, \quad \mathbf{F}_{\mathrm{vol}} = J^{\frac{1}{3}}\mathbf{I}. \tag{5.2}$$

Following the assumption of a multiplicative decomposition of $\mathbf{F}$ into an elastic $\mathbf{F}_{\mathrm{e}}$, and a plastic $\mathbf{F}_{\mathrm{p}}$ contribution[4,29] and considering also the volumetric and isochoric decomposition, we can write:

$$\mathbf{F} = \bar{\mathbf{F}}_{\mathrm{e}}\mathbf{F}_{\mathrm{p}}\mathbf{F}_{\mathrm{vol}}, \qquad \bar{\mathbf{F}} = J^{-\frac{1}{3}}\mathbf{F}_{\mathrm{e}}\mathbf{F}_{\mathrm{p}} = \bar{\mathbf{F}}_{\mathrm{e}}\mathbf{F}_{\mathrm{p}}, \tag{5.3}$$

with the Jacobians such that $J_{\mathrm{e}} = \det \mathbf{F}_{\mathrm{e}}$, $J_{\mathrm{p}} = \det \mathbf{F}_{\mathrm{p}}$ and $\bar{J} = \det \bar{\mathbf{F}} = 1$.

The symmetric isochoric right Cauchy-Green tensor is

$$\bar{\mathbf{C}} = \bar{\mathbf{F}}^{\mathrm{T}}\bar{\mathbf{F}}\,, \tag{5.4}$$

and the elastic and plastic counterparts are similarly, i.e.

$$\bar{\mathbf{C}}_{\mathrm{e}} = \bar{\mathbf{F}}_{\mathrm{e}}^{\mathrm{T}}\bar{\mathbf{F}}_{\mathrm{e}}\ ,\ \mathbf{C}_{\mathrm{p}} = \mathbf{F}_{\mathrm{p}}^{\mathrm{T}}\mathbf{F}_{\mathrm{p}}\,. \tag{5.5}$$

We consider that fibers are embedded in a continuum and move coupled with the ground substance. As such, the stretch λ_{f} of a certain fiber is defined as the ratio between its length at the deformed and reference configuration, i.e

$$\lambda_{\mathrm{f}}\mathbf{m} = \mathbf{F}\mathbf{m}_0\,, \tag{5.6}$$

where $\mathbf{m}$ and $\mathbf{m}_0$ are the unit vector of the fiber direction in the deformed and the reference configuration, respectively. Considering the multiplicative decomposition into the elastic and plastic part, we write $\lambda_{\mathrm{f}} = \lambda_{\mathrm{e}}\lambda_{\mathrm{p}}$, where λ_{e} can be designated as the elastic stretch and λ_{p} the permanent deformation variable or the permanent deformation stretch.

Considering the volumetric decomposition, we can define the first invariant as

$$\bar{\mathrm{I}}_1 = \bar{\mathbf{C}} : \mathbf{I}\,, \tag{5.7}$$

and the isochoric pseudo-invariant introduced by Holzapfel[21] as

$$\mathrm{I}_4 = \mathbf{m}_0 \cdot \mathbf{C}\mathbf{m}_0 = {\lambda_{\mathrm{f}}}^2\,, \tag{5.8}$$

with $\bar{\mathrm{I}}_4 = J^{-\frac{2}{3}}\mathrm{I}_4$ and $\bar{\lambda}_{\mathrm{f}} = J^{-\frac{1}{3}}\lambda_{\mathrm{f}}$, where I_4 represents the square of the stretch in the fiber direction $\mathbf{m}_0$.

Integrating the elastic and plastic contributions, we can write

$$\mathrm{I}_{1\mathrm{e}} = \mathbf{C}_{\mathrm{e}} : \mathbf{I}\,, \tag{5.9}$$

$$\mathrm{I}_{4\mathrm{e}} = \mathbf{m}_0 \cdot \mathbf{C}_{\mathrm{e}}\mathbf{m}_0 = {\lambda_{\mathrm{e}}}^2,\quad \lambda_{\mathrm{e}} = \frac{\lambda_{\mathrm{f}}}{\lambda_{\mathrm{p}}}, \tag{5.10}$$

and considering the isochoric components, with $\bar{\mathbf{C}}_{\mathrm{e}} = J^{-\frac{2}{3}}\mathbf{C}_{\mathrm{e}}$,

$$\bar{\mathrm{I}}_{1\mathrm{e}} = \bar{\mathbf{C}}_{\mathrm{e}} : \mathbf{I}\,, \tag{5.11}$$

$$\bar{\mathrm{I}}_{4\mathrm{e}} = \mathbf{m}_0 \cdot \bar{\mathbf{C}}_{\mathrm{e}}\mathbf{m}_0 = {\bar{\lambda}_{\mathrm{e}}}^2,\quad \bar{\lambda}_{\mathrm{e}} = \frac{\bar{\lambda}_{\mathrm{f}}}{\lambda_{\mathrm{p}}}. \tag{5.12}$$

We assumed that the permanent deformation would occur along the fiber direction, $\mathbf{m}_0$, and defined the permanent deformation tensor $\mathbf{F}_{\mathrm{p}}$ as a function of the permanent stretch λ_{p} as[19]

$$\mathbf{F}_{\mathrm{p}} = \mathbf{I} + \left(\lambda_{\mathrm{p}} - 1\right)\mathbf{m}_0 \otimes \mathbf{m}_0\,, \tag{5.13}$$

where its inverse can be given explicitly as

$${\mathbf{F}_{\mathrm{p}}}^{-1} = \mathbf{I} - \frac{\lambda_{\mathrm{p}} - 1}{\lambda_{\mathrm{p}}}\mathbf{m}_0 \otimes \mathbf{m}_0\,. \tag{5.14}$$

5.2.2. Constitutive and balance equations for hyperelastic materials

A hyperelastic material postulates the existence of a Helmholtz free-energy function Ψ defined per unit reference volume[21]. To simulate a transversely isotropic hyperelastic material including permanent deformation, we apply the following representation of Ψ, i. e.

$$\Psi = \Psi_{\mathrm{vol}}(\mathrm{J}) + \bar{\Psi}_{\mathrm{m}}(\bar{\mathrm{I}}_{1\mathrm{e}}) + \bar{\Psi}_{\mathrm{f}}(\bar{\lambda}_{\mathrm{e}}) \,, \tag{5.15}$$

where $\Psi_{\mathrm{ich}} = \bar{\Psi}_{\mathrm{m}} + \bar{\Psi}_{\mathrm{f}}$ represents the isochoric contribution. The index m and f refer to the ground matrix and fiber contributions, respectively.

In this work, we decided to use a modification of Holzapfel-Gasser-Ogden model[24] (HGO), since it is a versatile model for soft tissues and has previously shown to be a good fit for our experimental data [49]. It has the following isochoric free-energy functions

$$\bar{\Psi}_{\mathrm{m}} = \mathrm{C}_{10}(\bar{\mathrm{I}}_{1\mathrm{e}} - 3) \,, \tag{5.16}$$

$$\bar{\Psi}_{\mathrm{f}} = \frac{\mathrm{k}_1}{2\mathrm{k}_2}\left\{\exp^{\mathrm{k}_2\left(\bar{\lambda}_{\mathrm{e}}{}^2-1\right)^2} - 1\right\} , \tag{5.17}$$

where C_{10}, k_1 and k_2 are the material parameters.

Let us now introduce the dissipation inequality in the form

$$\mathcal{D}_{\mathrm{int}} = \mathbf{S} : \frac{1}{2}\dot{\mathbf{C}} - \dot{\Psi} \geq 0 \,, \tag{5.18}$$

where $\mathbf{S}$ is the second Piola-Kirchhoff stress tensor.

Evaluating eq. (5.18), we can write

$$\mathcal{D}_{\mathrm{int}} = \left(\mathbf{S} - 2\frac{\partial \Psi_{\mathrm{vol}}}{\partial \mathbf{C}} - 2\frac{\partial \Psi_{\mathrm{ich}}}{\partial \mathbf{C}}\right) : \frac{1}{2}\dot{\mathbf{C}} + \mathbf{S}_{\mathrm{ich\,e}} : \frac{1}{2}\left(\mathbf{L}_{\mathrm{p}}^{\mathrm{T}}\mathbf{C}_{\mathrm{e}} + \mathbf{C}_{\mathrm{e}}\mathbf{L}_{\mathrm{p}}\right) \geq 0 \,, \tag{5.19}$$

where $\mathbf{L}_{\mathrm{p}} = \dot{\mathbf{F}}_{\mathrm{p}}\mathbf{F}_{\mathrm{p}}{}^{-1}$ is the plastic velocity gradient. This allows us to reach the definition of $\mathbf{S}$ as

$$\mathbf{S} = \mathbf{S}_{\mathrm{vol}} + \mathbf{S}_{\mathrm{ich}} \,, \tag{5.20}$$

$$\mathbf{S}_{\mathrm{vol}} = 2\frac{\partial \Psi_{\mathrm{vol}}}{\partial \mathbf{C}} , \tag{5.21}$$

$$\mathbf{S}_{\mathrm{ich\,e}} = 2\frac{\partial \Psi_{\mathrm{ich}}}{\partial \bar{\mathbf{C}}_{\mathrm{e}}} : \frac{\partial \bar{\mathbf{C}}_{\mathrm{e}}}{\partial \mathbf{C}_{\mathrm{e}}} = J^{-\frac{2}{3}}\mathbb{P}_{\mathrm{e}} : \bar{\mathbf{S}}_{\mathrm{e}} \,, \qquad \bar{\mathbf{S}}_{\mathrm{e}} = 2\frac{\partial \Psi_{\mathrm{ich}}}{\partial \bar{\mathbf{C}}_{\mathrm{e}}} , \tag{5.22}$$

$$\mathbf{S}_{\mathrm{ich}} = 2\frac{\partial \Psi_{\mathrm{ich}}}{\partial \mathbf{C}_{\mathrm{e}}} : \frac{\partial \mathbf{C}_{\mathrm{e}}}{\partial \mathbf{C}} = \mathbf{F}_{\mathrm{p}}{}^{-1}\mathbf{S}_{\mathrm{ich\,e}}\mathbf{F}_{\mathrm{p}}{}^{-\mathrm{T}} , \tag{5.23}$$

where $\mathbb{P}_{\mathrm{e}} = \mathbb{I} - \frac{1}{3}\mathbf{C}_{\mathrm{e}}{}^{-1}\otimes\mathbf{C}_{\mathrm{e}}$ is the elastic projection tensor in the material configuration. Further details and description on how to obtain $\bar{\mathbf{S}}_{\mathrm{e}}$ can be found in the literature[4,21].

The implementation of constitutive models requires the computation of a linearized tangent moduli, also designated as elasticity tensor. It can generally be defined in the material configuration as

$$\mathbb{C} = 2\frac{\partial \mathbf{S}}{\partial \mathbf{C}} = 2\frac{\partial \mathbf{S}_{\text{vol}}}{\partial \mathbf{C}} + 2\frac{\partial \mathbf{S}_{\text{ich}}}{\partial \mathbf{C}} = \mathbb{C}_{\text{vol}} + \mathbb{C}_{\text{ich}}\,, \tag{5.24}$$

where $\mathbb{C}_{\text{vol}}$ is obtained from the linearization of eq. (5.21) which following Holzapfel and Gasser[23] notation gives:

$$\mathbb{C}_{\text{vol}} = J\tilde{p}\mathbf{C}^{-1} \otimes \mathbf{C}^{-1} - 2Jp\mathbf{C}^{-1} \odot \mathbf{C}^{-1}\,, \tag{5.25}$$

where

$$p = \frac{\mathrm{d}\Psi_{\text{vol}}}{\mathrm{d}J} \qquad \tilde{p} = p + J\frac{\mathrm{d}p}{\mathrm{d}J}\,, \tag{5.26}$$

$$-(\mathbf{C}^{-1} \odot \mathbf{C}^{-1} =)_{IJKL} = -\frac{\left(\mathrm{C}_{IK}^{-1}\mathrm{C}_{JL}^{-1} + \mathrm{C}_{IL}^{-1}\mathrm{C}_{JK}^{-1}\right)}{2}. \tag{5.27}$$

To calculate $\mathbb{C}_{\text{ich}}$, we first need to obtain the equivalent elastic tensor $\mathbb{C}_{\text{ich e}}$, which can be derived as following[21,23]

$$\mathbb{C}_{\text{ich e}} = \mathbb{P}_{\text{e}} : \bar{\mathbb{C}}_{\text{e}} : \mathbb{P}_{\text{e}}^{\text{T}} + \frac{2}{3}\mathrm{Tr}_{\text{e}}\left(J^{-\frac{2}{3}}\bar{\mathbf{S}}\right)\tilde{\mathbb{P}}_{\text{e}} - \frac{2}{3}\left(\mathbf{C}_{\text{e}}{}^{-1} \otimes \mathbf{S}_{\text{ich e}} + \mathbf{S}_{\text{ich e}} \otimes \mathbf{C}_{\text{e}}{}^{-1}\right) \tag{5.28}$$

based on the following definitions[21]:

$$\begin{gathered}\mathrm{Tr}_{\text{e}}(\blacksquare) = (\blacksquare) : \mathbf{C}_{\text{e}} \quad , \quad \tilde{\mathbb{P}}_{\text{e}} = \mathbf{C}_{\text{e}}{}^{-1} \odot \mathbf{C}_{\text{e}}{}^{-1} - \frac{1}{3}\mathbf{C}_{\text{e}}{}^{-1} \otimes \mathbf{C}_{\text{e}}{}^{-1} \quad , \\ \mathbb{P}_{\text{e}} = \mathbb{I} - \frac{1}{3}\mathbf{C}_{\text{e}}{}^{-1} \otimes \mathbf{C}_{\text{e}}\,,\end{gathered} \tag{5.29}$$

$$\bar{\mathbb{C}}_{\text{e}} = 2J^{-\frac{4}{3}}\frac{\partial \bar{\mathbf{S}}_{\text{e}}}{\partial \bar{\mathbf{C}}_{\text{e}}} = 4J^{-\frac{4}{3}}\frac{\partial^2 \Psi_{\text{ich}}}{\partial \bar{\mathbf{C}}_{\text{e}} \partial \bar{\mathbf{C}}_{\text{e}}}. \tag{5.30}$$

Details on how to calculate $\bar{\mathbb{C}}_{\text{e}}$ are described in the literature[21,23].

Now we can finally linearize eq. (5.23) to obtain $\mathbb{C}_{\text{ich}}$, which following the work of Göktepe et al.[18] i.e.

$$\mathbb{C}_{\text{ich}} = 2\frac{\partial \mathbf{S}_{\text{ich}}}{\partial \mathbf{C}}\bigg|_{\mathbf{F}_{\text{p}}} + 2\left[\frac{\partial \mathbf{S}_{\text{ich}}}{\partial \mathbf{F}_{\text{p}}} : \frac{\partial \mathbf{F}_{\text{p}}}{\partial \lambda_{\text{p}}}\right] \otimes \frac{\partial \lambda_{\text{p}}}{\partial \mathbf{C}}\bigg|_{\mathbf{F}}. \tag{5.31}$$

The first two terms can be defined as follows

$$2\frac{\partial \mathbf{S}_{\text{ich}}}{\partial \mathbf{C}}\bigg|_{\mathbf{F}_{\text{p}}} = \left[\mathbf{F}_{\text{p}}^{-1}\overline{\otimes}\mathbf{F}_{\text{p}}^{-1}\right] : \mathbb{C}_{\text{ich e}} : \left[\mathbf{F}_{\text{p}}^{-\text{T}}\overline{\otimes}\mathbf{F}_{\text{p}}^{-\text{T}}\right], \tag{5.32}$$

$$\frac{\partial \mathbf{S}_{\text{ich}}}{\partial \mathbf{F}_{\text{p}}} = -\left[\mathbf{F}_{\text{p}}^{-1}\overline{\otimes}\mathbf{S}_{\text{ich}} + \mathbf{S}_{\text{ich}}\underline{\otimes}\mathbf{F}_{\text{p}}^{-1}\right] - \left[\mathbf{F}_{\text{p}}^{-1}\overline{\otimes}\mathbf{F}_{\text{p}}^{-1}\right] : \frac{1}{2}\mathbb{C}_{\text{ich e}} : \left[\mathbf{F}_{\text{p}}^{-\text{T}}\underline{\otimes}\mathbf{C}_{\text{e}} + \mathbf{C}_{\text{e}}\overline{\otimes}\mathbf{F}_{\text{p}}^{-\text{T}}\right], \quad (5.33)$$

where the tensor products abbreviations where applied: $\left(\star\,\overline{\otimes}\,\circ\right)_{ijkl} = (\star)_{ik}\otimes(\circ)_{jl}$ and $\left(\star\,\underline{\otimes}\,\circ\right)_{ijkl} = (\star)_{il}\otimes(\circ)_{jk}$ [27].

The third and fourth terms depend on the choice for the permanent deformation gradient. In this work, we applied the tensor defined in eq. (5.13), which gives the third term as follows:

$$\frac{\partial \mathbf{F}_{\text{p}}}{\partial \lambda_{\text{p}}} = \mathbf{m}_0\otimes\mathbf{m}_0\,. \quad (5.34)$$

The fourth term $\frac{\partial \lambda_{\text{p}}}{\partial \mathbf{C}}\Big|_{\mathbf{F}}$ depends on the evolution equation for the permanent stretch λ_{p}, and it is defined subsequently.

Most finite element software requires the stress and elasticity tensors in the spatial or current configuration. As such, we must apply a push forward operation to both the second Piola-Kirchhoff stress tensor defined in eq. (5.20) and to the material elasticity tensor defined in eq. (5.24) to obtain the Cauchy stress tensor $\boldsymbol{\sigma}$, and the spatial elasticity tensor $\mathbb{c}$ as

$$\boldsymbol{\sigma} = J^{-1}\mathbf{F}\mathbf{S}\mathbf{F}^{\text{T}}\,, \quad (5.35)$$

$$(\mathbb{c})_{ijkl} = J^{-1}\text{F}_{ia}\text{F}_{jb}\text{F}_{kc}\text{F}_{ld}(\mathbb{C})_{abcd}\,. \quad (5.36)$$

Remark: To ensure quadratic convergence of the solutions in the global Newton-Raphson procedure for the continuum elements and for the application of constitutive models in the commercial finite element software ABAQUS®, the consistent elasticity tensor must be calculated based on the Jaumann rate[14]. This implies adding the Jaumann rate contribution $\mathbb{c}_{\text{jr}}$, to eq. (5.36) such as

$$(\mathbb{c})_{ijkl} = J^{-1}\text{F}_{ia}\text{F}_{jb}\text{F}_{kc}\text{F}_{ld}(\mathbb{C})_{abcd} + \mathbb{c}_{\text{jr}}\,, \quad (5.37)$$

$$\mathbb{c}_{\text{jr}} = \frac{1}{2}\left[\mathbf{I}\overline{\otimes}\boldsymbol{\sigma} + \boldsymbol{\sigma}\overline{\otimes}\mathbf{I} + \mathbf{I}\underline{\otimes}\boldsymbol{\sigma} + \boldsymbol{\sigma}\underline{\otimes}\mathbf{I}\right]. \quad (5.38)$$

5.2.3. Evolution equations

We hypothesize that permanent deformation is a direct consequence of microstructural damage that accumulates with repetitive sub-maximal loading. Hence, we defined a low cycle fatigue damage variable D ($0 < \text{D} < 1$), that grows with the deformation cycles. Such damage variable can then be seen as a quantitative measurement of the microstructure degradation due to low-cycle fatigue, with $\text{D} = 0$ representing an undamaged material and $\text{D} = 1$ a point of degradation

that promotes a swift evolution of permanent deformation. So, when the material degrades cyclically, it starts to permanently deform, which will affect the mechanical properties.

Low-cycle fatigue damage

The damage variable was defined according to an experimentally driven previous work[49]. It was developed using the concept of accumulated equivalent strain Ξ_t^{acc}, as defined by Peña et al.[40]

$$\Xi_t^{\mathrm{acc}} = \int_0^t \left|\frac{\mathrm{d}\Psi_{\mathrm{ich}}}{\mathrm{d}s}\right| \mathrm{d}s\,. \tag{5.39}$$

This allows for a continuous damage accumulation within the deformation process with the following evolution equation

$$\frac{\mathrm{d}\Xi_t^{\mathrm{acc}}}{\mathrm{d}t} = \left|\frac{\mathrm{d}\Psi_{\mathrm{ich}}}{\mathrm{d}t}\right|. \tag{5.40}$$

The propagation and accumulation of the damage variable was defined

$$\mathrm{D} = \mathrm{D}_{\max}\left\{1 - \left(1 - \frac{\Xi_t^{\mathrm{acc}}}{\Xi_{\max}^{\mathrm{acc}}}\right)^{1/\mathrm{C}}\right\}, \tag{5.41}$$

which is a modification of the nonlinear cumulative expression of Lemaitre and Plumtree[36].

The parameters of this evolution are the maximum equivalent strain $\Xi_{\max}^{\mathrm{acc}}$, the exponent C and a weighting parameter $\mathrm{D}_{\max}$ $(0 < \mathrm{D}_{\max} \leq 1)$, while $\Xi_{\max}^{\mathrm{acc}}$ controls the speed and C the shape of this evolution, as illustrated in Figure 5.2a and b.

The criteria for the evolution can be defined as

$$\dot{\Xi}_t^{\mathrm{acc}} = \begin{cases} \dot{\Psi}_{\mathrm{ich}}, & \dot{\Psi}_{\mathrm{ich}} \geq 0\,, \\ 0, & \dot{\Psi}_{\mathrm{ich}} < 0\,. \end{cases} \tag{5.42}$$

Permanent deformation

To define the evolution of the permanent deformation, we adapted the concept proposed by Göktepe et al.[18] of a strain-driven evolution law, such as

$$\dot{\lambda}_{\mathrm{p}} = \mathrm{k}_{\mathrm{p}}(\mathrm{D})\phi_{\mathrm{p}}(\lambda_{\mathrm{e}})\,. \tag{5.43}$$

It is based on a weighting function, which in our case will be function of the continuous damage variable, D, such as:

$$\mathrm{k}_{\mathrm{p}} = (\xi_0 + \xi\mathrm{D})^{\gamma}\,. \tag{5.44}$$

The material parameters of the permanent deformation evolution are ξ_0, ξ and γ. The parameter ξ_0 (> 0) represents the starting point or minimum value of this weighting function, which translates into the starting point of the permanent deformation rate. The parameter ξ controls the speed of permanent deformation rate, while γ controls the shape of this evolution. The influence of the parameters is illustrated in Figure 5.2c, d and e.

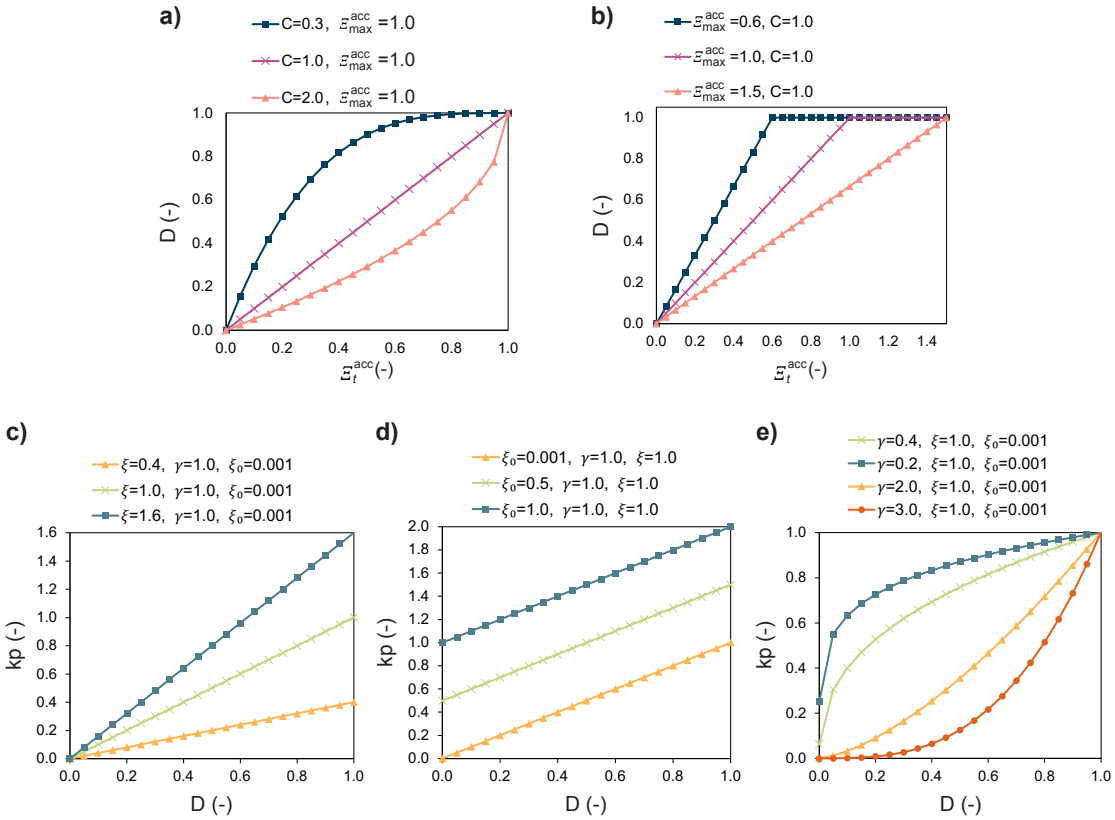

Figure 5.2 - (a-b) Damage evolution, eq. (5.41), as function of the material parameters Ξ_{max}^{acc} and C. Damage evolves linearly or nonlinearly, depending on C, until it reaches the maximum value of 1, which can occur faster or slower depending on Ξ_{max}^{acc}. **(c-e)** Permanent deformation weighting function (5.44) depends on the material parameters ξ_0, ξ and γ. Depending on ξ, the permanent deformation rate increases faster or slower with the damage variable, and linearly or nonlinearly, depending on γ.

Although the permanent deformation depends on the accumulated damage, we decided to include a second stretch-based criterion: $\phi_p = \lambda_e - \lambda_{crit}$[18] so that the permanent deformation is only activated if a critical stretch λ_{crit}, is achieved. This allows for a better control of the permanent deformation. Thus, we have the following criteria of this evolution

$$\dot{\lambda}_p = \begin{cases} k_p \phi_p, & \phi_p \geq 0 \cap D > 0 \cap \dot{\Psi}_{ich} \geq 0\,, \\ 0, & \phi_p < 0 \cap D = 0 \cap \dot{\Psi}_{ich} < 0\,. \end{cases} \tag{5.45}$$

This ensures that the permanent deformation only evolves if the damage is accumulating ($\dot{\Psi}_{ich} \geq 0$), if the elastic stretch is higher than a given critical stretch, $\phi_p \geq 0$, and finally if there is damage accumulated, $D > 0$.

5.2.4. Iterative scheme

To solve the permanent deformation evolution equation, we can take the following expression from the finite difference approximation, i.e.

$$\dot{\lambda}_{\mathrm{p}} = \frac{\lambda_{\mathrm{p}}^{n+1} - \lambda_{\mathrm{p}}^{n}}{\Delta t}\,, \qquad \Delta t = t_{n+1} - t_{n}\,, \tag{5.46}$$

which allows us to obtain the expression of the Euler Backward implicit scheme, such as:

$$\lambda_{\mathrm{p}}^{n+1} = \lambda_{\mathrm{p}}^{n} + \Delta t\dot{\lambda}_{\mathrm{p}} = \lambda_{\mathrm{p}}^{n} + \Delta t\mathrm{k}_{\mathrm{p}}\phi_{\mathrm{p}}\,. \tag{5.47}$$

To solve eq. (5.47), we can apply the Newton-Raphson method, introducing the residual R in the form

$$\mathrm{R} = \lambda_{\mathrm{p}}^{n+1} - \lambda_{\mathrm{p}}^{n} - \Delta t\mathrm{k}_{\mathrm{p}}\phi_{\mathrm{p}} = 0\,. \tag{5.48}$$

Differentiating R in respect to $\lambda_{\mathrm{p}}^{n+1}$ gives us the tangent moduli K, which takes on the form (see Appendix F for more details)

$$\mathrm{K} = \frac{\partial \mathrm{R}}{\partial \lambda_{\mathrm{p}}^{n+1}} = 1 - \Delta t\left(\frac{\partial \mathrm{k}_{\mathrm{p}}}{\partial \lambda_{\mathrm{p}}^{n+1}}\phi_{\mathrm{p}} + \frac{\partial \phi_{\mathrm{p}}}{\partial \lambda_{\mathrm{p}}^{n+1}}\mathrm{k}_{\mathrm{p}}\right). \tag{5.49}$$

Finally, we can obtain $\lambda_{\mathrm{p}}^{n+1}$ from the Newton-Raphson iterative method such as

$$\lambda_{\mathrm{p}}^{n+1}{}_{k} = \lambda_{\mathrm{p}}^{n+1}{}_{k-1} - \frac{\mathrm{R}}{\mathrm{K}}, \tag{5.50}$$

where the index k represents the current iteration. The final solution for $\lambda_{\mathrm{p}}^{n+1}$ is chosen when the residual R is less than an admissible tolerance defined by the user, which depends on each application.

The term $\frac{\partial \lambda_{\mathrm{p}}}{\partial \mathbf{C}}$, necessary for the calculation of the tangent moduli, can now be obtained as:

$$\frac{\partial \lambda_{\mathrm{p}}}{\partial \mathbf{C}} = \frac{\partial \lambda_{\mathrm{p}}}{\partial \lambda_{\mathrm{f}}}\frac{\partial \lambda_{\mathrm{f}}}{\partial \mathbf{C}} = \frac{\Delta t\mathrm{k}_{\mathrm{p}}}{\mathrm{K}\lambda_{\mathrm{p}}}\frac{1}{2\lambda_{\mathrm{f}}}\mathbf{m}_0 \otimes \mathbf{m}_0\,. \tag{5.51}$$

The algorithmic treatment for the update of the permanent deformation and damage variables is summarized in Table 5.1.

Table 5.1 - Algorithm for the damage accumulation and permanent set evolution.

Given $\mathbf{F}$, ${\lambda_p}^n$, Ψ^n, D^n
exit ← false;
it ← 0;
initialize maxit, tol (max iterations and convergence tolerance)
While it < maxit and exit ← false

$$
\begin{cases}
\text{it} \leftarrow \text{it} + 1 \\
\text{if it} = 1 \text{ then} \\
\quad \begin{cases} {\lambda_p}^k \leftarrow {\lambda_p}^n \\ \Psi^k\left({\lambda_p}^k\right), D^k(\Psi^k) \end{cases} \\
\text{else} \\
\quad \begin{cases} {\lambda_p}^k \leftarrow {\lambda_p}^{k+1} \\ D^k \leftarrow D^{k+1} \\ \Psi^k \leftarrow \Psi^{k+1} \end{cases} \\
\phi_p^k\left({\lambda_p}^k\right), \dot{\Psi}^k(\Psi^k, \Psi^n) \\
\quad \text{if } \phi_p^k \geq 0 \text{ and } D^k > 0 \text{ and } \dot{\Psi}^k > 0 \text{ then} \\
\quad \begin{cases}
k_p^k \leftarrow (\xi_0 + \xi D^k)^\gamma \\
R \leftarrow {\lambda_p}^k - {\lambda_p}^n - \Delta t k_p^k \phi_p^k \\
K \leftarrow 1 - \Delta t \left(\dfrac{\partial k_p^k}{\partial {\lambda_p}^k} \phi_p^k + \dfrac{\partial \phi_p}{\partial {\lambda_p}^k} k_p^k \right) \\
{\lambda_p}^{k+1} \leftarrow {\lambda_p}^k - \dfrac{R}{K} \\
\text{update } \mathbf{F}_p^{k+1}\left({\lambda_p}^{k+1}\right) \\
\text{update } \Psi^{k+1}\left(\mathbf{F}_p^{k+1}, \mathbf{F}\right) \\
\text{update } D^{k+1}\ (\Psi^{k+1}) \\
\quad \text{if } |R| < \text{tol then} \\
\quad \begin{cases} {\lambda_p}^{n+1} \leftarrow {\lambda_p}^{k+1} \\ D^{n+1} \leftarrow D^{k+1} \\ \text{exit} \leftarrow \text{true} \end{cases}
\end{cases} \\
\quad \text{else} \\
\quad \begin{cases} {\lambda_p}^{n+1} \leftarrow {\lambda_p}^n \\ D^{n+1} \leftarrow D^n \end{cases}
\end{cases}
$$

5.3. Numerical examples

5.3.1. Convergence analysis

To validate the constitutive model, we can apply a homogeneous deformation to a single material point and compare the numerical solution to the analytical solution. The analytical solution can be obtained by the direct derivative of the strain-energy function for an anisotropic undamaged material without permanent deformation. Using Matlab® software we were able to

successfully validate the constitutive equations implemented in our UMAT for an undamaged material without permanent deformation. To validate the damage and permanent set evolutions, a semi-analytical solution was further programmed in Matlab®. Thus, our Matlab® code included the analytical solution of the undamaged elastic stress and elasticity tensor and solved the evolution equations numerically, in the same manner as the UMAT subroutine. The Matlab® stress and elasticity tensors are semi-analytical solutions that were compared to the results given by the UMAT subroutine for a single material point and different deformation gradients. We obtained a perfect match between the Matlab® code and the UMAT subroutine, which supported the idea of a successful implementation. However, since the Matlab® solution is semi-analytical, it is still prone to implementation errors. So, as a final verification, we simulated characteristic deformation modes on a single 3-D unitary hexahedral finite element (C3D8H) using the UMAT subroutine and the software ABAQUS®. With this analysis we aimed to verify if quadratic convergence was achieved, as well as the objectivity and overall behavior of the response. The tested deformation modes were uniaxial stretch under force control, simple shear under force control, uniaxial cyclic loading under force control and uniaxial stretch under displacement control followed by a 90º rigid body rotation. Arbitrary material parameters were defined (Table 5.2) and the absolute tolerance value of the ABAQUS® Newton-Raphson scheme was changed to a smaller value (1E-16) so that more iterations were applied, and quadratic convergence could be achieved.

Table 5.2 - Arbitrary material parameters applied to verify quadratic convergence, objectivity, and overall behavior of the constitutive model.

Hyperelastic	**Damage**	**Permanent Deformation**
$C_{10} = 0.02$ MPa	$C = 1.0\ (-)$	$\lambda_{crit} = 1.0\ (-)$
$k_1 = 0.14$ MPa	$\Xi_{max}^{acc} = 3.0$ MPa	$\gamma = 1.0\ (-)$
$k_2 = 2.0\ (-)$	$D_{max} = 1.0\ (-)$	$\xi = 1.0\ s^{-1}$
		$\xi_0 = 0.3\ s^{-1}$

Figure 5.3 shows the evolution of the largest residual (normalized to the value of the first iteration of each time increment) with the iteration number (Figure 5.3a-d1) and the principal stresses as a function of the principal stretch or time (Figure 5.3a-d2) for the different deformation modes (Figure 5.3a-d). From Figure 5.3a-d1 we can see that quadratic convergence was achieved. Figure 5.3a-d2 shows the nonlinearity of the constitutive model for higher stretches and in the uniaxial cyclic tensile loading scenario (Figure 5.3c2) we can see the hysteresis and the permanent deformation from the two loading cycles. The objectivity of the constitutive model was confirmed by the uniaxial stretch followed by the 90º rotation (Figure 5.3d), since the rotation did not affect the stress tensor. Moreover, actual absolute zero residuals were reported by ABAQUS® in the rotation step. With this simple set of baseline numerical examples, we were able to validate both the behavior of the constitutive model and the numerical implementation.

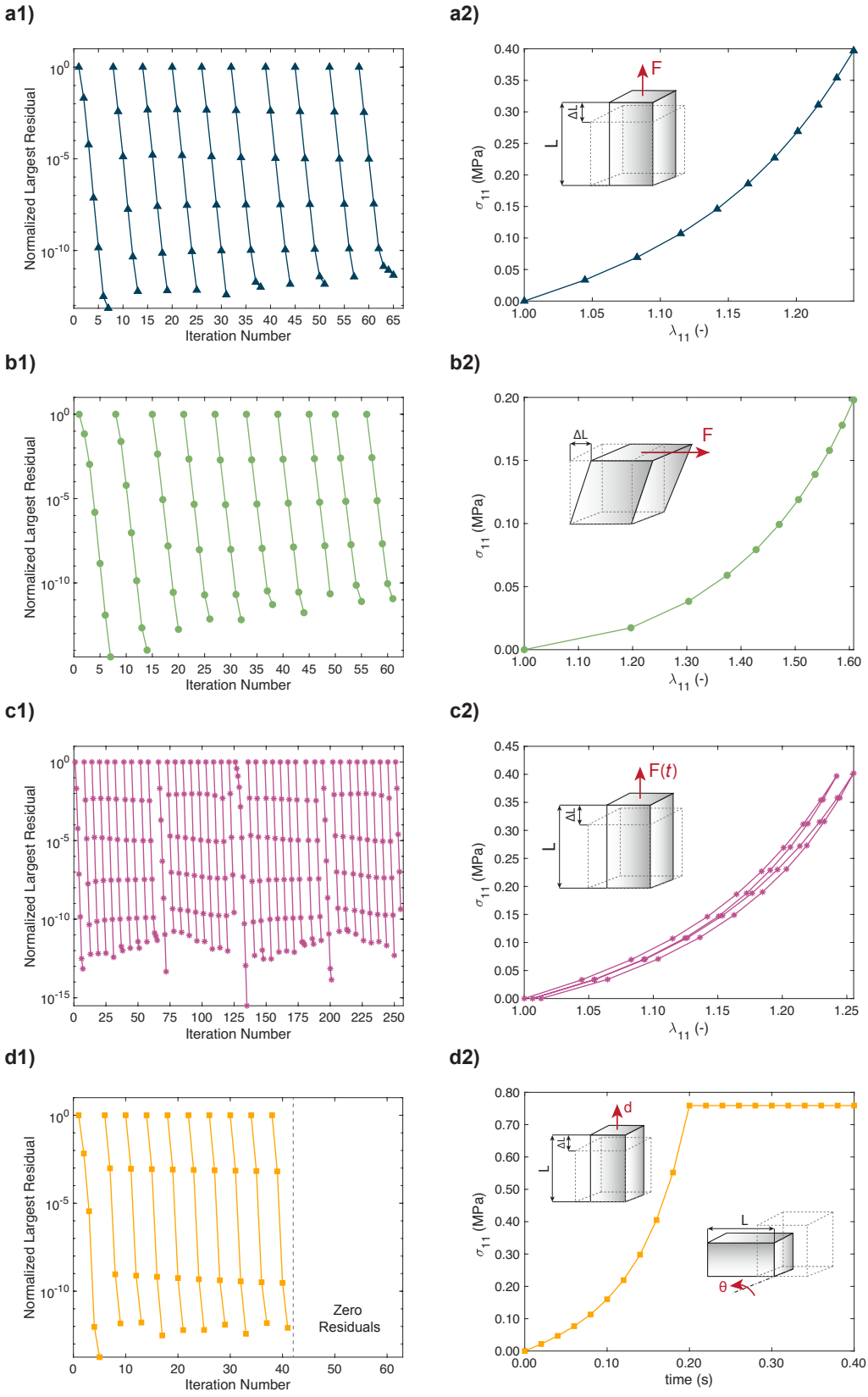

Figure 5.3 - a) Uniaxial stretch under force control, **b)** simple shear under force control, **c)** cyclic uniaxial stretch under force control, **d)** uniaxial stretch under displacement control followed by 90º rigid body rotation. **a-d1)** Evolution of the largest absolute residual of ABAQUS® Newton-Raphson iterative scheme (normalized to the maximum value of each time increment) with the iteration number. **a-c2)** Evolution of the maximum principal stretch with the principal stretch ratio. **d2)** Evolution of the maximum principal stretch with time.

5.3.2. Tensile behavior of a dog bone-shaped sample

In this numerical example we defined a dog bone-shaped sample of a hypothetical tissue to illustrate the material behavior captured with the constitutive model used in this work. The geometry and symmetry boundary conditions are illustrated in Figure 5.4. The mesh consists of 619 hexahedral (C3D8H) elements. Twenty loading cycles were defined, with each cycle consisting of applying the displacement in the direction of the material fibers to a stretch of $\lambda = 1.2$, and then unloading it to a stretch of $\lambda = 1.1$. A strain rate of $\dot{\varepsilon} = 1.0\ s^{-1}$ and a time increment of 0.05 *s* was applied. In the final cycle, after it reached the peak stretch of $\lambda = 1.2$, the specimen was released and allowed to return to the initial position without any displacement imposition. The material parameters of the hypothetical tissue are presented in Table 5.3.

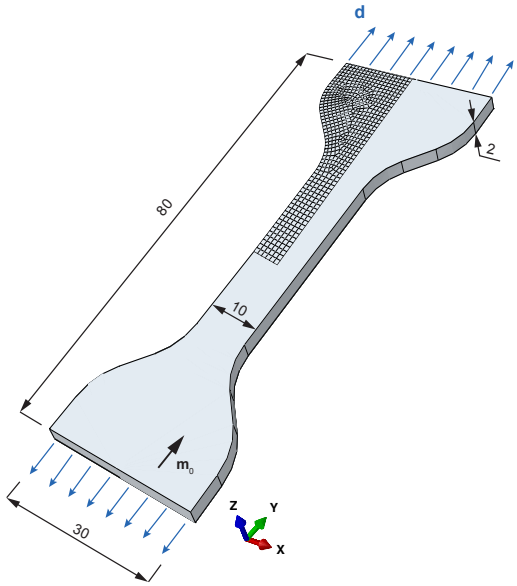

Figure 5.4 - Geometry of the dog bone sample (dimensions in mm) with a representation of the applied displacement. For the finite element simulation only 1/8 of the model was defined and meshed, considering symmetry boundary conditions. The fiber direction, $\mathbf{m}_0$, was defined as the direction of the applied displacement.

Table 5.3 - Material parameters of the hypothetical tissue applied to the dog bone sample

Hyperelastic	Damage	Permanent Deformation
$C_{10} = 1.0$ MPa	$C = 1.0\ (-)$	$\lambda_{crit} = 1.0\ (-)$
$k_1 = 0.610$ MPa	$\Xi^{acc}_{max} = 3.0$ MPa	$\gamma = 1.0\ (-)$
$k_2 = 0.560\ (-)$	$D_{max} = 1.0\ (-)$	$\xi = 1.0\ s^{-1}$
		$\xi_0 = 1E-5\ s^{-1}$

Figure 5.5a shows the profile of the applied stretch with time, with the location of the release point and the permanent deformation highlighted. Figure 5.5b shows the average result on the gauge section of the Cauchy stresses in the direction of the applied displacement as a function of the applied stretch. The hysteresis represents the energy dissipated by damage and permanent deformation, and the peak stress decrease shows the effect of damage on the mechanical

properties of the material. The overall material stiffness reduces in each cycle, despite the same displacement is applied in each cycle. Figure 5.5c shows the damage evolution with time: here we see that the damage variable is irreversible and only increases in the loading stages of the simulation.

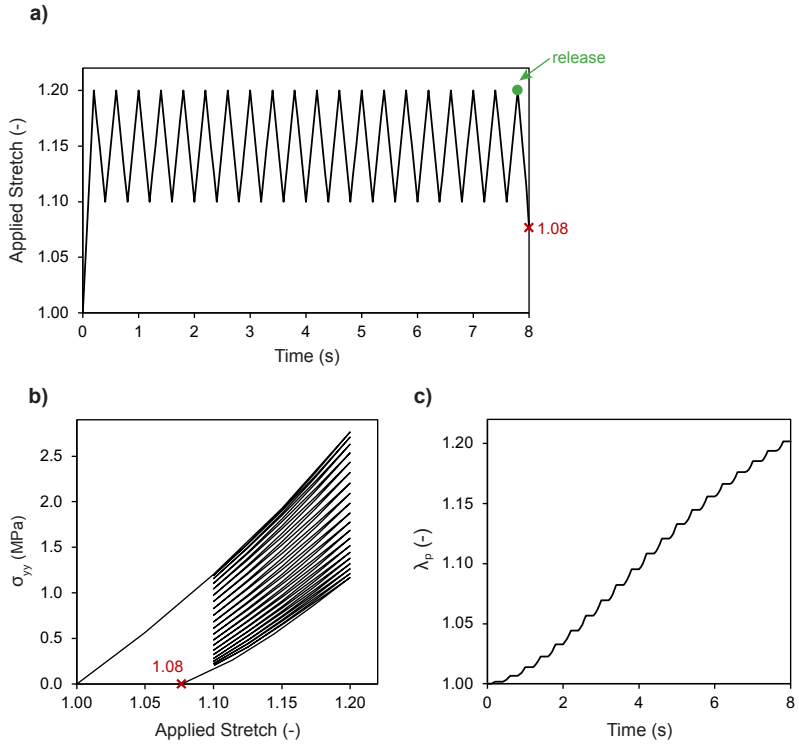

Figure 5.5 - a) Profile of the applied stretch with time. Note that the stretch was only imposed until the last cycle peak, illustrated as the release point. After that point the material was released from any applied displacement/loads and allowed to return to the unloaded state. After the simulation, the new unloaded state occurs for a stretch of 1.08, which represents the permanent deformation. **b)** Cauchy stresses in the direction of the applied displacement as a function of the stretch. The stresses are the average result of the gauge section finite elements. The energy dissipation due to the irreversible processes is visible due to the hysteresis of the curve. We can also verify the permanent deformation of 1.08 at the end of the test. **c)** Evolution of the permanent set variable with time (average result of the gauge section finite elements).

Figure 5.6a shows the fiber stretch distribution in the initial point ($\lambda_f = 1.0$) and at the end of the simulation. We can see that at the end of the simulation, the unloaded state changed, when compared with the initial stage, with a visible macroscopic permanent deformation. In Figure 5.6a we have a visual representation of the overall permanent deformation of the specimen, but we can also see that the gauge section is the most affected and the fiber residual stretches are higher in that region. Figure 5.6b and c show the distribution of the permanent deformation and the damage variables, respectively. Both variables present a similar distribution, with the gauge section uniformly affected and a small local concentration.

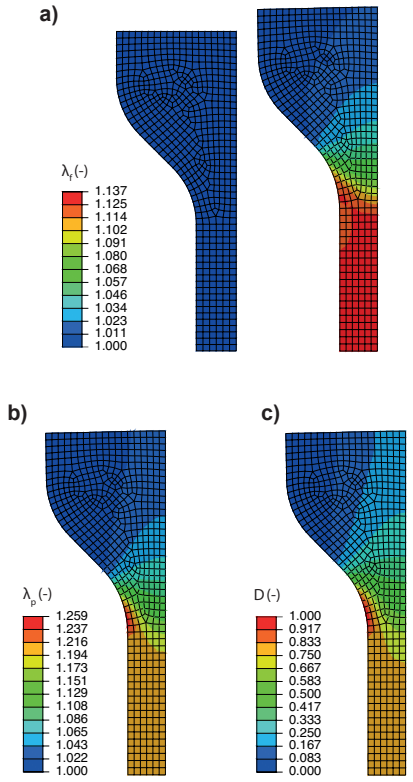

Figure 5.6 - a) Distribution of the fiber stretch λ_f at the simulation starting point and at the end, which is the new unloaded state. **b)** Permanent stretch λ_p at the end of the simulation. **c)** Damage variable at the end of the simulation.

5.3.3. Behavior of rectangular specimen under biaxial stretch

This numerical example illustrates a rectangular specimen of the same hypothetical tissue applied in example 5.3.2 (Table 5.3) under biaxial stretch. The mesh consists of 800 hexahedral (C3D8H) elements. Twenty loading cycles were defined and in each cycle the specimen is stretched in both directions to a stretch of $\lambda = 1.2$ and then unloaded to $\lambda = 1.1$. Two scenarios were analyzed: a) fibers vertically aligned (Figure 5.7a) and b) fibers oriented 45º in the x-y plane (Figure 5.7b). A strain rate of $\dot{\varepsilon} = 1.0\ s^{-1}$ and a time increment of 0.05 s was applied. In the final cycle, after it reached the peak stretch of $\lambda = 1.2$, the specimen was released and allowed to return to the initial position without any displacement imposition.

Figure 5.8a1 and a2 shows the Cauchy stresses in the x and y direction, respectively, for the scenario of the fibers vertically aligned. In this situation, there is only permanent deformation in the fiber direction, which causes the hysteresis and stress softening seen in Figure 5.8a2 and the overall permanent stretch of 1.10 in the y-direction (obtained at the end of the simulation, after releasing the loads). In the x direction there is no permanent deformation, and the stresses behave hyperelastically, without energy dissipation until the unloading stage. At this point, after releasing the loads, the specimen contracts in the x-direction since we are enforcing incompressibility and the permanent deformation is acting in the y-direction.

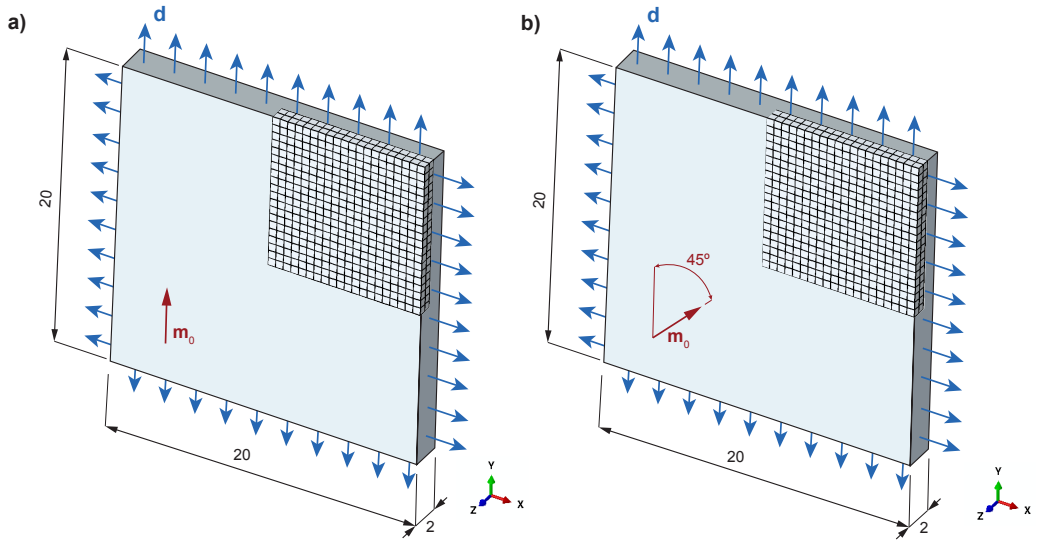

Figure 5.7- Geometry of the rectangular specimen (dimensions in mm) with a representation of the biaxial applied displacement. For the finite element simulation only 1/8 of the model was defined and meshed, considering symmetry boundary conditions. **a)** The fiber direction, $\mathbf{m}_0$, was defined in the vertical direction. **b)** fiber direction oriented with an angle of 45º in the x-y plane.

Figure 5.8b1 and b2 shows the Cauchy stresses in the x and y direction, respectively, for the scenario of the fibers oriented 45º in the x-y plane. In this situation, we can see that the same behavior in the x and y direction is obtained, with a permanent deformation of 1.03 captured in both directions at the end of the simulation, after the releasing of the loads. Since we have permanent deformation in both directions, we also obtained the stress softening and energy dissipation associated with this phenomenon in both the x and y directions. The Cauchy stresses shown in Figure 5.8 are the average within all finite elements. Figure 5.8a3 and b3 shows the average permanent deformation variable λ_p (in all finite elements) with time. We can see that a higher value is obtained when the fibers are oriented 45º in the x-y plane since we are allowing permanent deformation in both directions.

Figure 5.9b and c shows the distribution of the permanent deformation variable at the end of the simulation, in the new unloaded state. Figure 5.9a shows the unloaded specimen in the initial position, for an easier comparison. We can see that when the fibers are vertically aligned (Figure 5.9b), the new unloaded state captures the permanent deformation along fiber direction, with a homogeneous permanent deformation. When the fibers are oriented 45º in the x-y plane (Figure 5.9c), there is permanent deformation in both directions, which causes the specimen to become distorted in its new unloaded state.

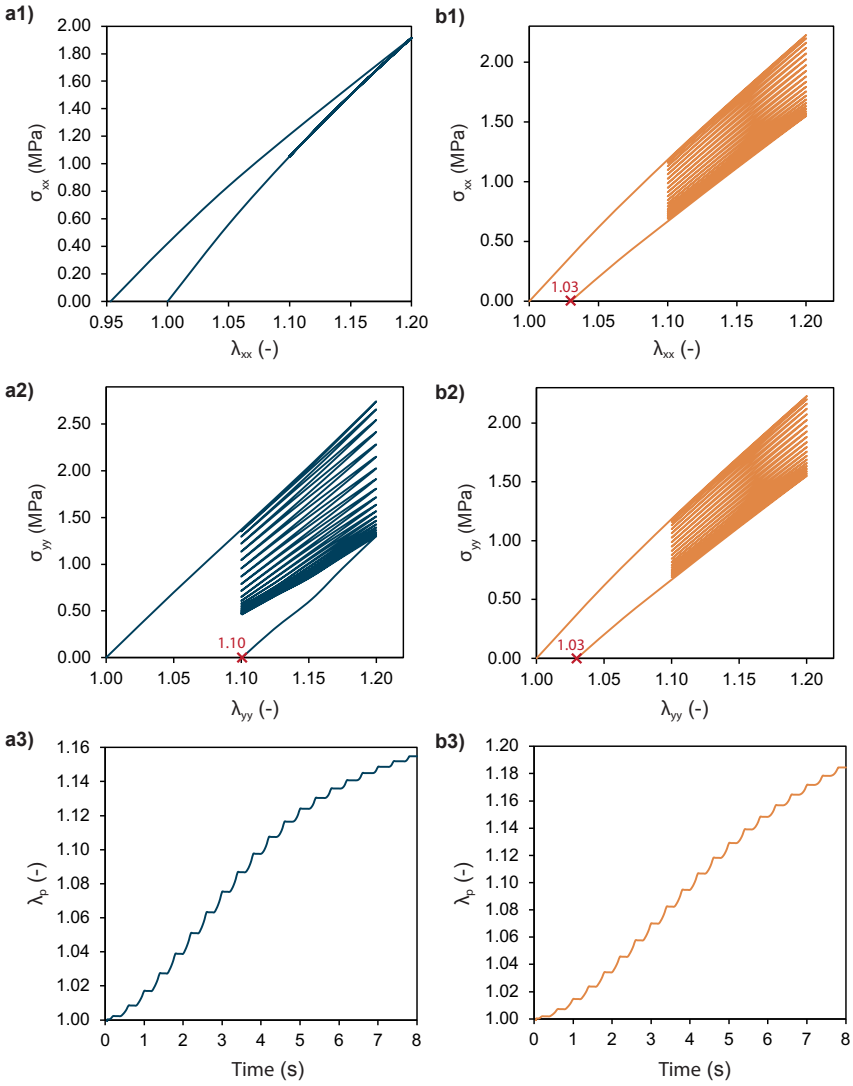

Figure 5.8- a) Results for the rectangular specimen with the fibers aligned vertically **b)** results for the rectangular specimen with the fibers oriented 45º in the x-y plane. Note that the stretch was only imposed until the last peak cycle. After that point the material was released from any applied displacement and allowed to return to the new unloaded state. **1)** Cauchy stresses in the x direction $\boldsymbol{\sigma}_{xx}$, as a function of the stretch in the same direction, λ_{xx}. **2)** Cauchy stresses in the y direction $\boldsymbol{\sigma}_{yy}$, as a function of the stretch in the same direction λ_{yy}. The stresses are the average within all finite elements. The stretches in **b1)** and **b2)** are the average of the top and side nodes, respectively, since in the final unloading stage the specimen becomes distorted due to permanent deformation (see Figure 5.9c). **3)** evolution of the permanent set variable λ_p with time (average result of all finite elements).

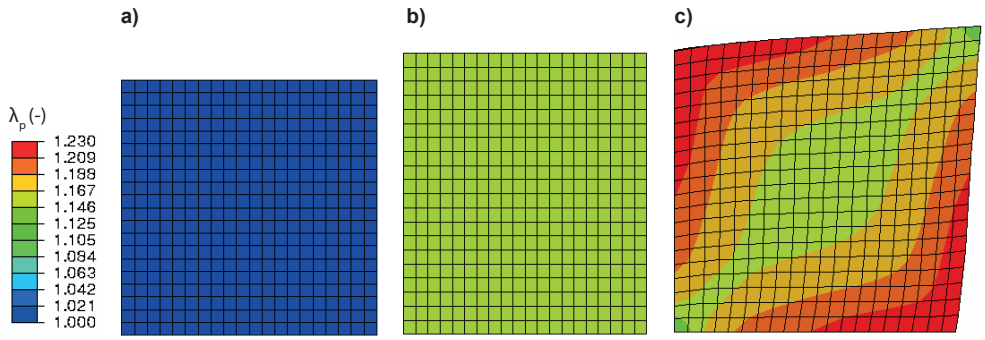

Figure 5.9- a) Non-deformed rectangular specimen. **b)** permanent stretch distribution at the end of the simulation with the fibers vertically aligned. **c)** permanent stretch distribution at the end of the simulation with the fibers oriented 45º in the x-y plane.

5.3.4. Permanent deformation of the pelvic floor muscles after vaginal delivery

This numerical example demonstrates the feasibility of our model in a complex 3-D simulation of the second stage of labor, while providing some preliminary results. The accomplishment of full cervical dilation marks the beginning of the second stage of labor, which ends with the delivery of the fetus.

This biomechanical model incorporates 3-D finite element models of the pelvic floor muscles and the fetal head, which is the largest part of the fetus and consequently the structure that typically can cause damage to the muscles. It also incorporates a rigid surface that acts as the pubic bone and limits the anterior region. Regarding the boundary conditions, the perimeter of the pelvic floor muscles and the 'pubic bone' surface were fixed. Figure 5.10 shows the finite element model of the pelvic floor muscles (20,804 hexahedral elements C3D8H) and the fetal head (19,520 tetrahedral elements C3D4) in the initial position, with the rigid surface rendered semi-transparent for visualization purposes. All the displacements of the fetal head were left free, and the fetal descent was defined by the superposed uterine and maternal forces applied to a reference node. Head flexion was applied to the same reference node so that approximately the smallest head diameter was presented in the birth canal at all instants. The remaining rotations of the fetal head were fixed. To improve numerical convergence, we applied the ABAQUS® automatic stabilization mechanism with a stabilization factor of 0.001. This allows for the stabilization of unstable nonlinear problems through the automatic addition of volume-proportional damping to the model. For further details see ABAQUS® documentation[9].

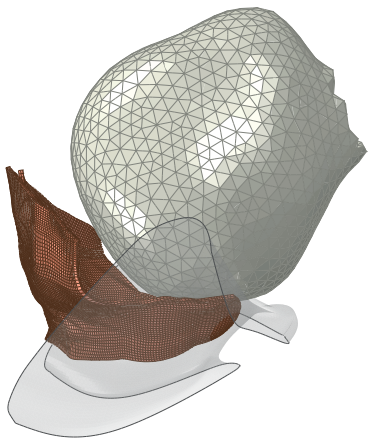

Figure 5.10 - Finite element model of the second stage of labor, which includes the pelvic floor muscles in red (C3D8H elements), the fetal head in grey (C3D4 elements) and a rigid surface for the anterior region constraint.

The expulsion of the fetus is achieved by the superposition of pressure from the uterine contraction and the maternal pushes [6]. The uterine contraction reaches an average pressure of 8.5 kPa at its peak, while the maternal push adds an average of 10.5 kPa[3,32]. These combined pressures result in a peak force of ~175 N on the fetal head, when calculated from its cross-sectional area.

There are different ways to coach labor in terms of how and when the volitional maternal pushes are performed, and these results in different loading conditions. However, the most common and popularized one is the 'directed pushing' management of labor. In this method, the mother is coached by the doctor or midwife to inhale deeply and push for a duration of ~10 seconds, 2-3 times per uterine contraction[30]. Each maternal push resembles the Valsalva maneuver, so we designated this loading profile as the 'Valsalva-push' pattern. This pushing pattern was applied to our simulation by defining a 90 s uterine contraction accompanied by three 10 s maternal pushes, as illustrated in Figure 5.11. A resting interval of 60 seconds was also applied between contractions. For more details regarding the simulation and the finite element models the reader is referred to Vila Pouca et al.[47].

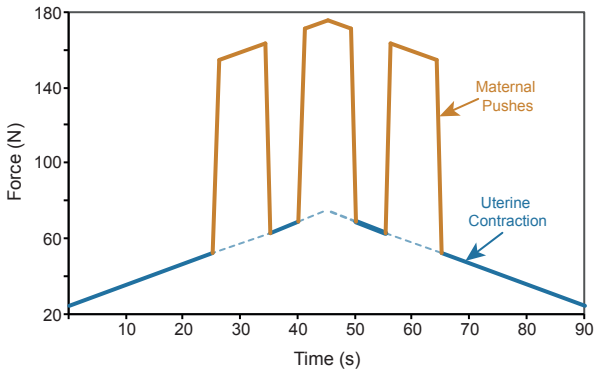

Figure 5.11 - Expulsive force placed on the fetal head during the simulated Valsalva directed maternal pushes superposed upon each 90 s uterine contraction.

The material model developed in this work was applied to the pelvic floor muscles, but with the addition of viscoelasticity. We decided to include viscoelasticity in this example since the pelvic floor muscles are highly viscoelastic and ignoring this feature while defining the material parameters could result in an overestimation of the permanent deformation (since viscoelasticity typically causes stress softening in the initial loading cycles before reaching equilibrium). This feature was added following the Generalized Maxwell Model, which is well described in the works of Holzapfel et al.[23,46]. In short, non-equilibrium stresses $\mathbf{Q}_\alpha$ governed by evolution equations, are calculated from the numerical solution of convolution integrals and added to the overall stresses. The parameter $\alpha = 1, \ldots, m$ is the number of viscoelastic processes. These non-equilibrium stresses define the way the viscoelastic process evolves, and each process can be represented by a spring in series with a dashpot. The material parameters are the number of viscoelastic processes α, the mechanical properties of the springs or free-energy parameters β_α, and the properties of the dashpots or relaxation times τ_α. The evolution equations can be defined as

$$\dot{\mathbf{Q}}_\alpha + \frac{\mathbf{Q}_\alpha}{\tau_\alpha} = \beta_\alpha \dot{\mathbf{S}}_{\text{ich}} \,, \tag{5.52}$$

where $\dot{\mathbf{S}}_{\text{ich}}$ is the rate of the stress tensor defined in eq. (5.23).

The material parameters were calibrated using ovine pelvic floor low-cycle fatigue experimental data [49] by applying a micro-genetic algorithm. The experiment consisted in the application of 60 sub-maximal loading cycles under displacement control. The resulting material parameters are shown in Table 5.4, while Figure 5.12 compares the stress-time data of the experimental data with the numerical results.

Table 5.4 - Material parameters of the pelvic floor muscles, calibrated from ovine experimental data [49].

Hyperelastic	**Damage**	**Permanent Deformation**	**Viscoelastic**
$C_{10} = 0.19$ MPa	$C = 1.00\ (-)$	$\lambda_{\text{crit}} = 1.00\ (-)$	$\alpha = 2\ (-)$
$k_1 = 0.17$ MPa	$\Xi_{\text{max}}^{\text{acc}} = 6.20$ MPa	$\gamma = 1.50\ (-)$	$\beta_1 = 3.67\ (-)$
$k_2 = 0.28\ (-)$	$D_{\text{max}} = 1.00\ (-)$	$\xi = 0.005\ \text{s}^{-1}$	$\tau_1 = 10.13$ s
		$\xi_0 = 0.01\ \text{s}^{-1}$	$\beta_2 = 0.58\ (-)$
			$\tau_2 = 5.66$ s

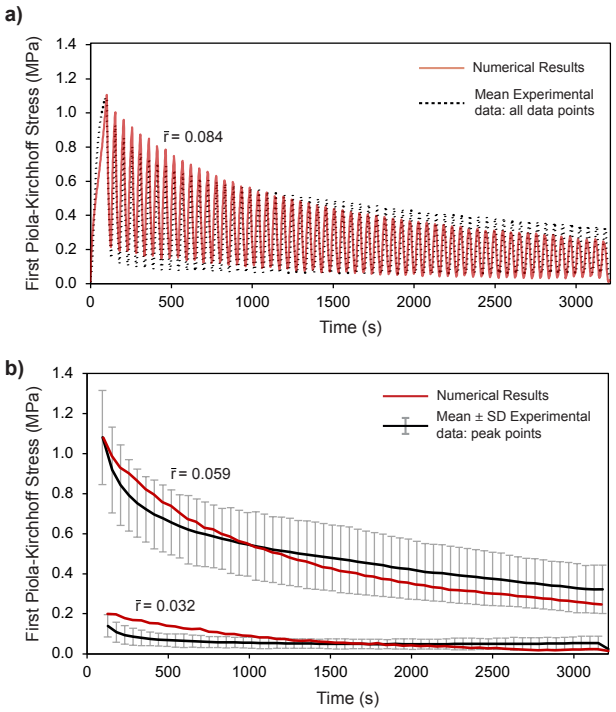

Figure 5.12 - Calibration of the constitutive material parameters for the averaged response of the fatigue tests from Vila Pouca et al[49]. **a)** Comparison of the numerical and experimental data for all 3212 data points. **b)** Comparison of the numerical and experimental data (mean ± SD) for the maximum and minimum peak points. SD: standard deviation; r̄: absolute error mean

After total fetal head expulsion, which occurred during the 5th contraction, the pelvic muscles were allowed to recover and permanent deformation was evaluated. Figure 5.13a shows the stretch of the hiatal length (defined as Level 1 in Figure 5.13c) throughout the simulation. The stretch values during the fetal head descent are consistent with a previous numerical study[39]. We can see that the maternal pushes cause these stretch controlled repetitive loading cycles, with 3

stretch peaks per contraction. The fetal head retracts during the resting stage, causing stretch to decrease. After complete fetal head expulsion and recovery, the overall permanent deformation stretch of Level 1 was 1.03. Figure 5.13b shows the permanent deformation variable λ_p throughout the simulation for the critical node (point of maximum λ_p). Figure 5.13c shows the distribution of λ_p in the complete pelvic muscles and identifies the critical node location and the hiatal length (Level 1) used to evaluate the stretch of Figure 5.13a. We can see that the critical node is located near the right lateral origin of the pubovisceral muscle, indicating that this is the location of higher microstructure disruption and consequently the most likely location for failure initiation. Nevertheless, the value of the permanent deformation variable λ_p of the muscle near the hiatus, opposed to the pubovisceral attachments are considerable, ranging between 1.07 and 1.15. The increase in hiatal area was also measured using ImageJ. Three measurements of the initial and final hiatal area were performed under the same conditions to minimize measurement errors. The average of these measurements was considered to calculate the increase in hiatal area, which in these conditions was 8%.

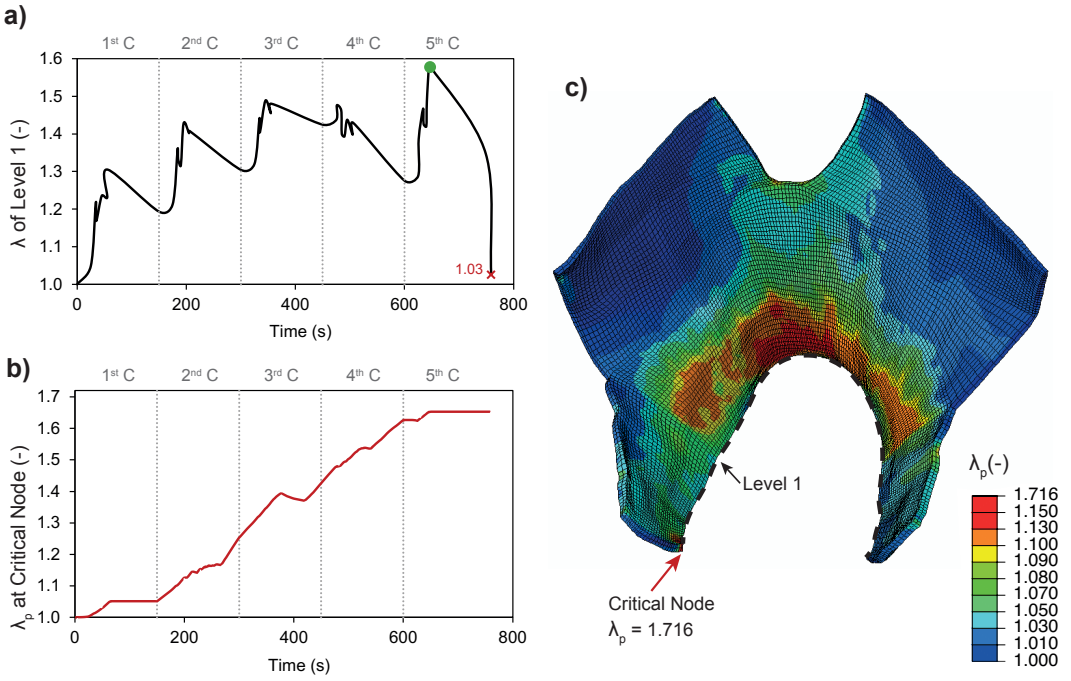

Figure 5.13 - a) Evolution of the hiatal length (Level 1) stretch value. The green dot indicates the point of complete fetal head expulsion. Following recovery, there is a permanent stretch of 1.03. **b)** Evolution of the permanent deformation variable λ_p at the critical node. Each contraction is identified by the grey dotted lines. **c)** Distribution of the permanent deformation variable λ_p on the pelvic floor muscles after the fetal head expulsion. The critical node location, and the peak nodal permanent deformation and Level 1 are identified.

5.4. Discussion

This work provides a numerical framework to incorporate permanent deformation as a direct consequence of low-cycle fatigue and microdamage accumulation resulting from two to several hundred loading cycles. In this regime, the damage can start to grow during the first cycle or just after, and it is associated with large permanent strains, which should not be neglected. The proposed evolution equations for the permanent deformation and damage variables are versatile, allowing linear or nonlinear evolutions depending on the shape parameters. From the first numerical examples, quadratic convergence and objectivity were verified, and the model proved able to predict the permanent deformation of a typical dog-bone shaped specimen as well as a rectangular specimen under biaxial loading. In the final example, the constitutive model was tested on the complex simulation of a vaginal delivery. The resulting stretch values of the hiatal length agree with published quantitative results, as well as the critical location, which has been extensively described to be near the origin of the pubovisceral muscle. The novelty of this work lies in the capability of simulating the increase in hiatal area after the vaginal delivery, which we believe has never been simulated before.

Nevertheless, there are limitations in this study. Since we have two versatile evolution equations, care is needed when calibrating the material parameters. To achieve more meaningful results, robust experimental data are needed so that appropriate linear/nonlinear relationship between the microdamage accumulation and the permanent deformation is chosen. Moreover, the present analysis is phenomenological and did not consider the spread of the fatigue damage to the fiber or macro scale under repetitive sub-maximal loading (see section 5.1). The constitutive model is also subject to mesh dependence and adding non-local averaging could mitigate this effect, although no localization phenomena were noted in any of our examples

In the context of the vaginal delivery, our results must be taken with care since the calibration was performed using non-pregnant female sheep experimental data and the average experimental stress-time curve. The present study points out the need for better measurements of the microdamage accumulation and permanent deformation at multiple length scales in pregnant pelvic floor tissues *in vivo.* The key tissues include the pubovisceral muscle and its connective tissue apophysis at its origin from the pubic bone, as well as the perineal membrane, not represented in this model, because tearing of this important passive collagenous structure is associated with increased hiatal size (for example [41]).

Nevertheless, we believe this work opens new possibilities to analyze low cycle fatigue-induced permanent deformation in soft tissues. In the context of childbirth, when appropriately calibrated, it will be an important tool to analyze the several obstetrical factors that can impact the evolution of permanent deformation and consequentially, the development of pelvic organ prolapse.

5.5. Conclusions

(1) The proposed methods make it possible to simulate low cycle fatigue-induced permanent deformation in soft tissues.

(2) The results suggest that low cycle-fatigue-induced permanent deformation in the pubovisceral muscle is a plausible mechanism that may underlie the widely recognized post-partum increase in hiatal length (and area) observed clinically.

(3) The study points out the pressing need for data on low cycle fatigue-induced damage in soft tissues *in vivo*, whether in muscle or its serial connective tissues, or in specialized passive connective tissue structures like the perineal membrane.

Acknowledgements

Authors acknowledge the support from the Portuguese Foundation of Science under grant SFRH/BD/136213/2018 and under the research project UIDB/50022/2020. The funding sources were not involved in preparing the manuscript and conducting the research.

References

1. Araujo AE, Delgado A, Maia JN, et al. Efficacy of spontaneous pushing with pursed lips breathing compared with directed pushing in maternal and neonatal outcomes : a clinical trial. *Authorea*. Published online 2020:1-11. doi:10.22541/au.160278519.95490262/v1

2. Ashton-Miller JA, DeLancey JOL. Functional anatomy of the female pelvic floor. *Ann N Y Acad Sci*. 2007;1101:266-296. doi:10.1196/annals.1389.034

3. Ashton-Miller JA, DeLancey JOL. On the biomechanics of vaginal birth and common sequelae. *Annu Rev Biomed Eng*. 2009;11(1):163-176. doi:10.1146/annurev-bioeng-061008-124823.On

4. Bilby BA, Lardner LRT, Stroh AN. Continuous distributions of dislocations and the theory of plasticity. *Actes du IXe congrès Int mécanique appliquée*. 1957;8:35-44.

5. Calvo B, Peña E, Martinez MA, Doblaré M. An uncoupled directional damage model for fibred biological soft tissues. Formulation and computational aspects. *Int J Numer Methods Eng*. 2007;69(10):2036-2057. doi:https://doi.org/10.1002/nme.1825

6. Casanova R, And AC, Goepfert AR, Hueppchen NA, Weiss PM, American College of Obstetricians and Gynecologists. *Beckmann and Ling's Obstetrics and Gynecology*. 8th Editio. Philadelphia : Wolters Kluwer; 2019.

7. Caudwell-Hall J, Kamisan Atan I, Martin A, et al. Intrapartum predictors of maternal levator ani injury. *Acta Obstet Gynecol Scand*. 2017;96(4):426-431. doi:https://doi.org/10.1111/aogs.13103

8. Chen J, Kim J, Shao W, et al. An anterior cruciate ligament failure mechanism. *Am J Sports Med*. 2019;47(9):2067-2076. doi:10.1177/0363546519854450

9. Dassault Systemes Simulia Corporation. Abaqus V. 6.14 documentation.

10. DeLancey JOL. What's new in the functional anatomy of pelvic organ prolapse? *Curr Opin Obstet Gynecol*. 2016;28(5):420-429. doi:10.1097/GCO.0000000000000312

11. Diani J, Brieu M, Vacherand JM. A damage directional constitutive model for Mullins effect with permanent set and induced anisotropy. *Eur J Mech - A/Solids*. 2006;25(3):483-496. doi:https://doi.org/10.1016/j.euromechsol.2005.09.011

12. Dong H, Liu M, Martin C, Sun W. A residual stiffness-based model for the fatigue damage of biological soft tissues. *J Mech Phys Solids*. 2020;143:104074. doi:https://doi.org/10.1016/j.jmps.2020.104074

13. Falkert A, Endress E, Weigl M, Seelbach-Göbel B. Three-dimensional ultrasound of the pelvic floor 2 days after first delivery: Influence of constitutional and obstetric factors. *Ultrasound Obstet Gynecol*. 2010;35(5):583-588. doi:10.1002/uog.7563

14. Ferreira JPS, Parente MPL, Jabareen M, Jorge RMN. A general framework for the

numerical implementation of anisotropic hyperelastic material models including non-local damage. *Biomech Model Mechanobiol*. 2017;16(4):1119-1140. doi:10.1007/s10237-017-0875-9

15. Fung Y. *Biomechanics: Mechanical Properties of Living Tissues*. Second Edi. Springer Science & Business Media; 1993.

16. Gasser TC, Holzapfel GA. A rate-independent elastoplastic constitutive model for biological fiber-reinforced composites at finite strains: continuum basis, algorithmic formulation and finite element implementation. *Comput Mech*. 2002;29(4):340-360. doi:10.1007/s00466-002-0347-6

17. Van Geelen H, Ostergard D, Sand P. A review of the impact of pregnancy and childbirth on pelvic floor function as assessed by objective measurement techniques. *Int Urogynecol J*. 2018;29(3):327-338. doi:10.1007/s00192-017-3540-z

18. Göktepe S, Abilez OJ, Kuhl E. A generic approach towards finite growth with examples of athlete's heart, cardiac dilation, and cardiac wall thickening. *J Mech Phys Solids*. 2010;58(10):1661-1680. doi:https://doi.org/10.1016/j.jmps.2010.07.003

19. Göktepe S, Abilez OJ, Parker KK, Kuhl E. A multiscale model for eccentric and concentric cardiac growth through sarcomerogenesis. *J Theor Biol*. 2010;265(3):433-442. doi:https://doi.org/10.1016/j.jtbi.2010.04.023

20. Hanson L. Second-stage labor care: challenges in spontaneous bearing down. *J Perinat Neonatal Nurs*. 2009;23(1):31. doi:10.1097/JPN.0b013e318196526b

21. Holzapfel GA. *Nonlinear Solid Mechanics: A Continuum Approach for Engineering*. John Wiley & Sons; 2000.

22. Holzapfel GA, Fereidoonnezhad B. Chapter 5 - Modeling of Damage in Soft Biological Tissues. In: Payan Y, Ohayon JBT-B of LO, eds. *Translational Epigenetics*. Vol 1. Academic Press; 2017:101-123. doi:https://doi.org/10.1016/B978-0-12-804009-6.00005-5

23. Holzapfel GA, Gasser TC. A viscoelastic model for fiber-reinforced composites at finite strains: Continuum basis, computational aspects and applications. *Comput Methods Appl Mech Eng*. 2001;190(34):4379-4403. doi:https://doi.org/10.1016/S0045-7825(00)00323-6

24. Holzapfel GA, Gasser TC, Ogden RW. A new constitutive framework for arterial wall mechanics and a comparative study of material models. *J Elast Phys Sci solids*. 2000;61(1):1-48. doi:10.1023/A:1010835316564

25. Holzapfel GA, Ogden RW, Sherifova S. On fibre dispersion modelling of soft biological tissues: a review. *Proc R Soc A Math Phys Eng Sci*. 2019;475(2224):20180736. doi:10.1098/rspa.2018.0736

26. Kamisan Atan I, Gerges B, Shek KL, Dietz HP. The association between vaginal parity

and hiatal dimensions: A retrospective observational study in a tertiary urogynaecological centre. *BJOG An Int J Obstet Gynaecol*. 2015;122(6):867-872. doi:10.1111/1471-0528.12920

27. Kuhl E, Garikipati K, Arruda EM, Grosh K. Remodeling of biological tissue: Mechanically induced reorientation of a transversely isotropic chain network. *J Mech Phys Solids*. 2005;53(7):1552-1573. doi:https://doi.org/10.1016/j.jmps.2005.03.002

28. Laganà AS, La Rosa VL, Rapisarda AMC, Vitale SG. Pelvic organ prolapse: the impact on quality of life and psychological well-being. *J Psychosom Obstet Gynecol*. 2018;39(2):164-166. doi:10.1080/0167482X.2017.1294155

29. Lee EH, Liu DT. Finite-Strain Elastic—Plastic Theory with Application to Plane-Wave Analysis. *J Appl Phys*. 1967;38(1):19-27. doi:10.1063/1.1708953

30. Lee N, Gao Y, Lotz L, Kildea S. Maternal and neonatal outcomes from a comparison of spontaneous and directed pushing in second stage. *Women and Birth*. 2019;32(4):e433-e440. doi:https://doi.org/10.1016/j.wombi.2018.10.005

31. Leveno KJ, Nelson DB, McIntire DD. Second-stage labor: how long is too long? *Am J Obstet Gynecol*. 2016;214(4):484-489. doi:https://doi.org/10.1016/j.ajog.2015.10.926

32. Lien K-C, DeLancey JOL, Ashton-Miller JA. Biomechanical analyses of the efficacy of patterns of maternal effort on second-stage progress. *Obstet Gynecol*. 2009;113(4):873-880. doi:10.1097/AOG.0b013e31819c82e1

33. Lipps DB, Wojtys EM, Ashton-Miller JA. Anterior cruciate ligament fatigue failures in knees subjected to repeated simulated pivot landings. *Am J Sports Med*. 2013;41(5):1058-1066. doi:10.1177/0363546513477836

34. Liu F, Xu L, Ying T, Tao J, Hu B. Three-dimensional ultrasound appearance of pelvic floor in nulliparous women and postpartum women one week after their first delivery. *Int J Med Sci*. 2014;11(3):234-239. doi:10.7150/ijms.7384

35. Martin C, Sun W. Modeling of long-term fatigue damage of soft tissue with stress softening and permanent set effects. *Biomech Model Mechanobiol*. 2013;12(4):645-655. doi:10.1007/s10237-012-0431-6

36. Milella PP. *Fatigue and Corrosion in Metals*. 1st ed. (Milella PP, ed.). Springer-Verlag Mailand; 2013. doi:10.1007/978-88-470-2336-9

37. Miller JM, Low LK, Zielinski R, Smith AR, Delancey JOL, Brandon C. Evaluating maternal recovery from labor and delivery: Bone and levator ani injuries. *Am J Obstet Gynecol*. 2015;213(2):188.e1-188.e11. doi:10.1016/j.ajog.2015.05.001

38. Mullins L. Softening of rubber by deformation. *Rubber Chem Technol*. 1969;42(1):339-362. doi:10.5254/1.3539210

39. Parente MPL, Jorge RMN, Mascarenhas T, Fernandes AA, Martins JAC. Deformation of the pelvic floor muscles during a vaginal delivery. *Int Urogynecol J Pelvic Floor Dysfunct*.

2008;19(1):65-71. doi:10.1007/s00192-007-0388-7

40. Peña E. Computational aspects of the numerical modelling of softening, damage and permanent set in soft biological tissues. *Comput Struct*. 2014;130:57-72. doi:https://doi.org/10.1016/j.compstruc.2013.10.002

41. Pipitone F, Swenson CW, DeLancey JOL, Chen L. Novel 3D MRI technique to measure perineal membrane structural changes with pregnancy and childbirth: Technique development and measurement feasibility. *Int Urogynecol J*. 2021;32(9):2413-2420. doi:10.1007/s00192-021-04795-x

42. Rebouah M, Chagnon G. Permanent set and stress-softening constitutive equation applied to rubber-like materials and soft tissues. *Acta Mech*. 2014;225(6):1685-1698. doi:10.1007/s00707-013-1023-y

43. Shek KL, Dietz HP. Intrapartum risk factors for levator trauma. *BJOG An Int J Obstet Gynaecol*. 2010;117(12):1485-1492. doi:10.1111/j.1471-0528.2010.02704.x

44. Shek KL, Dietz HP. The effect of childbirth on hiatal dimensions. *Obstet Gynecol*. 2009;113(6):1272-1278. doi:10.1097/AOG.0b013e3181a5ef23

45. Stær-Jensen J, Siafarikas F, Hilde G, Benth JŠ, Bø K, Engh ME. Postpartum Recovery of Levator Hiatus and Bladder Neck Mobility in Relation to Pregnancy. *Obstet Gynecol*. 2015;125(3).

46. Unterberger MJ, Schmoller KM, Wurm C, Bausch AR, Holzapfel GA. Viscoelasticity of cross-linked actin networks: experimental tests, mechanical modeling and finite-element analysis. *Acta Biomater*. 2013;9(7):7343-7353. doi:10.1016/j.actbio.2013.03.008

47. Vila Pouca MCP, Ferreira JPS, Parente MPL, Natal Jorge RM, Ashton-Miller JA. On the management of maternal pushing during the second stage of Labor: a biomechanical study considering passive tissue fatigue damage accumulation. *Am J Obstet Gynecol*. 2022;In Press. doi:https://doi.org/10.1016/j.ajog.2022.01.023

48. Vila Pouca MCP, Parente MPL, Natal Jorge RM, Ashton-Miller JA. Injuries in muscle-tendon-bone units: a systematic review considering the role of passive tissue fatigue. *Orthop J Sport Med*. 2021;9(8). doi:DOI: 10.1177/23259671211020731

49. Vila Pouca MCP, Parente MPL, Natal Jorge RM, Ashton-Miller JA. Investigating the birth-related caudal maternal pelvic floor muscle injury: The consequences of low cycle fatigue damage. *J Mech Behav Biomed Mater*. 2020;110:103956. doi:https://doi.org/10.1016/j.jmbbm.2020.103956

50. Vila Pouca MCP, Parente MPL, Natal Jorge RM, DeLancey JO., Ashton-Miller JA. Pelvic floor muscle injury during a difficult labor. Can tissue fatigue damage play a role? *Int J Urogynecology*. 2022;(33):211-220.

51. Wojtys EM, Beaulieu ML, Ashton-Miller JA. New perspectives on ACL injury: On the role of repetitive sub-maximal knee loading in causing ACL fatigue failure. *J Orthop Res*.

2016;34(12):2059-2068. doi:10.1002/jor.23441

52. Zhang W, Sacks MS. Modeling the response of exogenously crosslinked tissue to cyclic loading: The effects of permanent set. *J Mech Behav Biomed Mater*. 2017;75:336-350. doi:https://doi.org/10.1016/j.jmbbm.2017.07.013

1. Araujo AE, Delgado A, Maia JN, et al. Efficacy of spontaneous pushing with pursed lips breathing compared with directed pushing in maternal and neonatal outcomes : a clinical trial. *Authorea*. Published online 2020:1-11. doi:10.22541/au.160278519.95490262/v1

2. Ashton-Miller JA, DeLancey JOL. Functional anatomy of the female pelvic floor. *Ann N Y Acad Sci*. 2007;1101:266-296. doi:10.1196/annals.1389.034

3. Ashton-Miller JA, DeLancey JOL. On the biomechanics of vaginal birth and common sequelae. *Annu Rev Biomed Eng*. 2009;11(1):163-176. doi:10.1146/annurev-bioeng-061008-124823.On

4. Bilby BA, Lardner LRT, Stroh AN. Continuous distributions of dislocations and the theory of plasticity. *Actes du IXe congrès Int mécanique appliquée*. 1957;8:35-44.

5. Calvo B, Peña E, Martinez MA, Doblaré M. An uncoupled directional damage model for fibred biological soft tissues. Formulation and computational aspects. *Int J Numer Methods Eng*. 2007;69(10):2036-2057. doi:https://doi.org/10.1002/nme.1825

6. Casanova R, And AC, Goepfert AR, Hueppchen NA, Weiss PM, American College of Obstetricians and Gynecologists. *Beckmann and Ling's Obstetrics and Gynecology*. 8th Editio. Philadelphia : Wolters Kluwer; 2019.

7. Caudwell-Hall J, Kamisan Atan I, Martin A, et al. Intrapartum predictors of maternal levator ani injury. *Acta Obstet Gynecol Scand*. 2017;96(4):426-431. doi:https://doi.org/10.1111/aogs.13103

8. Chen J, Kim J, Shao W, et al. An anterior cruciate ligament failure mechanism. *Am J Sports Med*. 2019;47(9):2067-2076. doi:10.1177/0363546519854450

9. DeLancey JOL. What's new in the functional anatomy of pelvic organ prolapse? *Curr Opin Obstet Gynecol*. 2016;28(5):420-429. doi:10.1097/GCO.0000000000000312

10. Diani J, Brieu M, Vacherand JM. A damage directional constitutive model for Mullins effect with permanent set and induced anisotropy. *Eur J Mech - A/Solids*. 2006;25(3):483-496. doi:https://doi.org/10.1016/j.euromechsol.2005.09.011

11. Dong H, Liu M, Martin C, Sun W. A residual stiffness-based model for the fatigue damage of biological soft tissues. *J Mech Phys Solids*. 2020;143:104074. doi:https://doi.org/10.1016/j.jmps.2020.104074

12. Falkert A, Endress E, Weigl M, Seelbach-Göbel B. Three-dimensional ultrasound of the pelvic floor 2 days after first delivery: Influence of constitutional and obstetric factors. *Ultrasound Obstet Gynecol*. 2010;35(5):583-588. doi:10.1002/uog.7563

13. Ferreira JPS, Parente MPL, Jabareen M, Jorge RMN. A general framework for the numerical implementation of anisotropic hyperelastic material models including non-local damage. *Biomech Model Mechanobiol*. 2017;16(4):1119-1140. doi:10.1007/s10237-017-0875-9

14. Fung Y. *Biomechanics: Mechanical Properties of Living Tissues*. Second Edi. Springer Science & Business Media; 1993.

15. Van Geelen H, Ostergard D, Sand P. A review of the impact of pregnancy and childbirth on pelvic floor function as assessed by objective measurement techniques. *Int Urogynecol J*. 2018;29(3):327-338. doi:10.1007/s00192-017-3540-z

16. Göktepe S, Abilez OJ, Kuhl E. A generic approach towards finite growth with examples of athlete's heart, cardiac dilation, and cardiac wall thickening. *J Mech Phys Solids*. 2010;58(10):1661-1680. doi:https://doi.org/10.1016/j.jmps.2010.07.003

17. Göktepe S, Abilez OJ, Parker KK, Kuhl E. A multiscale model for eccentric and concentric cardiac growth through sarcomerogenesis. *J Theor Biol*. 2010;265(3):433-442. doi:https://doi.org/10.1016/j.jtbi.2010.04.023

18. Hanson L. Second-stage labor care: challenges in spontaneous bearing down. *J Perinat Neonatal Nurs*. 2009;23(1):31. doi:10.1097/JPN.0b013e318196526b

19. Holzapfel GA. *Nonlinear Solid Mechanics: A Continuum Approach for Engineering*. John Wiley & Sons; 2000.

20. Holzapfel GA, Fereidoonnezhad B. Chapter 5 - Modeling of Damage in Soft Biological Tissues. In: Payan Y, Ohayon JBT-B of LO, eds. *Translational Epigenetics*. Vol 1. Academic Press; 2017:101-123. doi:https://doi.org/10.1016/B978-0-12-804009-6.00005-5

21. Holzapfel GA, Gasser TC. A viscoelastic model for fiber-reinforced composites at finite strains: Continuum basis, computational aspects and applications. *Comput Methods Appl Mech Eng*. 2001;190(34):4379-4403. doi:https://doi.org/10.1016/S0045-7825(00)00323-6

22. Holzapfel GA, Gasser TC, Ogden RW. A new constitutive framework for arterial wall mechanics and a comparative study of material models. *J Elast Phys Sci solids*. 2000;61(1):1-48. doi:10.1023/A:1010835316564

23. Holzapfel GA, Ogden RW, Sherifova S. On fibre dispersion modelling of soft biological tissues: a review. *Proc R Soc A Math Phys Eng Sci*. 2019;475(2224):20180736. doi:10.1098/rspa.2018.0736

24. Kamisan Atan I, Gerges B, Shek KL, Dietz HP. The association between vaginal parity and hiatal dimensions: A retrospective observational study in a tertiary urogynaecological centre. *BJOG An Int J Obstet Gynaecol*. 2015;122(6):867-872. doi:10.1111/1471-0528.12920

25. Kuhl E, Garikipati K, Arruda EM, Grosh K. Remodeling of biological tissue: Mechanically induced reorientation of a transversely isotropic chain network. *J Mech Phys Solids*. 2005;53(7):1552-1573. doi:https://doi.org/10.1016/j.jmps.2005.03.002

26. Laganà AS, La Rosa VL, Rapisarda AMC, Vitale SG. Pelvic organ prolapse: the impact on quality of life and psychological well-being. *J Psychosom Obstet Gynecol*. 2018;39(2):164-166. doi:10.1080/0167482X.2017.1294155

27. Lee EH, Liu DT. Finite-Strain Elastic—Plastic Theory with Application to Plane-Wave Analysis. *J Appl Phys*. 1967;38(1):19-27. doi:10.1063/1.1708953

28. Lee N, Gao Y, Lotz L, Kildea S. Maternal and neonatal outcomes from a comparison of spontaneous and directed pushing in second stage. *Women and Birth*. 2019;32(4):e433-e440. doi:https://doi.org/10.1016/j.wombi.2018.10.005

29. Leveno KJ, Nelson DB, McIntire DD. Second-stage labor: how long is too long? *Am J Obstet Gynecol*. 2016;214(4):484-489. doi:https://doi.org/10.1016/j.ajog.2015.10.926

30. Lien K-C, DeLancey JOL, Ashton-Miller JA. Biomechanical analyses of the efficacy of patterns of maternal effort on second-stage progress. *Obstet Gynecol*. 2009;113(4):873-880. doi:10.1097/AOG.0b013e31819c82e1

31. Lipps DB, Wojtys EM, Ashton-Miller JA. Anterior cruciate ligament fatigue failures in knees subjected to repeated simulated pivot landings. *Am J Sports Med*. 2013;41(5):1058-1066. doi:10.1177/0363546513477836

32. Liu F, Xu L, Ying T, Tao J, Hu B. Three-dimensional ultrasound appearance of pelvic floor in nulliparous women and postpartum women one week after their first delivery. *Int J Med Sci*. 2014;11(3):234-239. doi:10.7150/ijms.7384

33. Martin C, Sun W. Modeling of long-term fatigue damage of soft tissue with stress softening and permanent set effects. *Biomech Model Mechanobiol*. 2013;12(4):645-655. doi:10.1007/s10237-012-0431-6

34. Milella PP. *Fatigue and Corrosion in Metals*. 1st ed. (Milella PP, ed.). Springer-Verlag Mailand; 2013. doi:10.1007/978-88-470-2336-9

35. Miller JM, Low LK, Zielinski R, Smith AR, Delancey JOL, Brandon C. Evaluating maternal recovery from labor and delivery: Bone and levator ani injuries. *Am J Obstet Gynecol*. 2015;213(2):188.e1-188.e11. doi:10.1016/j.ajog.2015.05.001

36. Mullins L. Softening of Rubber by Deformation. *Rubber Chem Technol*. 1969;42(1):339-362. doi:10.5254/1.3539210

37. Parente MPL, Jorge RMN, Mascarenhas T, Fernandes AA, Martins JAC. Deformation of the pelvic floor muscles during a vaginal delivery. *Int Urogynecol J Pelvic Floor Dysfunct*. 2008;19(1):65-71. doi:10.1007/s00192-007-0388-7

38. Peña E. Computational aspects of the numerical modelling of softening, damage and permanent set in soft biological tissues. *Comput Struct*. 2014;130:57-72. doi:https://doi.org/10.1016/j.compstruc.2013.10.002

39. Pipitone F, Swenson CW, DeLancey JOL, Chen L. Novel 3D MRI technique to measure perineal membrane structural changes with pregnancy and childbirth: Technique development and measurement feasibility. *Int Urogynecol J*. 2021;32(9):2413-2420. doi:10.1007/s00192-021-04795-x

40. Rebouah M, Chagnon G. Permanent set and stress-softening constitutive equation applied to rubber-like materials and soft tissues. *Acta Mech*. 2014;225(6):1685-1698. doi:10.1007/s00707-013-1023-y

41. Shek KL, Dietz HP. Intrapartum risk factors for levator trauma. *BJOG An Int J Obstet Gynaecol*. 2010;117(12):1485-1492. doi:10.1111/j.1471-0528.2010.02704.x

42. Shek KL, Dietz HP. The effect of childbirth on hiatal dimensions. *Obstet Gynecol*. 2009;113(6):1272-1278. doi:10.1097/AOG.0b013e3181a5ef23

43. Stær-Jensen J, Siafarikas F, Hilde G, Benth JŠ, Bø K, Engh ME. Postpartum Recovery of Levator Hiatus and Bladder Neck Mobility in Relation to Pregnancy. *Obstet Gynecol*. 2015;125(3).

44. Unterberger MJ, Schmoller KM, Wurm C, Bausch AR, Holzapfel GA. Viscoelasticity of cross-linked actin networks: experimental tests, mechanical modeling and finite-element analysis. *Acta Biomater*. 2013;9(7):7343-7353. doi:10.1016/j.actbio.2013.03.008

45. Vila Pouca MCP, Ferreira JPS, Parente MPL, Natal Jorge RM, Ashton-Miller JA. On the Management of Maternal Pushing During the Second Stage of Labor: A Biomechanical Study Considering Passive Tissue Fatigue Damage Accumulation. *Am J Obstet Gynecol*. (Submitted.

46. Vila Pouca MCP, Parente MPL, Natal Jorge RM, Ashton-Miller JA. Injuries in muscle-tendon-bone units: a systematic review considering the role of passive tissue fatigue. *Orthop J Sport Med*. 2021;9(8). doi:DOI: 10.1177/23259671211020731

47. Vila Pouca MCP, Parente MPL, Natal Jorge RM, Ashton-Miller JA. Investigating the birth-related caudal maternal pelvic floor muscle injury: The consequences of low cycle fatigue damage. *J Mech Behav Biomed Mater*. 2020;110:103956. doi:https://doi.org/10.1016/j.jmbbm.2020.103956

48. Vila Pouca MCP, Parente MPL, Natal Jorge RM, DeLancey JO., Ashton-Miller JA. Pelvic floor muscle injury during a difficult labor. Can tissue fatigue damage play a role? *Int J Urogynecology*. (In Press).

49. Wojtys EM, Beaulieu ML, Ashton-Miller JA. New perspectives on ACL injury: On the role of repetitive sub-maximal knee loading in causing ACL fatigue failure. *J Orthop Res*. 2016;34(12):2059-2068. doi:10.1002/jor.23441

50. Zhang W, Sacks MS. Modeling the response of exogenously crosslinked tissue to cyclic loading: The effects of permanent set. *J Mech Behav Biomed Mater*. 2017;75:336-350. doi:https://doi.org/10.1016/j.jmbbm.2017.07.013

Afterword

General discussion

Pelvic floor muscle injuries, particularly at the pubovisceral portion of the levator ani, show a prevalence of 13-41% after vaginal delivery (see Introduction). These injuries are strongly associated with the development of pelvic floor dysfunctions later in life, making vaginal delivery a primary risk factor. Women with pelvic floor dysfunctions can experience pelvic organ prolapse, urinary and fecal incontinence, sexual dysfunctions, among others, which causes an overall impact in the quality of life. Surgical repairs can be performed to help with pelvic floor dysfunctions, however, there is still a failure rate of ~30% and high risk of recurrence and complications. So, the focus should be in preventing the injury in the first place. This dissertation was an attempt to improve our current understanding of this injury mechanism, by proposing a new hypothesis, testing it experimentally and applying computational tools to provide further insights on how to improve the management of labor and reduce the risk of injury.

Material fatigue damage in soft tissues has been largely overlooked. Only in the last decade this issue was raised, experimentally tested and demonstrated to be a cause of failure of the anterior cruciate ligament, in the knee (see sections 1.1 and 2.4). There are also concerns with material fatigue when testing bioprosthetic tissues and materials (i.e. bioprosthetic heart valves). However, it is still generally not recognized by the medical community as a possible damage mechanism or damage contributor. In the engineering field, fatigue is estimated to be responsible for 90% of all mechanical service failures, so it is only reasonable to consider material fatigue as an additional damage mechanism for soft biological tissues. Despite this reasoning, it is true that soft tissues have the ability to heal, which can make a difference when dealing with fatigue damage, particularly for high-cycle fatigue. In the case of ultra-low/low-cycle fatigue, when the number of repetitions is relatively small and the loads are sub-maximal but still significant, the damage can start to grow in the first cycle and it is accompanied by plastic strain and ductile fracture initiation. So, damage and plastic deformation can develop fast in low-cycle fatigue and become significant to a point where it might not be completely recoverable. Vaginal delivery is a traumatic event for the pelvic floor muscles, where strenuous loads are repeated for a duration of

2-3 hours with short resting stages. It can almost be compared to the loading pattern of an earthquake, which is an event that causes ultra-low-cycle fatigue failure in metal structures. So, I believe a vaginal delivery, particularly a difficult one, fits the criteria for the development of ultra-low/low-cycle fatigue damage, and this damage can be a significant contributor for the levator ani injury extensively reported at the origin of the pubovisceral muscle.

The first aim of this thesis was to evaluate the feasibility of fatigue damage being a contributor to musculoskeletal injuries. A larger series of muscle and tendon injuries were assessed via systematic review and analyzed, among other factors, for its site, activity at time of injury and possible contribution of fatigue. The contribution of fatigue was considered only for well-trained athletes and people actively or previously engaged in frequent sports activity or the military when evident trauma (i.e a car accidents, forceful hits, work accidents involving machinery,…) was not reported. Mid-substance tendon and musculotendinous injuries were the most common injury sites and with the exception of avulsion injuries, who were mainly caused by traumas, fatigue could be involved in the cause of injury in all sites. Moreover, the systematic review also included *ex vivo* and *in vivo* laboratory studies in animal models, who showed histological signs of microdamage at the musculotendinous junction due to repetitive loading. This microdamage affected the mechanical properties when the repetitive loads were sub-maximal, but close to the ultimate failure load. So, although we cannot obtain a conclusive proof of fatigue damage by this systematic review, the indirect evidence is significant: First, the results of the laboratory studies showed a clear sign of fatigue damage accumulation; Second, most of the injuries at the musculoskeletal system could not be linked to a specific event. They are most common in well-trained athletes and occur during their normal sports activity, without any particular strange movement or fall being involved. This suggests that engaging regular and intense sports activity increases the injury possibility since the strenuous repetitions involved cause damage to accumulate. If the resting times are not enough for the tissues to heal or if the damage accumulation becomes partially irrecoverable, this might lead to failure during a commonly performed movement by the athletes, that would not cause injury in the first place.

The second aim was to stablish the main hypothesis of this research. Here we reviewed what are the characteristics of muscle/ligament origin and insertions and why are they typically prone to injury, the specific characteristics of the pubovisceral muscle origin and the evidence of fatigue damage in soft tissues. We saw that muscle/ligament origin and insertions are the locations where the muscle attaches to the bone through a tendon, which is mainly made of collagen. This interface between muscle and collagen and also between collagen and bone, being junctions of dissimilar materials, are typically locations where stresses concentrate. Consequently, these locations are prone to damage. Particularly regarding the pubovisceral muscle, the attachment to the bone is made through an aponeurosis, which is the designation for a sheet like tendon. So, the area and points of attachment are larger than when the muscle converges to a tendon, which has an almost

circular a smaller cross-section compared to the muscle. Nevertheless, the junction between dissimilar materials is the same as throughout the musculoskeletal system since aponeurosis have the same structural composition as tendons. Finally, from Chapter 1, we had the indirect evidence of fatigue damage in soft tissues elsewhere in the body. So, by analyzing this information we formed the clinical opinion that the origin of the pubovisceral muscle can be weakened by an accumulation of damage after a series of strenuous submaximal loading cycles, such as what occurs during labor.

In Chapter 3, a series of tests were performed, with the null hypothesis that the origin of the pubovisceral muscle accumulates damage due to low-cycle sub-maximal repetitive loading and that the microscopic damage would appear at the tendon-bone interface, as it was seen with the anterior cruciate ligament in the knee. So, using sheep as our animal model, we stablished and performed a low-cycle fatigue test protocol of 60 loading cycles, where in each cycle a specimen is stretched between 60% and 45% failure displacement. After the fatigue tests, the specimens were immediately fixed, prepped for histology and the microstructure analyzed under light microscopy.

Damage accumulation was verified both by the observation of a continuous stress softening throughout the fatigue tests and by the microstructure, which showed significant differences compared to untested controls. The null hypothesis was partially rejected since the damage accumulation was seen in the muscle close to the musculotendinous junction, rather than at the tendon-bone interface. With these experiments, we were able to see that even a small number of cycles, such as 60, is able to cause disruption of the muscle fibers and at the macroscopic level, besides the measured stress softening, there was also a visible and significant permanent deformation in the specimen.

Interestingly, these results are consistent with the damage mechanisms reported in metals for the ultra-low cycle fatigue regime, when hundreds or less strenuous cycles are performed (note that in this work we preferred the term low-cycle fatigue since it is more comprehensive and even in engineering materials there is not yet an agreement in the limits for low cycle and ultra-low cycle fatigue in terms of number of cycles). Our stress curves showed damage developing from the initial cycle and an average permanent deformation strain of almost 0.5 was measured after the tests. So, it is reasonable to assume an accumulation of plastic strains. These are also effects reported in metals and are consistent with the transitioning damage process between monotonic ductile damage and low-cycle fatigue (in the order of thousands of cycles). Due to the difference in nature of the materials, the microscopic underlying mechanisms are different in soft tissues than in metals. The most common effects seen in the muscle were larger spacing between the muscle fibers and muscle fibers that seemed elongated and crimped, which is interesting since it seems that they individually suffered from permanent deformation, which then translated to the

specimen at a macroscopic level. We also saw some individual muscle fiber rupture, which might be analogous to the 'fracture initiation' in the muscle.

Finally, motivated by these results we developed a low-cycle fatigue damage constitutive model and incorporated it into a visco-hyperelastic transversely isotropic model for the application of 3-D finite element analysis. The model showed a good correlation with the experimental data and constituted the first modeling framework for the analysis of more complex scenarios.

Since there is no consensus regarding the management of the second stage of labor, different practices are performed, causing different loading patterns (from the maternal pushes) to affect the pelvic floor muscles. So, the fourth aim was to verify the influence of the maternal pushes in the damage accumulation of the pelvic floor muscles, with the ultimate goal of defining the best approach in terms of pelvic floor damage. To achieve this aim, the low-cycle fatigue constitutive model developed and calibrated in Chapter 3 was incorporated into a finite element model of the second stage of labor. We tested four possible loading patterns, varying the number of maternal pushes per contraction and their duration, and found the best approach to be performing 3 maternal pushes per contraction, each for a duration of 5 seconds. Increasing the number of maternal pushes or performing them for 10 seconds caused higher damage and did not reduce the simulated labor. It is of clinical interest to avoid prolonged second stages of labor since it may cause maternal exhaustion and negative fetal outcomes. This is the reason why it is most common to coach the mother to push for a duration of ~10 seconds, about 3 times per contraction. However, from our results we believe it is beneficial to reduce the duration of each push, since it will reduce the damage accumulation in the tissue. Moreover, it will lead to higher resting stages, which will help to reduce maternal exhaustion and, from a mechanical point of view, a decrease in the stretches due to the muscle viscoelasticity.

Besides the complete failure reported at the origin of the pubovisceral muscle after labor, an enlarged hiatus is also an effect seen after vaginal delivery. This might be caused by the accumulation of permanent strains and so, be an effect of the repetitive loading, as seen experimentally in sheep pelvic muscle. Although this type of injury does not cause a macroscopic failure, microscopic damage exists and prevents a complete recovery. The enlarged hiatus is also associated with the development of pelvic floor disorders, so although the damage accumulation might not be sufficient to cause a complete failure, it might still have a significant negative impact in the future. So, the fifth aim was to incorporate the macroscopic permanent deformation into our low-cycle fatigue constitutive model to obtain a finite element model capable to analyze this secondary injury in more complex scenarios. The constitutive model was successfully implemented, validated and tested with simpler numerical examples. Finally, it was adjusted for the experimental data of Chapter 3 and a preliminary simulation of the second stage of labor was performed. The model showed agreement with the literature, with hiatal stretches reaching ~1.6

during the passage of the fetal head, and, for the first time, predicted an increase hiatal area of 8%.

Major findings

The major findings of this dissertation are as follows:

- Musculoskeletal injuries at the tendon-bone interface, mid-substance tendon, musculotendinous junction and muscle belly are susceptible to fatigue damage in well-trained athletes or people greatly engaging in sports activities (Chapter 1);
- Indirect evidence indicates the possibility that the origin of the pubovisceral muscle can accumulate sufficient damage due to the strenuous pushes in the second stage of labor to weaken the tissue to a point of partial or complete tear (Chapter 2);
- The analogous origin of the pubovisceral muscle in sheep accumulates microdamage due to low cycle fatigue (60 cycles at 60% failure stretch). Microstructural damage is seen at the muscle near the musculotendinous junction, affects the mechanical properties and cause visible macroscopic permanent deformation. The fatigue damage seems to progress at the muscle fiber level, from permanent elongation to fiber crimps and then to individual fiber rupture (Chapter 3);
- The maternal pushes influence the low-cycle fatigue damage accumulation in the pelvic floor muscles, being the origin of the pubovisceral muscle the most affected. The best approach for the management of labor in terms of reducing the damage accumulation is for the mother to perform 3 pushes per contraction for no longer than 5 seconds each push. Increasing the number of maternal pushes per contraction or increasing their duration caused higher damage and did not reduce the duration of the second stage of labor (Chapter 4);
- Permanent deformation as an effect of low-cycle fatigue can be modeled using continuum mechanics with a good agreement to the experimental data. Preliminary results for a normal labor, with a fetal head size in the 50th percentile, predicted an increase in the hiatal area of 8% (Chapter 5).

Final remarks and future work

This thesis aimed to investigate the possibility of ultra-low/low-cycle fatigue as a damage mechanism in soft tissues, particularly at the origin of the pubovisceral muscle during a difficult labor. Despite our findings, this work has limitations and unanswered questions that warrant further studies.

The systematic review showed the potential for fatigue damage accumulation in the musculoskeletal system to be at least a contribution to injury. However, this was not proved, and it is still necessary to confirm our findings. This is not an easy task since microscopic imaging techniques are usually invasive and destructive and methods such as MRI or CT scans might not have the necessary resolution. Nevertheless, as a starting point it would be interesting to follow professional athletes and perform systematic MRI or CT scans in search for signs of damage (i.e inflammation, edema, …) and track the recovery times and the cases where it developed to a more serious injury. In the event of surgical repair, the site of injury could be easily identified and a small biopsy of tissue collected, prepared for histology, and analyzed under light microscopy for damage accumulation signs.

The experimental assessment of damage accumulation due to cyclic repetitive sub-maximal loading was evaluated in non-pregnant female sheep. Besides the inherent limitations of using an animal model, it also does not capture the hormonally induced mechanical adaptations occurring during pregnancy. So, testing more specimens, both from pregnant female sheep and from human specimens, are necessary to reach more statistically definitive conclusions. Moreover, despite the experimental protocol being developed taking into account the loading pattern of a vaginal delivery, it is still necessary to confirm if this damage accumulation occurs due to a vaginal delivery. To test this hypothesis, the same sheep animal model of the origin of the pubovisceral muscle could be histologically prepared and analyzed under light microscopy for non-pregnant nullipara female sheep, for primipara pregnant female sheep whose specimens would be non-pregnant controls, for primipara pregnant female sheep and for multiparas or primiparas female sheep immediately after the vaginal delivery and 6 months after the vaginal delivery. This study would allow to analyze the microscopic differences between non-pregnant and pregnant tissues, verify the existence of damage accumulation due to the vaginal delivery and if underlying mechanisms are similar to the *in vitro* damage found in this thesis, and finally analyze the grade of tissue recovery.

It is also worth noting that to perform the computational simulations, several simplifications were performed. Although simplifications are necessary and we believe they do not compromise these preliminary results, the geometrical models could be improved by the introduction fetal head molding and a pelvic floor geometry obtained from a younger woman. Regarding the material model, active muscle contraction could be incorporated into the constitutive equation, with the effects of maternal exhaustion. This would allow a more comprehensive analysis, with a better prediction of the duration of the second stage of labor, and therefore be better tool to improve the management of labor.

Despite these limitations, hopefully this work will instigate further research in this area, and if our findings are confirmed, lead to the develop of new strategies for injury prevention.

Publications and presentations related with this study

Peer-reviewed publications

11. Vila Pouca MCP, Ferreira JPS, Parente MPL, Natal Jorge RM, Ashton-Miller JA. On the management of maternal pushing during the second stage of labor: a biomechanical study considering passive tissue fatigue damage accumulation. *American Journal of Obstetrics and Gynecology.* (January 2022). In Press. DOI: https://doi.org/10.1016/j.ajog.2022.01.023

10. Vila Pouca MCP, Parente MPL, Natal Jorge RM, Ashton-Miller JA, DeLancey JOL. Pelvic Floor Muscle Injury during a Difficult Labor. Can Tissue Fatigue Damage Play a Role? *International Urogynecology Journal.* (November 2021) 33, 211-220. DOI: https://doi.org/10.1007/s00192-021-05012-5

9. Stansfield E, Fischer B, Grunstra NDS, **Vila Pouca, MCP**, Mitteroecker P. The evolution of pelvic canal shape and rotational birth in humans. *BMC Biology*. (October 2021) 19, 224. DOI: https://doi.org/10.1186/s12915-021-01150-w

8. Vila Pouca MCP, Parente MPL, Natal Jorge RM, Ashton-Miller JA. Injuries in muscle-tendon-bone units: a systematic review considering the role of passive tissue fatigue. *Orthopaedic Journal of Sports Medicine*. (August 2021); 9(8). DOI: 10.1177/23259671211020731

7. Fidalgo DS, **Vila Pouca MCP**, Oliveira DA, et al. Mechanical Effects of a Maylard Scar During a Vaginal Birth After a Previous Caesarean. *Annals of Biomedical Engineering*. (June 2021). DOI:10.1007/s10439-021-02805-z

6. Moura R, Borges M, **Vila Pouca MCP**, et al. A numerical study on fetal head molding during labor. *International Journal for Numerical Methods in Biomedical Engineering*. (November 2020); 37(1):e3411. DOI: https://doi.org/10.1002/cnm.3411

5. Vila Pouca MCP, Parente MPL, Natal Jorge RM, Ashton-Miller JA. Investigating the birth-related caudal maternal pelvic floor muscle injury: The consequences of low cycle fatigue damage. *Journal of the Mechanical Behavior of Biomedical Materials.* (October 2020); 110:103956. DOI: https://doi.org/10.1016/j.jmbbm.2020.103956

4. Oliveira DA, Silva MET, **Vila Pouca MCP**, Parente MPL, Mascarenhas T, Natal Jorge RM. Biomechanical Simulation of Vaginal Childbirth: The Colors of the Pelvic Floor Muscles BT - Computational Biomechanics for Medicine. In: Nash MP, Nielsen PMF, Wittek A, Miller K, Joldes GR, eds. Springer, Cham; (August 2019):1-17. DOI: 10.1007/978-3-030-15923-8_1

3. Oliveira D, **Vila Pouca M**, Ferreira J, Mascarenhas T. Episiotomy: the biomechanical impact of multiple small incisions during a normal vaginal delivery. *Interface Focus*. (October 2019); 9(5):20190027. DOI:10.1098/rsfs.2019.0027

2. Vila Pouca MCP, Ferreira JPS, Oliveira DA, Parente MPL, Mascarenhas MT, Natal Jorge RM. Simulation of the uterine contractions and foetus expulsion using a chemo-mechanical constitutive model. *Biomechanics and Modelling in Mechanobiology*. (January 2019); 18(3):829-843. DOI:10.1007/s10237-019-01117-5

1. Vila Pouca MCP, Ferreira JPS, Oliveira DA, Parente MPL, Mascarenhas T, Natal Jorge RM. On the effect of labour durations using an anisotropic visco-hyperelastic-damage approach to simulate vaginal deliveries. *Journal of the Mechanical Behavior of Biomedical Materials*. (December 2018); 88:120-126. DOI:10.1016/j.jmbbm.2018.08.011

Oral communications

1. Vila Pouca MCP, Ferreira JPS, Parente MPL, Natal Jorge RM. (2021) Maternal pushes during the second stage of labor: a biomechanical study of fatigue damage accumulation. 17th International Symposium on Computer Methods in Biomechanics and Biomedical Engineering (CMBBE), online edition (Bonn, Germany).

2. Vila Pouca MCP, Parente MPL, Natal Jorge RM, Ashton-Miller JA. (2021) Can cyclic loading weaken the origin of the ovine pubovisceral muscle? 26th Congress of the European Society of Biomechanics (ESB), online edition (Milano, Italy).

3. Vila Pouca MCP, Ferreira JPS, Oliveira DA, Parente MPL, Natal Jorge RM. (2018) Simulation of the uterine contractions and foetus expulsion using a chemo-mechanical constitutive model. 10th European Solid Mechanics Conference (ESMC), Bologna, Italy.

4. Vila Pouca MCP, Ferreira JPS, Oliveira DA, Parente MPL, Natal Jorge RM. (2018) On the Anisotrsopic visco-hyperelastic modelling of the pelvic floor muscles during childbirth. 15th International Symposium on Computer Methods in Biomechanics and Biomedical Engineering (CMBBE), Lisboa, Portugal.

Appendix

A

The PubMed, Web of Science, Scopus and Pro-Quest databases were searched using the following search strings, one at a time:

1. "musculotendinous injury" OR "musculotendinous injuries OR "musculotendinous failure" "musculotendinous tear" OR "muscle-tendon injury" OR "muscle-tendon injuries" OR "musculotendinous defect" OR "musculotendinous junction tear" OR musculotendinous junction injury" OR musculotendinous junction injuries" OR "musculotendinous junction failure" OR "musculotendinous junction defect" OR "muscle-tendon failure" OR "muscle-tendon tear" OR "myotendinous injury" OR "myotendinous injuries" OR "myotendinous tear" OR "myotendinous failure" OR "myotendinous defect" OR "myotendinous junction tear" OR "myotendinous junction failure" OR "myotendinous junction defect" OR "tendon-muscle injuries" OR tendon-muscle injury" OR tendon-muscle failure" OR "tendon-muscle tear" OR "tendon-muscle defect"

2."tendon-bone injury" OR "tendon-bone injuries" OR "tendon-bone tear" OR "tendon-bone defect" OR "bone-tendon injury" OR "bone-tendon injuries" OR "bone-tendon tear" OR "bone-tendon defect" OR "tendinous avulsion" OR "tendon avulsion" OR "aponeurosis avulsion" OR "aponeurotic avulsion" OR "musculotendinous avulsion" OR "myotendinous avulsion"

3."muscle belly tear" OR "muscle belly injuries" OR "muscle belly injury" OR "muscle belly failure" OR "muscle belly defect" OR "intramuscular tear" OR "intramuscular failure" OR "intramuscular defect" OR "intramuscular injury" OR "intramuscular injuries" OR "muscle substance tears" OR "muscle substance failure" OR "muscle substance defect" OR "muscle substance injury" OR "muscle substance injuries" OR "muscle tear" OR "muscle defect" OR "muscle failure"

4."tendon tear" OR "aponeurosis tear" OR "tendinous tear" OR "tendon failure" OR "tendon defect" OR "tendinous failure" OR "tendinous defect" OR "tendinous failure" OR "aponeurosis failure" OR "aponeurosis defect"

B

To access quality and risk of bias of the laboratory studies, the ARRIVE[72] guidelines checklist was implemented. Items 9, 14 and 17 were not considered since they were not relevant in the context of all the laboratory studies included in the analysis. To the remaining items, a score was given, depending on the number of details involved. The sum of the points of all items represents the maximum possible score, or a perfect 100% evaluation. Each article was evaluated in these 17 items and a percentual score was determined afterwards. Non-Applicable items were not counted and were deducted from the maximum possible score for that study. The items under evaluation, adapted from Kilkenny, et al 2010[72], and the score for each item it is presented in Table B.1 and the evaluation performed and the score for each laboratory study in Table B.2.

Table B.1 - ARRIVE guidelines checklist and score defined for the evaluation.

Item		Recommendations	Score
Title	**1**	Provide an accurate and concise description of the content	1
Abstract	**2**	Provide background, objectives, animal used, methods, results and conclusions	6
Introduction	**3**	Include sufficient scientific background. Explain how and why animal species and model being used can address the scientific objectives.	2
	4	Describe the objectives of the study or hypothesis being tested	1
Methods	**5**	Include ethical review permissions	1
	6	Include the number of experimental and control groups Include steps taken to minimize effects of subjective bias (e.g. randomisation) Define the experimental unit	3
	7	Provide details regarding the anaesthesia formulation and dose, route of administration, surgical procedure and method of euthanasia	4
	8	Provide details of the animals used: species, development stage, weight and source of animals	4
	10	Specify the total number of animals used and how the number of animals was arrived at	2
	11	Give full details of how animals were allocated to experimental groups	1
	12	Define the experimental outcomes assessed	1
	13	Provide details of the statistical methods Specify the unit of analysis for each dataset Describe any methods used to assess whether the data met the assumptions of the statistical approach	3
Results	**15**	Report the number of animals in each group included in the analysis If any animals or data where not included in the analysis explain why	2
	16	Report the results for each analysis carried out with a measure of precision	1
Discussion	**18**	Interpret the results Comment on the study limitations	2
	19	Comment on whether, and how, the findings of this study are likely to translate to other species or systems, including any relevance to human biology	1
	20	List all funding sources	1
		TOTAL	36

Adapted from Kilkenny, et al 2010[72]

Table B.2 - Quality evaluation and score of the laboratory studies included in this study.

Author	ARRIVE items																	TOTAL	Max Score	% Score
	1	2	3	4	5	6	7	8	10	11	12	13	15	16	18	19	20			
(Garrett et al. 1987)[43]	1	3	1	1	0	2	3	2	1	0	1	3	2	1	1	0	0	22	35	63%
(Garrett et al. 1988)[42]	1	2	1	1	0	2	3	2	1	0	0	2	2	1	1	0	0	19	36	53%
(Taylor et al. 1993)[125]	1	3	1	1	0	2	3	2	1	0	1	2	2	0	1	0	0	20	36	56%
(Noonan et al. 1994)[94]	1	3	1	1	0	2	2	2	1	0	1	2	0	1	2	0	0	19	36	53%
(Sun et al. 1994)[122]	1	4	1	1	0	3	3	2	1	1	1	2	2	1	1	0	0	24	36	67%
(Gottsauner-Wolf et al. 1995)[49]	1	4	1	1	0	3	0	2	1	1	1	2	2	1	1	0	1	22	33	67%
(Hasselman et al. 1995)[54]	1	5	1	1	0	2	0	2	1	0	1	2	2	1	2	0	1	22	36	61%
(Law, Caputo, and Tidball 1995)[74]	1	5	1	1	0	1	1	2	1	0	1	2	1	1	1	0	0	19	36	53%
(Mair et al. 1996)[81]	1	3	2	1	0	1	3	1	0	0	1	2	0	1	1	0	0	17	36	47%
(Sano et al. 1997)[107]	1	5	1	1	0	2	NA	2	1	NA	1	2	2	1	1	0	1	21	32	66%
(Tsuang et al. 1998)[129]	1	6	2	1	0	1	3	2	0	0	1	2	0	1	1	0	1	22	36	61%

NA – non-applicable

For the observational cohort studies, the STROBE[132] guidelines checklist was implemented. Item 17 was not considered since it was not relevant in the included cohort studies. As with the laboratory studies, a score was given to each item, depending on the number of details involved. Once again, Non-Applicable items were not counted and were deducted from the maximum possible score for that study. The items under evaluation, adapted from Vandenbroucke, et al 2007[132], and the score for each item it is presented in Table B.3 and the evaluation performed and the score for each laboratory study in Table B.4.

Table B.3 - STROBE guidelines checklist and score defined for the evaluation.

Item		Recommendations	Score
Title and Abstract	**1**	a) Indicate the study design in the title or abstract b) Provide in the abstract a balanced summary of what was done and what was found	3
Introduction	**2**	Explain the scientific background	1
	3	State specific objectives	1
Methods	**4**	Present the type of study design early in the paper	1
	5	Describe the recruiting site and relevant dates (e.g. periods of recruitment)	2
	6	Give the eligibility criteria and the methods of selection of participants	2
	7	Define what was included and/or excluded in the analysis	1
	8	Give details of methods of assessment	1
	9	Describe any efforts to address potential source of bias	1
	10	Explain how the study size was arrived	1
	11	Explain how quantitative variables were handled in the analysis	1
	12	a) Describe all statistical methods b) Explain how missing data was addressed (e.g. patients lost to follow-up)	2
Results	**13**	a) Report numbers of individuals at each stage of the study (e.g. numbers potentially eligible, confirmed eligible, included in the study, completing follow-up, and analysed) b) Give reasons for non-participation at each stage	2
	14	a) Give characteristics of study participants (sex, age, activity at time of injury) b) Indicate number of participants with missing data c) Summarize follow-up time	5
	15	Report numbers of outcome events or summary measures over time	1
	16	Give unadjusted estimates and, if applicable, confounded-adjusted estimates and their precision	1
Discussion	**18**	Summarize key results	1
	19	Discuss limitations of the study	1
	20	Give a cautious overall interpretation of results	
	21	Discuss the generalisability of the study results	
	22	Give the source of funding	1
		TOTAL	32

Adapted from Vandenbroucke, et al 2007[132]

Table B.4 - Quality evaluation and score of the cohort studies included in this study.

	STROBE items																							
Author	**1**	**2**	**3**	**4**	**5**	**6**	**7**	**8**	**9**	**10**	**11**	**12**	**13**	**14**	**15**	**16**	**18**	**19**	**20**	**21**	**22**	**TOTAL**	**Max Score**	**% Score**
(Durig et al. 1977)[29]	2	1	0	0	1	2	0	0	0	0	0	NA	2	4	1	1	1	0	1	0	0	16	30	53%
(Ferretti et al. 1983)[35]	2	1	1	0	0	2	1	1	0	0	1	NA	2	3	1	NA	1	0	1	0	0	17	29	59%
(Ferretti et al. 1985)[36]	2	1	0	1	2	2	0	1	0	1	1	2	2	3	1	NA	1	0	1	0	0	21	31	68%
(Nimityongskul, Montague, and Anderson 1988)[92]	2	1	0	0	2	1	0	1	0	0	NA	2	2	5	1	NA	1	0	0	0	0	18	30	60%
(Fleckenstein et al. 1989)[38]	3	1	1	1	0	2	0	1	0	0	1	2	2	2	1	0	1	0	1	0	0	19	32	59%
(Farley et al. 1992)[32]	3	0	1	0	1	2	1	1	1	1	1	2	2	2	1	0	1	0	1	0	0	21	32	66%
(Pomeranz and Heidt 1993)[102]	3	1	0	1	1	2	0	1	0	0	1	1	2	3	1	1	1	1	1	0	0	21	32	66%
(Speer, Lohnes, and Garrett 1993)[120]	2	1	1	1	2	1	1	1	1	1	NA	NA	2	2	1	NA	1	0	1	0	0	19	28	68%
(Yoshioka et al. 1994)[145]	2	1	0	0	0	0	0	1	0	0	1	NA	1	5	1	NA	1	0	0	0	0	13	29	45%
(Hughes et al. 1995)[60]	3	1	1	1	2	2	1	0	0	0	NA	NA	2	5	1	NA	1	0	1	0	0	21	28	75%
(Simonet, Saylor III, and Sim 1995)[115]	3	1	0	1	1	0	0	0	0	0	0	NA	2	5	0	NA	1	0	1	0	0	15	29	52%
(Takami et al. 1995)[124]	3	1	0	1	1	1	1	0	0	1	NA	NA	2	5	1	NA	1	0	0	0	0	18	28	64%
(Evans, Bowrey, and Newman 1998)[31]	3	1	0	0	2	2	0	1	0	0	NA	NA	2	5	1	NA	1	1	1	1	0	21	28	75%
(Maffulli 1998)[80]	3	1	0	1	1	2	0	1	0	0	1	2	2	3	1	1	1	1	1	1	0	23	32	72%

Table B.4 - continued

Author	STROBE items																					TOTAL	Max Score	% Score
	1	2	3	4	5	6	7	8	9	10	11	12	13	14	15	16	18	19	20	21	22			
(Temple et al. 1998)[126]	3	1	0	1	2	0	0	1	0	0	NA	NA	2	5	1	NA	1	0	0	1	0	18	28	64%
(Connell et al. 1999)[20]	3	1	1	0	2	2	1	1	0	0	1	NA	2	5	1	NA	1	1	1	1	0	24	29	83%
(Carrino et al. 2000)[16]	3	1	1	1	1	2	0	1	0	0	NA	NA	2	5	1	NA	1	1	1	1	0	22	29	76%
(De Smet and Best 2000)[27]	3	1	1	0	2	1	0	1	0	0	NA	NA	2	5	1	NA	1	0		0	0	18	29	62%
(Karjalainen et al. 2000)[68]	3	1	1	0	0	2	1	1	0	0	1	NA	2	4	1	NA	1	0	1	0	0	19	29	66%
(Panni, Tartarone, and Maffulli 2000)[96]	3	1	1	1	2	2	0	1	1	0	1	NA	2	5	1	NA	1	1	1	0	0	24	29	83%
(Tung et al. 2001)[130]	3	1	1	0	1	2	0	1	0	0	NA	NA	2	4	1	NA	1	1	1	0	0	19	28	68%
(Weishaupt, Schweitzer, and Morrison 2001)[139]	3	1	1	1	2	1	0	1	0	0	NA	NA	2	5	1	NA	1	1	1	1	1	23	28	82%
(Williams et al. 2001)[142]	3	1	1	1	0	1	0	1	0	0	NA	NA	2	2	1	NA	1	1	1	0	0	16	28	57%
(Bass and Connell 2002)[8]	3	1	1	1	2	2	0	1	0	0	NA	NA	2	4	1	NA	1	1	1	0	0	21	28	75%
(Bianchi et al. 2002)[11]	3	1	1	1	0	2	0	0	0	0	NA	NA	2	5	1	NA	1	0	0	0	0	17	28	61%
(Sonnery-Cottet et al. 2002)[119]	3	1	1	1	2	2	1	1	0	0	1	2	2	5	1	1	1	1	1	1	0	28	32	88%
(Connell, Jhamb, and James 2003)[19]	1	1	1	0	2	2	0	1	0	0	0	NA	2	5	1	NA	1	1	1	0	0	19	29	66%
(T. K. Kim, Rauh, and McFarland 2003)[73]	3	1	1	1	1	2	1	1	1	0	1	2	2	4	1	1	1	1	1	1	0	27	32	84%

Table B.4 - continued

Author	STROBE items																					TOTAL	Max Score	% Score
	1	2	3	4	5	6	7	8	9	10	11	12	13	14	15	16	18	19	20	21	22			
(Mansat, Frankle, and Cofield 2003)[83]	3	1	1	0	1	2	0	1	0	0	0	NA	2	4	1	NA	1	0	0	0	0	17	29	59%
(Äärimaa et al. 2004)[1]	3	1	1	1	2	2	1	1	0	0	NA	2	2	5	1	1	1	0	1	0	0	25	31	81%
(T. M. Cross et al. 2004)[23]	3	1	1	1	2	2	1	1	0	0	1	2	2	5	1	1	1	1	1	0	0	27	32	84%
(Freccero and Berkowitz 2006)[40]	3	1	0	1	2	2	1	1	0	1	1	2	2	3	1	1	1	0	1	0	0	24	32	75%
(Ilaslan, Iannotti, and Recht 2007)[62]	3	1	0	1	1	2	0	1	1	0	NA	NA	2	3	1	NA	1	1	1	0	0	19	28	68%
(Irmola et al. 2007)[63]	2	1	0	1	2	2	0	1	0	0	NA	NA	2	4	1	NA	1	0	0	0	0	17	28	61%
(Lempainen et al. 2007)[75]	3	1	1	1	2	2	0	1	0	0	NA	NA	2	5	1	NA	1	1	0	0	1	22	28	79%
(Gyftopoulos et al. 2008)[51]	2	1	1	1	2	2	0	1	0	0	1	NA	2	3	1	NA	1	1	1	0	0	20	29	69%
(Lunn et al. 2008)[78]	3	1	1	1	2	2	0	0	0	0	0	2	2	5	1	1	1	1	1	0	0	24	32	75%
(Silder et al. 2008)[114]	3	1	1	0	0	1	0	1	1	0	1	2	2	5	1	NA	1	0	0	0	1	21	31	68%
(Gaskin et al. 2009)[44]	3	1	1	1	0	2	1	1	0	0	NA	NA	2	4	1	NA	1	1	1	0	0	20	28	71%
(Basic-Jukic et al. 2009)[7]	3	1	0	0	2	2	0	1	0	0	1	NA	2	4	1	NA	1	0	0	0	0	18	29	62%
(Walch et al. 2009)[136]	3	1	1	0	1	2	0	1	0	0	0	2	2	4	1	0	1	0	0	0	0	19	32	59%
(Pochini et al. 2010)[101]	3	1	0	1	1	2	1	1	1	0	1	2	2	5	1	1	1	1	1	0	0	26	32	81%

Table B.4 - continued

Author	STROBE items																					TOTAL	Max Score	% Score
	1	2	3	4	5	6	7	8	9	10	11	12	13	14	15	16	18	19	20	21	22			
(Pedret et al. 2011)[97]	2	1	0	1	1	2	0	1	0	0	1	NA	2	5	1	NA	1	0	0	0	0	18	29	62%
(Makridis et al. 2014)[82]	3	1	1	1	1	2	1	1	0	0	0	2	1	4	1	1	1	1	1	0	0	23	32	72%
(Crema et al. 2016)[22]	3	1	1	1	2	2	1	1	1	0	0	2	2	5	1	1	1	1	1	0	1	28	32	88%
(Lukac et al. 2016)[77]	3	1	1	1	2	2	1	1	0	0	0	NA	2	4	1	NA	1	1	0	0	0	21	29	72%
(Entwisle et al. 2017)[30]	3	1	1	0	1	2	0	1	0	0	1	NA	2	5	1	NA	1	1	1	0	0	21	29	72%
(Godoy et al. 2018)[47]	3	1	1	1	0	2	1	1	0	0	1	2	2	5	1	1	1	1	1	0	0	25	32	78%
(Roe et al. 2018)[105]	3	1	1	0	2	1	0	1	0	0	0	2	0	1	1	0	1	0	0	0	1	15	32	47%
(Miranda and Bureau 2019)[90]	3	1	1	1	2	1	1	1	0	0	1	2	2	3	1	NA	1	1	1	1	0	24	31	77%

NA – non-applicable

Finally, for the case report studies, the CARE[41] guidelines checklist was implemented. Items 2, 7 and 12 were not considered. The system of points for each item was defined as with the previous checklists. The items under evaluation, adapted from Gagnier et al 2013[41], and the score for each item it is presented in Table B.5 and the evaluation performed and the score for each laboratory study in Table B.6.

Table B.5 - CARE guidelines checklist and score defined for the evaluation.

Item		Recommendations	Score
Title	**1**	The words Case Report should be in the title along with the area of focus	1
Abstract	**3**	Describe: a) what is unique about the case b) the main symptoms of the patient c) the main diagnosis, therapeutic interventions, and outcomes d) what are the main "take-away" lessons from this case	4
Introduction	**4**	One or two paragraphs summarizing why this case is unique with references	1
Patient Information	**5**	a) De-identified demographic information and other patient specific information b) Main concerns and symptoms of the patient c) Medical, family, and psychosocial history including relevant genetic information d) Relevant past intervention and their outcomes	4
Clinical Findings	**6**	Describe the relevant physical examinations and other significant clinical findings	1
Diagnostic Assessment	**8**	a) Diagnostic methods b) Diagnostic reasoning	2
Therapeutic Intervention	**9**	a) Types of intervention (e.g. pharmacological, surgical, conservative,…) b) Administration of intervention	2
Follow-up and Outcomes	**10**	a) Clinician and patient-assessed outcomes b) Important follow-up diagnostic and other results c) Intervention adherence and tolerability d) Adverse and unanticipated events	4
Discussion	**11**	a) Discussion of the strengths and limitations in your approach to this case b) Discussion of the relevant medical literature c) The rationale for conclusions d) The primary take-away lessons of this case report	4
Informed consent	**13**	Indicate if the patient provided informed consent	1
		TOTAL	24

Adapted from Gagnier et al 2013[41].

Table B.6 - Quality evaluation and score of the case report studies included in this study.

Author	CARE items										TOTAL	Max Score	% Score
	1	3	4	5	6	8	9	10	11	13			
(Wenger 1973)[140]	0	4	0	2	0	2	1	2	2	0	13	24	54%
(Kawashima et al. 1975)[69]	1	1	0	2	1	1	2	4	3	0	15	24	63%
(Shields and Ashby 1975)[112]	0	0	1	2	1	1	1	4	3	0	13	24	54%
(Miller 1977)[89]	0	0	1	3	1	0	2	3	4	0	14	24	58%
(Bowers 1981)[12]	0	2	1	2	1	1	2	2	3	0	14	24	58%
(Farrar et al. 1981)[33]	0	0	1	4	1	2	2	3	4	0	17	24	71%
(Smith 1981)[117]	1	0	1	1	1	2	1	0	1	0	8	24	33%
(Vastamäki, Brummer, and Solonen 1981)[133]	1	1	1	1	0	2	1	3	3	0	13	24	54%
(Aso and Torisu 1984)[5]	0	2	1	2	1	2	1	1	3	0	13	24	54%
(Sherman, Snyder, and Fox 1984)[111]	1	0	1	4	1	2	1	2	4	0	16	24	67%
(White and Riley Jr. 1985)[141]	1	0	1	3	1	2	1	2	4	0	15	24	63%
(Andersen 1986)[2]	0	0	0	1	1	1	2	2	4	0	11	24	46%
(Bach, Warren, and Wickiewicz 1987))[6]	1	0	1	3	1	1	2	4	4	0	17	24	71%
(de Waal Malefijt and Beeker 1987)[28]	1	3	1	3	1	2	1	2	2	0	16	24	67%
(Clay 1988)[18]	0	0	0	2	1	2	1	2	4	0	12	24	50%
(Menz and Nettle 1989)[87]	0	0	1	3	1	1	2	2	4	0	14	24	58%
(Gruel 1990)[50]	0	2	1	2	1	2	1	0.5	4	0	13.5	24	56%
(de Roos and Zeeman 1991)[26]	0	2	1	2	1	1	2	1	2	0	12	24	50%
Tiger, Mayer, and Glazer 1993)[127]	0	3	1	2	1	2	1	0	3	0	13	24	54%
(Goodier, Maffulli, and Good 1994)[48]	0	1	1	3	1	2	2	2	4	0	16	24	67%
(Butcher, Siekanowicz, and Pettrone 1996)[14]	0	2	1	3	1	2	1	2	4	0	16	24	67%
(Ohashi et al. 1996)[95]	0	3	1	2	1	2	1	0	4	0	14	24	58%
(Wagner and Cooney 1997)[135]	1	2	1	3	1	2	2	1	3	0	16	24	67%
(Asinger and el-Khoury 1998)[4]	0	0	1	4	1	2	1	1	4	0	14	24	58%
(Canovas, Nicolau, and Bonnel 1998)[15]	0	2	1	2	1	2	1	1	4	0	14	24	58%

Table B.6 - continued

Author	CARE items										TOTAL	Max Score	% Score
	1	3	4	5	6	8	9	10	11	13			
(Hertel and Lambert 1998)	0	0	1	4	1	2	2	4	4	0	18	24	75%
(Sollender, Rayan, and Barden 1998)[118]	0	3	1	3	1	2	2	3	3	0	18	24	75%
(Takami et al. 1998)[123]	0	2	1	3	1	1	1	1	2	0	12	24	50%
(Cooper and Selesnick 2000)[21]	1	0	1	3	1	2	2	3	4	0	17	24	71%
(Henry and Scerpella 2000)[55]	1	0	1	3	1	2	2	3	4	0	17	24	71%
(Kameyama and Shiraishi 2000)[66]	1	0	1	3	1	2	2	4	4	0	18	24	75%
(Street and Burks 2000)[121]	1	0	1	4	1	3	1	12	4	0	27	24	113%
(Rose and Frassica 2001)[106]	1	0	1	4	1	2	2	4	4	0	19	24	79%
(Pina, Garcia, and Sabater 2002)[99]	0	4	1	2	1	2	2	3	4	0	19	24	79%
(Rajasekhar, Kakarlapudi, and Bhamra 2002)[103]	0	0	1	2	1	2	2	1	4	0	13	24	54%
(Singh and Pooley 2002)[116]	1	2	1	3	1	2	2	1	4	0	17	24	71%
(Toczylowski et al. 2002)[128]	1	0	1	3	1	1	2	3	3	0	15	24	63%
(Michael James DePalma MD 2004)[25]	0	3	1	3	1	2	1	3	3	0	17	24	71%
(Maehara and Sakaguchi 2004)[79]	1	0	1	1	1	2	2	4	3	0	15	24	63%
(Mellado et al. 2004)[86]	1	1	1	2	1	2	1	4	4	0	17	24	71%
(Warme and Whitaker 2004)[138]	1	2	1	4	1	2	2	1	4	1	19	24	79%
(Giuffre and Lisle 2005)[46]	0	2	0	2	1	2	1	0	4	0	12	24	50%
(Wang et al. 2005)[137]	1	3	0	2	1	2	1	2	4	0	16	24	67%
(Kankaya et al. 2006)[67]	0	1	0	2	1	2	2	1	1	0	10	24	42%
(Mechrefe, Walsh, and DiGiovanni 2006)[85]	1	0	1	2	1	2	2	3	4	0	16	24	67%
(Rochman, SanGiovanni, and Uribe 2006)[104]	1	0	0	2	1	2	1	1	2	0	10	24	42%
(Sierra et al. 2006)[113]	1	0	1	3	1	2	2	4	3	0	17	24	71%
(Gidwani and Bircher 2007)[45]	1	3	1	2	1	1	2	1	4	1	17	24	71%
(Kibuule and Fehringer 2007)[71]	1	0	1	2	1	2	2	1	4	0	14	24	58%
(Nishida et al. 2007)[93]	1	3	1	2	1	2	1	3	4	0	18	24	75%

Table B.6 - continued

Author	CARE items												
	1	**3**	**4**	**5**	**6**	**8**	**9**	**10**	**11**	**13**	**TOTAL**	**Max Score**	**% Score**
(Levine and Savoie III 2008)[76]	0	0	1	4	1	2	2	1	4	0	15	24	63%
(Schache et al. 2008)[108]	1	4	1	2	1	2	2	2	4	0	19	24	79%
(Winblad, Escobedo, and Hunter 2008)[143]	0	0	1	2	1	2	0	0	2	0	8	24	33%
(Shah, Montgomery, and Bastidas 2009)[109]	0	0	1	2	1	2	2	2	4	0	14	24	58%
(Floor, Van Der Veen, and Devilee 2010)[39]	0	4	1	4	1	2	2	2	4	0	20	24	83%
(Hasegawa and Schofer 2010)[53]	1	4	1	2	1	2	1	1	4	0	17	24	71%
(Pitts, Garner, and Ortiguera 2010)[100]	1	0	1	2	1	2	1	3	4	0	15	24	63%
(Jansen, Cormier, and Patel 2012)[65]	1	0	1	2	1	2	2	3	4	1	17	24	71%
(Khiami et al. 2012)[70]	0	4	1	2	1	2	2	3	4	0	19	24	79%
(Yoon et al. 2012)[144]	1	0	1	2	1	2	2	3	4	0	16	24	67%
(Hart 2013)[52]	0	0	0	2	1	1	2	2	0	0	8	24	33%
(Naito et al. 2013)[91]	1	3	1	1	1	2	1	2	3	0	15	24	63%
(Valente, Mancuso, and Alecci 2013)[131]	0	3	1	2	1	2	2	2	4	0	17	24	71%
(Benazzo, Marullo, and Pietrobono 2014)[10]	0	1	1	3	1	2	2	3	1	1	15	24	63%
(Huri et al. 2014)[61]	1	4	1	2	1	2	2	2	4	1	20	24	83%
(Sharma et al. 2014)[110]	0	3	1	2	1	2	2	2	4	0	17	24	71%
(Bunshah et al. 2015)[13]	0	4	1	3	1	2	2	3	4	1	21	24	88%
(Cetinkaya et al. 2015)[17]	0	4	1	2	1	2	2	1	4	1	18	24	75%
(Fitzpatrick, Cagle, and Flatow 2016)[37]	1	2	0	2	1	1	2	2	4	0	15	24	63%
(Jaiswal et al. 2016)[64]	1	2	1	2	1	1	2	2	4	0	16	24	67%

C

Table C.1 - Characteristics of the included laboratory studies.

Author	no. of specimens	Model	Study Design	Muscle/Tendon (proportion)	Injury Site (proportion)	Major Findings
(Garrett et al. 1987)[43]	48	New Zealand White Rabbit	EDL stretched to failure: passive and stimulated at 64 Hz, at 16 Hz	EDL (1.00)	MTJ (1.00)	> UTF in stimulated muscles; No difference in UTD ; All EDL tear at MTJ
(Garrett et al. 1988)[42]	198	New Zealand White Rabbit	Five architecturally different muscles stretched to failure at different strain rates	EDL (0.18) TA(0.18) P(0.40) RF(0.14) GST(0.09)	MTJ (1.00)	All muscles fail at MTJ; rate of stretch doesn't influence site of injury; UTS > muscles with more pennate structure
(Taylor et al. 1993)[125]	24	New Zealand White Rabbit	Control EDLs stretched to failure. Tested EDLs subjected to nondisruptive stretch (prior to failure of the control) followed by stretch until failure	EDL (1.00)	MTJ (1.00)	Nondisruptive injury lowered 37% the UTF and 21% the UTD compared with controls. Histology showed incomplete disruptions at MTJ.
(Noonan et al. 1994)[94]	56	New Zealand White Rabbit	Control EDLs and TAs stretched to failure. Passive stretch of EDLs and TAs to 20% and 30% of the control UTF followed by stretch until failure.	EDL (0.50) TA (0.50)	MTJ (1.00)	Histology of injury at 30% UTF show areas of fiber rupture and hemorrhage near the MTJ. Failure parameters not influenced by neither 20% or 30% UTF injury.
(Sun et al. 1994)[122]	48	New Zealand White Rabbit	GST muscles stretched to failure at different strain rates.	TS (1.00)	M, within 0.1-30mm of the MTJ (1.0)	Muscle-tendon units show viscoelastic behaviour. All failures occur at or near the MTJ independently of strain rate. > UTF with faster strain rates.
(Gottsauner-Wolf et al. 1995)[49]	20	Adult Mongrel Dogs	SP were stretched to failure at 10 cm/sec	SP (1.00)	MTJ (1.00)	All SP fail at MTJ; Histology show loss of intracellular staining capacity to Masson's stain, tears and cracks disrupting the intracellular structures, and loss of striation.
(Hasselman et al. 1995)[54]	204	New Zealand White rabbits	Control EDLs and TAs actively stretched to failure. Active stretch of EDLs and TAs to 60%, 70%, 80% and 90% of the UTF of the ipsilateral control	EDL (0.50) TA (0.50)	MTJ (1.00)	Histology in the 70% group showed focal hemorrhage at the distal MTJ in both muscles. In the 80% and 90%, hemorrhage occurred at the distal MTJ and in muscle fibers near the MTJ. 60% histology showed no damage, 70% showed hemorrhage, acute inflammatory cells, edema, and focal muscle fiber disruption. 80% and the 90% groups showed hemorrhage and a number of lightly stained fibers and more spread damage.

Table C.1 - continued

Author	no.of specimens	Model	Study Design	Muscle/Tendon (proportion)	Injury Site (proportion)	Major Findings
(Law, Caputo, and Tidball 1995)[74]	14	Mouse	EDLs stretched passively and actively to failure at 2cm/s	EDL (1.00)	M, near MTJ (1.00)	No significant difference in UTS and UTSS between active and passive EDLs. Muscle fibers failed transversely
(Mair et al. 1996)[81]	96	New Zealand White Rabbit	Control EDLs stretched to failure. EDLs were fatigued by setting the muscle to the length of maximal isometric tetanic force until force dropped 25% or 50%, followed by stretch until failure.	EDL (1.00)	NR	Fatigued muscles absorb less 8-31% energy than control muscles. UTD did not change between control and fatigued EDLs.
(Sano et al. 1997)[107]	31	Cadaveric Human (mean age 62 yo)	SPT was divided in 3 strips and the middle strip was loaded to failure at 25.4 mm/s.	SPT (1.00)	TB (0.65) T (0.35)	Degenerative changes at the SPT insertion reduce its tensile strength. Histology on tested specimens showed that thin fibers on the articular side of the supraspinatus tendon seemed to contribute to the disruption of fibers. 10 of 20 strips showed avulsion of tendon fibers at the sites of granulation tissue
(Tsuang et al. 1998)[129]	60	New Zealand White Rabbit	TS of one limb was cyclically loaded for one hour at a rate of 0.5cm/min to 12, 20 and 25% strain. After, it was loaded at 0.5cm/min until failure. The TS of the other limb was stretched to failure at 0.5cm/min.	TS (1.00)	0.1-1mm of MTJ in SL, 5-10mm of MTJ in GST lateral head, 15-30mm of MTJ in GST medial head	UTD is affected by cyclic stretches at 20%. Load-deformation curve significantly change for cyclic stretches of 25%. After 60 min cyclic stretch at 25% strain, UTF decreased 10%, UTD decreased 20% and the slope of load-deformation increased 28%. Injury can be reproduced at 25% strain of the TS muscle tendon unit.

M: muscle belly; MTJ: musculotendinous junction ; T: tendon ; TB: tendon-bone ; UTF: ultimate tensile force; UTD: ultimate tensile displacement; UTS: ultimate tensile strain ; UTSS: ultimate tensile stress
EDL: extensor digitorum longus ; P: peroneus; RF: rectus femoris; GST: gastrocnemius; TA: tibialis anterior; SP: supraspinatus ; SPT: supraspinatus tendon ; TS: triceps surae ; SL: soleus ; ACT: achilles tendon

D

Table D.1 - Characteristics of the included observational studies.

Author	No. of patients	Age	No. patients surgery (proportion)	Relevant conditions (proportion)	Muscle or Tendon (proportion)	Injury Site (proportion)	Diagnosis (proportion)	Activity at injury (proportion)	Common injury symptoms
(Wenger 1973)[140]	4	17.8 ± 0.5	4 (1.00)	NR	PT (1.00)	AV (1.00)	X-ray (0.5), surgery (1.00)	American football (1.00)	inability to flex distal interphalangeal joint
(Kawashima et al. 1975)[69]	2	25.5 ± 3.5	2 (1.00)	NR	PM (1.00) LD (0.5)	M (0.5) MTJ (1.0)	X-ray (0.5), surgery (1.00)	work accident (1.00)	both M and MTJ injuries showed tenderness, palpable gap and hematoma
(Shields and Ashby 1975)[112]	2	20.5 ± 12.0	2 (1.00)	NR	PAT (1.00)	AV (1.00)	X-ray (1.00) and surgery (1.00)	high jump (1.00)	swelling of the knee
(Miller 1977)[89]	6	45.3 ± 9.7	2 (0.33)	NR	GST (1.00)	MTJ (1.00)	physical examination, surgery (1.00)	tennis: sudden dorsiflexion of the ankle with knee extended (1.00)	Defect in the medial head of the GST, palpable and tender, and small mass
(Durig et al. 1977)[29]	19	49.0 (33-64)	12 (0.63)	NR	GST (1.00)	MTJ (1.00)	physical examination, surgery (1.00)	maximal dorsiflexion of the foot with full extension of the knee (1.00)	Palpable dehiscence in the MTJ; proximal displacement of the medial head of the GST; decreased muscle tone; hematoma and edema
(Bowers 1981)[12]	1	13.0	1 (1.00)	Osgood-Schlatter's disease (1.00)	PAT (1.00)	AV (1.00)	X-ray (1.00), surgery (1.00)	basketball (1.00)	inability to extend the knee, swelling
(Farrar et al. 1981)[33]	3	48 ± 16.2	2 (0.67)	chronic renal failure (0.33)	TT (1.00)	AV (1.00)	X-ray (1.00), surgery (1.00)	car accident (0.33) fall (0.67)	swelling; palpable depression proximal to the olecranon; flecks of avulsed osseous material.
(Smith 1981)[117]	1	36.0	1 (1.00)	NR	PT (1.00)	AV (1.00)	X-ray (1.00), surgery (1.00)	fall (1.00)	swelling, inability to flex distal joint
(Vastamäki, Brummer, and Solonen 1981)[133]	5	47 ± 10.7	5 (1.00)	NR	BT (1.00)	AV (1.00)	surgery (1.00)	skiing (0.2), lift heavy load (0.4), teaching gymnastic (0.2), exercise on horizontal bar (0.2)	diminish forearm flexion or supination, hematoma

Table D.1 - continued

Author	No. of patients	Age	No. patients surgery (proportion)	Relevant conditions (proportion)	Muscle or Tendon (proportion)	Injury Site (proportion)	Diagnosis (proportion)	Activity at injury (proportion)	Common injury symptoms
(Ferretti et al. 1983)[35]	15	22.1 ± 2.4	15 (1.00)	anabolic steroid injections (0.33)	PAT (0.78) QT (0.22)	TB (1.00)	NR	volleyball (0.6), basketball (0.2), high jump (0.07), soccer (0.07), ballet (0.07)	tenderness over patellar insertion of the PAT or the QT
(Aso and Torisu 1984)[5]	2	32 ± 5.7	1 (0.5)	NR	TR (1.00)	M (1.00)	X-ray (1.00), surgery (0.50), CT (0.5)	kendo (0.5), volleyball (0.5)	palpable soft mass in the posterior part of the arm, tenderness, hematoma
(Sherman, Snyder, and Fox 1984)[111]	1	34.0	1 (1.00)	professional body builder	TT (1.00)	AV (1.00)	X-ray (1.00), surgery (1.00)	fall: strike on the wall (1.00)	swelling, retraction of the TT insertion
(Ferretti et al. 1985)[36]	110	NR	15 (0.14)	steroid injections (NR). All patients are athletes	PAT (0.65) QT (0.25) TBT (0.10)	TB (1.00)	X-ray, physical examination (1.00)	sports activity (1.00). Specifics NR	local tenderness, localized puffiness
(White and Riley Jr. 1985)[141]	1	12.0	1 (1.00)	NR	SCT (1.00)	AV (1.00)	X-ray (1.00)	climbing a wall (1.00)	avulsion of bone fragment, tenderness at the anterior part of the glenohumeral region
(Andersen 1986)[2]	1	44.0	1 (1.00)	NR	TT (1.00)	AV (1.00)	X-ray (1.00), surgery (1.00)	parachute landing on outstretched arm (1.00)	tenderness around the elbow, fragments of bone at medial epicondyle of the humerus and small fragment proximal to the olecranon
(Bach, Warren, and Wickiewicz 1987)[6]	1	33.0	1 (1.00)	anabolic steroid injections (1.00)	TR (1.00)	MTJ (1.00)	physical examination (1.00), surgery (1.00)	weightlifting (1.00)	palpable defect and scar formation at MTJ
(de Waal Malefijt and Beeker 1987)[28]	1	66.0	1 (1.00)	renal insufficiency treated with hemodialysis	TT (1.00)	AV (1.00)	physical examination (1.00), surgery (1.00)	NR	ecchymosis and subcutaneous soft tissue defect, degeneration of the distal end of the tendon, calcification
(Clay 1988)[18]	1	24.0	1 (1.00)	NR	ED (1.00) EIT (1.00)	MTJ (1.00) AV (1.00)	surgery (1.00)	work accident (1.00)	inability to extend index finger, tender lump, mass on the back of the hand
(Nimityongskul, Montague, and Anderson 1988)[92]	8	15.7 (14.2-16.4)	7 (0.88)	Osgood-Schlatter's disease (0.75)	TBT (1.00)	AV (1.00)	NR	NR	NR

Table D.1 - continued

Author	No. of patients	Age	no. patients surgery (proportion)	Relevant conditions (proportion)	Muscle or Tendon (proportion)	Injury Site (proportion)	Diagnosis (proportion)	Activity at injury (proportion)	Common injury symptoms
(Fleckenstein et al. 1989)[38]	19	NR	0 (0.00)	N	lower extremities (specific muscle and proportion NR)	MTJ (0.52)	Positive MRI (1.00)	running a 30k race (0.52)	Signs of hemorrhage and edema
(Menz and Nettle 1989)[87]	1	16.0	1 (1.00)	fracture of the distal tibial shaft 4 years prior to MTJ injury (1.00)	EHL (1.00)	MTJ (1.00)	physical examination (1.00), surgery (1.00)	football (1.00)	inability to extend the toe, ischaemic changes in the muscle and central fibrous tissue
(Gruel 1990)[50]	2	15.5 ± 0.7	2 (1.00)	NR	POPT (1.00)	AV (1.00)	physical examination, X-ray, surgery (1.00)	skiing (0.5) American football (0.5)	small bone fragment in the region of the lateral condyle, tense or large effusion, hemarthrosis
(de Roos and Zeeman 1991)[26]	1	20.0	1 (1.00)	N	FPT (1.00)	T (1.00)	physical examination, surgery (1.00)	fight (1.00)	swelling at the palm of the hand, absence of function of the small finger
(Farley et al. 1992)[32]	100	56.0	100 (1.00)	N	NR (0.70), SPT (0.18), SPT, TMT and IPT (0.09), SCT (0.04)	T (0.30)	MRI (1.00), surgery (1.00)	NR	muscular atrophy, retraction of the MTJ, subacromial fluid, tendinous thinning, for full thickness tears of SPT, SPT and TMT/IPT and SCT (0.3). Tendinitis, tendon degeneration, partial thickness tear of RC (0.7)
(Pomeranz and Heidt 1993)[102]	14	(20-29)	NR	professional athletes	QF (0.14) BF (0.43) SM (0.36) ST (0.07)	MTJ (0.43) M (0.5) T (0.07)	MRI (1.00)	professional athletes (1.00) specific sport NR	M injuries showed edema and hemorrhage, MTJ showed fluid collections.
(Speer, Lohnes, and Garrett 1993)[120]	50	28.0 (17-42)	NR	N	ADL (0.26) BF (0.22) RF (0.20) GST (0.20) SM (0.08) ST (0.04)	MTJ (1.00)	Positive MRI (0.46) Positive CT scan (0.54)	NR	Consistently seen inflammation and edema. CT showed signs of hemorrhage and proximal retraction
Tiger, Mayer, and Glazer 1993)[127]	1	52.0	1 (1.00)	NR	TT (1.00)	AV (1.00)	MRI (1.00)	fall (1.00)	tenderness, edema, tendon retraction, hemorrhage
(Goodier, Maffulli, and Good 1994)[48]	1	18.0	1 (1.00)	N	PAT (1.00)	AV (1.00)	X-ray (1.00), surgery (1.00)	soccer (1.00)	hemarthrosis, avulsion of bone fragment, palpable defect at TBT site

Table D.1 - continued

Author	No. of patients	Age	no. patients surgery (proportion)	Relevant conditions (proportion)	Muscle or Tendon (proportion)	Injury Site (proportion)	Diagnosis (proportion)	Activity at injury (proportion)	Common injury symptoms
(Yoshioka et al. 1994)[145]	7	22.7 ± 4.8	NR	well trained athletes	BF (0.71) RF (0.14) RF and VM (0.14)	MTJ (0.86) M (0.29)	Positive MRI (1.00)	sprinting (0.43) high jump (0.14) long jump (0.14) tennis (0.14) basketball (0.14)	Fan like lesion in MTJ and signs of hemorrhage and tissue edema
(Hughes et al. 1995)[60]	10	22.7 ± 7.6	2 (0.20)	N	RF (1.00)	MTJ (1.0)	Positive MRI (0.8) Positive CT scan (0.3)	sprinting (0.70) placekicking (0.10) NR (0.20)	Palpable mass of soft tissue in RF; The mass appears as a bull's eye with a round enhancing mass centered about the intramuscular tendon of the indirect head. Proximal retraction of the torn muscle fibers
(Simonet, Saylor III, and Sim 1995)[115]	10	25.5 (28-32)	10 (1.00)	professional hockey players	IAB (1.00)	MTJ (1.00)	physical examination (1.00), surgery (1.00)	ice hockey (1.00)	tenderness along the internal inguinal ring and/or along the floor of the inguinal canal
(Takami et al. 1995)[124]	10	30.2 ± 15.8	8 (0.80)	N	EDC (0.7) EIP (0.4) EPL (0.1)	MTJ (1.00)	physical examination (1.00), surgery (1.00)	work accident (0.5) gymnastic (0.4) judo (0.1)	tenderness on the dorsum of the forearm, loss of extension at the metacarpophalangeal joint of the finger.
(Butcher, Siekanowicz, and Pettrone 1996)[14]	2	24.5 ± 5.0	2 (1.00)	N	PMT (1.00)	AV (1.00)	surgery (1.00)	bench press (1.00)	soft tissue mass on the anteromedial chest wall with ecchymosis, weakness in adduction forward lesion and internal rotation
(Ohashi et al. 1996)[95]	4	25.0 ± 2.5	1 (0.25)	NR	PM (1.00)	MTJ (1.00)	MRI (0.75) CT (0.25)	bench press (0.75) wrestling (0.25)	ecchymosis, palpable defect in the region of the PMT, retraction of the muscle belly, hematoma
(Wagner and Cooney 1997)[135]	1	61.0	1 (1.00)	Insulin dependent diabetes (1.00)	TR (1.00)	MTJ (1.00)	X-Ray (1.00), MRI (1.00), surgery (1.00)	rollerskating (1.00)	palpable defect in the distal third of the posterior aspect, nodular mass near TT, calcific pseudocapsule
(Asinger and el-Khoury 1998)[4]	2	73.0 ± 10.6	0 (0.00)	N	TFL (1.00)	MTJ (1.00)	MRI (1.00)	fall (0.50) NR (0.50)	palpable soft tissue mass on the anterolateral pelvis, retracted muscle
(Canovas, Nicolau, and Bonnel 1998)[15]	1	28.0	1 (1.00)	chondroma of the distal phalange (1.00)	FPT (1.00)	AV (1.00)	X-ray (1.00), surgery (1.00)	lifting a plate (1.00)	swelling, ecchymosis, no active flexion at the distal interphalangeal joint. Small bone fleck and tendon retraction

Table D.1 - continued

Author	No. of patients	Age	no. patients surgery (proportion)	Relevant conditions (proportion)	Muscle or Tendon (proportion)	Injury Site (proportion)	Diagnosis (proportion)	Activity at injury (proportion)	Common injury symptoms
(Evans, Bowrey, and Newman 1998)[31]	4	32.8 ± 4.3	4 (1.00)	anabolic steroid injections (0.50)	BT (0.67) TT (0.33)	AV (0.5) T (0.5)	surgery (1.00)	fall (0.25) weightlifting (0.25) rugby (0.25) lifting container (0.25)	NR
(Hertel and Lambert 1998)[56]	1	34.0	1 (1.00)	NR	SP (0.5) IPT (0.5)	MTJ (0.50) AV (0.50)	X-ray (1.00), MRI (1.00), surgery (1.00)	fall (1.00)	fragment of bone above the posterosuperior glenoid rim, muscle retraction and atrophic
(Maffulli 1998) [80]	174	40.1 ± 13.2	133 (0.76)	NR	ACT (1.00)	T (1.00)	physical examination (1.00), surgery (1.00)	NR	minimal or absent plantar flexion when squeezing the calf muscles, hematoma
(Sollender, Rayan, and Barden 1998)[118]	4	42.0	4 (1.00)	oral anabolic steroids (1.00), tendinopathy (0.5)	TT (1.00)	AV (1.00)	surgery (1.00), X-ray (0.25)	softball (0.25), weightlifting (0.75)	resisted elbow extension, bone flake on lateral radiographs
(Takami et al. 1998)[123]	1	23.0	1 (1.00)	NR	FPL (1.00)	MTJ (1.00)	physical examination, surgery (1.00)	bowling (1.00)	ecchymosis, tenderness, complete loss of active flexion at the interphalangeal tenderness of the thumb
(Temple et al. 1998)[126]	7	31.9 ± 21.3	0 (0.00)	NR	RF (1.00)	MTJ (1.0)	Positive MRI (1.00)	sprinting (0.14) running (0.14) football (0.14) soccer (0.14) golf (0.14) softball (0.28)	Mass at the MTJ of the RF. Tissue biopsy confirmed chronic inflammation and reactive fibrosis. Proximal and distal retraction. edema along the fascial plane.
(Connell et al. 1999)[20]	15	28.3 ± 4.4	8 (0.53)	NR	PM (0.4) PMT (0.6)	MTJ (0.40) TB (0.60)	Positive MRI (1.00)	weightlifting (0.6) football (0.13) wrestling (0.07) fall from ladder (0.07) lifting a heavy object (0.07)	Palpable defect on PM and asymmetry of the muscle. Acute injuries demonstrated edema and hemorrhage and chronic injuries showed scarring and fibrosis
(Carrino et al. 2000)[16]	10	26.9 ± 5.9	6 (0.6)	NR	PMT (0.70) PM (0.20) N (0.1)	TB (0.70) MTJ (0.20)	MRI (1.00) surgery (0.6)	bench press (0.9) helicopter accident (0.1)	Both MTJ and TB showed edema, hematoma and retraction
(Cooper and Selesnick 2000)[21]	2	24.0 ± 4.2	2 (1.00)	tendinosis (0.5) Osgood-Schlatter disease (0.5)	PAT (1.00)	TB (1.00)	MRI (1.00) surgery (1.00)	jai alai (0.5) basketball player banged the knee on a car door (0.5)	localized tenderness over the PAT insertion, bone edema

Table D.1 - continued

Author	No. of patients	Age	no. patients surgery (proportion)	Relevant conditions (proportion)	Muscle or Tendon (proportion)	Injury Site (proportion)	Diagnosis (proportion)	Activity at injury (proportion)	Common injury symptoms
(De Smet and Best 2000)[27]	15	(18-22)	NR	college athletes	BF (0.40) BF and ST (0.33) ST (0.20) SM (0.07)	MTJ (0.47) M (0.53)	positive MRI (1.00)	football (0.27) hockey (0.07) long jump and triple jump (0.47) track (0.20)	Featherlike pattern of edema surrounding the MTJ; hematoma in injury site; high frequency of perifascial fluid
(Henry and Scerpella 2000)[55]	1	42.0	1 (1.00)	N	LDT (1.00)	AV (1.00)	surgery (1.00)	water sky (1.00)	soft tissue swelling and palpable tender mass in the posterior axilla, no bony fragment, tendon retraction
(Kameyama and Shiraishi 2000)[66]	1	49.0	1 (1.00)	non-insulin dependent diabetes (1.00)	ED (1.00) EDM (1.00)	MTJ (1.00)	X-ray (1.00), surgery (1.00)	work accident (1.00)	swelling of the wrist, volar dislocation of the distal radioulnar joint
(Karjalainen et al. 2000)[68]	100	33.0 (15-58)	28 (0.28)	N	ACT (1.00) SL (0.03)	T (0.54) TB (0.28) MTJ (0.02)	MRI (1.00)	competitive or recreational sports (1.00)	thickening of the Achilles tendon in the anteroposterior, direction, intratendinous lesion, inflammation, edema
(Panni, Tartarone, and Maffulli 2000)[96]	42	24.4 (18-32)	9 (0.21)	N	PAT (1.00)	TB (1.00), T (0.67)	X-ray (1.00) ultrasonographic evaluation (1.00)	amateur volleyball (0.5) semi professional basketball (0.31) amateur soccer (0.17) parachutist (0.02)	local tenderness on palpation of the PAT with the knee fully extended and at the lower pole of the PAT, hypotrophy of the QD, ossification of the fibrocartilaginous zone in TB, fibrillation and loss of the normal tendinous crimp
(Street and Burks 2000)[121]	1	39.0	1 (1.00)	HS injury at 20 yo playing college football and at 38 years old playing baseball	ST, SM, BF (1.00)	AV ITB (1.00)	MRI (1.00) surgery	moving heavy boxes (1.00)	palpable defect in the proximal HS tendon ~6-8cm below the ischial tuberosity. Muscle retraction.
(Rose and Frassica 2001)[106]	1	30.0	1 (1.00)	systemic lupus erythematosus and fibromyalgia. Prednisone (20 mg/day) (1.00)	PAT (1.00)	T (1.00)	surgery (1.00)	standing (1.00)	bilateral knee effusion, tenderness, absence of active knee. Ruptured tendons in midsubstance, thin and attenuated

Table D.1 - continued

Author	No. of patients	Age	no. patients surgery (proportion)	Relevant conditions (proportion)	Muscle or Tendon (proportion)	Injury Site (proportion)	Diagnosis (proportion)	Activity at injury (proportion)	Common injury symptoms
(Tung et al. 2001)[130]	16	56.0 (33-74)	16 (1.00)	N	SCT (1.00) SPT (0.69) IPT (0.19)	T (1.00)	MRI (1.00) surgery (1.00)	NR	Medial luxation or subluxation and tendinopathy of BT, tear of the superior glenoid labrum, or fluid within either or both the superior subscapularis recess or subcoracoid bursa
(Weishaupt, Schweitzer, and Morrison 2001)[139]	20	47.0 (14-66)	0 (0.00)	N	GST (0.96) ACT (0.04)	MTJ (0.96) T (0.04)	MRI (1.00)	basketball/tennis/running (0.5) stepping out of car/bus/bed (0.3) walking/hiking (0.15) running away from an assault (0.05)	MTJ injuries showed V shaped hematoma, M belly retraction,
(Williams et al. 2001)[142]	20	50.0 (35-77)	3 (0.15)	N	BT (1.00)	T (0.5) AV (0.5)	MRI (1.00) surgery (0.15)	NR	bursitis, marrow edema
(Bass and Connell 2002)[8]	12	33.1 ± 9.5	1 (0.08)	NR	TFL origin (1.00)	TB (0.92) AV (0.08)	sonograms (1.00)	running (0.67) tennis (0.17) walking (0.08) triathlon (0.08)	anterior groin pain, point tenderness over anterior iliac crest, TFL origin enlarged.
(Bianchi et al. 2002)[11]	17	26.0	0 (0.00)	N	RF (1.00)	MTJ (1.00)	physical examination (1.00) MRI (0.47) sonograms (1.00)	sprinting or kicking football ball (NR)	RF exquisitely tender to deep palpation in proximal portion. Bull's eye appearance in central aponeurosis. Smaller lesions showed hemorrhagic infiltration, more severe included also hematoma and complete tear showed fluid collection between retracted muscle and central aponeurosis.
(Pina, Garcia, and Sabater 2002)[99]	1	43.0	1 (1.00)	corticosteroids treatment for allergic asma	TT (1.00)	AV (1.00)	physical examination, x-ray, surgery (1.00)	fall with extended arm (1.00)	swelling in the elbow, palpable depression proximal to the olecranon, flake of bone seen in x-ray, retraction of the proximal end of the tendon
(Rajasekhar, Kakarlapudi, and Bhamra 2002)[103]	1	42.0	1 (1.00)	NR	TT (1.00)	AV (1.00)	physical examination, x-ray, surgery (1.00)	fall (1.00)	diffuse swelling and tenderness in the elbow, palpable gap just above the olecranon, flake fracture of the olecranon,

Table D.1 - continued

Author	No. of patients	Age	no. patients surgery (proportion)	Relevant conditions (proportion)	Muscle or Tendon (proportion)	Injury Site (proportion)	Diagnosis (proportion)	Activity at injury (proportion)	Common injury symptoms
(Singh and Pooley 2002)[116]	1	31.0	1 (1.00)	N	TR (1.00)	M (1.00)	physical examination, surgery (1.00)	professional ice hockey, direct hit by a stick (1.00)	palpable gap in the substance of the TR muscle, edema, muscle retraction
(Sonnery-Cottet et al. 2002)[119]	51	50.8 (35 - 67)	51 (1.00)	NR	SPT (0.69), SPT and IPT (0.22), SPT and SCT (0.10) BT (0.16)	T (1.00)	x-ray, CT (1.00)	recreational tennis (0.63) competitive tennis (0.37)	progressive symptoms in 29 patients (0.57) and traumatic in 22 (0.43). Pain during day and night, pseudoparalytic shoulder
(Toczylowski et al. 2002)[128]	2	65.0 ± 9.9	1 (0.5)	N	BT (1.00)	AV (1.00)	physical examination (1.00) surgery, MRI (0.50)	competitive ice dancer (0.5) recreational tennis (0.5)	tenderness, swelling, extensive ecchymosis, soft tissue defect just proximal to the antecubital fossa
(Connell, Jhamb, and James 2003)[19]	10	27.9 ± 4.6	0 (0.00)	N	IAB (1.00)	M (1.00)	MRI (1.00) sonography (0.1)	cricket (0.7) javelin thrower (0.1) golf (0.1) row (0.1)	edema, hemorrhage, hematoma tracking between myofascial coverings of internal and external oblique muscle. Fibrosis and scar tissue at follow up
(Kim, Rauh, and McFarland 2003)[73]	314	44.5 ± 17.3	314 (1.00)	N	SCT (0.19) SPT (0.58) IPT (0.06) BT (0.28)	T (1.00)	physical examination, arthroscopy (1.00)	sports (0.58) fall (0.12) NR (0.3)	activity, rest and night pain, weakness and lack of strength, limitation in throwing
(Mansat, Frankle, and Cofield 2003)[83]	22	56.5 ± 10.2	22 (1.00)	NR	SCT (0.13) SCT and SPT (0.26) SCT, SPT and IPT (0.61)	T (1.00)	X-ray (1.00) physical examination (1.00)	fall with extended arm (0.43) NR (0.57)	rest and night pain, functional impairment, motion range limitation, weakness
(Äärimaa et al. 2004)[1]	33	28.1 ± 6.7	33 (1.00)	anabolic steroid (0.36)	PM (0.33) PMT (0.67)	AV (0.30) T (0.36) MTJ (0.33)	X-ray (1.00) ultrasound (0.73) MRI (0.09)	powerlifting (0.36) bench press (0.27) bodybuilding (0.09) workout (0.09) gymnastics (0.03) ice hockey (0.03) horse pulled (0.03) getting out of pool (0.03) work injury (0.03) parachute (0.03)	pain, weakness
(Cross et al. 2004)[23]	18	24.4 ± 3.3	0 (0.00)	N	RF (0.68) VI (0.27) VL (0.05)	MTJ (0.55) M (0.45)	Positive MRI (0.88)	australian rules football (1.00)	Maximal tenderness on the midline of the anterior thigh; Maximal tenderness often ~3 cm from the site of maximal MRI muscle injury. edema, hemorrhage and muscle detritus

Table D.1 - continued

Author	No. of patients	Age	no. patients surgery (proportion)	Relevant conditions (proportion)	Muscle or Tendon (proportion)	Injury Site (proportion)	Diagnosis (proportion)	Activity at injury (proportion)	Common injury symptoms
(Michael James DePalma MD 2004)[25]	1	34.0	1 (1.00)	PAT tendinopathy (1.00)	PAT (1.00)	AV (1.00)	X-ray, physical examination (1.00)	recreational basketball (1.00)	large effusion and palpable gap in the PAT. Inability to extend the knee. PAT alta with avulsed bone fragments
(Maehara and Sakaguchi 2004)[79]	1	26.0	1 (1.00)	N	GST origin (1.00)	AV (1.00)	X-ray, physical examination, CT, MRI (1.00)	ski (1.00)	tenderness over the proximal and posterior part of the medial condyle of the femur, bone fragment in the popliteal space
(Mellado et al. 2004)[86]	2	42.5 ± 9.2	2 (1.00)	N	PMT (0.5) PM (0.5)	AV (0.5) M (0.5)	physical examination, MRI, surgery (1.00)	fall (0.50) bench press (0.50)	soft tissue edema, loss of axillary fold, AV injury showed local ecchymosis
(Warme and Whitaker 2004)[138]	1	34.0	1 (1.00)	recreational weightlifter (1.00)	PMT (1.00)	AV (1.00)	physical examination, surgery (1.00)	rappel (1.00)	ecchymosis on the medial aspect of proximal humerus, swelling and palpable bulge within M belly, tender to palpation.
(Giuffre and Lisle 2005)[46]	1	42.0	1 (1.00)	NR	BT (1.00)	T (1.00)	physical examination, ultrasound, surgery (1.00)	moving heavy crates (1.00)	local bruising in the antecubital fossa, hematoma
(Wang et al. 2005)[137]	1	52.0	1 (1.00)	engaged sports every day (1.00)	PM (1.00)	MTJ (1.00)	Ultrasound, MRI (1.00)	pulled out of a river by the arm (1.00)	swelling of chest wall, hematoma, muscle retraction
(Freccero and Berkowitz 2006)[40]	29	28.0	29 (1.00)	NR	PBT (1.00)	T (1.00)	surgery (1.00)	NR	NR
(Kankaya et al. 2006)[67]	1	11.0	1 (1.00)	N	FPT (1.00)	AV (1.00)	surgery (1.00)	explosion of a firework (1.00)	tender and edematous hand
(Mechrefe, Walsh, and DiGiovanni 2006)[85]	1	32.0	1 (1.00)	N	TBLT (1.00)	AV (1.00)	X-ray (1.00) surgery (1.00)	car accident (1.00)	weak dorsiflexion of the foot,
(Rochman, SanGiovanni, and Uribe 2006)[104]	1	19.0	0 (0.00)	N	PL (1.00) PB (1.00)	M (1.00)	physical examination (1.00), MRI (1.00), surgery (1.00)	running in american football practice (1.00)	diffuse edema was present along the anterolateral aspect of the leg, lower extremity nontender to palpation. After exercise-induced showed fusiform swelling and tenderness to palpation. MRI showed edema.

Table D.1 - continued

Author	No. of patients	Age	no. patients surgery (proportion)	Relevant conditions (proportion)	Muscle or Tendon (proportion)	Injury Site (proportion)	Diagnosis (proportion)	Activity at injury (proportion)	Common injury symptoms
(Sierra et al. 2006)[113]	15	50.3 ± 16.5	11 (0.73)	anabolic steroid (0.07), septic olecranon/bursitis (0.13)	TT (0.93) TR (0.07)	AV (0.81), T (0.125), M (0.0625)	physical examination (1.00), surgery (0.73)	pulling on cord (0.07), direct blow (0.33), fall (0.27), transferring from wheelchair to bed (0.07), car accident (0.07), getting up from chair (0.07), extend elbow (0.07), NR (0.07)	palpable defect just proximal to the olecranon.
(Gidwani and Bircher 2007)[45]	12	21.3 ± 11.6	0 (0.75)	N	HST (1.00)	AV (1.00)	physical examination (1.00), X-ray (1.00), MRI (1.00), surgery (0.75)	martial arts (0.25), soccer (0.17), gymnastics (0.08), sprinting (0.08), rugby (0.08), ski jump (0.08), running (0.08), tennis (0.08), waterskiing (0.08)	wasting of the HS, palpable gap at the HS origin,
(Ilaslan, Iannotti, and Recht 2007)[62]	24	73.0 (54-87)	3 (0.13)	subacromial steroid injections (0.25), systemic steroid use (0.13)	DLT (1.00) SPT, IPT and SCT (0.42) SPT and IPT (0.5) , SPT (0.08))	MTJ in DLT (0.79) TB in DLT (0.21) T in RC (1.00)	MRI (1.00)	NR	RC atrophy, sub-cutaneous fluid, edema, tendon retraction in case of AV injury
(Irmola et al. 2007)[63]	5	22.8 ± 3.5	5 (1.00)	NR	RF tendon of the direct head	AV (1.00)	MRI (1.00), ultrasound (1.00), X-ray (0.4)	soccer (0.8), track (0.2)	sudden and sever pain in anterior thigh, weakness, tendon retraction,
(Kibuule and Fehringer 2007)[71]	1	12.0	1 (1.00)	N	TT (1.00)	T (1.00)	physical examination (1.00), surgery (1.00)	wrestling with friend at home (1.00)	soft tissue swelling, palpable defect proximal to the olecranon
(Lempainen et al. 2007)[75]	18	27.5 ± 7.3	18 (1.00)	N	BF (0.61) SM (0.28) ST (0.11)	MTJ (0.83) AV (0.11) T (0.06)	physical examination (1.00), surgery (1.00) MRI or ultrasound (1.00)	sprinting (0.22), soccer (0.22), ice hockey (0.06), floorball (0.06), long jump (0.06), marathon (0.06), triathlon (0.06), road cycling (0.06), orienteering (0.06), golf (0.06), dancing (0.06), baseball (0.06)	weakness, stiffness of distal part of posterior thigh, localized swelling, hematoma, retracted muscle belly and palpable defect

Table D.1 - continued

Author	No. of patients	Age	no. patients surgery (proportion)	Relevant conditions (proportion)	Muscle or Tendon (proportion)	Injury Site (proportion)	Diagnosis (proportion)	Activity at injury (proportion)	Common injury symptoms
(Nishida et al. 2007)[93]	2	41.5 ± 36.1	0 (0.00)	N	BCH (1.00)	M (1.00)	MRI (1.00), X-ray (1.00)	judo (0.50) golf (0.5)	swelling in the anterolateral aspect of the mid arm, inability to extend elbow, hemorrhage,
(Gyftopoulos et al. 2008)[51]	20	32.0 (12-54)	0 (0.00)	N	RF (1.00)	MTJ (1.00)	MRI (1.00)	NR	bull's eye appearance in MRI, tendon thickening, partial muscle retraction, hematoma, edema, fluid. Older injuries, muscle atrophy, fatty replacement, fibrous encasement
(Levine and Savoie III 2008)[76]	1	42.0	1 (1.00)	N	LDT (1.00)	AV (1.00)	X-ray (1.00) MRI (1.00)	water skiing (1.00)	ecchymosis, swelling, palpable tender mass in the posterior aspect of the axilla, retracted tendon
(Lunn et al. 2008)[78]	19	46.9 ± 9.6	5 (0.26)	N	IP (1.00)	MTJ (0.42) T (0.47) INC (0.11)	Positive MRI (1.00) Positive CT scan (0.37)	progressive onset (0.89) traumatic onset (0.11)	T or MTJ rupture and edema with fluid at the junction tracking around the muscle fascicles and involving the IP. Muscle retraction after tear.
(Silder et al. 2008)[114]	14	31.3 ± 13.7	0 (0.00)	N	BF (0.86) ST (0.07) BF and ST (0.07)	MTJ (1.00)	MRI (1.00)	soccer (0.21) sprinting (0.57) hurdling (0.07) softball (0.07) 10k race (0.07)	Scar tissue observed along the MTJ, in the site of prior injury.
(Schache et al. 2008)[108]	1	20.0	1 (1.00)	N	BF (1.00) ST (1.00)	MTJ (1.00)	MRI, surgery (1.00)	australian rules football (1.00)	marked tenderness around the proximal and middle thirds of the lateral aspect of the hamstring muscle group, hematoma
(Winblad, Escobedo, and Hunter 2008)[143]	1	17.0	0 (0.00)	N	BCH (1.00)	M (1.00)	MRI (1.00)	american football (1.00)	swelling, edema, hematoma,
(Gaskin et al. 2009)[44]	16	57.0 (40 - 72)	15 (0.94)	NR	SPT (0.75) BT and SCT (0.13) BT (0.13)	T (1.00)	MRI (1.00)	NR	NR

Table D.1 - continued

Author	No. of patients	Age	no. patients surgery (proportion)	Relevant conditions (proportion)	Muscle or Tendon (proportion)	Injury Site (proportion)	Diagnosis (proportion)	Activity at injury (proportion)	Common injury symptoms
(Basic-Jukic et al. 2009)[7]	9	52.8 ± 8.8	9 (1.00)	hemodialysis (0.44) renal allograft from deceased donor (0.44) automated peritoneal dialysis and hemodialysis (0.11) steroids (0.11)	QT (0.5) ACT (0.19) SCT (0.13) BT (0.06) IAT (0.06) SPT (0.06)	AV (1.00)	NR	normal activity (1.00)	NR
(Shah, Montgomery, and Bastidas 2009)[109]	1	39.0	1 (1.00)	N	GST (1.00)	MTJ (1.00)	surgery (1.00)	american football (1.00)	swelling, ecchymoses
(Walch et al. 2009)[136]	59	46.4	24 (0.41)	calcific tendonitis (0.61)	IP (1.00)	MTJ (1.00)	MRI (0.73) Positive CT scan (0.27)	progressive onset (0.78) traumatic onset (0.22)	Evidence of edema, fatty infiltration, retraction of the muscle with modification of the architecture of the muscle fibers.
(Floor, Van Der Veen, and Devilee 2010)[39]	2	44.5 ± 0.7	2 (1.00)	N	BF (1.00) SM (1.00) ST (1.00)	M (0.5) T (0.5)	MRI, surgery (1.00)	water skiing (1.00)	swelling, ecchymosis, loss of strength at flexion of the knee, hematoma, muscle retraction
(Hasegawa and Schofer 2010)[53]	1	31.0	1 (1.00)	N	PMT (1.00)	TB (1.00)	MRI (1.00)	bench press (1.00)	swelling, ecchymosis, abnormal contour of the axillary fold, edema, hematoma, retraction of the musculotendinous fibers
(Pitts, Garner, and Ortiguera 2010)[100]	1	16.0	0 (0.00)	N	PMT (1.00)	AV (1.00)	MRI (1.00)	wrestling (1.00)	tenderness in the area of the BT and PM insertion, hematoma
(Pochini et al. 2010)[101]	20	32.7 ± 5.4	10 (0.50)	anabolic steroids (0.7)	PMT (0.85) PM (0.15)	AV (0.85) M (0.10) MTJ (0.05)	MRI (NR) ultrasound (NR)	bench press (0.60), jiu-jitsu (0.20), skating (0.05), soccer (0.05), gymnastics (0.05)	pain, ecchymosis, palpable defect in anterior axillar region, edema
(Pedret et al. 2011)[97]	7	26.3 ± 6.1	0 (0.00)	elite athletes (1.00)	GRC (1.00)	MTJ (1.00)	ultrasound (1.00) MRI (0.57)	dance (0.43), soccer (0.29), taekwondo (0.29), tennis (0.29)	posteromedial thigh pain at the junction between the proximal and middle thirds of the thigh, ecchymosis, crescent moon appearance in the posterior part of the GRC
(Jansen, Cormier, and Patel 2012)[65]	1	28.0	1 (1.00)	N	RF (1.00)	MTJ (1.00)	ultrasound (1.00)	soccer (1.00)	mass over the RF and a palpable gap distal to it, muscle retraction.

Table D.1 - continued

Author	No. of patients	Age	no. patients surgery (proportion)	Relevant conditions (proportion)	Muscle or Tendon (proportion)	Injury Site (proportion)	Diagnosis (proportion)	Activity at injury (proportion)	Common injury symptoms
(Khiami et al. 2012)[70]	1	28.0	1 (1.00)	N	TT (1.00)	T (1.00)	MRI (1.00)	weightlifting (1.00)	lack of strength in extension, retraction of the deep portion of the tendon
(Yoon et al. 2012)[144]	4	16.8 ± 4.8	4 (1.00)	N	TT (1.00)	AV (1.00)	MRI (0.5) X.ray (1.00)	judo (0.25), fall (0.25), soccer (0.25), colliding with a wall (0.25)	hematoma, ecchymosis, small fragment of bone posterior to the tip of the olecranon, tendon retraction
(Hart 2013)[52]	1	50.0	1 (1.00)	NR	QT (1.00)	T (1.00)	MRI (1.00) X-ray (1.00)	slipped on the wet floor (1.00)	inability to extend leg, effusion, hematoma, retraction of the QT
(Naito et al. 2013)[91]	1	18.0	1 (1.00)	N	TT (1.00)	AV (1.00)	X-ray (1.00) CT (1.00)	fall (1.00)	swelling at the back of elbow, fragment of bone avulsed from the olecranon,
(Valente, Mancuso, and Alecci 2013)[131]	1	24.0	1 (1.00)	N	BF (1.00)	MTJ (1.00)	NMR (1.00), surgery (1.00)	american football (1.00)	diffuse swelling in the posterolateral region of the knee, retraction of the tendon, serosanguineous fluid collection,
(Benazzo, Marullo, and Pietrobono 2014)[10]	1	23.0	0 (0.00)	NR	SP (1.00)	MTJ (1.00)	MRI (1.00)	fall (1.00)	tenderness over the supraspinatus fossa, hematoma, edema,
(Huri et al. 2014)[61]	1	16.0	1 (1.00)	N	RF (1.00)	MTJ (1.00)	MRI (1.00), surgery (1.00)	soccer (1.00)	swelling and mild tenderness on the anterior aspect of the thigh, prominence on the thigh, edema,
(Makridis et al. 2014)[82]	67	68.0 (25 - 87)	73 (1.00)	NR	GMEDT (0.66) GMEDT and GMINT(0.33)	T (1.00)	MRI (1.00) surgery (1.00)	NR	pain within 30 sec of standing or immediate pain, retraction, muscle atrophy.
(Sharma et al. 2014)[110]	1	34.0	1 (1.00)	N	TT (1.00)	AV (1.00)	physical examination, X-ray (1.00)	assault by hard and blunt object (1.00)	severe tenderness and swelling on the posterior aspect of the elbow, palpable depression proximal to the olecranon, piece of avulsed bone from the olecranon, hematoma, retraction of the TT

Table D.1 - continued

Author	No. of patients	Age	no. patients surgery (proportion)	Relevant conditions (proportion)	Muscle or Tendon (proportion)	Injury Site (proportion)	Diagnosis (proportion)	Activity at injury (proportion)	Common injury symptoms
(Bunshah et al. 2015)[13]	1	40.0	1 (1.00)	weightlifter (1.00), anabolic steroid (1.00)	TT (1.00)	AV (1.00)	physical examination, X-ray, MRI (1.00)	fall (1.00)	ecchymosis and moderate swelling over the posterior aspect of the arm above the elbow, fleck of bone proximal to the tip of the olecranon, hematoma
(Cetinkaya et al. 2015)[17]	1	22.0	0 (0.00)	NR	VIT (1.00)	T (1.00)	physical examination, MRI (1.00)	rugby player (1.00)	Tenderness in the anterior of the suprapatellar region in the right thigh, mass in the mid-anterior of the right thigh, hematoma
(Crema et al. 2016)[22]	275	25.0 ± 5.2	NR	professional football players	BF (0.65) ST (0.26) SM (0.17)	MTJ (0.53), M (0.47), T (0.08)	MRI (1.00)	American football (1.00)	edema and tear seen as high signal intensity; signal abnormalities around the MTJ and MFJ, involvement of proximal and/or distal T
(Fitzpatrick, Cagle, and Flatow 2016)[37]	1	53.0	0 (0.00)	N	TMJ (1.00)	MTJ (1.00)	physical examination, MRI (1.00)	waterski (1.00)	visible asymmetry in the posterior axillary fold, no appreciable weakness, fluid signal gap at the site of complete tearing
(Jaiswal et al. 2016)[64]	3	38.0 ± 14.7	3 (1.00)	N	TT (0.67) TR (0.33)	AV (0.67) MTJ (0.33)	X-ray (0.33), ultrasound (0.67), surgery (1.00)	gym (0.33), fall (0.67)	MTJ injury showed a palpable gap in posterior region, inability to extend arm, swelling, ecchymoses. AV injuries revealed tenderness, swelling, ecchymosis and fleck of bone proximal to the insertion
(Lukac et al. 2016)[77]	67	42.3 ± 11.3	NR	NR	GST (1.00)	MTJ (1.00)	ultrasound (1.00)	recreational activities (0.45), daily activities (0.24), professional sport (0.07), occupational trauma (0.06) NR (0.18)	intense pain in the calf, that increases during dorsiflexion, liquid collections between the aponeurosis of the GST and the SL
(Entwisle et al. 2017)[30]	55	26.4	NR	professional athletes (0.78)	BF (1.00)	MTJ (1.00)	MRI (1.00)	australian football (0.67), soccer (0.07), cricket (0.05), rugby (0.02), athletics (0.02), hockey (0.02)	peritendinous “feathery” edema and bloodfluid, retraction in case of complete tears, chronic scarring in recurrent injuries

Table D.1 - continued

Author	No. of patients	Age	no. patients surgery (proportion)	Relevant conditions (proportion)	Muscle or Tendon (proportion)	Injury Site (proportion)	Diagnosis (proportion)	Activity at injury (proportion)	Common injury symptoms
(Godoy et al. 2018)[47]	46	34.0 ± 9	26 (0.57)	anabolic steroids (0.04)	PM (0.48), PMT (0.52)	MTJ (0.48), T (0.52)	MRI (1.00), surgery (0.57)	bench press (0.5), ski/snowboarding (0.11), NR (0.09), obstacle race (0.07), wrestling (0.07), hockey (0.04), sudden upper extremity abduction (0.04), baseball (0.02), cross-fit (0.02), soccer (0.02), watersports (0.02)	T injury showed triangular-shaped peri-bicipital hematoma and anterior displacement of the BT. MTJ injury showed normal BT displacement and hematoma in MTJ. Both showed hemorrhage and edema.
(Roe et al. 2018)[105]	307	(18 - >30)	NR	professional athletes (1.00)	BF (0.69) SM and ST (0.09) HS (0.21)	M (0.53), MTJ (0.25) NR (0.21)	team medical staff (specific NR)	Gaelic football (1.00)	NR
(Miranda and Bureau 2019)[90]	363	57.7 ± 12.1	NR	NR	RC (0.42) SP (0.0047) IP (0.0059) SC (0.0012) TMIN (0.0012) N (0.57)	TB (0.42) MTJ (0.013) N (0.57)	MRI (1.00)	NR	MTJ showed edema and retraction and fibrous scarring, atrophy and fatty infiltration in chronic lesions.

E

The finite element model of the pelvic floor muscles was comprised of 20,804 hexahedral hybrid elements (C3D8H). The average volume of each finite element was 1.16 mm^3, and the tissue volume of the pelvic floor muscles is 24,088 mm^3, with a ratio between the average finite element volume and the total model volume of 0.005% (Figure E.1). Hexahedral elements were chosen because of their better precision compared to other 3D finite elements.

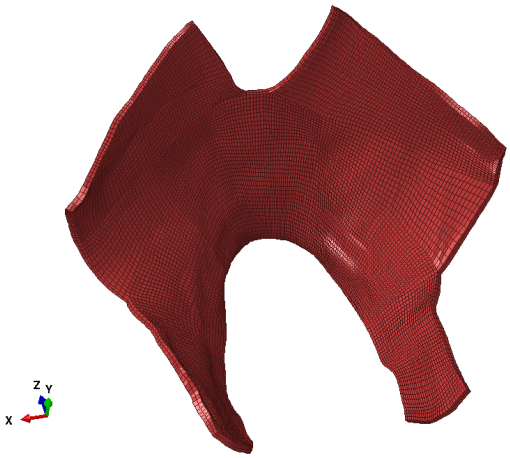

Figure E.1 – Finite element mesh of the levator ani muscles.

The fetal head was modeled using 19,520 tetrahedral elements (C3D4H). In this case, we consider tetrahedral elements the best choice because they perform faster, and no mechanical analysis was to be made of the fetal head. For both the fetal head and the pelvic floor, hybrid elements were used since we believe it is the best choice when the material is incompressible or near incompressible. They have a mixed formulation that allows one to overcome numerical problems caused by incompressibility, such as volume strain "locking". More details are available in ABAQUS® Documentation[24].

The constitutive model applied to the Levator Ani muscles include the Holzapfel-Gasser-Ogden (HGO) model[59] to capture the transversely isotropic hyperelastic behavior, the Generalized Maxwell model, as described by Holzapfel and Gasser[58], to capture the viscoelastic behavior and a fatigue damage model, previously developed based on experimental evidence[134], to capture the damage accumulation due to sub-maximal repetitive loadings. In this work we also included a non-local damage averaging of the integral-type to attenuate the mesh influence on the damage contours.

As we wanted to simulate the behavior of a soft tissue, which is nearly incompressible due to the high water content[84], we can typically express the strain energy function in a decoupled form, defining a contribution for the volumetric and the isochoric components separately. In this way, applying a penalty function to the volumetric contribution will assure the material to be incompressible. The isochoric component can also be further decoupled to add the specificities

of the different constituents of the soft tissue[57]. In particular, this model considers the presence of a single family of muscle fibers embedded in a ground substance (or ground matrix) material (a family of fibers is a group of fibers that are assumed to have a preferred direction). As such, the complete strain energy function can be defined in a decoupled form as:

$$\Psi = \Psi_{\text{vol}} + \left[\left(1 - \widehat{\text{D}_{\text{m}}}\right) \cdot \left(\overline{\Psi}_{\text{m}} + \Psi_{\text{m}}^{\text{vsc}}\right)\right] + \left(1 - \widehat{\text{D}_{\text{f}}}\right) \cdot \left(\overline{\Psi}_{\text{f}} + \Psi_{\text{f}}^{\text{vsc}}\right) \tag{E.1}$$

where Ψ_{vol} is the volumetric contribution, $\overline{\Psi}_{\text{m}}$ is the isochoric contribution of the ground matrix, $\overline{\Psi}_{\text{f}}$ is the isochoric contribution of the family of fibers, Ψ_{*}^{vsc} $_{*=\text{m,f}}$ are the viscous effects and $\widehat{\text{D}_{*}}\left(0 < \widehat{\text{D}_{*}} < 1\right)$ $_{*=\text{m,f}}$ are the non-local continuous damage variables. Both the viscous effects and the damage variables affect each isochoric component of the strain energy. The indices m and f refer to the ground matrix and fibers contribution, respectively.

Each contribution can be defined as:

$$\Psi_{\text{vol}} = \text{K}\left(\frac{J^2 - 1}{2} - \ln\left(J\right)\right) \tag{E.2}$$

$$\overline{\Psi}_{\text{m}} = \text{C}_{10}(\bar{\text{I}}_1 - 3) \tag{E.3}$$

$$\overline{\Psi}_{\text{f}} = \frac{\text{k}_{11}}{2\text{k}_{12}}\{\exp[\text{k}_{12}(\bar{\text{I}}_4 - 1)^2] - 1\} \tag{E.4}$$

$$\Psi_{*}^{\text{vsc}} = \sum_{\alpha=1}^{m} \Upsilon_{\alpha *} \quad _{*=\text{m,f}} \tag{E.5}$$

where $J = \det \mathbf{F}$, designated as Jacobian, represents the local rate of change of the deformed configuration volume v with respect to the reference configuration volume V, with $\mathbf{F}$ the deformation gradient. The symmetric right Cauchy-Green deformation tensor can be defined as $\mathbf{C} = \mathbf{F}^{\text{T}}\mathbf{F}$, with the corresponding first invariant $\text{I}_1 = \text{tr}\,\mathbf{C}$. The deformation gradient can be decomposed into a volumetric (dilatational) $\mathbf{F}_{\text{vol}} = J^{1/3}$ and volume preserving (distortional) part $\bar{\mathbf{F}} = J^{-1/3}\,\mathbf{F}$, with $\det \bar{\mathbf{F}} = 1$. Accordingly, the isochoric right Cauchy-Green tensor becomes $\bar{\mathbf{C}} = \bar{\mathbf{F}}^{\text{T}}\bar{\mathbf{F}}$, with its first invariant now defined as $\bar{\text{I}}_1 = \text{tr}\,\bar{\mathbf{C}}$. The stretch $\bar{\lambda}_{\text{f}}$ in the direction $\mathbf{m}_0$ of the fiber family relates with the pseudo-invariant $\bar{\text{I}}_4$ such as $\bar{\lambda}_{\text{f}}^{\,2} = \bar{\text{I}}_4 = \mathbf{m}_0 \cdot \bar{\mathbf{C}} \cdot \mathbf{m}_0$. The scalar value functions $\Upsilon_{\alpha *}$ $_{*=\text{m,f}}$ may be viewed as a dissipative potential and determines the viscoelastic contribution of each process α, which is also the number of parallel elements in the Maxwell model[58]. Each Maxwell element can be represented by a spring in series with a dashpot. The spring represents the solid behavior and is characterized by a free energy parameter $\beta_{\alpha *}$ $_{*=\text{m,f}}$

and the dashpot characterizes the viscous behavior and is function of a relaxation time $\tau_{\alpha *}$ $_{*=m,f}$[58].

The parameters of the transversely isotropic visco-hyperelastic model are: K for the volumetric contribution, C_{10}: for the ground matrix contribution, k_{11}, k_{12}: for the fibers contribution and $\beta_{\alpha *}$ $_{*=m,f}$ and $\tau_{\alpha *}$ $_{*=m,f}$ for the viscoelastic contribution.

More details concerning this transversely isotropic visco-hyperelastic model can be found elsewhere[58,59].

The continuous damage model was developed using the concept of accumulated equivalent strain Ξ_t^{acc}, as defined by Peña et al[98]:

$$\Xi_t^{\mathrm{acc}} = \int_0^t \left| \frac{d\bar{\Psi}}{ds} \right| ds \tag{E.6}$$

This allows for a continuous damage accumulation within the deformation process, with a simple equation of damage evolution:

$$\frac{d\Xi_t^{\mathrm{acc}}}{dt} = \left| \frac{d\bar{\Psi}}{dt} \right| \tag{E.7}$$

The damage propagation and accumulation was defined using a modification of the Lemaitre and Plumtree nonlinear cumulative expression[88]. As described in our previous work[134], the ratio between the number of cycles and the number of cycles to fatigue failure was replaced with the ratio between the accumulated equivalent strain and its maximum value. A parameter was also added so that the weight of the damage variable can be easily changed:

$$D_* = D_{max*} \left\{ 1 - \left(1 - \frac{\Xi_{t*}^{\mathrm{acc}}}{\Xi_{max*}^{\mathrm{acc}}} \right)^{1/C_*} \right\}_{*=m,f} \tag{E.8}$$

The parameters of this damage evolution are the maximum equivalent strain $\Xi_{max*}^{\mathrm{acc}}$ $_{*=m,f}$, the exponent C_* $_{*=m,f}$ and the weighting parameter D_{max*} $(0 < D_{max*} \leq 1)_{*=m,f}$. The criteria for the evolution can be defined as:

$$\dot{\Xi}_{t*}^{acc} = \begin{cases} \dfrac{d\bar{\Psi}_*}{dt}, & \dot{\Xi}_{t*}^{\mathrm{acc}} \geq 0 \\ 0, & \dot{\Xi}_{t*}^{acc} < 0 \end{cases}_{*=m,f} \tag{E.9}$$

This damage model is a so-called 'local' model. This designation appears since the solution is dependent on the spatial discretization. In other words, the solution is mesh dependent and upon mesh refinement the effects are even more prominent[3,34]. To overcome this issue, non-local theory approaches can be applied to eliminate or reduce the mesh dependency. In this work, we chose to apply an integral-type averaging scheme coupled to the material law[34]. Using the non-local

averaging of the integral type, the non-local damage variable $\widehat{D_*}_{\ *=m,f}$ can be expressed by means of a spatially weighted averaging integral as:

$$\widehat{D_*} = \int_V \chi(\boldsymbol{x},\boldsymbol{\eta})\, D_{*\ *=m,f}\, dV(\boldsymbol{\eta}) \tag{E.10}$$

where $\chi(\boldsymbol{x},\boldsymbol{\eta})$ is a weighted average operator, $D_{*\ *=m,f}$ is the local damage. $\widehat{D_*}_{\ *=m,f}$ represents the measurement of non-local damage at a generic material point $\boldsymbol{x}$, which has been averaged over a finite volume V, containing a set of points $\boldsymbol{\eta}$. The size of the non-local volume is dictated by a constitute parameter designated as characteristic length L_c (Figure E.2)

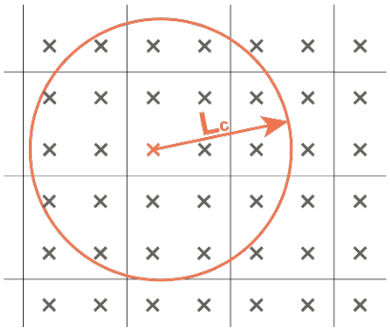

Figure E.2 – Non-local damage at a material point $\boldsymbol{x}$ results from an averaging operation of the local quantities of the material points inside the non-local averaging volume. This volume is defined by radius L_c , which is the characteristic length..

The averaging operator can be defined as:

$$\chi(\boldsymbol{x},\boldsymbol{\eta}) = \frac{\varpi(\boldsymbol{x},\boldsymbol{\eta})}{\Omega_r(\boldsymbol{x})} \tag{E.11}$$

where $\varpi(\boldsymbol{x},\boldsymbol{\eta})$ is the weighting function and $\Omega_r(\boldsymbol{x})$ the representative volume, defined as follows:

$$\varpi(\boldsymbol{x},\boldsymbol{\eta}) = \begin{cases} \left(1 - \dfrac{\|\boldsymbol{x}-\boldsymbol{\eta}\|^2}{{L_c}^2}\right)^2, & \|\boldsymbol{x}-\boldsymbol{\eta}\| \le L_c \\ 0, & \|\boldsymbol{x}-\boldsymbol{\eta}\| > L_c \end{cases} \tag{E.12}$$

$$\Omega_r(\boldsymbol{x}) = \int_V \varpi(\boldsymbol{x},\boldsymbol{\eta}) dV(\boldsymbol{\eta}) \tag{E.13}$$

The only parameter of the non-local implementation is the characteristic length. This parameter must be chosen with care since it can have a significant impact on the results. If too small a value is chosen, the non-local solution approaches the local solution, and the mesh dependency can still occur. On the other hand, if too large a value is chosen it will cause over-homogenization and the results will lose significance. Further details on the non-local damage averaging can be found elsewhere[3,9,34].

The constitutive parameters were obtained using a custom made micro-genetic algorithm by calibrating experimental results with numerical data, as detailed in Vila Pouca et al[134]. No

restriction to the domains of the ground matrix and muscle fibers was imposed. The only exception is the non-local damage parameter, the characteristic length L_c, which was defined to be approximately the length of three finite elements[34]. The calibration was performed by replicating the conditions of the laboratory experiments in the computer simulations. Then, the set of parameters was iteratively changed (randomly by the algorithm), and the experimental force-displacement curve was compared with the computational force-displacement curve until the least error was achieved. The set of material parameters that allowed the best approximation between the experimental force-displacement curve and the computational (numerical) was the set of parameters used in the simulations. Since these material models are phenomenological, the material properties do not have a physical meaning and cannot be obtained by observation.

The complete set of calibrated material parameters to simulate the levator ani muscles behavior is presented in Table E.1. Despite the lack of restrictions to the domain of the material parameters, the micro-genetic algorithm was able to capture the faster rate of the muscle fibers damage, compared to the ground matrix. This can be seen by comparing the values of $\Xi^{acc}_{max\,m}$ and $\Xi^{acc}_{max\,f}$, which are respectively 4.07 and 2.25 MPa. Since this parameter represents the accumulated equivalent strain at failure, it indicates that the fiber damage accumulates at a faster rate, which agrees with our experimental observations[134]. This translated to the numerical results, with maximum damage values of the ground matrix of ~0.1 for all pushing patterns. As such, we decided to neglect the damage in the ground matrix in the Results section and analyze only the damage results of the muscle fibers.

Table E.1- Levator ani constitutive model parameters, obtained from the micro-genetic algorithm optimization [134].

Hyperelastic	**Viscoelastic**	**Local Damage**	**Non-local Damage**
$C_{10} = 0.14$ MPa	$\beta_{1\,m} = \beta_{1\,f1} = 5.08\ (-)$	$D_{max\ m} = 0.9\ (-)$	$L_c = 3.0$ mm
$k_{11} = 0.05$ MPa	$\tau_{1\,m} = \tau_{1\,f1} = 33.59\ s$	$\Xi^{acc}_{max\,m} = 4.07$ MPa	
$k_{12} = 0.23\ (-)$	$\beta_{2\,m} = \beta_{2\,f1} = 0.79\ (-)$	$C_m = 1.65\ (-)$	
	$\tau_{2\,m} = \tau_{2\,f1} = 44.14\ s$	$D_{max\ f1} = 1.0\ (-)$	
		$\Xi^{acc}_{max\,f1} = 2.25$ MPa	
		$C_{f1} = 0.27\ (-)$	

F

In order to perform the update of the permanent deformation and damage variables, the tangent moduli K presented in eq. (5.49) must be calculated

$$\mathrm{K} = \frac{\partial \mathrm{R}}{\partial \lambda_{\mathrm{p}}^{n+1}} = 1 - \Delta t \left(\frac{\partial \mathrm{k_p}}{\partial \lambda_{\mathrm{p}}^{n+1}} \phi_{\mathrm{p}} + \frac{\partial \phi_{\mathrm{p}}}{\partial \lambda_{\mathrm{p}}^{n+1}} \mathrm{k_p} \right). \tag{5.49}$$

For simplification, the index $n+1$ will be suppressed in the following equations.

Starting with the derivative $\partial \phi_{\mathrm{p}} / \partial \lambda_{\mathrm{p}}$ and recalling that $\phi_{\mathrm{p}} = \lambda_{\mathrm{e}} - \lambda_{\mathrm{crit}}$ and $\lambda_{\mathrm{e}} = \bar{\lambda}_{\mathrm{f}} / \lambda_{\mathrm{p}}$, we can write

$$\frac{\partial \phi_{\mathrm{p}}}{\partial \lambda_{\mathrm{p}}} = -\frac{\bar{\lambda}_{\mathrm{f}}}{{\lambda_{\mathrm{p}}}^2}. \tag{F.1}$$

Recalling that $\mathrm{k_p} = (\beta_0 + \beta \mathrm{D})^{\gamma}$ and that $\mathrm{D} = \mathrm{D_{max}} \left\{ 1 - \left(1 - \frac{\Xi_t^{\mathrm{acc}}}{\Xi_{\mathrm{max}}^{\mathrm{acc}}} \right)^{1/\mathrm{C}} \right\}$, where $\dot{\Xi}_t^{\mathrm{acc}} = \dot{\Psi}_{\mathrm{ich}}^0$. Knowing that Ψ_{iso}^0 will be a function of λ_{p}, we can see that $\mathrm{k_p}$ is implicitly dependent of λ_{p}.

For this reason, we can use the chain rule to obtain the derivative $\partial \mathrm{k_p} / \partial \lambda_{\mathrm{p}}$ such as

$$\frac{\partial \mathrm{k_p}}{\partial \lambda_{\mathrm{p}}} = \frac{\partial \mathrm{k_p}}{\partial \mathrm{D}} \frac{\partial \mathrm{D}}{\partial \Xi_t^{\mathrm{acc}}} \frac{\partial \Xi_t^{\mathrm{acc}}}{\partial \lambda_{\mathrm{p}}}. \tag{F.2}$$

The first two terms are easily obtained as

$$\frac{\partial \mathrm{k_p}}{\partial \mathrm{D}} = \beta \gamma (\beta_0 + \beta \mathrm{D})^{\gamma - 1}, \tag{F.3}$$

$$\frac{\partial \mathrm{D}}{\partial \Xi_t^{\mathrm{acc}}} = \frac{\mathrm{D_{max}}}{\Xi_{\mathrm{max}}^{\mathrm{acc}} \cdot \mathrm{C}} \left(1 - \frac{\Xi_t^{\mathrm{acc}}}{\Xi_{\mathrm{max}}^{\mathrm{acc}}} \right)^{(1/\mathrm{C})-1}. \tag{F.4}$$

To obtain the third term we used the finite difference approximation to obtain a direct relationship of Ξ_t^{acc} with Ψ_{ich}, such that $(\Xi_t^{\mathrm{acc}})^{n+1} = (\Psi_{\mathrm{ich}})^{n+1} - (\Psi_{\mathrm{ich}})^n + (\Xi_t^{\mathrm{acc}})^n$.

Recalling that we are in the current time increment, $n+1$, the derivative of $\frac{\Xi_t^{\mathrm{acc}}}{\partial \lambda_{\mathrm{p}}^{n+1}}$ will be equal to the derivative $\frac{\Psi_{\mathrm{ich}}^0}{\partial \lambda_{\mathrm{p}}^{n+1}}$. As such,

$$\frac{\partial \Xi_t^{\mathrm{acc}}}{\partial \lambda_{\mathrm{p}}} = \frac{\partial \bar{\Psi}_{\mathrm{m}}(\bar{\mathrm{I}}_{1\mathrm{e}})}{\partial \lambda_{\mathrm{p}}} + \frac{\partial \bar{\Psi}_{\mathrm{f}}(\bar{\lambda}_{\mathrm{e}})}{\partial \lambda_{\mathrm{p}}}. \tag{F.5}$$

Recalling our choice for the free-energy function

$$\bar{\Psi}_{\mathrm{m}} = \mathrm{C_{10}} (\bar{\mathrm{I}}_{1\mathrm{e}} - 3), \tag{F.6}$$

$$\bar{\Psi}_{\mathrm{f}} = \frac{\mathrm{k_1}}{2\mathrm{k_2}} \left\{ \exp^{\mathrm{k_2} \left(\bar{\lambda}_{\mathrm{e}}^{\,2} - 1 \right)^2} - 1 \right\}, \tag{F.7}$$

we obtain the following expression from the fiber contribution,

$$\frac{\partial \bar{\Psi}_{\mathrm{f}}}{\partial \lambda_{\mathrm{p}}} = 2k_1 \frac{\bar{\lambda}_{\mathrm{f}}^{\,2}}{\lambda_{\mathrm{p}}^{\,5}} \left(\lambda_{\mathrm{p}}^{\,2} - \bar{\lambda}_{\mathrm{f}}^{\,2} \right) \exp^{k_2 \left(\bar{\lambda}_{\mathrm{e}}^{\,2} - 1 \right)^2} , \tag{F.8}$$

and for the ground substance contribution,

$$\frac{\partial \bar{\Psi}_{\mathrm{m}}}{\partial \lambda_{\mathrm{p}}} = \frac{\partial \bar{\Psi}_{\mathrm{m}}}{\partial \bar{\mathrm{I}}_{1\mathrm{e}}} \left(\frac{\partial \bar{\mathrm{I}}_{1\mathrm{e}}}{\partial \bar{\mathbf{C}}_{\mathrm{e}}} : \frac{\partial \bar{\mathbf{C}}_{\mathrm{e}}}{\partial \lambda_{\mathrm{p}}} \right), \tag{F.9}$$

where,

$$\frac{\partial \bar{\Psi}_{\mathrm{m}}}{\partial \bar{\mathrm{I}}_{1\mathrm{e}}} = C_{10} , \tag{F.10}$$

$$\frac{\partial \bar{\mathrm{I}}_{1\mathrm{e}}}{\partial \bar{\mathbf{C}}_{\mathrm{e}}} = \mathbf{I} , \tag{F.11}$$

$$\frac{\partial \bar{\mathbf{C}}_{\mathrm{e}}}{\partial \lambda_{\mathrm{p}}} = -\mathbf{F}_{\mathrm{p}}^{-\mathrm{T}} \frac{\partial \mathbf{F}_{\mathrm{p}}^{\mathrm{T}}}{\partial \lambda_{\mathrm{p}}} \bar{\mathbf{C}}_{\mathrm{e}} - \bar{\mathbf{C}}_{\mathrm{e}} \frac{\partial \mathbf{F}_{\mathrm{p}}}{\partial \lambda_{\mathrm{p}}} \mathbf{F}_{\mathrm{p}}^{-1} . \tag{F.12}$$

G

Chapter 1 co-author consent form

Marco Paulo Lages Parente, Renato Manuel Natal Jorge, James Anthony Ashton-Miller, the undersigned, as co-authors of the paper entitled "Injuries in Muscle-Tendon-Bone-Units. A systematic review considering the role of passive tissue fatigue" submitted to the journal The Orthopaedic Journal of Sports Medicine, agree to the inclusion of its contents, the including figures and tables, in the Ph.D. thesis of Maria Castro Paupério Vila Pouca, entitled "Biomechanical analysis of low-cycle fatigue damage during the second stage of labor".

Signed,

Author 1	Marco Parente PRINT	Marco Parente SIGN	DATE: 20/10/2021 D/M/YYYY
Author 2	Renato Natal Jorge PRINT	 SIGN	DATE: 20/10/2021 D/M/YYYY
Author 3	James Ashton-Miller PRINT	James Ashton-Miller SIGN	DATE: 28/10/2021 D/M/YYYY

Chapter 2 co-author consent form

Marco Paulo Lages Parente, Renato Manuel Natal Jorge, John O.L. DeLancey, James Anthony Ashton-Miller, the undersigned, as co-authors of the paper entitled "Pelvic muscle injury during a difficult labor. Can tissue fatigue play a role?" submitted to the International Urogynecology Journal, agree to the inclusion of its contents, the including figures and tables, in the Ph.D. thesis of Maria Castro Paupério Vila Pouca, entitled "Biomechanical analysis of low-cycle fatigue damage during the second stage of labor".

Signed,

Author 1	Marco Parente PRINT	Marco Parente SIGN	DATE: 20 / 10 / 2021 D/M/YYYY
Author 2	Renato Natal Jorge PRINT	 SIGN	DATE: 20 / 10 / 2021 D/M/YYYY
Author 3	James Ashton-Miller PRINT	James Ashton-Miller SIGN	DATE: 28 / 10 / 2021 D/M/YYYY
Author 4	John DeLancey PRINT	J DeLancey SIGN	DATE: 28 / 10 / 2021 D/M/YYYY

Chapter 3 co-author consent form

Marco Paulo Lages Parente, Renato Manuel Natal Jorge, James Anthony Ashton-Miller, the undersigned, as co-authors of the paper entitled "Investigating the birth-related caudal maternal pelvic floor muscle injury. The consequences of low-cycle fatigue damage" submitted to the Journal of the Mechanical Behavior of Biomedical Materials, agree to the inclusion of its contents, the including figures and tables, in the Ph.D. thesis of Maria Castro Paupério Vila Pouca, entitled "Biomechanical analysis of low-cycle fatigue damage during the second stage of labor".

Signed,

Author 1	Marco Parente PRINT	Marco Parente SIGN	DATE: 20 / 10 / 2021 D/M/YYYY
Author 2	Renato Natal Jorge PRINT	 SIGN	DATE: 20 / 10 / 2021 D/M/YYYY
Author 3	James Ashton-Miller PRINT	James Ashton-Miller SIGN	DATE: 28 / 10 / 2021 D/M/YYYY

Chapter 4 co-author consent form

João Pedro Sousa Ferreira, Marco Paulo Lages Parente, Renato Manuel Natal Jorge, James Anthony Ashton-Miller, the undersigned, as co-authors of the paper entitled "On the management of maternal pushing during the second stage of labor: A biomechanical study considering passive tissue fatigue damage" submitted to the American Journal of Obstetrics and Gynecology, agree to the inclusion of its contents, the including figures and tables, in the Ph.D. thesis of Maria Castro Paupério Vila Pouca, entitled "Biomechanical analysis of low-cycle fatigue damage during the second stage of labor".

Signed,

Author 1	João Ferreira PRINT	 SIGN	DATE: **20 / 10 / 2021** D/M/YYYY
Author 2	Marco Parente PRINT	 SIGN	DATE: 20 / 10 / 2021 D/M/YYYY
Author 3	Renato Natal Jorge PRINT	 SIGN	DATE: 20/10/2021 D/M/YYYY
Author 4	James Ashton-Miller PRINT	 SIGN	DATE: 28 / 10 / 2021 D/M/YYYY

Chapter 5 co-author consent form

Pedro Areias, Serdar Göktepe, James Anthony Ashton-Miller, Renato Manuel Natal Jorge, Marco Paulo Lages Parente, the undersigned, as co-authors of the paper entitled "Modeling permanent deformation during low-cycle fatigue: Application to the pelvic muscles during labor" submitted to the journal Computer Methods in Applied Mechanics and Engineering, agree to the inclusion of its contents, the including figures and tables, in the Ph.D. thesis of Maria Castro Paupério Vila Pouca, entitled "Biomechanical analysis of low-cycle fatigue damage during the second stage of labor".

Signed,

Author 1	Pedro Areias PRINT	Pedro Areias SIGN	DATE: 27 / 10 / 2021 D/M/YYYY
Author 2	Serdar Göktepe PRINT	 SIGN	DATE: 27/ 10/ 2021 D/M/YYYY
Author 3	James Ashton-Miller PRINT	James Ashton-Miller SIGN	DATE: 28 / 10 / 2021 D/M/YYYY
Author 4	Renato Natal Jorge PRINT	 SIGN	DATE: 20 / 10 / 2021 D/M/YYYY
Author 5	Marco Parente PRINT	Marco Parente SIGN	DATE: 20 / 10 / 2021 D/M/YYYY

References

1. Äärimaa V, Rantanen J, Heikkilä J, Helttula I, Orava S. Rupture of the pectoralis major muscle. *Am J Sports Med*. 2004;32(5):1256-1262. doi:10.1177/0363546503261137

2. Andersen E. Triceps tendon avulsion. *Injury*. 1986;17(4):279-280.

3. Andrade FXC, César de Sá JMA, Andrade Pires FM. A ductile damage nonlocal model of integral-type at finite strains: formulation and numerical issues. *Int J Damage Mech*. 2011;20(4):515-557. doi:10.1177/1056789510386850

4. Asinger DA, el-Khoury GY. Tensor fascia lata muscle tear: evaluation by MRI. *Iowa Orthop J*. 1998;18:146-149.

5. Aso K, Torisu T. Muscle belly tear of the triceps. *Am J Sports Med*. 1984;12(6):485-487. doi:10.1177/036354658401200614

6. Bach BR, Warren RF, Wickiewicz TL. Triceps rupture:A case report and literature review. *Am J Sports Med*. 1987;15(3):285-289. doi:10.1177/036354658701500319

7. Basic-Jukic N, Juric I, Racki S, Kes P. Spontaneous tendon ruptures in patients with end-stage renal disease. *Kidney Blood Press Res*. 2009;32(1):32-36. doi:10.1159/000201792

8. Bass CJ, Connell DA. Sonographic findings of tensor fascia lata tendinopathy: Another cause of anterior groin pain. *Skeletal Radiol*. 2002;31(3):143-148. doi:10.1007/s00256-001-0459-7

9. Bažant ZP, Jirásek M. Nonlocal integral formulations of plasticity and damage: survey of progress. *J Eng Mech*. 2002;128(11):1119-1149. doi:10.1061/(ASCE)0733-9399(2002)128:11(1119)

10. Benazzo F, Marullo M, Pietrobono L. Supraspinatus rupture at the musculotendinous junction in a young woman. *J Orthop Traumatol*. 2013;15(3):231-234. doi:http://dx.doi.org/10.1007/s10195-013-0271-x

11. Bianchi S, Martinoli C, Waser NP, Bianchi-Zamorani MP, Federici E, Fasel J. Central aponeurosis tears of the rectus femoris: sonographic findings. *Skeletal Radiol*. 2002;31(10):581-586. doi:10.1007/s00256-002-0559-z

12. Bowers KDJ. Patellar tendon avulsion as a complication of Osgood-Schlatter's disease. *Am J Sports Med*. 1981;9(6):356-359. doi:10.1177/036354658100900603

13. Bunshah JJ, Raghuwanshi S, Sharma D, Pandita A. Triceps tendon rupture: An uncommon orthopaedic condition. *BMJ Case Rep*. 2015;2015. doi:10.1136/bcr-2014-206446

14. Butcher JD, Siekanowicz A, Pettrone F. Pectoralis Major Rupture: Ensuring Accurate Diagnosis and Effective Rehabilitation. *Phys Sportsmed*. 1996;24(3):37.

15. Canovas F, Nicolau F, Bonnel F. Avulsion of the flexor digitorum profundus tendon associated with a chondroma of the distal phalanx. *J Hand Surg Br*. 1998;23(1):130-131.

16. Carrino JA, Chandnanni VP, Mitchell DB, Choi-Chinn K, DeBerardino TM, Miller MD. Pectoralis major muscle and tendon tears: diagnosis and grading using magnetic resonance imaging. *Skeletal Radiol*. 2000;29(6):305-313.

17. Cetinkaya E, Aydin CG, Akman YE, et al. A rare knee extensor mechanism injury: Vastus intermedius tendon rupture. *Int J Surg Case Rep*. 2015;14:186-188. doi:10.1016/j.ijscr.2015.07.035

18. Clay NR. A pulled muscle. Partial avulsion of the extensor indicis proprius tendon following a hyperflexion injury. *Injury*. 1988;19(2):127-128. doi:10.1016/0020-1383(88)90092-7

19. Connell DA, Jhamb A, James T. Side Strain: A Tear of Internal Oblique Musculature. *Am J Roentgenol*. 2003;181(6):1511-1517. doi:10.2214/ajr.181.6.1811511

20. Connell DA, Potter HG, Sherman MF, Wickiewicz TL. Injuries of the pectoralis major muscle: evaluation with MR imaging. *Radiology*. 1999;210(3):785-791. doi:10.1148/radiology.210.3.r99fe43785

21. Cooper ME, Selesnick FH. Partial rupture of the distal insertion of the patellar tendon: A report of two cases in professional athletes. *Am J Sports Med*. 2000;28(3):402-406.

22. Crema MD, Guermazi A, Tol JL, Niu J, Hamilton B, Roemer FW. Acute hamstring injury in football players: Association between anatomical location and extent of injury--A large single-center MRI report. *J Sci Med Sport*. 2016;19(4):317-322. doi:http://dx.doi.org/10.1016/j.jsams.2015.04.005

23. Cross TM, Gibbs N, Houang MT, Cameron M. Acute Quadriceps Muscle Strains: Magnetic

Resonance Imaging Features and Prognosis. *Am J Sports Med*. 2004;32(3):710-719. doi:10.1177/0363546503261734

24. Dassault Systemes Simulia Corporation. Abaqus V. 6.14 documentation.

25. Depalma MJ, Perkins RH. Patellar Tendinosis: Acute Patellar Tendon Rupture and Jumper's Knee. *Phys Sportsmed*. 2004;32(5):41-45.

26. DeRoos WK, Zeeman RJ. A flexor tendon rupture in the palm of the hand. *J Hand Surg Am*. 1991;16(4):663-665.

27. DeSmet AA, Best TM. MR imaging of the distribution and location of acute hamstring injuries in athletes. *AJR Am J Roentgenol*. 2000;174(2):393-399. doi:10.2214/ajr.174.2.1740393

28. DeWaal Malefijt MC, Beeker TW. Avulsion of the triceps tendon in secondary hyper parathyroidism: A case report. *Acta Orthop*. 1987;58(4):434-435. doi:10.3109/17453678709146376

29. Dürig M, Schuppisser JP, Gauer EF, et al. Spontaneous rupture of the gastrocnemius muscle. *Injury*. 1977;9(2):143-145. doi:10.1016/0020-1383(77)90009-2

30. Entwisle T, Ling Y, Splatt A, Brukner P, Connell D. Distal Musculotendinous T Junction Injuries of the Biceps Femoris: An MRI Case Review. *Orthop J Sport Med*. 2017;5(7):2325967117714998. doi:10.1177/2325967117714998

31. Evans NA, Bowrey DJ, Newman GR. Ultrastructural analysis of ruptured tendon from anabolic steroid users. *Injury*. 1998;29(10):769-773. doi:10.1016/S0020-1383(98)00183-1

32. Farley TE, Neumann CH, Steinbach LS, Jahnke AJ, Petersen SS. Full-thickness tears of the rotator cuff of the shoulder: diagnosis with MR imaging. *AJR Am J Roentgenol*. 1992;158(2):347-351. doi:10.2214/ajr.158.2.1729796

33. Farrar EL 3rd, Lippert FG 3rd, Farrar III EL, Lippert III FG. Avulsion of the triceps tendon. *Clin Orthop Relat Res*. 1981;No. 161(161):242-246.

34. Ferreira JPS, Parente MPL, Jabareen M, Jorge RMN. A general framework for the numerical implementation of anisotropic hyperelastic material models including non-local damage. *Biomech Model Mechanobiol*. 2017;16(4):1119-1140. doi:10.1007/s10237-017-0875-9

35. Ferretti A, Ippolito E, Mariani P, Puddu G. Jumper's knee. *Am J Sports Med*. 1983;11(2):58-62. doi:10.1177/036354658301100202

36. Ferretti A, Puddu G, Mariani PP, Neri M. The natural history of jumper's knee. Patellar or quadriceps tendonitis. *Int Orthop*. 1985;8(4):239-242. doi:10.1007/bf00266866

37. Fitzpatrick D, Cagle P, Flatow E. Isolated Teres Major Rupture: A case report with a suggested dedicated imaging protocol and review of the literature. *J Radiol Case Rep*. 2016;10(4):31-36. doi:10.3941/jrcr.v10i4.2674

38. Fleckenstein JL, Weatherall PT, Parkey RW, Payne JA, Peshock RM. Sports-related muscle injuries: evaluation with MR imaging. *Radiology*. 1989;172(3):793-798. doi:10.1148/radiology.172.3.2772190

39. Floor S, Van Der Veen AH, Devilee RJ. Two patients with a complete proximal rupture of the hamstring. *Arch Orthop Trauma Surg*. 2010;130(4):523-526. doi:10.1007/s00402-009-0950-5

40. Freccero DM, Berkowitz MJ. The relationship between tears of the peroneus brevis tendon and the distal extent of its muscle belly: an MRI study. *Foot ankle Int*. 2006;27(4):236-239. doi:10.1177/107110070602700402

41. Gagnier JJ, Riley D, Altman DG, Moher D, Sox H, Kienle G. The CARE guidelines: consensus-based clinical case reporting guideline development. *Dtsch Arztebl Int*. 2013;110(37):603-608. doi:10.3238/arztebl.2013.0603

42. Garrett WEJ, Nikolaou PK, Ribbeck BM, Glisson RR, Seaber A V. The effect of muscle architecture on the biomechanical failure properties of skeletal muscle under passive extension. *Am J Sports Med*. 1988;16(1):7-12. doi:10.1177/036354658801600102

43. Garrett WEJ, Safran MR, Seaber A V, Glisson RR, Ribbeck BM. Biomechanical comparison of stimulated and nonstimulated skeletal muscle pulled to failure. *Am J Sports Med*. 1987;15(5):448-454. doi:10.1177/036354658701500504

44. Gaskin CM, Anderson MW, Choudhri A, Diduch DR. Focal partial tears of the long head of the biceps brachii tendon at the entrance to the bicipital groove: MR imaging findings, surgical correlation, and clinical significance. *Skeletal Radiol*. 2009;38(10):959-965. doi:http://dx.doi.org/10.1007/s00256-009-0720-z

45. Gidwani S, Bircher MD. Avulsion injuries of the hamstring origin - A series of 12 patients and management algorithm. *Ann R Coll Surg Engl*. 2007;89(4):394-399. doi:10.1308/003588407X183427

46. Giuffre BM, Lisle DA. Case Report: Tear of the distal biceps branchii tendon: A new method of ultrasound evaluation. *Australas Radiol*. 2005;49(5):404-406. doi:http://dx.doi.org/10.1111/j.1440-1673.2005.01469.x

47. Godoy IRB, Martinez-Salazar EL, Simeone FJ, Bredella MA, Palmer WE, Torriani M. MRI of pectoralis major tears: association between ancillary findings and tear severity. *Skeletal Radiol*. 2018;47(8):1127-1135. doi:http://dx.doi.org/10.1007/s00256-018-2893-9

48. Goodier D, Maffulli N, Good CJ, Good J. Tibial tuberosity avulsion associated with patellar tendon avulsion. *Acta Orthop Belg*. 1994;60(2):336-338.

49. Gottsauner-Wolf F, Grabowski JJ, Chao EY, An KN. Effects of freeze/thaw conditioning on the tensile properties and failure mode of bone-muscle-bone units: a biomechanical and histological study in dogs. *J Orthop Res*. 1995;13(1):90-95. doi:10.1002/jor.1100130114

50. Gruel JB. Isolated avulsion of the popliteus tendon. *Arthroscopy*. 1990;6(2):94-95.

51. Gyftopoulos S, Rosenberg ZS, Schweitzer ME, Bordalo-Rodrigues M. Normal anatomy and strains of the deep musculotendinous junction of the proximal rectus femoris: MRI features. *AJR Am J Roentgenol*. 2008;190(3):W182-6. doi:10.2214/AJR.07.2947

52. Hart ES. Acute Quadriceps Tendon Rupture. *Orthop Nurs*. 2013;32(1):53-54.

53. Hasegawa K, Schofer JM. Rupture of the Pectoralis Major: A Case Report and Review. *J Emerg Med*. 2010;38(2):196-200. doi:10.1016/j.jemermed.2008.01.025

54. Hasselman CT, Best TM, Seaber A V, Garrett WEJ. A threshold and continuum of injury during active stretch of rabbit skeletal muscle. *Am J Sports Med*. 1995;23(1):65-73. doi:10.1177/036354659502300111

55. Henry JC, Scerpella TA. Acute traumatic tear of the latissimus dorsi tendon from its insertion: A case report. *Am J Sports Med*. 2000;28(4):577-579.

56. Hertel R, Lambert SM. Supraspinatus rupture at the musculotendinous junction. *J shoulder Elb Surg*. 1998;7(4):432-435.

57. Holzapfel GA. *Nonlinear Solid Mechanics: A Continuum Approach for Engineering*. John Wiley & Sons; 2000.

58. Holzapfel GA, Gasser TC. A viscoelastic model for fiber-reinforced composites at finite strains: Continuum basis, computational aspects and applications. *Comput Methods Appl Mech Eng*. 2001;190(34):4379-4403. doi:https://doi.org/10.1016/S0045-7825(00)00323-6

59. Holzapfel GA, Gasser TC, Ogden RW. A new constitutive framework for arterial wall mechanics and a comparative study of material models. *J Elast Phys Sci solids*. 2000;61(1):1-48. doi:10.1023/A:1010835316564

60. Hughes C 4th, Hasselman CT, Best TM, Martinez S, Garrett WEJ. Incomplete, intrasubstance strain injuries of the rectus femoris muscle. *Am J Sports Med*. 1995;23(4):500-506. doi:10.1177/036354659502300422

61. Huri G, Dubin JM, Ozgonen K, Kaya D, Doral MN. A unique rectus femoris injury in an adolescent professional soccer player: A case report. *JBJS Case Connect*. 2014;4(4). doi:10.2106/JBJS.CC.M.00290

62. Ilaslan H, Iannotti JP, Recht MP. Deltoid muscle and tendon tears in patients with chronic rotator cuff tears. *Skeletal Radiol*. 2007;36(6):503-507. doi:10.1007/s00256-007-0279-5

63. Irmola T, Heikkilä JT, Orava S, Sarimo J. Total proximal tendon avulsion of the rectus femoris muscle. *Scand J Med Sci*. 2007;17(4):378-382. doi:http://dx.doi.org/10.1111/j.1600-0838.2006.00564.x

64. Jaiswal A, Kacchap ND, Tanwar YS, Kumar D, Kumar B. Rupture of the triceps tendon – A case series. *Chinese J Traumatol - English Ed*. 2016;19(4):235-238. doi:10.1016/j.cjtee.2016.06.006

65. Jansen JA, Cormier S, Patel J V. Acute rectus femoris rupture at the distal musculotendinous junction in a football player: A case report and surgical technique. *Curr Orthop Pract*. 2012;23(4):390-392. doi:10.1097/BCO.0b013e31825b2249

66. Kameyama M, Shiraishi T. Traumatic rupture of the extensor digitorum communis and extensor digiti minimi at the musculotendinous junction associated with volar dislocation of the distal radioulnar joint--a case report. *Hand Surg*. 2000;5(2):165-168.

67. Kankaya Y, Oruç M, Uysal A, Koçer U. Multiple Closed flexor Tendon Avulsions From Their Insertions by a High-energy Explosion. *J Hand Surg Am*. 2006;31(6):663-664. doi:10.1016/j.jhsb.2006.07.014

68. Karjalainen PT, Soila K, Aronen HJ, et al. MR imaging of overuse injuries of the Achilles tendon. *AJR Am J Roentgenol*. 2000;175(1):251-260. doi:10.2214/ajr.175.1.1750251

69. Kawashima M, Sato M, Torisu T, Himeno R, Iwabuchi A. Rupture of the pectoralis major. Report of 2 cases. *Clin Orthop Relat Res*. 1975;(109):115-119. doi:10.1097/00003086-197506000-00015

70. Khiami F, Tavassoli S, De Ridder Baeur L, Catonné Y, Sariali E. Distal partial ruptures of triceps brachii tendon in an athlete. *Orthop Traumatol Surg Res*. 2012;98(2):242-246. doi:10.1016/j.otsr.2011.09.022

71. Kibuule LK, Fehringer E V. Distal triceps tendon rupture and repair in an otherwise healthy pediatric patient: A case report and review of the literature. *J Shoulder Elb Surg*. 2007;16(3):e1-e3. doi:10.1016/j.jse.2006.06.002

72. Kilkenny C, Browne WJ, Cuthill IC, Emerson M, Altman DG. Improving Bioscience Research Reporting: The ARRIVE Guidelines for Reporting Animal Research. *PLOS Biol*. 2010;8(6):e1000412.

73. Kim TK, Rauh PB, McFarland EG. Partial tears of the subscapularis tendon found during arthroscopic procedures on the shoulder: A statistical analysis of sixty cases. *Am J Sports Med*. 2003;31(5):744-750.

74. Law DJ, Caputo A, Tidball JG. Site and mechanics of failure in normal and dystrophin-deficient skeletal muscle. *Muscle Nerve*. 1995;18(2):216-223. doi:10.1002/mus.880180211

75. Lempainen L, Sarimo J, Mattila K, Heikkilä J, Orava S. Distal tears of the hamstring muscles: Review of the literature and our results of surgical treatment. *Br J Sports Med*. 2007;41(2):80-83. doi:10.1136/bjsm.2006.031211

76. Levine JW, Savoie III FH. Traumatic rupture of the latissimus dorsi. *Orthopedics*. 2008;31(8):799. doi:10.3928/01477447-20080801-14

77. Lukac D, Jakovljevic DK, Klasnja A, Drapsin M, Slavic D, Karan V. Ultrasonographic evaluation of the ruptured medial head of gastrocnemius muscle . *Rev Bras Med do Esporte*. 2016;22(5):381-385. doi:10.1590/1517-869220162205158755

78. Lunn J V, Castellanos-Rosas J, Tavernier T, Barthelemy R, Walch G. A novel lesion of the infraspinatus characterized by musculotendinous disruption, edema, and late fatty infiltration. *J shoulder Elb Surg*. 2008;17(4):546-553. doi:10.1016/j.jse.2007.11.016

79. Maehara H, Sakaguchi Y. Avulsion Fracture of the Medial Head of the Gastrocnemius Muscle: A Case Report. *J Bone Jt Surg - Ser A*. 2004;86(2):373-375. doi:10.2106/00004623-200402000-00024

80. Maffulli N. The clinical diagnosis of subcutaneous tear of the Achilles tendon: A prospective study in 174 patients. *Am J Sports Med*. 1998;26(2):266-270.

81. Mair SD, Seaber A V, Glisson RR, Garrett WE, Garrett Jr. WE. The role of fatigue in susceptibility to acute muscle strain injury. *Am J Sports Med*. 1996;24(2):137-143. doi:10.1177/036354659602400203

82. Makridis KG, Lequesne M, Bard H, Djian P. Clinical and MRI results in 67 patients operated for gluteus medius and minimus tendon tears with a median follow-up of 4.6 years. *Orthop Traumatol Surg Res*. 2014;100(8):849-853. doi:10.1016/j.otsr.2014.08.004

83. Mansat P, Frankle MA, Cofield RH. Tears in the subscapularis tendon: Descriptive analysis and results of surgical repair. *Jt Bone Spine*. 2003;70(5):342-347. doi:10.1016/S1297-319X(03)00044-7

84. Marino M. Constitutive modeling of soft tissues. In: Narayan R, ed. *Encyclopedia of Biomedical Engineering*. Vol 1-3. Elsevier; 2019:81-110. doi:https://doi.org/10.1016/B978-0-12-801238-3.99926-4

85. Mechrefe AP, Walsh EF, DiGiovanni CW. Anterior tibial tendon avulsion with distal tibial fracture entrapment: case report. *Foot ankle Int*. 2006;27(8):645-647. doi:10.1177/107110070602700816

86. Mellado JM, Calmet J, Giné J, Saurí A. Pectoralis major muscle and tendon tears: Report of two cases with surgical correlation and postoperative follow-up. *Eur J Radiol Extra*. 2004;50(3):101-104. doi:10.1016/j.ejrex.2004.03.005

87. Menz P, Nettle WJ. Closed rupture of the musculotendinous junction of extensor hallucis longus.

Injury. 1989;20(6):378-381.

88. Milella PP. *Fatigue and Corrosion in Metals*. 1st ed. (Milella PP, ed.). Springer-Verlag Mailand; 2013. doi:10.1007/978-88-470-2336-9

89. Miller WA. Rupture of the musculotendinous juncture of the medial head of the gastrocnemius muscle. *Am J Sports Med*. 1977;5(5):191-193. doi:10.1177/036354657700500505

90. Miranda MO, Bureau NJ. Supraspinatus Myotendinous Junction Injuries: MRI Findings and Prevalence. *AJR Am J Roentgenol*. 2019;212(1):W1-W9. doi:10.2214/AJR.18.19776

91. Naito K, Homma Y, Morita M, Mogami A, Obayashi O. Triceps tendon avulsion: a case report and discussion about the olecranon ossification nucleus. *Eur J Orthop Surg Traumatol*. 2013;23 Suppl 2:S193-6. doi:10.1007/s00590-012-1127-4

92. Nimityongskul P, Montague WL, Anderson LD. Avulsion fracture of the tibial tuberosity in late adolescence. *J Trauma - Inj Infect Crit Care*. 1988;28(4):505-509. doi:10.1097/00005373-198804000-00015

93. Nishida Y, Tsukushi S, Yamada Y, Hosono K, Ishiguro N. Brachialis Muscle Tear Mimicking an Intramuscular Tumor: A Report of Two Cases. *J Hand Surg Am*. 2007;32(8):1237-1241. doi:10.1016/j.jhsa.2007.06.002

94. Noonan TJ, Best TM, Seaber A V, Garrett WEJ. Identification of a threshold for skeletal muscle injury. *Am J Sports Med*. 1994;22(2):257-261. doi:10.1177/036354659402200217

95. Ohashi K, El-Khoury GY, Albright JP, Tearse DS. MRI of complete rupture of the pectoralis major muscle. *Skeletal Radiol*. 1996;25(7):625-628.

96. Panni AS, Tartarone M, Maffulli N. Patellar tendinopathy in athletes. Outcome of nonoperative and operative management. *Am J Sports Med*. 2000;28(3):392-397. doi:10.1177/03635465000280031901

97. Pedret C, Balius R, Barcelo P, et al. Isolated tears of the gracilis muscle. *Am J Sports Med*. 2011;39(5):1077-1080. doi:10.1177/0363546510394436

98. Peña E. Computational aspects of the numerical modelling of softening, damage and permanent set in soft biological tissues. *Comput Struct*. 2014;130:57-72. doi:https://doi.org/10.1016/j.compstruc.2013.10.002

99. Pina A, Garcia I, Sabater M. Traumatic avulsion of the triceps brachii. *J Orthop Trauma*. 2002;16(4):273-276. doi:10.1097/00005131-200204000-00010

100. Pitts RT, Garner HW, Ortiguera CJ. Pectoralis major avulsion in a skeletally immature wrestler: A case report. *Am J Sports Med*. 2010;38(5):1034-1037. doi:10.1177/0363546509351559

101. Pochini A de C, Ejnisman B, Andreoli C V, et al. Pectoralis major muscle rupture in athletes: A prospective study. *Am J Sports Med*. 2010;38(1):92-98. doi:10.1177/0363546509347995

102. Pomeranz SJ, Heidt RSJ. MR imaging in the prognostication of hamstring injury. Work in progress. *Radiology*. 1993;189(3):897-900. doi:10.1148/radiology.189.3.8234722

103. Rajasekhar C, Kakarlapudi TK, Bhamra MS. Avulsion of the triceps tendon. *Emerg Med J*. 2002;19(3):271-272.

104. Rochman R, SanGiovanni TP, Uribe JW. Muscle belly tears of the peroneal muscles: A case report. *Foot Ankle Int*. 2006;27(12):1159-1160. doi:10.1177/107110070602701227

105. Roe M, Murphy JC, Gissane C, Blake C. Hamstring injuries in elite Gaelic football: an 8-year investigation to identify injury rates, time-loss patterns and players at increased risk. *Br J Sports Med*. 2018;52(15):982-988. doi:10.1136/bjsports-2016-096401

106. Rose PS, Frassica FJ. Atraumatic bilateral patellar tendon rupture: A case report and review of the literature. *J Bone Jt Surg*. 2001;83(9):1382-1386.

107. Sano H, Ishii H, Yeadon A, Backman DS, Brunet JA, Uhthoff HK. Degeneration at the insertion weakens the tensile strength of the supraspinatus tendon: a comparative mechanical and histologic study of the bone-tendon complex. *J Orthop Res*. 1997;15(5):719-726. doi:10.1002/jor.1100150514

108. Schache AG, Koulouris G, Kofoed W, Morris HG, Pandy MG. Rupture of the conjoint tendon at the proximal musculotendinous junction of the biceps femoris long head: A case report. *Knee Surgery, Sport Traumatol Arthrosc*. 2008;16(8):797-802. doi:10.1007/s00167-008-0517-y

109. Shah S, Montgomery W, Bastidas M. A unique myotendinous avulsion injury of the achilles tendon. *Curr Orthop Pract*. 2009;20(4):464-466. doi:10.1097/BCO.0b013e31819cadf1

110. Sharma P, Vijayargiya M, Tandon S, Gaur S. Triceps tendon avulsion: a rare injury. *Ethiop J Health Sci*. 2014;24(1):97-99. doi:10.4314/ejhs.v24i1.14

111. Sherman OH, Snyder SJ, Fox JM. Triceps tendon avulsion in a professional body builder. A case report. *Am J Sports Med*. 1984;12(4):328-329. doi:10.1177/036354658401200415

112. Shields CL, Ashby ME. Diagnosis in patellar tendon avulsion. *J Natl Med Assoc*. 1975;67(3):231-232.

113. Sierra RJ, Weiss NG, Shrader MW, Steinmann SP. Acute triceps ruptures: Case report and retrospective chart review. *J Shoulder Elb Surg*. 2006;15(1):130-134. doi:10.1016/j.jse.2005.01.004

114. Silder A, Heiderscheit BC, Thelen DG, Enright T, Tuite MJ. MR observations of long-term musculotendon remodeling following a hamstring strain injury. *Skeletal Radiol*. 2008;37(12):1101-1109. doi:10.1007/s00256-008-0546-0

115. Simonet WT, Saylor III HL, Sim L. Abdominal wall muscle tears in hockey players. *Int J Sports Med*. 1995;16(2):126-128. doi:10.1055/s-2007-972978

116. Singh RK, Pooley J. Complete rupture of the triceps brachii muscle. *Br J Sports Med*. 2002;36(6):467. doi:http://dx.doi.org/10.1136/bjsm.36.6.467

117. Smith JH. Avulsion of a profundus tendon with simultaneous intraarticular fracture of the distal phalanx—Case report. *J Hand Surg Am*. 1981;6(6):600-601. doi:10.1016/S0363-5023(81)80141-4

118. Sollender JL, Rayan GM, Barden GA. Triceps tendon rupture in weight lifters. *J shoulder Elb Surg*. 1998;7(2):151-153.

119. Sonnery-Cottet B, Edwards TB, Noel E, Walch G. Rotator cuff tears in middle-aged tennis players: Results of surgical treatment. *Am J Sports Med*. 2002;30(4):558-564.

120. Speer KP, Lohnes J, Garrett WEJ. Radiographic imaging of muscle strain injury. *Am J Sports Med*. 1993;21(1):89-95; discussion 96. doi:10.1177/036354659302100116

121. Street CC, Burks RT. Chronic complete hamstring avulson causing foot drop: A case report. *Am J Sports Med*. 2000;28(4):574-576. doi:10.1177/03635465000280042201

122. Sun J-SS, Tsuang Y-HH, Liu T-KK, Hang Y-SS, Cheng C-KK. Failure sites and peak tensile forces of the composite triceps surae muscle by passive extension in the rabbit. *Clin Biomech*. 1994;9(5):310-314. doi:10.1016/0268-0033(94)90044-2

123. Takami H, Takahashi S, Ando M, Kabata K. Rupture of the flexor pollicis longus tendon at the musculotendinous junction in a bowler. *Arch Orthop Trauma Surg*. 1998;117(4-5):277-278.

124. Takami H, Takahashi S, Ando M, Suzuki K. Traumatic rupture of the extensor tendons at the musculotendinous junction. *J Hand Surg Am*. 1995;20(3):474-477. doi:10.1016/S0363-5023(05)80110-8

125. Taylor DC, Dalton JDJ, Seaber A V, Garrett WEJ. Experimental muscle strain injury. Early functional and structural deficits and the increased risk for reinjury. *Am J Sports Med*. 1993;21(2):190-194. doi:10.1177/036354659302100205

126. Temple HT, Kuklo TR, Sweet DE, Gibbons CL, Murphey MD. Rectus femoris muscle tear appearing as a pseudotumor. *Am J Sports Med*. 1998;26(4):544-548. doi:10.1177/03635465980260041301

127. Tiger E, Mayer DP, Glazer R. Complete avulsion of the triceps tendon: MRI diagnosis. *Comput Med Imaging Graph*. 1993;17(1):51-54. doi:10.1016/0895-6111(93)90074-W

128. Toczylowski HM, Balint CR, Steiner ME, Boardman M, Scheller Jr. AD. Complete rupture of the distal biceps brachii tendon in female patients: A report of 2 cases. *J Shoulder Elb Surg*. 2002;11(5):516-518. doi:10.1067/mse.2002.126617

129. Tsuang Y-H, Sun J-S, Chen I-H, et al. The effects of cyclic stretching on tensile properties of the rabbit's skeletal muscle. *Clin Biomech (Bristol, Avon)*. 1998;13(1):48-53.

130. Tung GA, Yoo DC, Levine SM, Brody JM, Green A. Subscapularis Tendon Tear: Primary and Associated Signs on MRI. *J Comput Assist Tomogr*. 2001;25(3):417-424.

131. Valente M, Mancuso F, Alecci V. Isolated rupture of biceps femoris tendon. *Musculoskelet Surg*. 2013;97(3):263-266. doi:10.1007/s12306-011-0171-2

132. Vandenbroucke JP, von Elm E, Altman DG, et al. Strengthening the Reporting of Observational Studies in Epidemiology (STROBE): Explanation and Elaboration. *PLOS Med*. 2007;4(10):e297.

133. Vastamäki M, Brummer H, Solonen KA. Avulsion of the distal biceps brachii tendon. *Acta Orthop*.

1981;52(1):45-48. doi:10.3109/17453678108991757

134. Vila Pouca MCP, Parente MPL, Natal Jorge RM, Ashton-Miller JA. Investigating the birth-related caudal maternal pelvic floor muscle injury: The consequences of low cycle fatigue damage. *J Mech Behav Biomed Mater*. 2020;110:103956. doi:https://doi.org/10.1016/j.jmbbm.2020.103956

135. Wagner JR, Cooney WP. Rupture of the triceps muscle at the musculotendinous junction: a case report. *J Hand Surg Am*. 1997;22(2):341-343. doi:10.1016/S0363-5023(97)80175-X

136. Walch G, Nove-Josserand L, Liotard J-P, Noel E. Musculotendinous infraspinatus ruptures: an overview. *Orthop Traumatol Surg Res*. 2009;95(7):463-470. doi:10.1016/j.otsr.2009.06.004

137. Wang Y-C, Jeng C-M, Shen P-W, et al. Pectoralis major muscle tear diagnosed with magnetic resonance imaging and ultrasound - A case report. *Tzu Chi Med J*. 2005;17(6):441-444+456.

138. Warme WJ, Whitaker DC. Pectoralis major tendon avulsion from rappelling. *Mil Med*. 2004;169(2):151-154. doi:10.7205/milmed.169.2.151

139. Weishaupt D, Schweitzer ME, Morrison WB. Injuries to the distal gastrocnemius muscle: MR findings. *J Comput Assist Tomogr*. 2001;25(5):677-682.

140. Wenger DR. Avulsion of the Profundus Tendon Insertion in Football Players. *Arch Surg*. 1973;106(2):145-149. doi:10.1001/archsurg.1973.01350140013006

141. White GM, Riley Jr. LH. Isolated avulsion of the subscapularis insertion in a child. A case report. *J Bone Jt Surg - Ser A*. 1985;67(4):635-636. doi:10.2106/00004623-198567040-00021

142. Williams BD, Schweitzer ME, Weishaupt D, et al. Partial tears of the distal biceps tendon: MR appearance and associated clinical findings. *Skeletal Radiol*. 2001;30(10):560-564. doi:10.1007/s002560100397

143. Winblad JB, Escobedo E, Hunter JC. Brachialis Muscle Rupture and Hematoma. *Radiol Case Reports*. 2008;3(4):251. doi:10.2484/rcr.v3i4.251

144. Yoon MY, Koris MJ, Ortiz JA, Papandrea RF. Triceps avulsion, radial head fracture, and medial collateral ligament rupture about the elbow: A report of 4 cases. *J Shoulder Elb Surg*. 2012;21(2):e12-e17. doi:10.1016/j.jse.2011.06.017

145. Yoshioka H, Anno I, Niitsu M, Takahashi H, Matsumoto K, Itai Y. MRI of muscle strain injuries. *J Comput Assist Tomogr*. 1994;18(3):454-460.